MICROCOPY RESOLUTION TEST CHART

NATIONAL BUREAU OF STANDARDS-1963-A

AD-A151 712

DNA-TR-84-11

LABORATORY INVESTIGATION OF CONTAINMENT OF UNDERGROUND EXPLOSIONS

J.C. Cizek
A.L. Florence
SRI International
333 Ravenswood Avenue
Menlo Park, California 94025

December 1983

Technical Report

APPROVED FOR PUBLIC RELEASE;
DISTRIBUTION UNLIMITED.

Prepared for
Director
DEFENSE NUCLEAR AGENCY
Washington, DC 20305

DTIC
ELECTE
MAR 26 1985
S   D
B

85   02   04   024

REPORT DOCUMENTATION PAGE		READ INSTRUCTIONS BEFORE COMPLETING FORM
1. REPORT NUMBER DNA-TR-84-11	2. GOVT ACCESSION NO. AD-A151 712	3. RECIPIENT'S CATALOG NUMBER
4. TITLE (and Subtitle) LABORATORY INVESTIGATION OF CONTAINMENT OF UNDERGROUND EXPLOSIONS		5. TYPE OF REPORT & PERIOD COVERED **Technical Report**
		6. PERFORMING ORG. REPORT NUMBER SRI Project 5372
7. AUTHOR(s) J.C. Cizek A.L. Florence		8. CONTRACT OR GRANT NUMBER(s) DNA 002-83-C-0024
9. PERFORMING ORGANIZATION NAME AND ADDRESS SRI International 333 Ravenswood Avenue Menlo Park, California 94025		10. PROGRAM ELEMENT, PROJECT, TASK AREA & WORK UNIT NUMBERS Task J24AMXJA-00001
11. CONTROLLING OFFICE NAME AND ADDRESS Director Defense Nuclear Agency Washington, DC 20305		12. REPORT DATE December 1983
		13. NUMBER OF PAGES 258
14. MONITORING AGENCY NAME & ADDRESS(if different from Controlling Office)		15. SECURITY CLASS (of this report) UNCLASSIFIED
		15a. DECLASSIFICATION/DOWNGRADING SCHEDULE N/A since UNCLASSIFIED

16. DISTRIBUTION STATEMENT (of this Report)

Approved for public release, distribution unlimited.

17. DISTRIBUTION STATEMENT (of the abstract entered in Block 20, if different from Report)

19. KEY WORDS (Continue on reverse side if necessary and identify by block number)

Nuclear	Cavity	Granite
Underground	Hydrofracture	Differential compacting
Explosion	Fracture	Overburden
Containment	Tuff	Depth-of-burial
Residual stress	Alluvium	

20. ABSTRACT (Continue on reverse side if necessary and identify by block number)

In support of the DNA program for stemming and containment of under-
ground nuclear tests, laboratory techniques were applied to investigate the
mechanics of containing gases in cavities formed by underground nuclear
explosions.

One experimental technique uses constant flow rate hydrofracture from
a central exploded cavity in a cylinder of geologic material or simulant
externally pressurized to represent overburden.

DD FORM 1473 EDITION OF 1 NOV 65 IS OBSOLETE
1 JAN 73

20. ABSTRACT (Continued)

A second experimental technique uses the measurement of particle velocity in the material surrounding an exploded cavity to provide outward and rebound motion at several radii for geologic materials and simulants.

Additional experimental techniques use direct measurements of the transient and long-term stress and strain surrounding an exploded cavity.

Hydrofracture, particle velocity, stress, and strain results for a rock-matching grout representing saturated Nevada Test Site tuff show the following:

- A beneficial residual stress forms around an exploded cavity, and containment of gases is achieved at normal overburden.

- Permanent volume compression exists in the region surrounding an exploded cavity.

- Containment may be possible with depth-of-burial and overburden less than those of normal practice.

- Strain rate changes do not have significant effect on particle velocity when the scale factor is doubled.

Hydrofracture and particle velocity results for G-tunnel and P-tunnel tuffs show the following:

- A beneficial residual stress forms around an exploded cavity.

- A larger exploded cavity is formed in the P-tunnel tuff, thus reducing cavity gas pressure and the possibility of spontaneous fracture.

- Permanent volume dilatation exists in the region near an exploded cavity, suggesting that microcracks are formed.

Hydrofracture and particle velocity results for weak grout and reconstituted desert fines representing test site alluvium show the following:

- Containment may be achieved because cavities are large and pressures are low.

- The residual stress field around an exploded cavity in the grout is weak but it aids containment by providing crack growth stability.

- Postshot loss of confining tectonic stress resulting from differential compaction may result in cavity fracture.

Particle velocity results for dome salt show the following:

- Negligible residual stress forms around an exploded cavity because the weak material produces no rebound motion.

- A relatively small exploded cavity forms, which keeps the pressure high.

20. ABSTRACT (Continued)

- Microcracks associated with volume dilatation probably develop near the exploded cavity.

- Extensive dynamic fractures from the cavity develop.

Hydrofracture and particle velocity results for granite and granite simulant representative of hard rock show the following:

- Dynamic fracture of the cavity is likely.

- A beneficial residual stress may form around an exploded cavity, and gases may be contained in a region near the cavity.

PREFACE

CONVERSION FACTORS

To Convert From	To	Multiply By
bar	kilo pascal (kPa)	$1.000 \times E +2$
foot	meter (m)	$3.048 \times E -1$
inch	meter (m)	$2.540 \times E -2$
mil	meter (m)	$2.540 \times E -5$
ounce	kilogram (kg)	$2.834 \times E -2$
poise	kilogram/meter-second (kg/m·s)	$1.000 \times E -1$
pound-force (lbf avoirdupois)	newton (N)	4.448
pound-force/inch^2 (psi)	kilo pascal (kPa)	6.894
pound-mass (lbm avoirdupois)	kilogram (kg)	$4.535 \times E -1$

TABLE OF CONTENTS

3

4

LIST OF ILLUSTRATIONS

5

LIST OF ILLUSTRATIONS (Continued)

LIST OF ILLUSTRATIONS (Continued)

The exploded cavity hydrofracture technique was applied to cylinders of RMG 2C4 and cylindrical cores of NTS tuff to assess the effects of material properties and other parameter variations on the residual stress field of the basic containment experiment. The reference parameters of the basic experiment were the material (2C4), charge size (3/8 gram PETN), overburden pressure [1000 psi (6.895 MPa)], viscosity of the hydrofracture fluid (1 centipoise), and rate of fluid flow into the exploded cavity (122.4 cm^3/min). Surface gages monitored fracture arrival in selected tests.

An independent series of basic tests was performed on spheres and cylinders of RMG 2C4 and cylinders of geologic material to obtain particle velocity profiles in the region surrounding exploded cavities. These records provide valuable restraints on the calculational modeling of dynamic material properties.[13,14]

A final series of tests was performed on RMG 2C4 spheres to measure directly dynamic and residual stress and strain in the region surrounding an exploded cavity.

The specific areas of investigation were as follows:

- Material property hydrofracture. Cylindrical cores of NTS G-tunnel tuff, taken from the vicinity of the working point of a Sandia National Laboratory (SNLA) 1 ton high explosive test, were hydrofractured immediately following charge detonation, and the pressures were compared with those for RMG 2C4.

- Differential compaction. The radial confining pressure on exploded cavity cylinders of weak (1-day-old) RMG 2C4 was released following charge detonation to simulate the tectonic stress change associated with differential compaction. The axial load was maintained constant. The release rate of the radial pressure was varied to study sudden and long-term differential compaction. A hydrofracture test was performed shortly after the pressure release.

- Depth-of-burial. Exploded cavity RMG 2C4 cylinders with a charge embedded at various depths and subjected to a range of external pressures were hydrofractured to determine the effects of depth-of-burial on containment. A free surface was provided at the top of the cylinders to simulate a finite depth-of-burial. In a separate series of tests,

21

Our laboratory investigations during the last year have focused on containment. One purpose of the experimental program has been to understand the mechanisms of underground nuclear explosions and containment of the cavity gases. An essential part of this understanding is the generation of data under controlled reproducible conditions for validation of the continuum mechanics computer codes of calculators working for the DNA program.[11-14]

Although the experiments are not strictly scalable to underground nuclear events, they are designed so that much of the physical behavior is represented. Consequently, the effects on containment of various physical conditions in past or planned nuclear events can receive a preliminary assessment.

In our basic containment experiments, a small sphere of PETN[*] powder explosive in a thin-walled Lucite container is cast at the center of a sphere of rock-matching grout (RMG 2C4). After aging, the grout has properties similar to those of Nevada Test Site (NTS) tuff. Also cast in the grout sphere is a stainless steel access tube located on a radius and ending just short of the Lucite container. External pressure is applied hydraulically to the sphere to represent overburden pressure. The explosive is detonated to create the exploded cavity. The end of the steel tube is located so that it just protrudes into the exploded cavity. Fluid is pumped into the cavity at a constant rate until fracture is initiated and propagated to the outside of the RMG sphere. During the pumping, fluid pressure and flow are monitored so that a hydrofracture record can be constructed.

The effect of the explosively generated residual stress field on containment is assessed by conducting a separate hydrofracture test on a sphere with an unexploded cavity comparable in size to the exploded cavity.

---

[*]Pentaerythritol tetranitrate ($C_5H_8O_{12}N_4$).

SECTION 1

INTRODUCTION, SUMMARY, AND CONCLUSIONS

1.1 INTRODUCTION

During an underground nuclear explosion, spherically divergent
ground motion is produced in the medium surrounding the expanding
cavity. This motion is eventually brought to rest by the outward energy
radiation of stress waves; by the energy dissipation of crushing, dis-
tortion, and crack formation; and by the combined resistance of tensile
tangential stresses and overburden pressure. This combined resistance
eventually causes a rebound of the medium that may cause further plastic
work around the cavity and intensify the residual stress field.

Radioactive gases produced by the explosion must not be released
into the atmosphere. Consequently, tunnels from the cavity must be
stemmed, and the cavity gases must be contained by the adjacent sur-
rounding medium. Containment of the gases may be aided by the residual
stress field created by the explosion. The extent of this aid is
governed by residual stress field strength relative to cavity gas
pressure, relaxation, and potential weaknesses in the field strength
caused by nearby geological and man-made features typical of those found
at the Nevada Test Site. Although containment has been achieved for
many years and stemming has generally been successful in recent nuclear
tests, the complexities associated with underground testing require that
planned events still receive extensive containment evaluation.

Over the years, the DNA stemming and containment program has
consisted of five parts: code development for ground motion, tunnel
closure, and grout flow calculations; material properties determination;
laboratory investigations; scaled high explosive tests; and field
diagnostics. Over the past several years, SRI has been conducting
laboratory investigations.[1-10]

LIST OF TABLES

LIST OF ILLUSTRATIONS (Concluded)

LIST OF ILLUSTRATIONS (Continued)

16

LIST OF ILLUSTRATIONS (Continued)

LIST OF ILLUSTRATIONS (Continued)

14

LIST OF ILLUSTRATIONS (Continued)

13

LIST OF ILLUSTRATIONS (Continued)

LIST OF ILLUSTRATIONS (Continued)

LIST OF ILLUSTRATIONS (Continued)

10

LIST OF ILLUSTRATIONS (Continued)

9

LIST OF ILLUSTRATIONS (Continued)

8

particle velocity components parallel to the free surface were measured at various depths.

- Particle velocity technique validation. A series of tests was performed in RMG 2C4, GS4, and granite cylinders to assess the effects of gage installation in geologic cores on particle velocity records. The areas examined were gage wire material (copper versus aluminum), gages cast in place versus gages embedded in precast material, and the groove width (wide versus narrow).

- Scaling effects. Strain rate effects in RMG 2C4 were assessed by doubling the charge diameter and gage radii (increasing the weight of explosive by a factor of 8) in a series of particle velocity tests.

- Material property particle velocity measurements. Particle velocity pulses were measured at various distances from the explosive charge in coupled exploded cavity cylinders of geologic material and simulant. The materials tested were SNLA G-tunnel tuff, P-tunnel tuff, Grand Saline (Texas) dome salt, California grey/white granite, granite simulant GS4, and alluvium reconstituted from NTS desert fines.

- Strain measurements. Dynamic circumferential strain and subsequent strain relaxation were measured at several distances from an exploded cavity in RMG 2C4 by means of embedded constantan wire loops. Radial and circumferential components of strain were independently monitored by strain gage grids encapsulated in room temperature vulcanizing (RTV) plastic.

- Stress measurements. Dynamic radial stress and subsequent stress relaxation were measured near an exploded cavity in RMG 2C4 by means of embedded piezoresistive ytterbium grids encapsulated in RTV.

In addition, the pressure pulses generated in the overburden fluid during exploded cavity tests were monitored for quality control and to provide additional data for verifying calculations. Volume strain in the region surrounding an exploded cavity was determined from the particle velocity records for several materials. Finally, an elastic analysis was performed to assess the extent of the plastic region surrounding an exploded cavity in granite by studying particle velocity attenuation.

Section 2 describes existing experimental techniques and recent developments. Section 3 presents and discusses the hydrofracture, particle velocity, stress, and strain results. The tests performed are

22

tabulated according to specific areas of investigation in Section 3.1.
Appendix A contains the particle displacement records obtained from the
particle velocity measurements, and Appendix B contains the pressure
pulses measured in the overburden fluid during exploded cavity tests.
Appendix C describes the elastic analysis for determining particle
velocity attenuation, and Appendix D describes the procedure for
generating volume strain from particle velocity records. Appendix E
contains the procedure for measuring particle velocity in alluvium
reconstituted from desert fines. Appendix F describes material proper-
ties for rock-matching grout RMG 2C4, reconstituted alluvium, granite
simulants GS3 and GS4, and a variety of NTS tuffs.

1.2 SUMMARY

The principal findings of the above investigations were as follows:

- Reproducibility of hydrofracture and particle velocity
  records is good for all configurations and materials
  tested.

- For SNLA G-tunnel tuff, exploded cavity hydrofracture
  pressures are comparable to those for RMG 2C4. Particle
  velocity pulses are also similar in the plastic region,
  but peak velocity attenuation is less in tuff as the
  elastic region is approached. Volume dilatation occurs in
  the tuff only (Figures 3.1 and 3.33 through 3.41).

- Loss of radial confining pressure following charge
  detonation (differential compaction) in a weak RMG results
  in cavity fracture (Figures 3.2 through 3.4).

- Depth-of-burial and overburden variations define a failure
  threshold in RMG 2C4 (Figures 3.5 through 3.7 and 3.111
  through 3.114).

- Changes in particle velocity gage wire material and groove
  width have negligible influence on particle velocity
  records in RMG 2C4. Gages cast in place and gages
  embedded in precast material yielded similar results
  (Figures 3.8 through 3.27).

- Doubling the charge and gage diameters causes a small
  increase of the scaled particle displacement for RMG 2C4
  (Figure A.5).

- For P-tunnel tuff, peak particle velocities are higher and
  pulse duration is longer than in SNLA G-tunnel tuff.

23

Dilatation occurs in both materials (Figures 3.42 through 3.49).

- Grand Saline dome salt shows no rebound following outward motion. Permanent dilatation and dynamic cracking occur near the cavity (Figures 3.50 through 3.56).

- Dynamic fracture results from charge detonation in an uncut cylinder of California grey/white granite. Thickness of a bonded interface influences particle velocity records. Stepped and plane interfaces yield similar results (Figures 3.57 through 3.77).

- For granite simulant GS4, no cracks form in a cast exploded cavity sphere; however, dynamic cracking occurs along the bonded interface in a precast cylinder. Particle velocity records showed little sensitivity to a propagating fracture (Figures 3.78 through 3.85).

- Particle accelerations at the wavefront in exploded cavity alluvium cylinders increase with initial saturation. Dilatation occurs in 88%-saturated material (Figures 3.86 through 3.110).

- Loops of constantan wire embedded in an exploded cavity RMG 2C4 sphere yield strains consistent with results obtained from particle velocity tests (Figure 3.115).

- Peak dynamic stress in an exploded cavity RMG 2C4 sphere, as measured by an ytterbium grid encapsulated in RTV, agrees with a calculated result. Pulse shape is influenced by the inclusion effect of an embedded gage (Figure 3.118).

1.3 CONCLUSIONS

Based on hydrofracture, particle velocity, stress, and strain results for the rock-matching grout 2C4, the implications for underground explosions in similar tuff-like materials are as follows:

- A beneficial residual stress will form around a coupled exploded cavity, and containment of high pressure gases will be achieved at normal overburden pressure.

- A well-defined failure threshold relating depth-of-burial and overburden exists. Containment may be possible with depth-of-burial and overburden less than those of normal practice.

- Strain rate effects are not changed significantly when the scale factor is doubled.

24

- The response of an embedded stress gage package will be influenced by inclusion effects.

Based on hydrofracture and particle velocity results for SNLA G-tunnel tuff and particle velocity results for P-tunnel tuff, the implications for containment in these materials are as follows:

- A beneficial residual stress will form around a coupled exploded cavity, and containment of high pressure gases at normal overburden pressure is expected.

- The larger exploded cavity formed in the P-tunnel tuff reduces cavity pressure and the possibility of spontaneous fracture.

- Volumetric dilatation occurs in a region near the exploded cavity and this suggests that microcracks are formed.

Based on hydrofracture results for weak RMG 2C4 and particle velocity results for reconstituted desert fines, the implications for underground tests in alluvium are as follows:

- An exploded cavity may provide adequate containment at normal overburden because large cavities are formed and pressures are relatively low.

- Postshot loss of confining tectonic stress resulting from differential compaction may result in cavity fracture. The resulting asymmetric stress field will encourage crack growth in vertical planes.

- Pore pressure will develop in a material with sufficient initial saturation. The pore fluid may aid containment by quenching cavity gases and lowering cavity pressure.

Based on particle velocity results for Grand Saline dome salt, the implications for underground tests in this material are as follows:

- Negligible residual stress will form around the exploded cavity because the weak material is incapable of producing rebound motion. Containment may be jeopardized because a relatively small exploded cavity is formed.

- Microcracks associated with volume dilatation will develop near the exploded cavity.

- Extensive dynamic cavity fractures will probably develop.

25

Based on hydrofracture and particle velocity results for California grey/white granite and granite simulant GS4, the implications for underground explosions in hard rock are as follows:

- Dynamic fracture of the cavity is likely.

- A beneficial residual stress field may form around a coupled exploded cavity, and containment of gases in a region near the cavity may be possible.

Laboratory research during the next phase of the containment program should include the following:

- Stress Measurements. With the particle velocity data augmented by stress measurements, the constraints on material modeling will be much more severe, and consequently the combined data will be an extremely valuable aid to calculators.

- Particle Velocity Measurements. Past experiments with G-tunnel tuff have given particle velocity records with peaks that are much more rounded than for other tuffs at stations close to the charge. This result has been attributed to the high level of heterogeneity and anisotropy of the G-tunnel tuff. The circular wire gage gives the average radial velocity. Consequently, to determine angular dependency, we recommend experiments with particle velocity gages having sensing wires extending only over a small arc. The additional work on G-tunnel tuff is important because of the program in which the results of the SNLA 1-ton test, our laboratory tests, and the theoretical material modeling research are coordinated.

- Saturation Percentage. We should continue to determine the dependence of particle velocity (and stress) measurements on saturation percentage for NTS tuff and alluvium.

- Hydrofracture Measurements. Currently, we have only one hydrofracture record for tuff. More experiments should be performed to consolidate the hydrofracture data.

- NTS Features. Further hydrofracture experimentation is recommended to obtain the effect of key NTS features on the residual stress field and hence on containment.

26

SECTION 2

EXPERIMENTAL TECHNIQUES

2.1 CONCEPTS

Hydrofracture

The experiment shown schematically in Figure 2.1 was devised[4] to simulate in the laboratory several conditions associated with underground nuclear tests. A small amount of PETN powder explosive sealed in a thin-walled Lucite sphere represents the device. The charge is cast at the center of a rock-matching grout sphere (or cylinder). After aging, the grout has properties similar to those of an NTS tuff. Also cast in the grout sphere is a stainless steel access tube located on a radius and ending near the charge [Figure 2.1(a)]. External pressure is applied hydraulically to the sphere to represent overburden pressure [Figure 2.1(b)]. The explosive is detonated to form the exploded cavity. The end of the steel tube is located so that it just protrudes into the explosively formed cavity [Figure 2.1(c)]. Fluid is pumped into the cavity at a constant rate until a fracture has initiated and propagated to the outside of the grout sphere [Figure 2.1(d)]. Fluid pressure and flow are monitored while fluid is being pumped so that a hydrofracture record can be constructed.

Alternative configurations and techniques have been developed to simulate test site conditions. These include the following:

- Performing hydrofracture tests on cylindrical cores of geologic test site material.

- Applying independent axial and radial confining pressures to a cylinder to simulate tectonic stress. The confining stress may be relieved at a controlled rate following charge detonation to simulate the effects of differential compaction.

- Embedding an explosive charge near the free end surface of a cylinder to simulate reduced depth-of-burial.

27
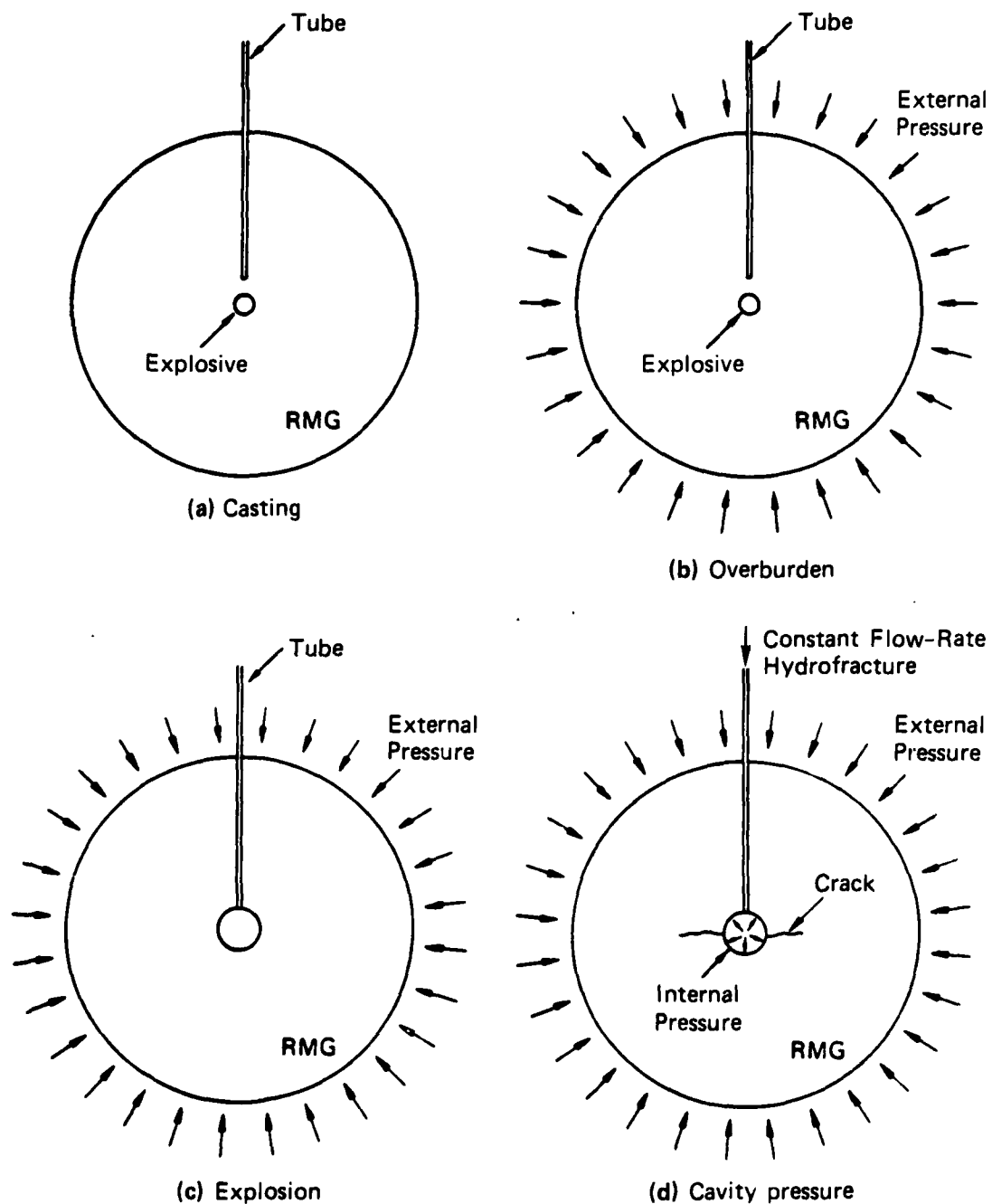
FIGURE 2.1 SEQUENCE OF OPERATIONS IN CONTAINMENT EXPERIMENTS

MA-3702-103B

The hydrofracture experiments determine the effect of the residual stress field on containment by allowing comparison of the cavity pressures required to crack grout specimens with and without residual stresses. In the experiments without a residual stress field, spherical cavities are cast in the grout; these unexploded cavities are comparable in size to the corresponding coupled exploded cavities.

Particle Velocity

The experiment shown schematically in Figure 2.2 was devised[15] to provide laboratory measurements of particle velocity in the material around an exploded cavity. Circular loops of wire are embedded symmetrically about an explosive source and move radially to follow particle motion. A voltage proportional to velocity is generated in each gage as the wires cut externally induced magnetic flux lines.

The experimental procedure with grout specimens readily allows embedding of stress and strain gage packages for measurement of transient and residual stress and strain.

2.2 EXISTING EXPERIMENTAL TECHNIQUES

Figure 2.3 shows the experimental apparatus for hydrofracture tests. A 12-inch-diameter (30.48-cm) RMG sphere is shown inside a steel vessel containing water that can be pressurized to the desired overburden. The sphere is suspended from the lid by the stainless steel tube cast in the grout. The fluid in the vessel is maintained at a constant pressure throughout the test by incorporating a high pressure nitrogen reservoir and valve in the water supply line. A quartz gage mounted in the bottom of the vessel monitors the pressure pulse generated by charge detonation.

The constant flow-rate system shown schematically in Figure 2.4 conforms with standard hydrofracture practice. The specifications of this system have been described in a previous report.[8]

Uniform Axial
Magnetic Field

Geologic
Specimen

Spherical
Explosive
Source

Horizontal
Plane
of Source

Concentric
Circular-Loop
Particle
Velocity
Gages

JA-317583-76B
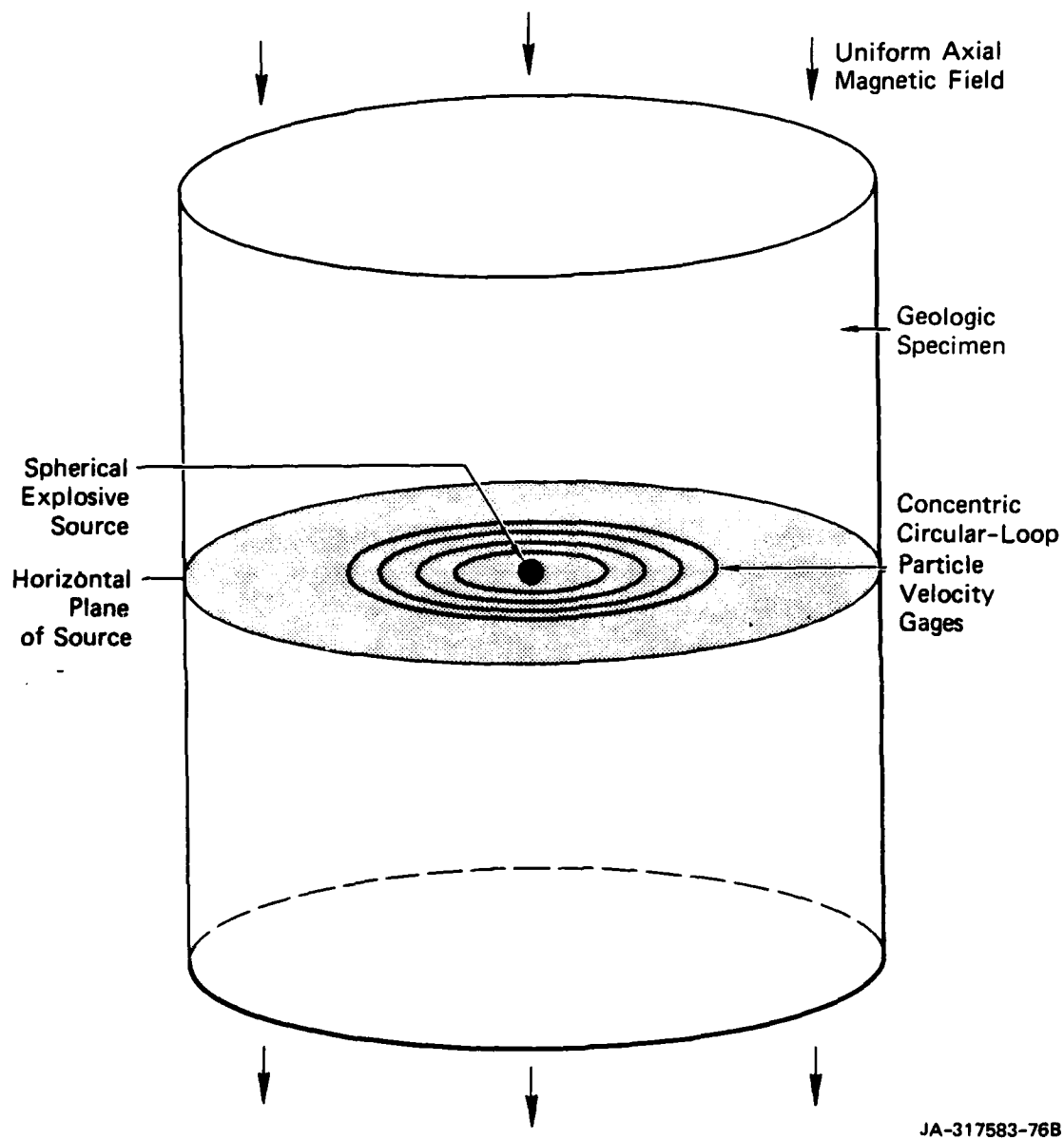
FIGURE 2.2 SCHEMATIC OF CONFIGURATION FOR PARTICLE VELOCITY EXPERIMENTS
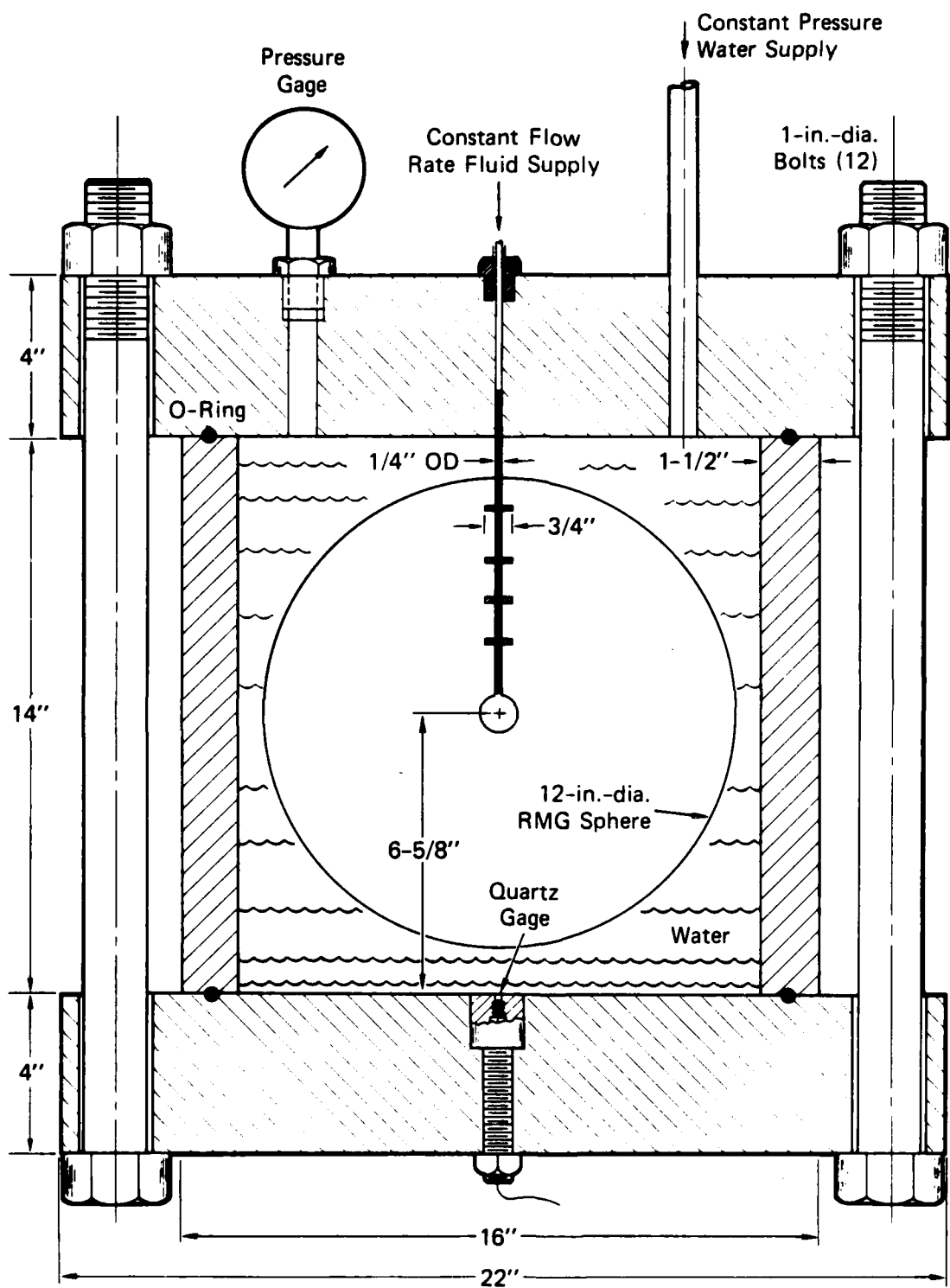
FIGURE 2.3   CONTAINMENT EXPERIMENT APPARATUS

31
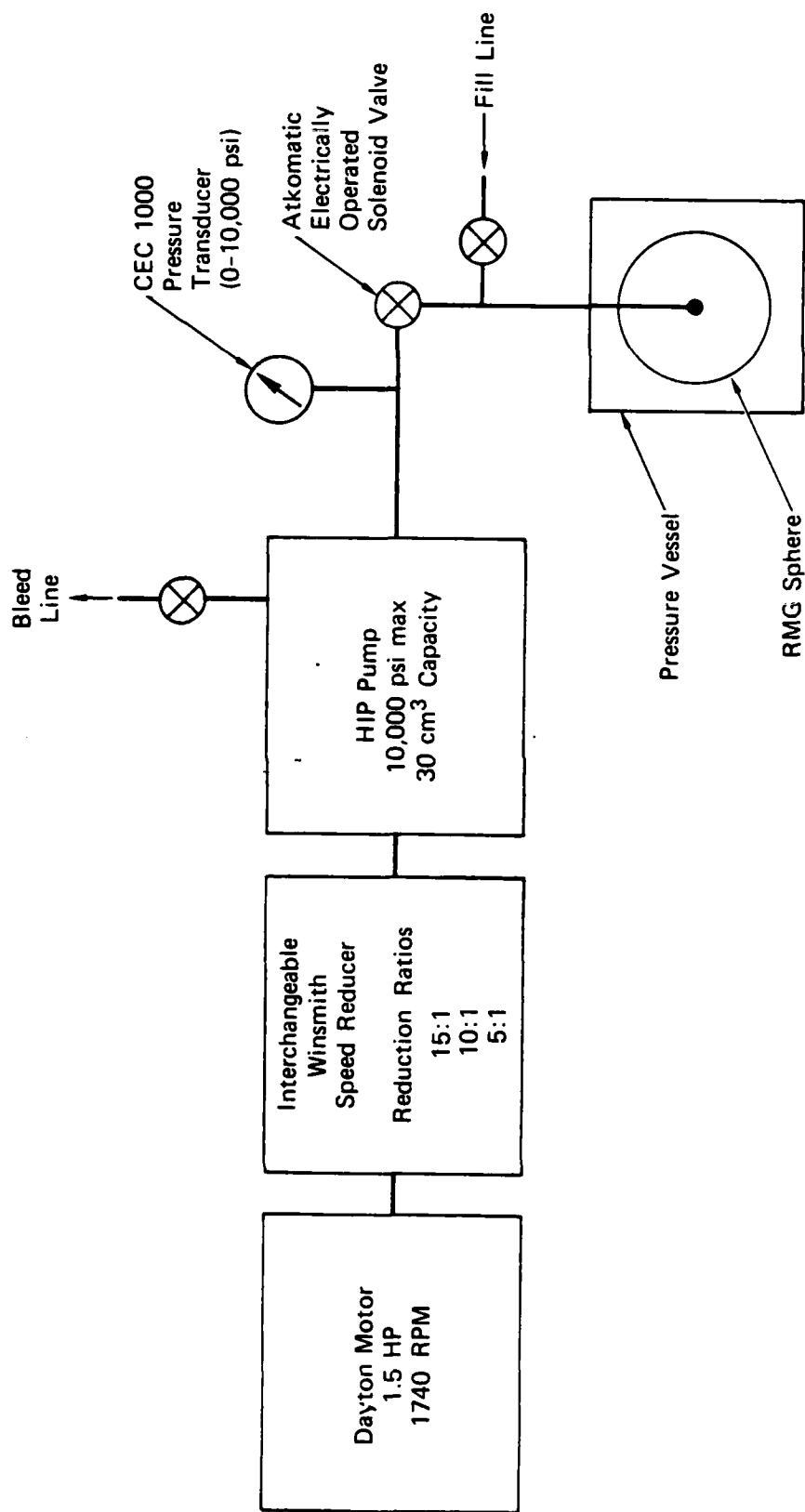
FIGURE 2.4 CONSTANT FLOW-RATE HYDROFRACTURE SYSTEM

Bleed Line

Dayton Motor
1.5 HP
1740 RPM

Interchangeable
Winsmith
Speed Reducer

Reduction Ratios

15:1
10:1
5:1

HIP Pump
10,000 psi max
30 cm³ Capacity

CEC 1000
Pressure
Transducer
(0-10,000 psi)

Atkomatic
Electrically
Operated
Solenoid Valve

Fill Line

Pressure Vessel

RMG Sphere

JA-1289-14

32

Compliance of the hydrofracture system is measured by performing a pressure test in which the cavity is replaced by a rigid vessel of equivalent volume. The pressure-volume curve for this test is then used to compensate for the effects of system compliance on the hydrofracture records.

Brief descriptions of existing experimental techniques for exploded cavity hydrofracture tests in cast and geologic materials, particle velocity measurements in cast and geologic materials, and surface fracture detection are given below.

Hydrofracture Tests in Cast Materials

The basic configuration for exploded cavity hydrofracture tests in cast materials is shown in Figure 2.5. In an alternative configuration, a cylinder replaces the sphere. The charge consists of 3/8 gram of PETN in a 10-mm-OD Lucite case with a wall thickness of 20 mil (0.508 mm). A 10-mil-thick (0.254-mm) coating of Homalite epoxy seals the charge. A constant explosive density of 1 g/cm^3 was used for reproducibility; PETN weight varied slightly from charge to charge as a result of variations in machining accuracy. Hence, 3/8 gram was the nominal weight of the explosive. Charge assembly has been described in a previous report.[8]

Cavity gas pressure was measured and hydrofracture was performed by following the sequence of steps shown in Figure 2.6. Before charge detonation, the entire system was filled with hydrofracture fluid. The steel ball sealed the end of the access tube [Figure 2.6(a)]. Charge detonation expanded the cavity past the end of the tube [Figure 2.6(b)], and the ball continued to seal the access tube until cavity gas and hydrofracture fluid pressures reached equilibrium [Figure 2.6(c)]. The fluid pressure was measured by a transducer located in the supply line. Pumping began immediately with charge detonation.

Hydrofracture Tests in Geologic Materials

The basic configuration for exploded cavity hydrofracture tests in cylinders of geologic material is shown in Figure 2.7. A sequence of

33

Steel Tube
0.25 in. OD
0.15 in. ID

Steel
Ferrule

12-in.-dia.
RMG Sphere

Steel Piston
0.14-in.-dia.
0.50-in.-long

Detonator
Wires

Explosive
Charge
Epoxied to
Steel Piston
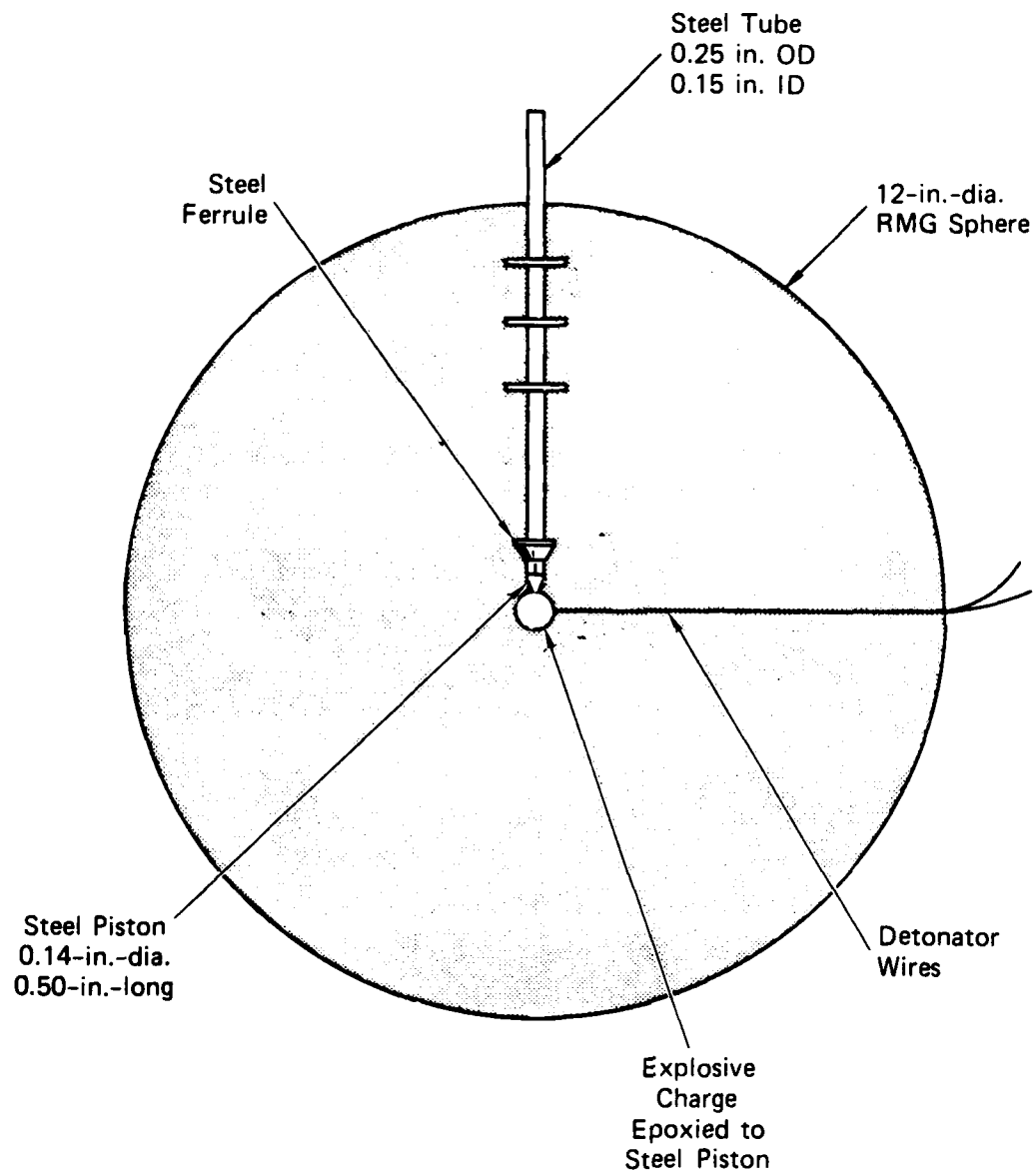
MA-5958-92A

FIGURE 2.5 OVERALL CONFIGURATION FOR UNVENTED EXPLODED CAVITY TESTS

34
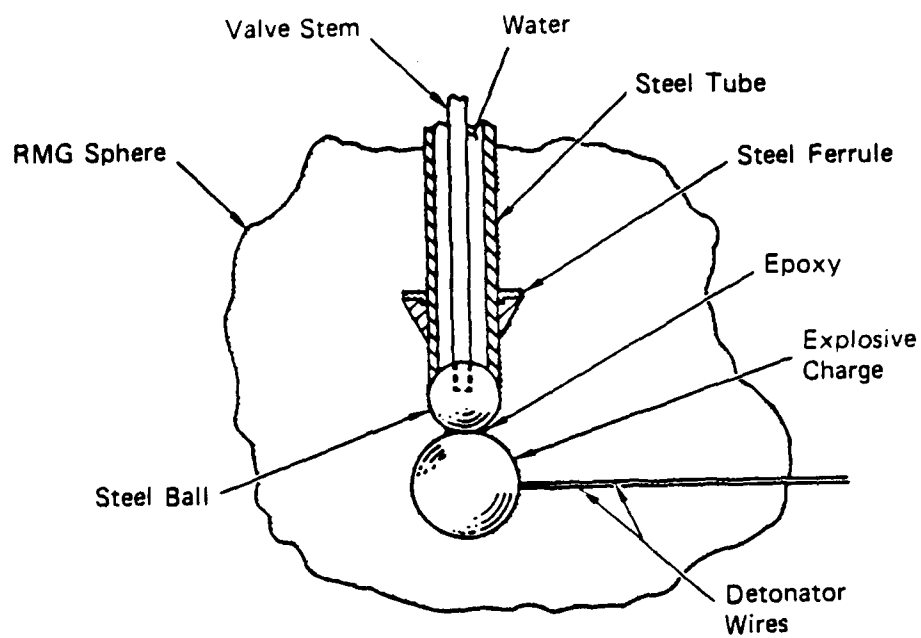
(a) Initial Configuration
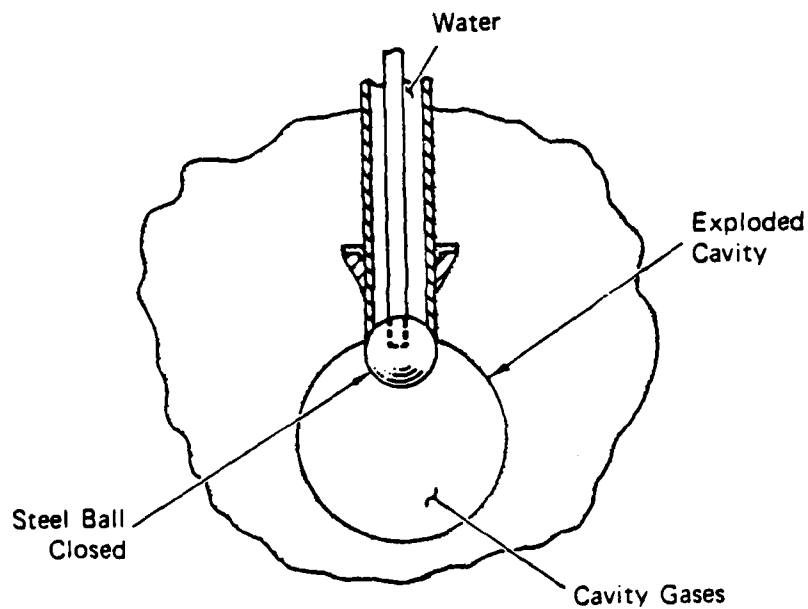
(b) Charge Exploded

MA-5958-96A

FIGURE 2.6   SEQUENCE OF OPERATIONS FOR UNVENTED EXPLODED CAVITY TESTS

35

Table 3.1 (concluded)

Series	General Description	Test Results (Figure)	Material	Test Numbers	Observations
9B	Material property	3.70–3.77	California grey/white granite	361,377	Dynamic fractures result from charge detonation in an uncut granite cylinder. Stepped and plane bonded interfaces result in similar particle velocity records.
10	Material property	3.78–3.85	GS4	357,358	No cracks are formed in a cast GS4 exploded cavity sphere. Dynamic cracking occurs along the bonded interface in a precast cylinder.
11	Material property	3.86–3.100	Alluvium (dry, 40%, 88% saturated)	379,380 381,382 383,384	Particle acceleration at the wavefront increases with initial saturation of alluvium Dilatation occurs in 88%-saturated material.
12	Material property	3.101–3.110	Alluvium (2000-psi pore pressure)	362,363 368	Air voids significantly influence particle velocity response even when initial pore pressure is 2000 psi.
13	Depth-of-burial below a free surface	3.111–3.114	RMG 2C4	347,348	Dynamic cracking of a free surface influences particle velocity response by extending pulse duration.
Stress and Strain Measurements					
14	Loop and point strain gages	3.115–3.117	RMG 2C4	372,373	Dynamic strain result from loops of constantan wire agree with results obtained from particle velocity records. Strain relaxation was measured in RMG 2C4.
15	Ytterbium stress gage	3.119–3.120	RMG 2C4	371	Peak dynamic stress results from gage agree with calculation; pulse shape is influenced by inclusion effect of an embedded gage. Residual stress decay was measured in RMG 2C4.

49

SUMMARY OF CONTAINMENT INVESTIGATIONS

Series	General Description	Test Results (Figure)	Material	Test Numbers	Observations
Exploded Cavity Hydrofracture Tests					
1	Material property	3.1	SNLA G-tunnel tuff	359,360	Hydrofracture pressures for tuff are similar to those for RMG 2C4, indicating significant residual stress in tuff.
2	Differential compaction	3.2-3.4	Weak RMG 2C4	333,334 339,344	Loss of confining stress following charge detonation in a weak RMG results in cavity fracture because of static crushing.
3	Depth-of-burial below a free surface	3.5-3.7	RMG 2C4	337,338 342,343 346	A well-defined failure threshold relates depth-of-burial and overburden.
Particle Velocity Measurements					
4	Technique validation	3.8-3.27	RMG 2C4	353,354 355,356	Effects of gage wire material, groove width, and precast cores on particle velocity records are negligible for RMG 2C4.
5	Scaling effects	3.28-3.32	RMG 2C4	335,356	Doubling linear dimensions has negligible effect on particle velocity records, indicating no strain rate effects in RMG 2C4 over the scaled range.
6	Material property	3.33-3.41	SNLA G-tunnel tuff	340,341	Particle velocity pulses for tuff are similar to those for RMG 2C4; however, dilatation is observed in tuff only.
7	Material	3.42-3.49	P-tunnel tuff	350	Peak particle velocities are higher and pulse durations longer in P-tunnel tuff than in SNLA G-tunnel tuff; dilatation occurs in both materials.
8	Material property	3.50-3.56	Grand Saline dome salt	364,365	Particle velocity records for salt show no rebound following outward motion; permanent dilatation and dynamic cracking occur in a region near the cavity.
9A	Technique improvements	3.57-3.69	California grey/white granite	349,351 352,366 367,369 370	Thickness of bonded interface influences particle velocity response in granite. Dynamic fracture was detected along the interface by embedded gages.

SECTION 3

EXPERIMENTAL RESULTS

3.1 TEST SERIES

Hydrofracture tests previously performed[5-10] on exploded and
unexploded spheres and cylinders provide a data base for comparing
pressure records and assessing the contribution of residual stress to
containment. The current hydrofracture tests were performed on exploded
cavity cylinders to assess the influence of material properties and
specific test site features on containment. Particle velocity tests
were performed to provide data for material modeling in computer codes,
to validate existing techniques, and to assess potential technique
improvements. Stress and strain tests were performed to provide addi-
tional data for material modeling and to monitor the formation and decay
of a residual field surrounding an exploded cavity. The specific
parameters studied during the investigation include material properties,
scaling effects, differential compaction, and depth-of-burial. This
section provides a complete description of the results. Conclusions
based on these findings are in Section 1.

The types of experiments performed and the principal observations
are summarized in Table 3.1. Additional observations are summarized in
Table 3.2. Exploded cavity hydrofracture tests are grouped in Series 1
through 3, particle velocity tests are grouped in Series 4 through 13,
and stress and strain tests are grouped in Series 14 and 15. In
general, at least two tests were performed in each series to establish a
measure of reproducibility. The specific areas of investigation were as
follows:

- Material Property Hydrofracture (Series 1). Results of
  previous tests on rock-matching grout RMG 2C4, a material
  that approximates the documented properties of NTS tuff,
  were chosen as the standard of comparison. Effects of
  material property variations on containment were studied

47

surrounding grout. The fractional change in resistance is equal to the product of the fractional strain and a gage factor. In a separate calibration test, stretching of a constantan wire under uniaxial stress yielded a gage factor of 2.0.

In the second configuration, a commercially available constantan grid[*] was encapsulated in a small sphere of RTV and cast in RMG 2C4. Gage packages were oriented in radial and circumferential directions at a given distance from the charge.

Stress Measurements in Cast Materials

The gage package developed for measuring stress in exploded cavity grout spheres is a commercially available piezoresistive ytterbium grid[**] encapsulated in RTV. The RTV was molded into disks and spheres so that the inclusion effects associated with simple geometries could be studied.

---

[*]BLH Electronics, Waltham, MA. Type FAE-035-12-56EL-1.

[**]Dynasen, Inc., Goleta, CA. Type Yb8-50-Ek.

Stainless Steel Access Tube
(0.250 in. OD, 0.180 in. ID)

Cylindrical Core
of Geologic Material

1 grain/ft MDF
Epoxied in Access
Tube

GS4
Stemming
Column

Circular
Particle Velocity
Grooves

Explosive Charge
Epoxied to Access
Tube

Bonded
Interface

Plug and Matching Hole
(0.900 in. dia., 0.500 in. long)
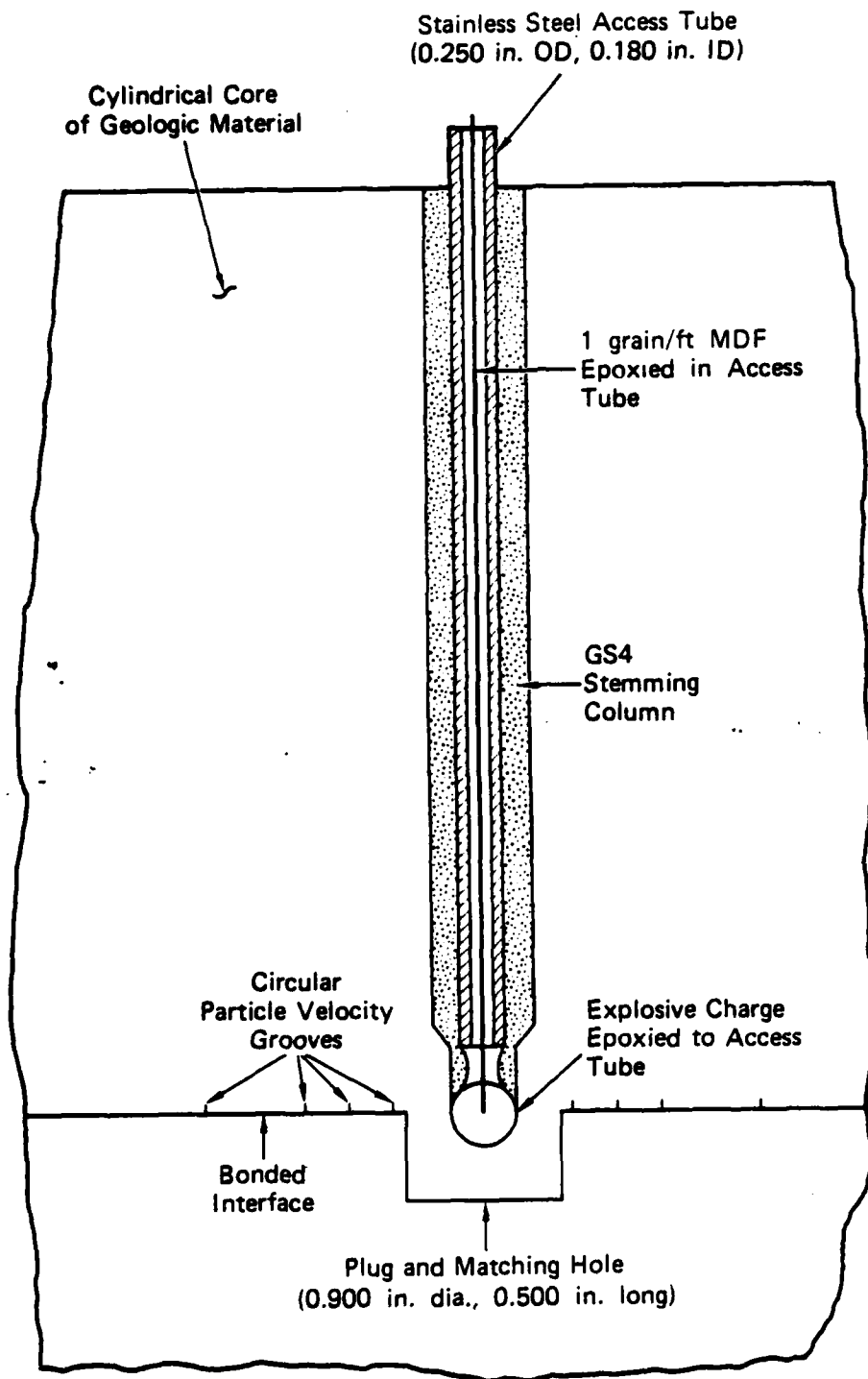
JA-5372-121

FIGURE 2.12   STEPPED INTERFACE CONFIGURATION FOR PARTICLE VELOCITY
TESTS IN CYLINDRICAL CORE OF GEOLOGIC MATERIAL

Particle Velocity Gage Installation

An alternative configuration for installing particle velocity gages in cylindrical cores of hard geologic material (see Section 2.2) is shown in Figure 2.12. The new technique required the precision grinding of an axial plug in the upper half of the cylinder and a matching hole in the lower half. A tapered axial hole having a hemispherical bottom that matched the charge was drilled in the upper half. Narrow circular grooves 9 mils (0.229 mm) wide were cut concentrically about the hole in the upper half. Particle velocity gages were epoxied in the grooves, and the sections of the cylinder were epoxied together in the region outside the plug. The charge and access tube were positioned in the axial hole and grouted in place with granite simulant GS4.

Dynamic Fracture Detection in Geologic Materials

The basic configuration for particle velocity tests in cylindrical cores of geologic material employs a bonded interface extending through the charge (Figure 2.9). A technique for detecting fractures along this interface was developed. After assembly of a standard particle velocity model, holes are drilled the length of the cylinder at desired distances from the axis. A commercially available fracture gage consisting of a series of brittle wires[*] is placed in each hole and positioned to bridge the bonded interface. The holes are then filled with epoxy, except for a thin region at the interface. Fracture along the interface changes the gage resistance, which is monitored electronically.

Strain Measurements in Cast Materials

Two basic configurations were developed to measure strain in exploded cavity grout spheres. In one configuration, concentric loops of constantan wire were cast symmetrically about the charge. The wires change in length and resistance as they follow the motion of the

---

[*]Micro-Measurements, Romulus, MI. Type TK-09-CPB02-005.

44

Depth-of-Burial

Nitrogen

Water
or Oil

Charge
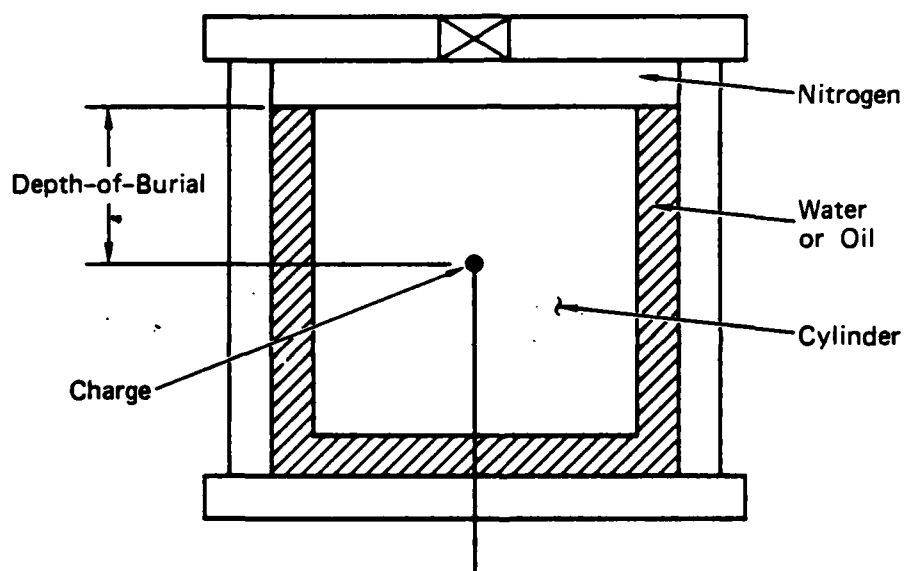
Cylinder

JA-5372-98A

FIGURE 2.11   CONFIGURATION FOR FAILURE CRITERION TESTS

43

Solenoid Valve Used
for Slow Release
of Confining Pressure

Hydraulic Line to
Confining Fluid

Grout Cylinder
(12 in. dia.,
12 in. long)

Explosively Ruptured
Diaphragm for Rapid
Release of Confining
Pressure

Evacuated Pipe

Explosive Charge

Hydraulic Line to
Flatjack Fluid

4"

14"

4"

13"

16"

22"
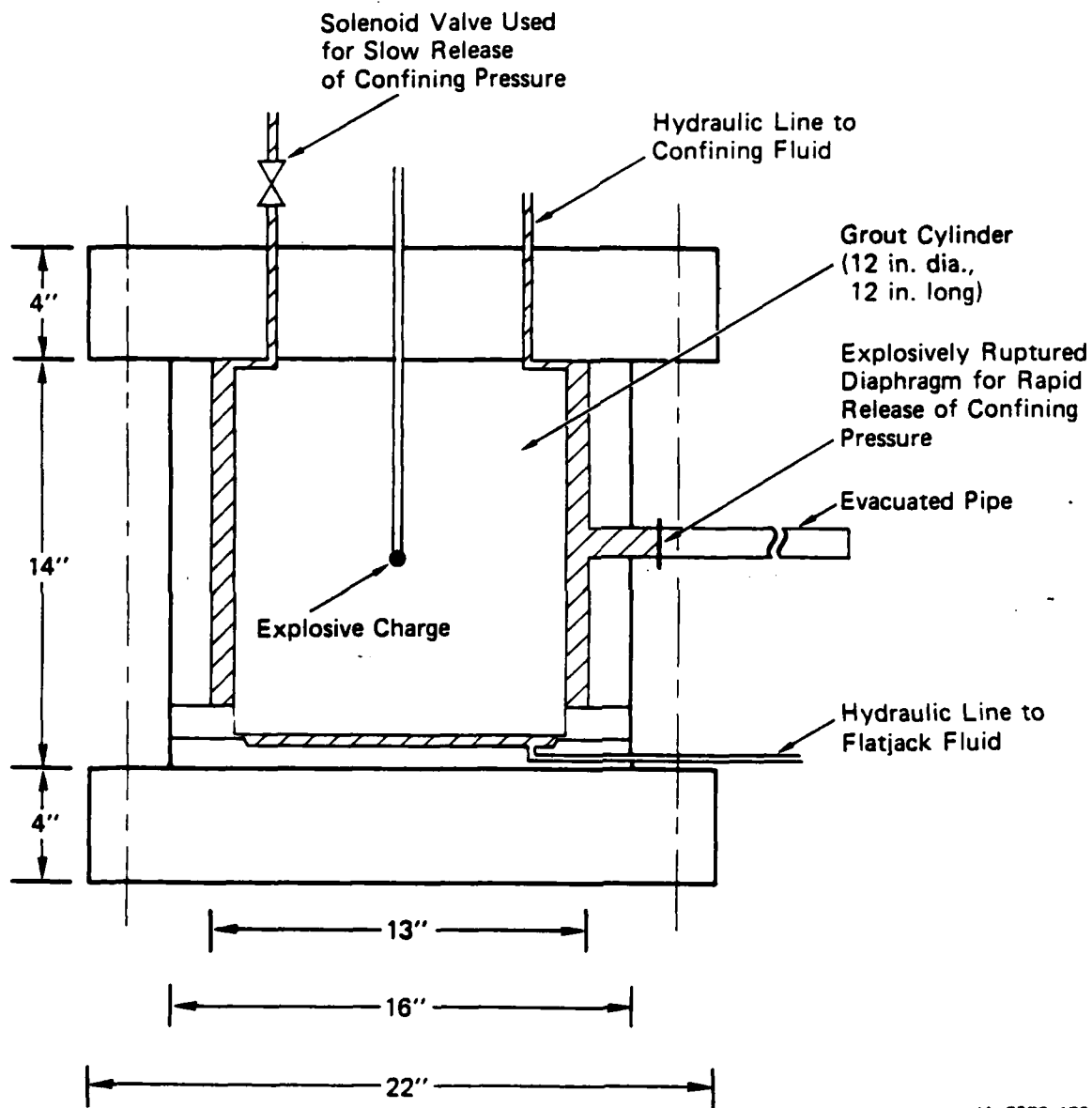
JA-5372-173

FIGURE 2.10 CONFIGURATION FOR DIFFERENTIAL COMPACTION TESTS

42

Surface Fracture Detection

Surface fracture of selected grout spheres and cylinders was detected by means of a 1/16-inch-wide (1.59-mm) stripe of electrically conductive silver-based paint. Selected regions of the surface were covered so that fracture could be detected with a minimum number of gages.

2.3 EXPERIMENTAL TECHNIQUE DEVELOPMENTS

Differential Compaction Simulation

Differential compaction in material near an underground explosion relieves the horizontal component of tectonic stress. This feature was simulated in the laboratory by relieving the confining hydrostatic pressure on a grout cylinder while maintaining a constant axial load. The apparatus is shown schematically in Figure 2.10. Confining pressure was applied hydraulically in the containment vessel. A hydraulic flat-jack located at the bottom of the vessel provided the axial load. For slow release of confining pressure, the water was vented through a valve in the top of the vessel. For rapid release of confining pressure, the water was vented through an explosively ruptured diaphragm located in the wall of the containment vessel.

Depth-of-Burial Simulation

The depth-of-burial of a nuclear device is an important parameter affecting both the safety and economy of underground tests. This feature was simulated in the laboratory by embedding a charge at various depths along the axis of a grout cylinder and by providing a gas interface at the top of the cylinder. The configuration for the depth-of-burial hydrofracture and particle velocity tests is shown in Figure 2.11. The hydrostatic confining pressure on the cylinder was also varied to simulate changes in overburden stress with depth.

41
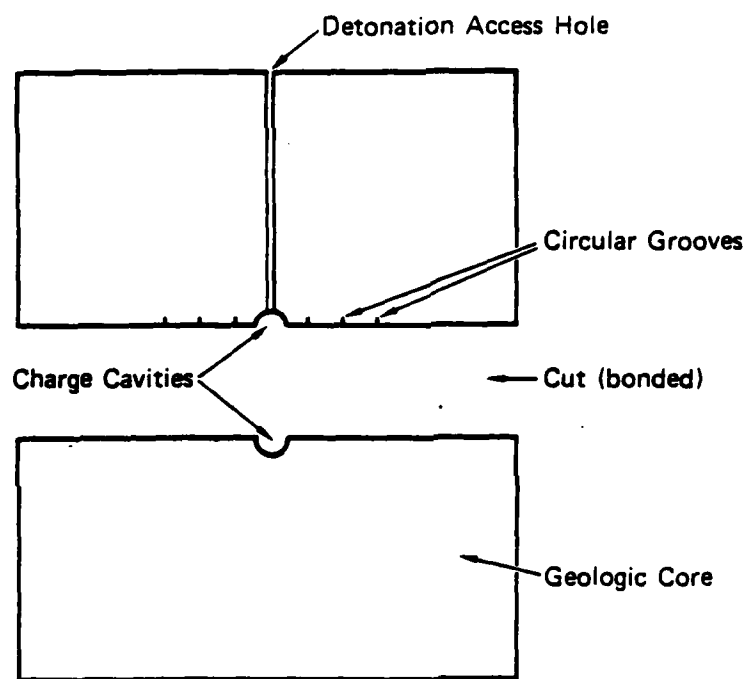
FIGURE 2.9   INSTALLATION OF PARTICLE VELOCITY LOOPS
IN GEOLOGIC CORES
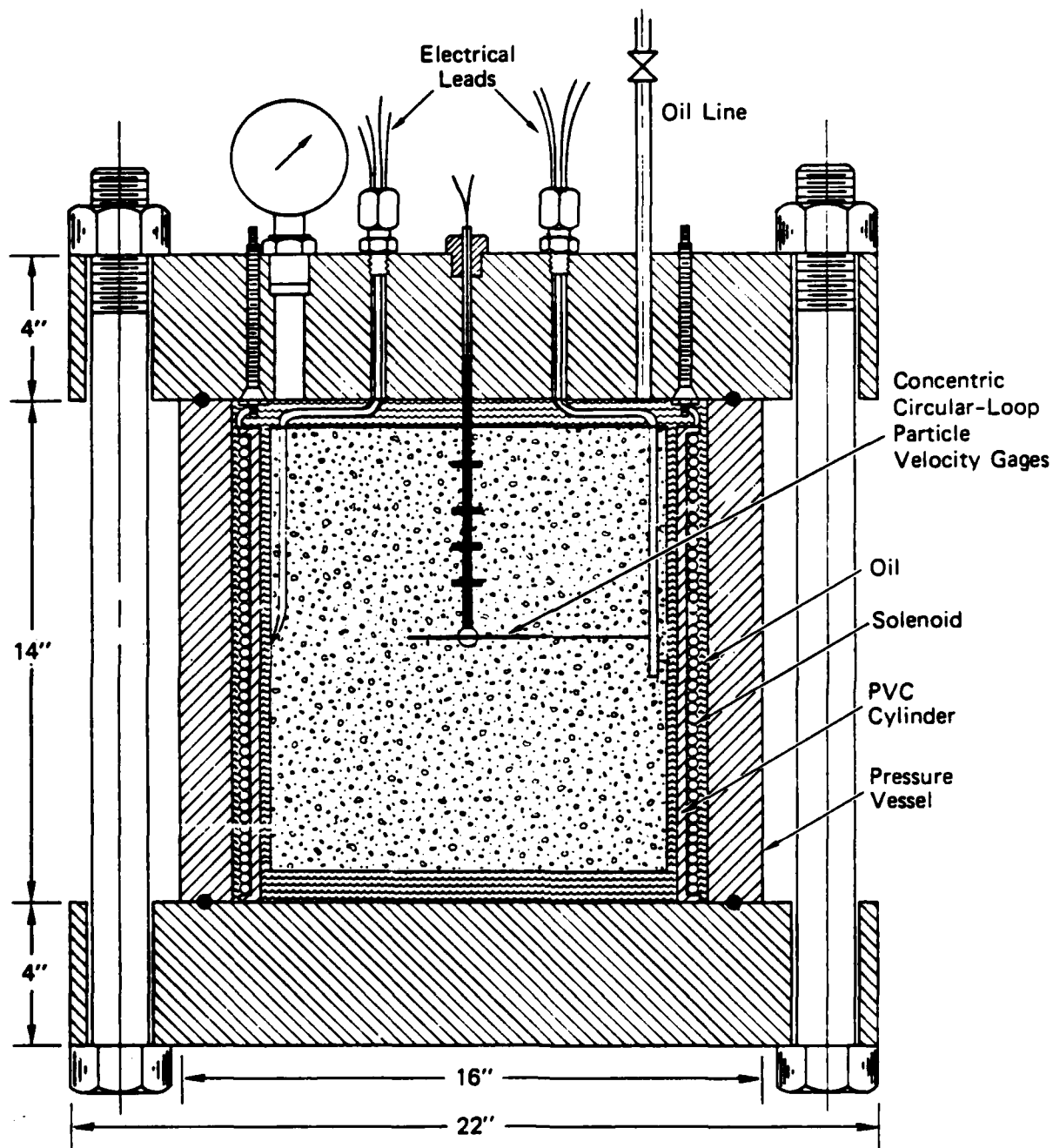
FIGURE 2.8 CONFIGURATION FOR PARTICLE VELOCITY EXPERIMENTS

(Vertical Cross Section)

drilling operations produced the tapered axial hole extending to the center of the cylinder. The bottom of the hole was formed into a hemispherical surface having a diameter equal to that of the charge to ensure proper coupling. The access tube with attached steel ball and explosive charge was then grouted into the hole.

Particle Velocity Measurements in Cast Materials

Particle velocity profiles for cast materials were obtained in 11-inch-diameter (27.94-cm) spheres (Figure 2.5) or 11-inch-diameter (27.94-cm) and 11-inch-long (27.94-cm) cylinders (Figure 2.8). Concentric circular loops of wire were cast symmetrically about the charge, and a magnetic field was generated normal to the plane of the loops by passing current through a coil that surrounds the sphere or cylinder. Charge detonation produces radial motion of the loops that cuts the magnetic flux lines. In accordance with Faraday's law, the voltage induced in each conducting loop is proportional to the particle velocity. A history of particle velocity at several radii was thus obtained for validation of material modeling in codes.

Particle Velocity Measurements in Geologic Materials

Particle velocity profiles for geologic materials were obtained in cylindrical cores from the test site. The cylinder was first sectioned along the midheight plane, and an axial hole was drilled in the upper half (Figure 2.9). Central hemispherical cavities were machined in matching faces of each section. Circular grooves were scribed concentrically about the cavity in the upper section, and particle velocity gage wire was epoxied in the grooves. The charge and access tube were epoxied in the axial hole, and the two halves of the cylinder were then epoxied together.
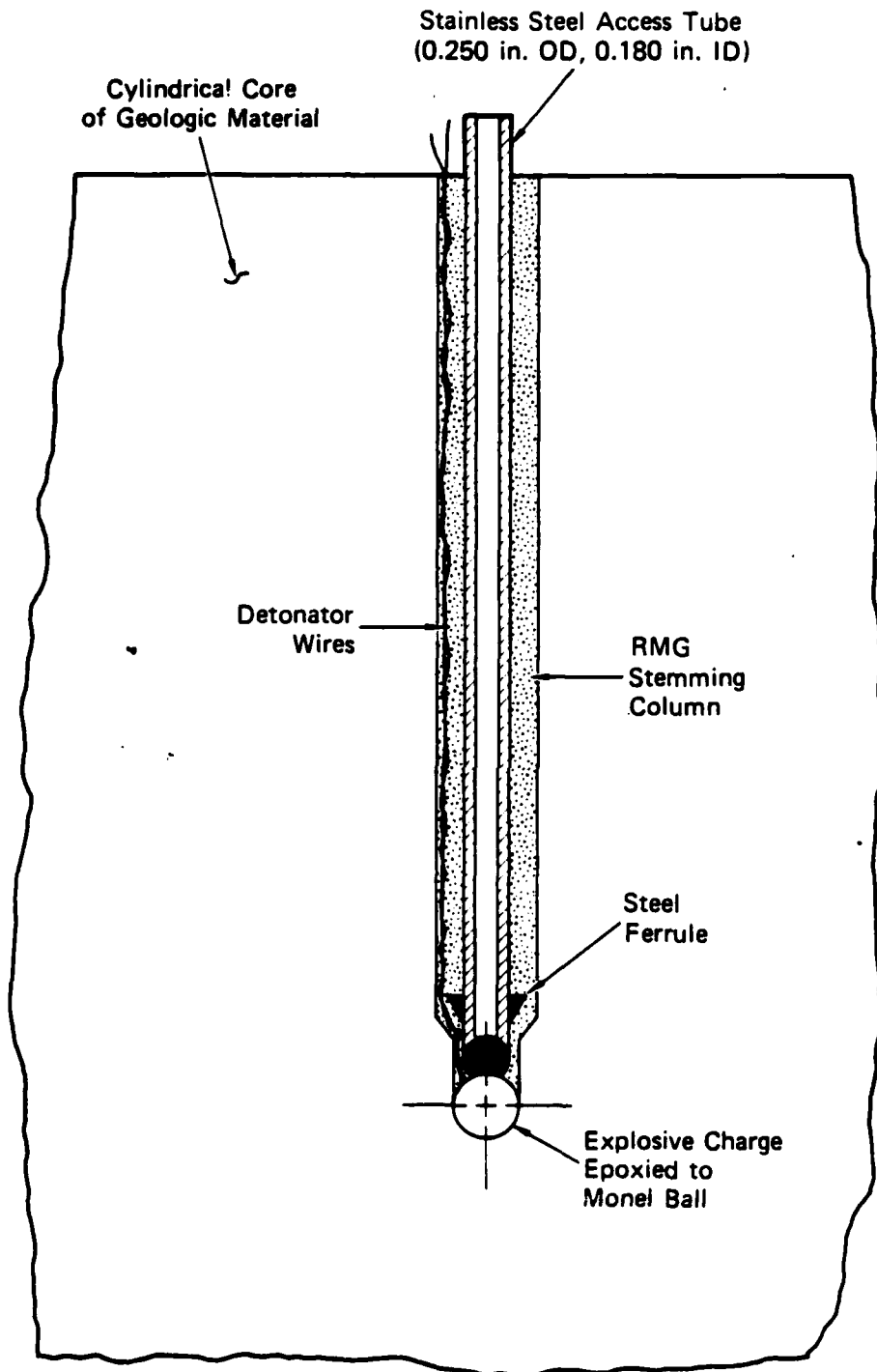
FIGURE 2.7 CONFIGURATION FOR EXPLODED CAVITY HYDROFRACTURE TESTS IN CYLINDRICAL CORE OF GEOLOGIC MATERIAL

37
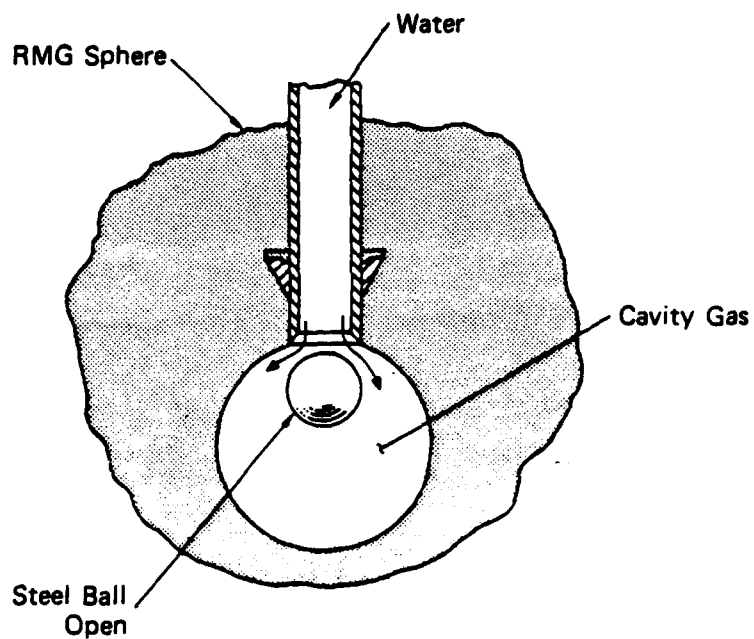
(c) Start of hydrofracture process

MA-5958-97A

FIGURE 2.6 SEQUENCE OF OPERATIONS FOR UNVENTED EXPLODED CAVITY
TESTS (Concluded)

Table 3.2

POSTTEST OBSERVATIONS

Material	Exploded Cavity Diameter[a] (cm)	Dynamic Fractures Developed During Test
Rock-matching grout (RMG 2C4)	2.05	None
Weak (1-day-old) RMG 2C4	2.86	None
Low-density grout (LD 2C4)[b]	2.38	None
NTS tuff (SNLA G-tunnel)	1.75	None (Tests 340 and 360); along bonded interface, extending 4 cm from cavity (Test 341); along stemming column (Test 359)
NTS tuff (P-tunnel)	2.14	None
NTS tuff (Strong G-tunnel)[b]	1.27	Along bonded interface, extending 4-5 cm from cavity (Test 295)
NTS tuff (N-tunnel)[b]	1.27	None (Test 327)
Salt (Grand Saline)	1.59	Three or four plane surfaces, extending 3 cm from cavity (Tests 364 and 365)
Granite (California grey/white)	1.17	Typically along bonded interface, extending 3-4 cm from cavity (7 tests); also through unsectioned material, extending 5 cm from cavity (Tests 375 and 376)
Granite simulant (GS4)	1.27	None in cast sphere (Test 357); along bonded interface in precast cylinder, extending 5 cm from cavity (Test 358)
Reconstituted alluvium (dry)	3.02	None
Reconstituted alluvium (40% saturated)	2.54	None
Reconstituted alluvium (88% saturated)	3.02	None

[a]Charge diameter = 1.05 cm.

[b]See reference 10.

by testing a G-tunnel tuff taken from near the working point of an SNLA high explosive test.

- Differential Compaction (Series 2). The effects of differential compaction at the test site were simulated in the laboratory by relieving the confining radial pressure on a weak grout cylinder following charge detonation while maintaining the axial load. The rate of pressure release was varied to study the effects on containment of sudden and long-term differential compaction.

- Depth-of-Burial Hydrofracture (Series 3) and Particle Velocity (Series 13). The effects of depth-of-burial on containment were assessed by performing hydrofracture tests on exploded cavity RMG 2C4 cylinders subjected to a range of external pressures and having the charge embedded at various depths. A free surface was simulated by providing a gas interface at the top of the cylinder. In a separate series of tests with the same configuration, particle velocity components parallel to the free surface were measured at various depths.

- Particle Velocity Technique Validation and Improvement (Series 4 and 9A). The effects of gage installation on particle velocity records for geologic cores were examined by performing a series of tests in cylinders of RMG 2C4, granite, and GS4. The parameters were gage wire material (copper versus aluminum), gages cast in place versus gages embedded in precast material, groove width (wide versus narrow), and shape of the bonded interface (plane versus stepped).

- Scaling Effects (Series 5). Strain rate effects are an important parameter in developing an equation of state for a material. Rate effects in RMG 2C4 were assessed by doubling the standard charge and gage diameters in a series of particle velocity tests. The weight of explosive was correspondingly increased by a factor of 8.

- Material Property Particle Velocity Measurements (Series 6, 7, 8, 9B, 10, 11, and 12). The particle velocity profile associated with charge detonation in a material provides a measure of the residual stress field intensity and represents a valuable source of data for verification of material modeling in codes. Particle velocity profiles were measured in several geologic materials and simulants. The materials tested were SNLA G-tunnel tuff, P-tunnel tuff, Grand Saline (Texas) dome salt, California grey/white granite, granite simulant GS4, and alluvium (with various saturations and pore pressures) reconstituted from NTS desert fines.

51

- Strain Measurements (Series 14). Direct measurement of
  strain in an exploded cavity test provides a means of
  verifying particle velocity records and allows for an
  assessment of residual strain relaxation. Circumferential
  strain was measured in RMG 2C4 by means of embedded
  circular loops of constantan wire. Radial and circum-
  ferential components of strain were independently measured
  by strain gage grids encapsulated in RTV.

- Stress Measurements (Series 15). Measurement of stress in
  an exploded cavity test provides a means of quantifying
  residual stress field strength and stress relaxation.
  Dynamic radial stress and subsequent stress relaxation
  were measured near an exploded cavity in RMG 2C4 by means
  of embedded piezoresistive ytterbium grids encapsulated in
  RTV.

3.2 EXPLODED CAVITY HYDROFRACTURE TESTS

Details of the exploded cavity hydrofracture experiments are shown
in Figures 2.1, 2.3, 2.4, 2.5, and 2.6. The modified configuration
shown in Figure 2.11 was used for depth-of-burial failure criterion
tests. The standard external pressure applied to the test specimens was
1000 psi (6.895 MPa). Water dyed with Rhodamine B was the hydrofracture
fluid.

Series 1: Material Property (SNLA G-Tunnel Tuff)

Cylindrical cores of G-tunnel tuff taken from near the working
point of a proposed SNLA 1-ton high explosives test were received from
NTS. The samples, which were 9-1/2 inches (24.13 cm) in diameter, were
cut to a length of 11 inches (27.94 cm) so that hydrofracture tests
could be performed. The configuration developed for exploded cavity
hydrofracture tests in cores of geologic material is described in
Section 2.2 (see Figure 2.7).

Figure 3.1 shows the exploded cavity hydrofracture pressures for
SNLA G-tunnel tuff (tests 359 and 360). For comparison, results of
previous tests (244, 245, 248, and 254) on 12-inch-diameter (30.48-cm)
RMG 2C4 spheres are included. The hydrofracture records for tuff in
test 360 and for RMG are similar, suggesting that comparable residual
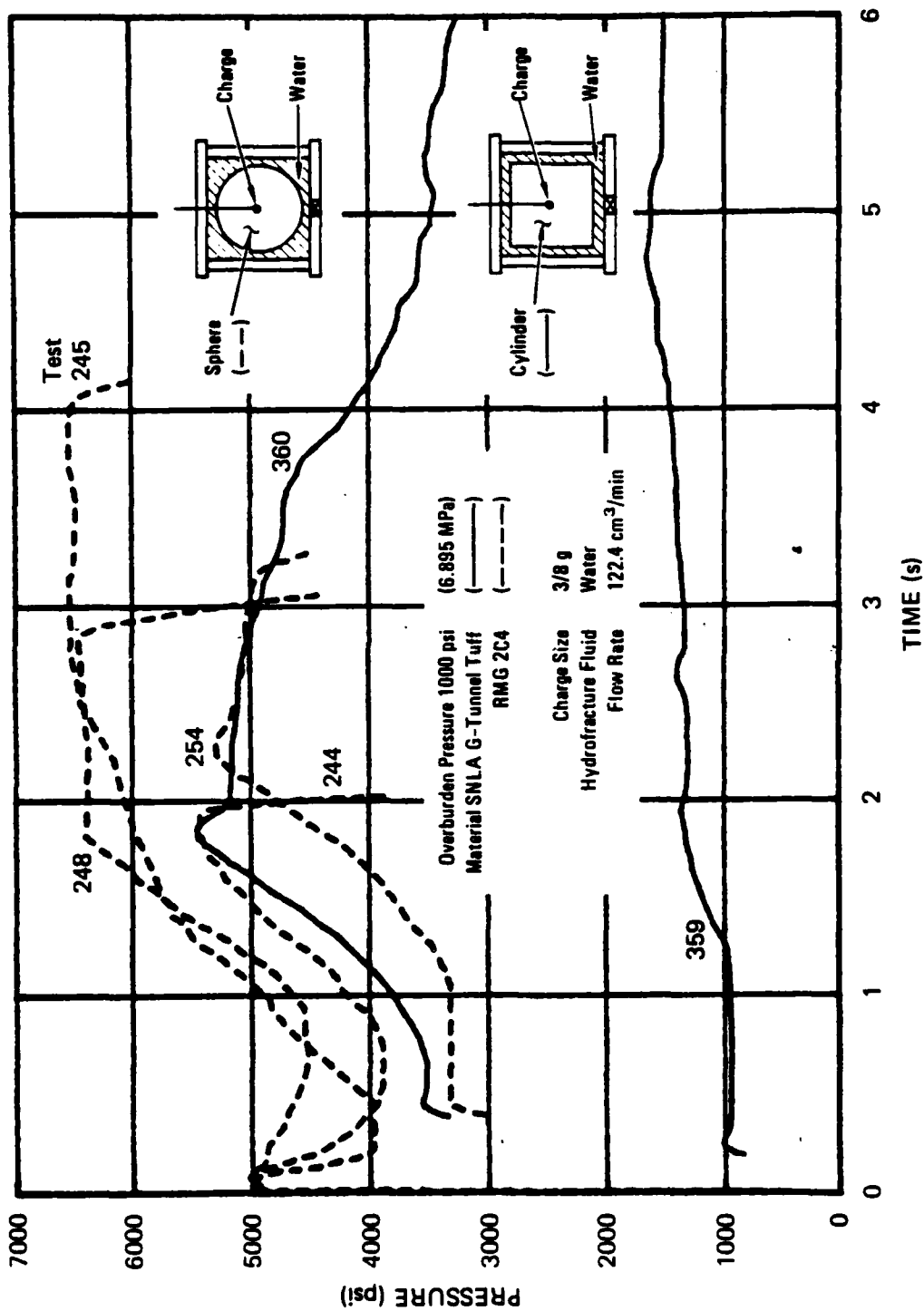
52

FIGURE 3.1 HYDROFRACTURE PRESSURES FOR UNVENTED EXPLODED CAVITY TESTS IN SNLA G-TUNNEL TUFF AND RMG 2C4

JA–5372–42

53

stress fields are developed in the two materials. Similar particle velocity response for the tuff and RMG (see Series 6) is additional evidence that comparable residual stress fields are formed. Hydrofracture of the tuff cylinder in test 360 resulted in a nearly horizontal fracture surface through the cavity. Hence, the grout stemming column had no apparent influence on containment.

The low hydrofracture pressures for tuff in test 359 (Figure 3.1) indicate the existence of a vent path that allowed gases and hydrofracture fluid to escape from the exploded cavity. In fact, posttest examination of the cylinder revealed two vertical fracture planes intersecting the grouted axial hole. Although the grout stemming column was not fractured, weak bonding between the grout and tuff permitted the venting. The low hydrofracture pressure obtained in this test caused by fracture from a weak grout/tuff interface implies that care is necessary in the design and construction of stemming of line-of-sight tunnels.

Pressure records in the overburden fluid obtained from quartz gage measurements are shown in appendix Figure B.1 for tuff and RMG. Similarity of the pulses for a given material indicates charge reproducibility. Higher pressures for the tuff are attributed in part to differences in the size and geometry of the tuff and RMG models.

Series 2: Differential Compaction in Weak RMG 2C4

Differential compaction represents a test site asymmetry that allows for a local relief of the horizontal tectonic stress component near an exploded cavity. This feature was simulated by relieving the radial component of overburden pressure on an exploded cavity cylinder after charge detonation. Because weak materials (e.g., alluvium) are potentially most vulnerable to the effects of differential compaction, the material tested was a weak (approximately 1-day-old) 2C4 grout. Unconfined crush strength determined from two tests was 600 psi (4.137 MPa). Splitting tensile strength determined from two tests was 60 psi (0.414 MPa).

A preliminary standard hydrofracture test (339) at constant 1000 psi (6.895 MPa) overburden pressure was conducted on a weak 2C4 grout cylinder to assess the basic containment capability of the material. Figure 3.2 shows the pressure record for test 339. For comparison, hydrofracture records for tests on standard 2C4 grout and low-density (LD) 2C4 grout are also shown. The LD 2C4 has an air void content (13%) similar to that of alluvium. Hydrofracture pressures for weak 2C4 grout are less than those of the other materials, but cavity gases appear to be contained after charge detonation.

The first differential compaction test (333) was performed with axial and confining pressures initially at 1000 psi (6.895 MPa). Figure 2.10 shows the test configuration. After charge detonation, the axial pressure was maintained while the confining pressure was relieved slowly as shown in Figure 3.3. No hydrofracture fluid was pumped into the cavity. When the confining pressure dropped to approximately 600 psi (4.137 MPa), a loss of cavity pressure was observed. For reference, test 344 (Figure 3.3) was performed to measure the pressure of cooling cavity gases in a weak 2C4 grout exploded cavity cylinder subjected to 1000 psi (6.895 MPa) overburden.

The second differential compaction test (334) was performed with axial and confining pressures initially at 500 psi (3.447 MPa). After charge detonation, the axial pressure was maintained while the confining pressure was relieved slowly, as shown in Figure 3.4. No hydrofracture fluid was pumped into the cavity. When the confining pressure dropped to approximately 100 psi (0.689 MPa), a loss of cavity pressure was observed.

A final differential compaction test (345) was performed with axial and confining pressures initially at 1000 psi (6.895 MPa). After charge detonation, the axial pressure was maintained while the confining pressure was relieved rapidly in approximately 20 ms. Measurements showed that loss of cavity pressure coincided with the loss of confining pressure.
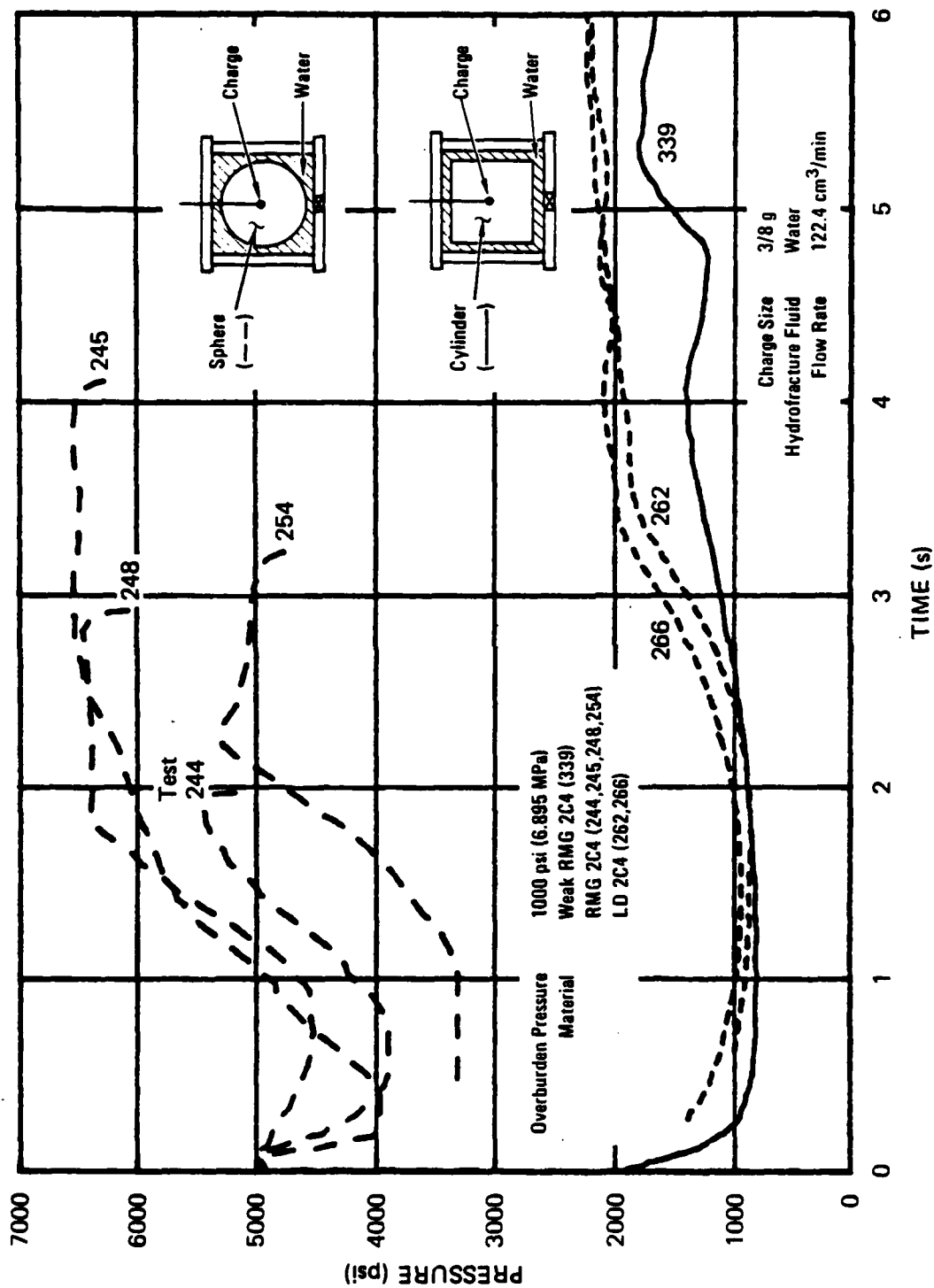
FIGURE 3.2   HYDROFRACTURE PRESSURES FOR UNVENTED EXPLODED CAVITY TESTS — MATERIAL PROPERTY
EFFECT (WEAK RMG 2C4 VERSUS RMG 2C4 AND LD 2C4)
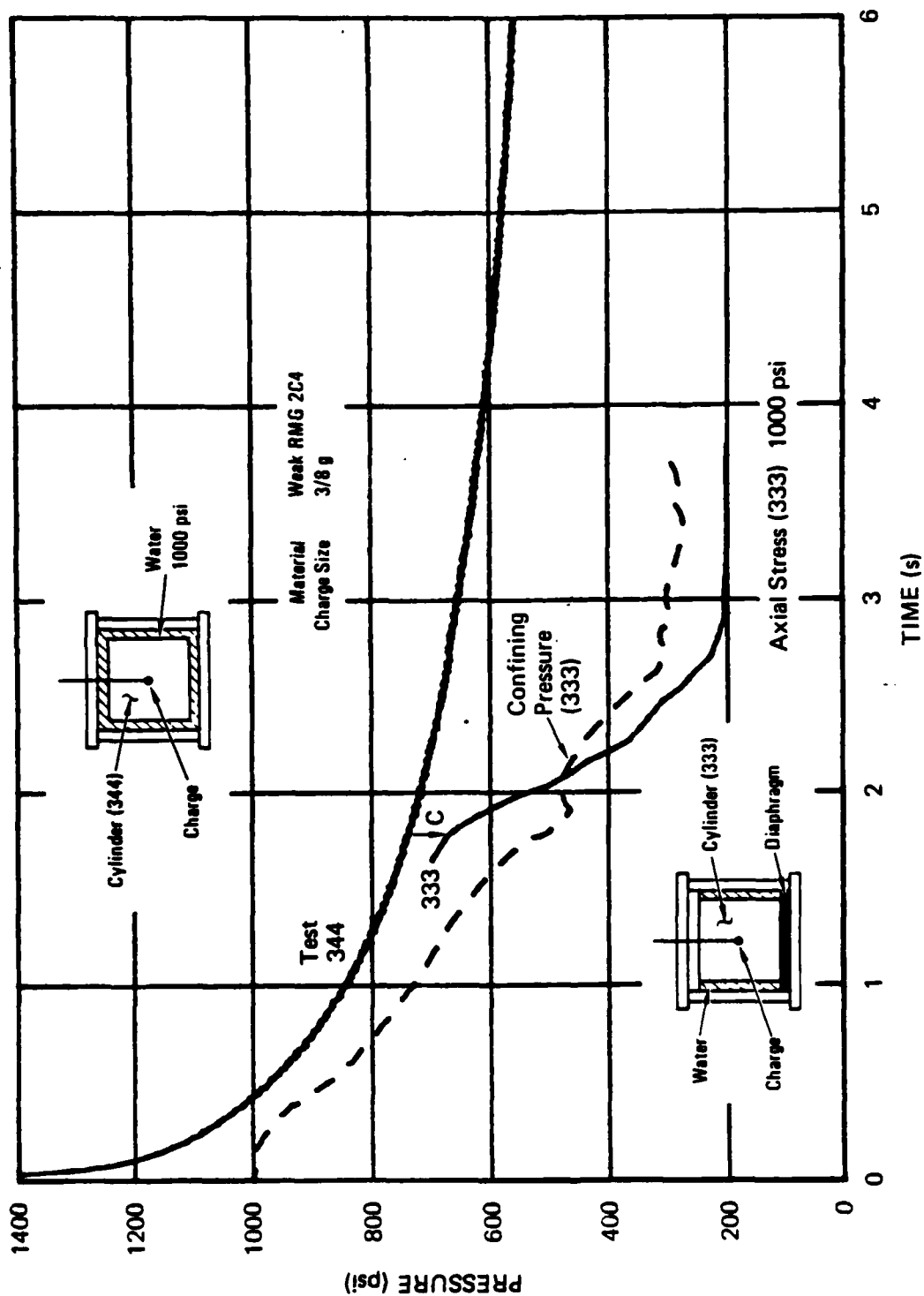
FIGURE 3.3 HYDROFRACTURE PRESSURES FOR UNVENTED EXPLODED CAVITY TEST
IN WEAK RMG 2C4 – DIFFERENTIAL COMPACTION EFFECT (TEST 333)

57
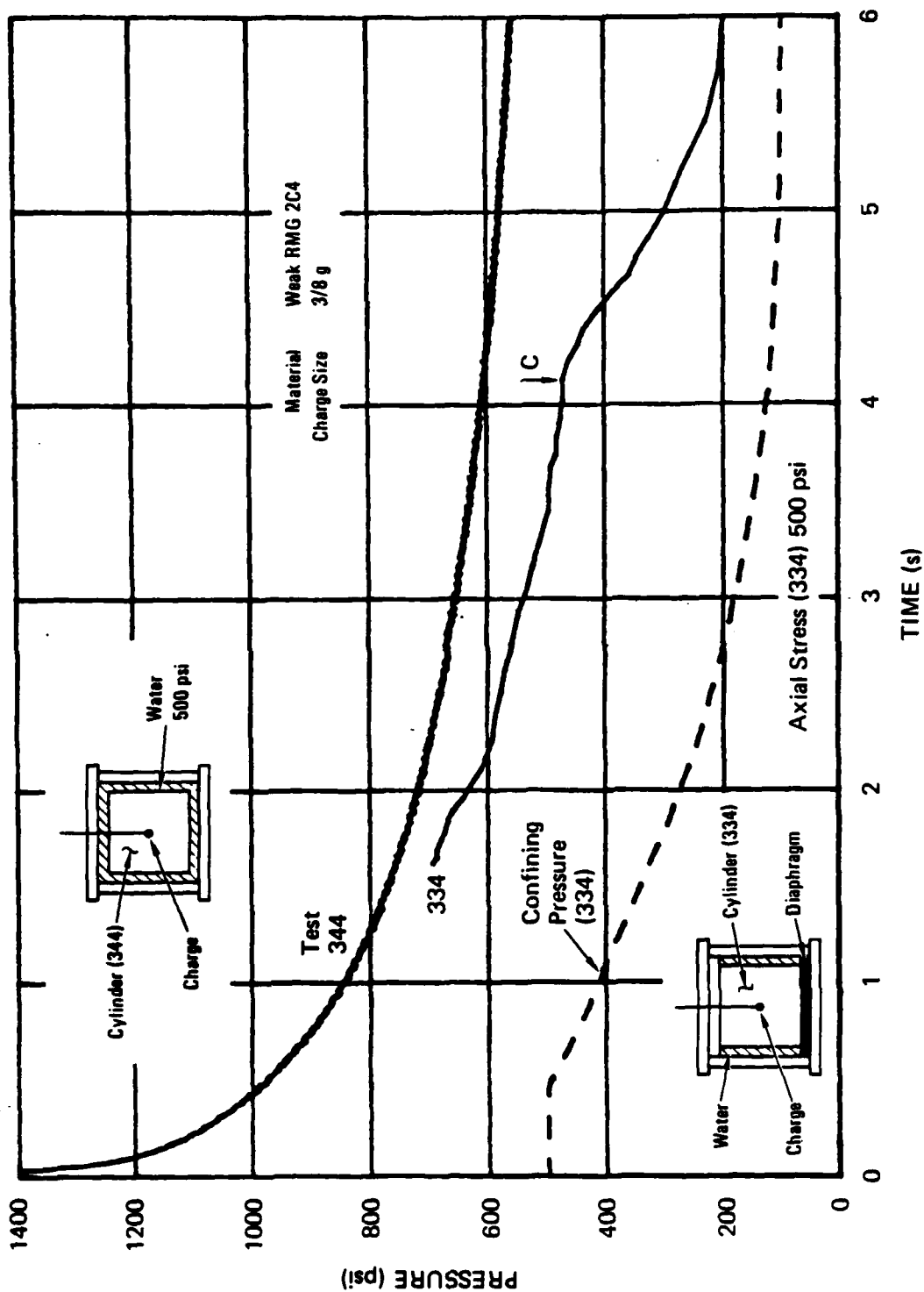
FIGURE 3.4   HYDROFRACTURE PRESSURES FOR UNVENTED EXPLODED CAVITY TEST
IN WEAK RMG 2C4 – DIFFERENTIAL COMPACTION EFFECT (TEST 334)

58

In all three differential compaction tests, the cylinders fractured through the cavity along vertical planes of least principal stress. The differences between the axial and confining stresses at fracture for tests 333 and 334 were about 450 and 400 psi (3.103 and 2.758 MPa), respectively. The unconfined strength of the 1-day-old 2C4 grout was 600 psi (4.137 MPa). Hence, in test 333 cavity pressure caused failure before the confining pressure dropped enough to cause overall failure of the cylinder. In test 334, complete removal of the confining pressure with no cavity pressure would not have caused failure of the cylinder so the cavity pressure combined with reduced confining pressure caused failure.

Series 3: Depth-of-Burial Failure Criterion Below an Air/RMG 2C4 Interface

Depth-of-burial represents an important containment parameter affecting both the safety and economy of underground tests. A depth-of-burial study was conducted in exploded cavity RMG 2C4 cylinders by providing a free surface at one end in the form of a gas interface, varying the distance between the charge and the free surface, and varying the overburden pressure. Hydrofracture tests were performed to determine the threshold of failure. Fracture gages were painted on the free surface to detect dynamic fracture.

In tests 342 and 343, the depth-of-burial was 2 inches (5.08 cm). The overburden pressure was 1000 psi (6.895 MPa) in test 342 and 1500 psi (10.342 MPa) in test 343. The configuration and hydrofracture pressure records for these tests are shown in Figure 3.5. Also shown in the figure for comparison are the configuration and hydrofracture records for standard exploded cavity tests on RMG 2C4 spheres. The shallow depth-of-burial in tests 342 and 343 resulted in dynamic cracking from the cavity to the free surface and venting of cavity gases.

In tests 337, 338, and 346, the depth of burial was 4 inches (10.16 cm). In test 337, the overburden pressure was 1000 psi (6.895 MPa), whereas in tests 338 and 346, the overburden pressure was 500 psi (3.447
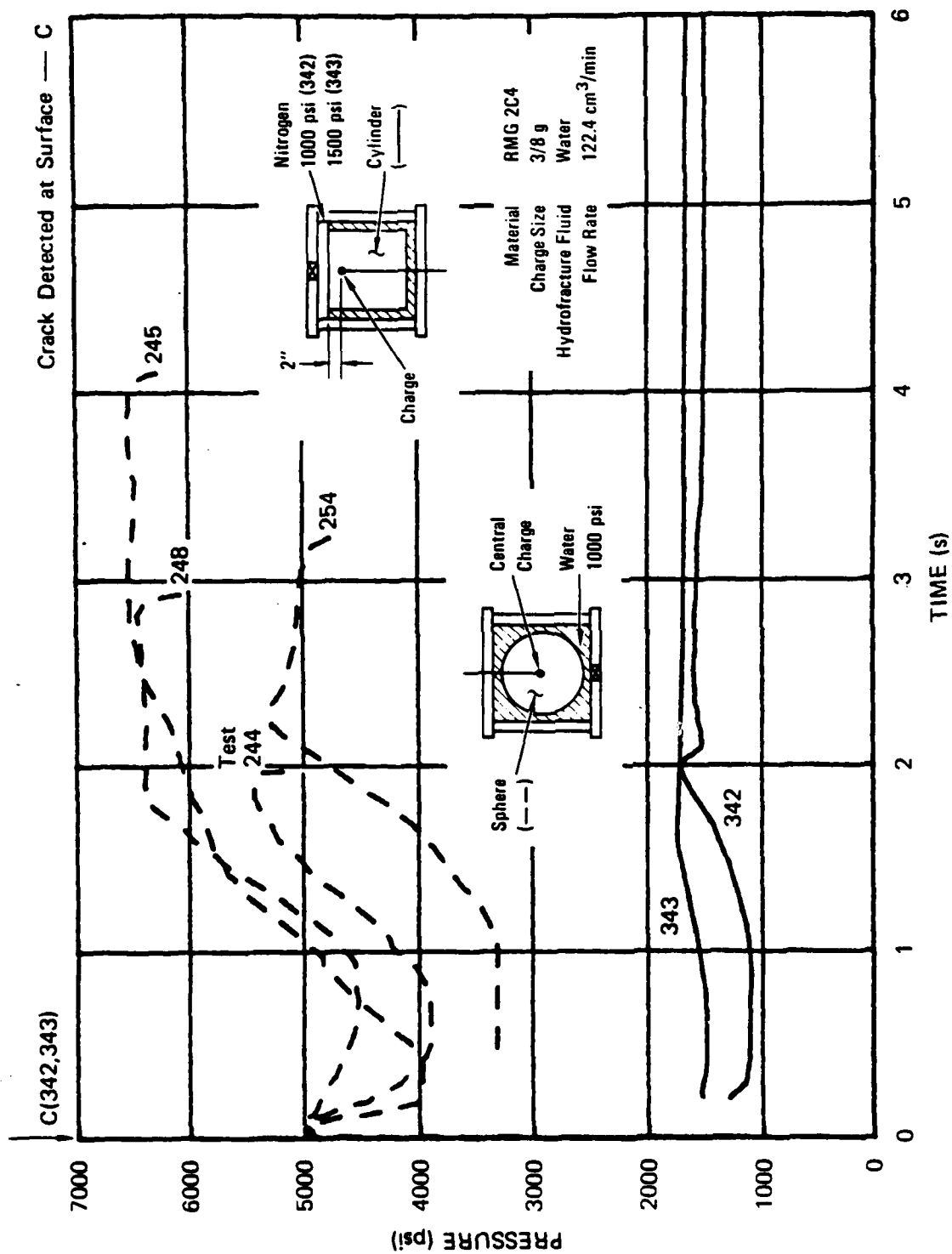
FIGURE 3.5   HYDROFRACTURE PRESSURES FOR UNVENTED EXPLODED CAVITY TESTS IN RMG 2C4 — DEPTH-OF-BURIAL EFFECT (TESTS 342 AND 343)

JA-5372-2

60

MPa). The configuration and hydrofracture pressure records for these
tests are shown in Figure 3.6. Dynamic surface cracking was observed
when the overburden pressure was 500 psi (3.447 MPa). However, in test
338, a typical hydrofracture record was obtained, whereas in test 346,
cracking extended from the cavity to the free surface, and the cavity
gases vented. No dynamic cracking was observed in test 337 in which the
overburden pressure was 1000 psi (6.895 MPa), and a typical hydro-
fracture record was obtained.

The depth-of-burial results are summarized in Figure 3.7. A
failure threshold curve consistent with all available results is
included.

3.3 PARTICLE VELOCITY MEASUREMENTS

The basic configuration for particle velocity measurements is shown
in Figure 2.8. The techniques developed to construct the models and
perform the tests are described in Sections 2.2 and 2.3. Shown in the
particle velocity figures are the times at which the generated wave
reflects from the surface of the sphere or cylinder and returns to each
gage. Hence, before these times the results are representative of
motion in an infinite medium.

Series 4: Technique Validation in RMG 2C4

The standard technique developed for particle velocity measurements
in RMG 2C4 consists of casting loops of copper wire symmetrically about
an explosive charge in a sphere of grout. An alternative technique,
required for tests in cores of geologic material, is to precast a grout
cylinder, section the cylinder along the midheight plane, embed the wire
loops in circular grooves, and epoxy the cylinder along the plane of the
gages (see Figure 2.9). A series of four experiments was performed to
validate these techniques.

In test type 1, we considered the effects of gage wire material on
the particle velocity records. Copper (density 9.0 g/cm^3) was replaced
by aluminum (density 2.7 g/cm^3) to assess inertial effects in RMG

61
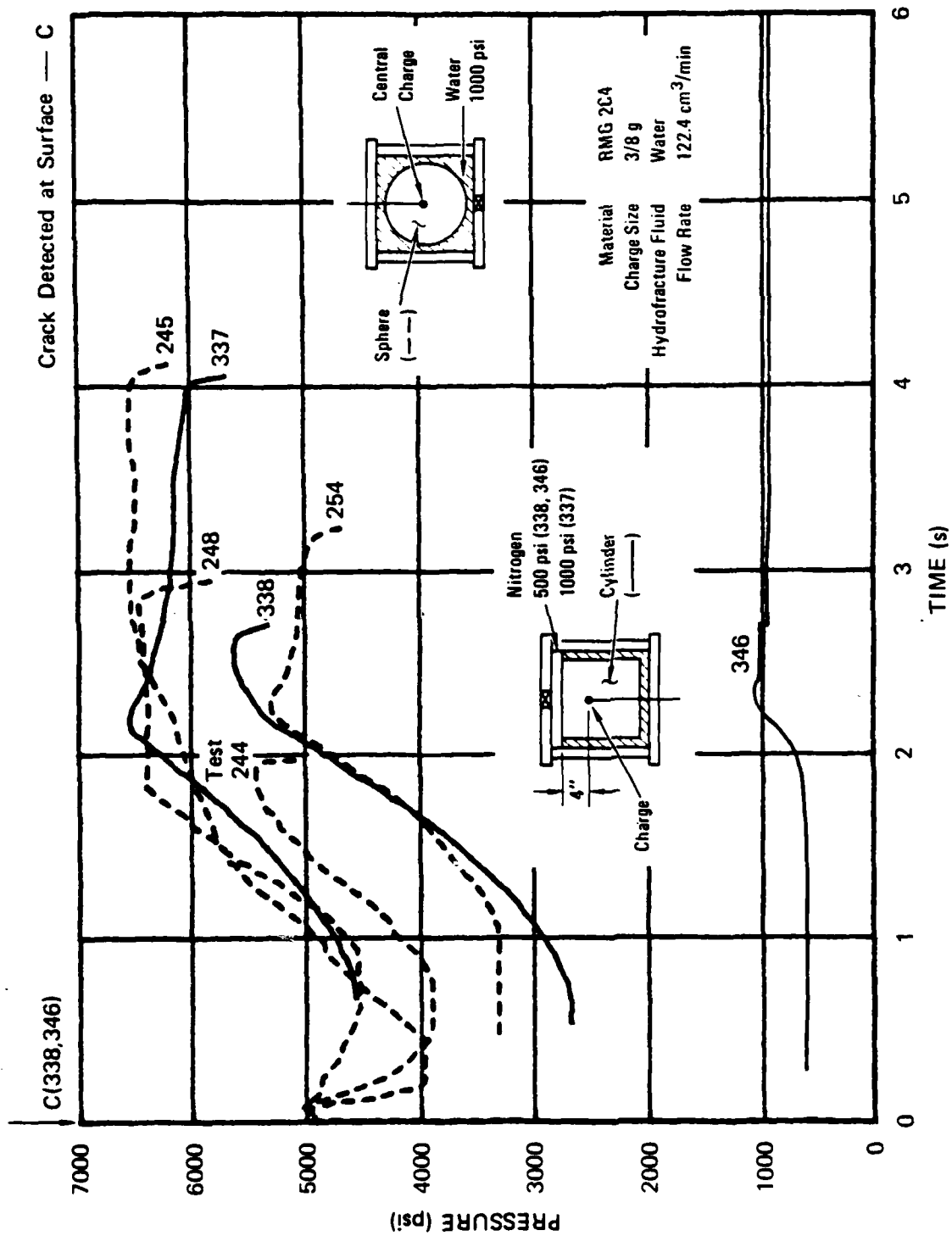
FIGURE 3.6 HYDROFRACTURE PRESSURES FOR UNVENTED EXPLODED CAVITY TESTS IN RMG 2C4 — DEPTH-OF-BURIAL EFFECT (TESTS 337, 338, AND 346)

62
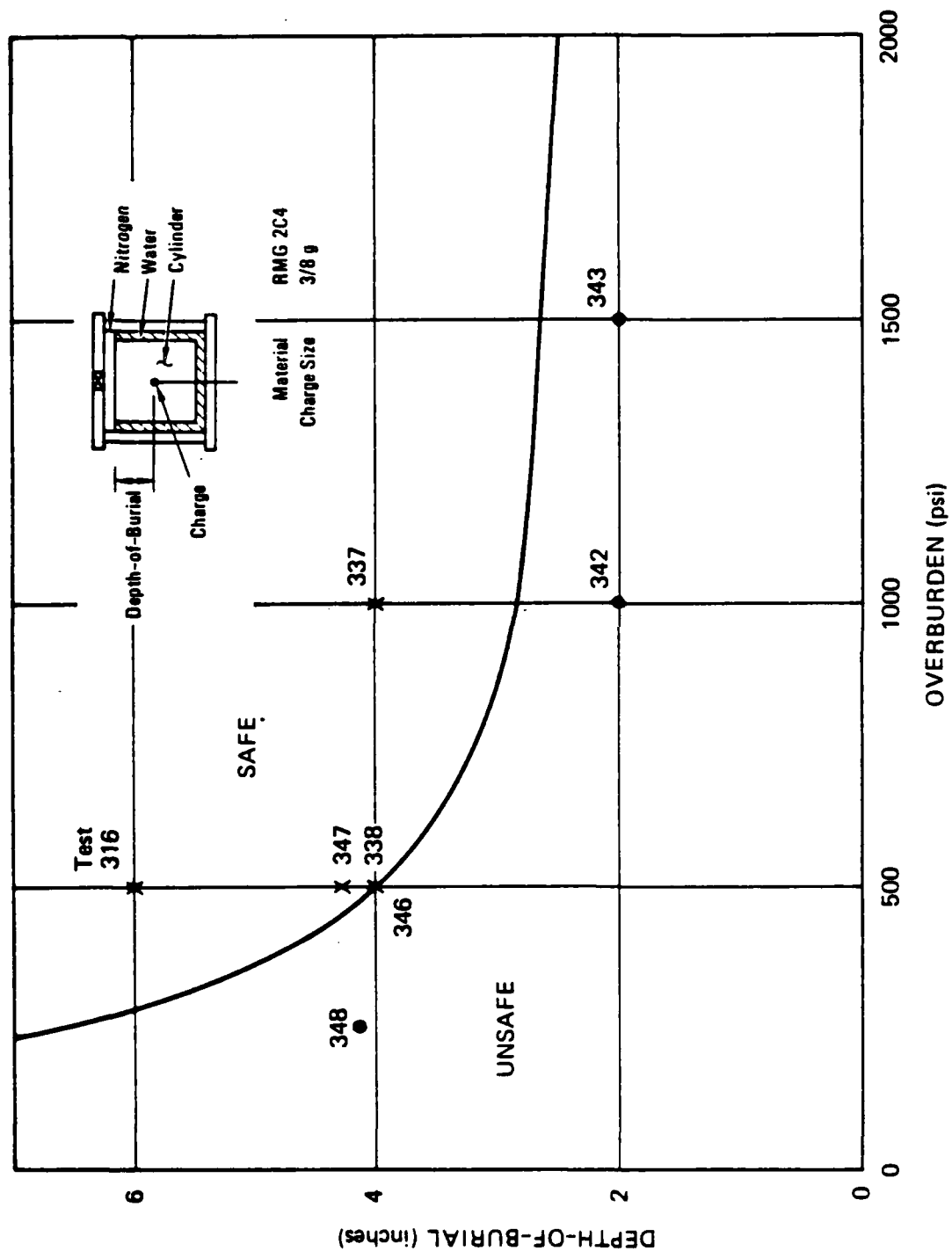
FIGURE 3.7 FAILURE THRESHOLD FOR EXPLODED CAVITY TESTS IN RMG 2C4

JA-5372-1

63
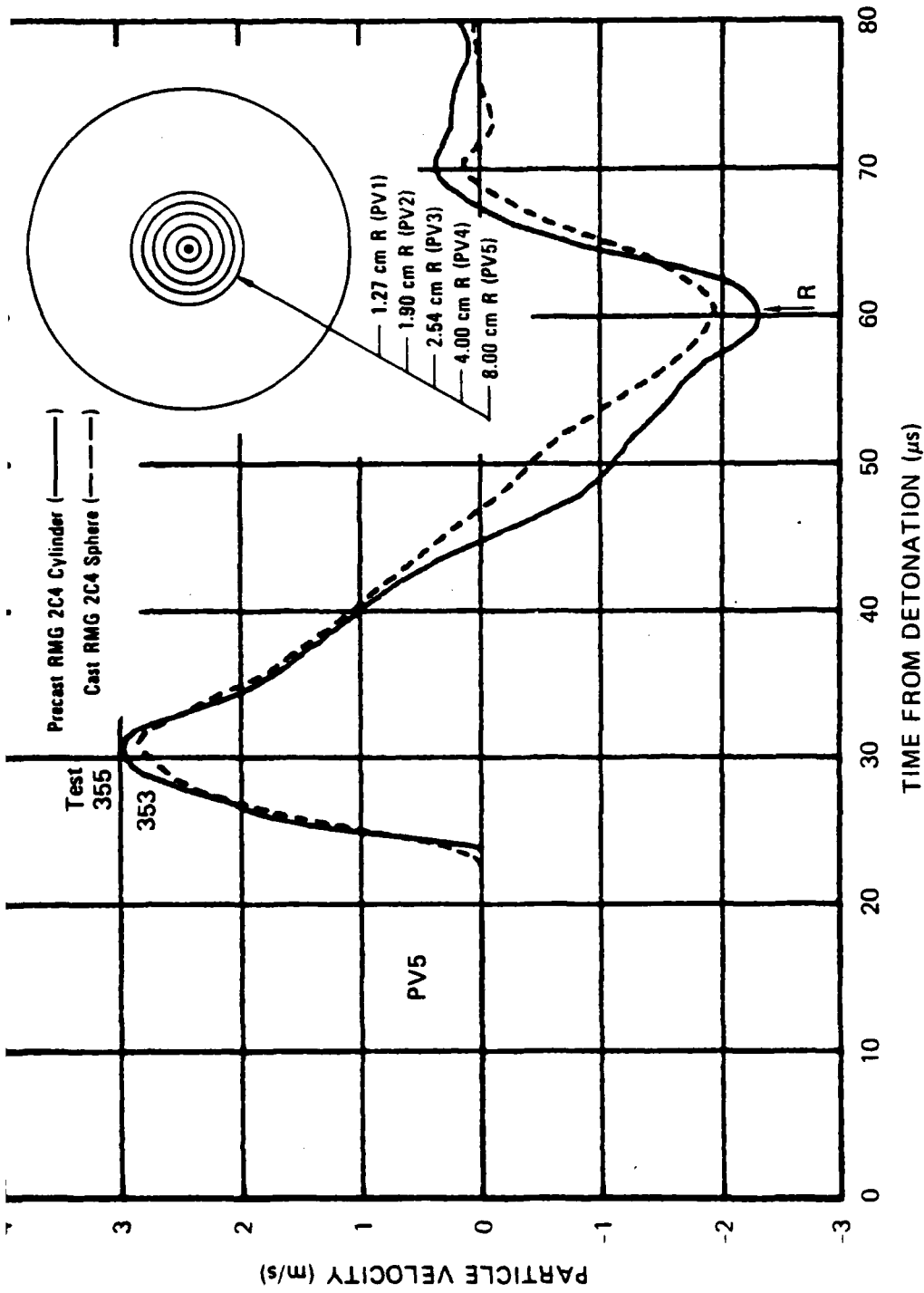
FIGURE 3.20 PARTICLE VELOCITY 8.00 cm FROM THE CENTER COUPLED EXPLOSIONS IN RMG 2C4 — CAST VERSUS PRECAST WITH WIDE GROOVES, ALUMINUM GAGE WIRE

77
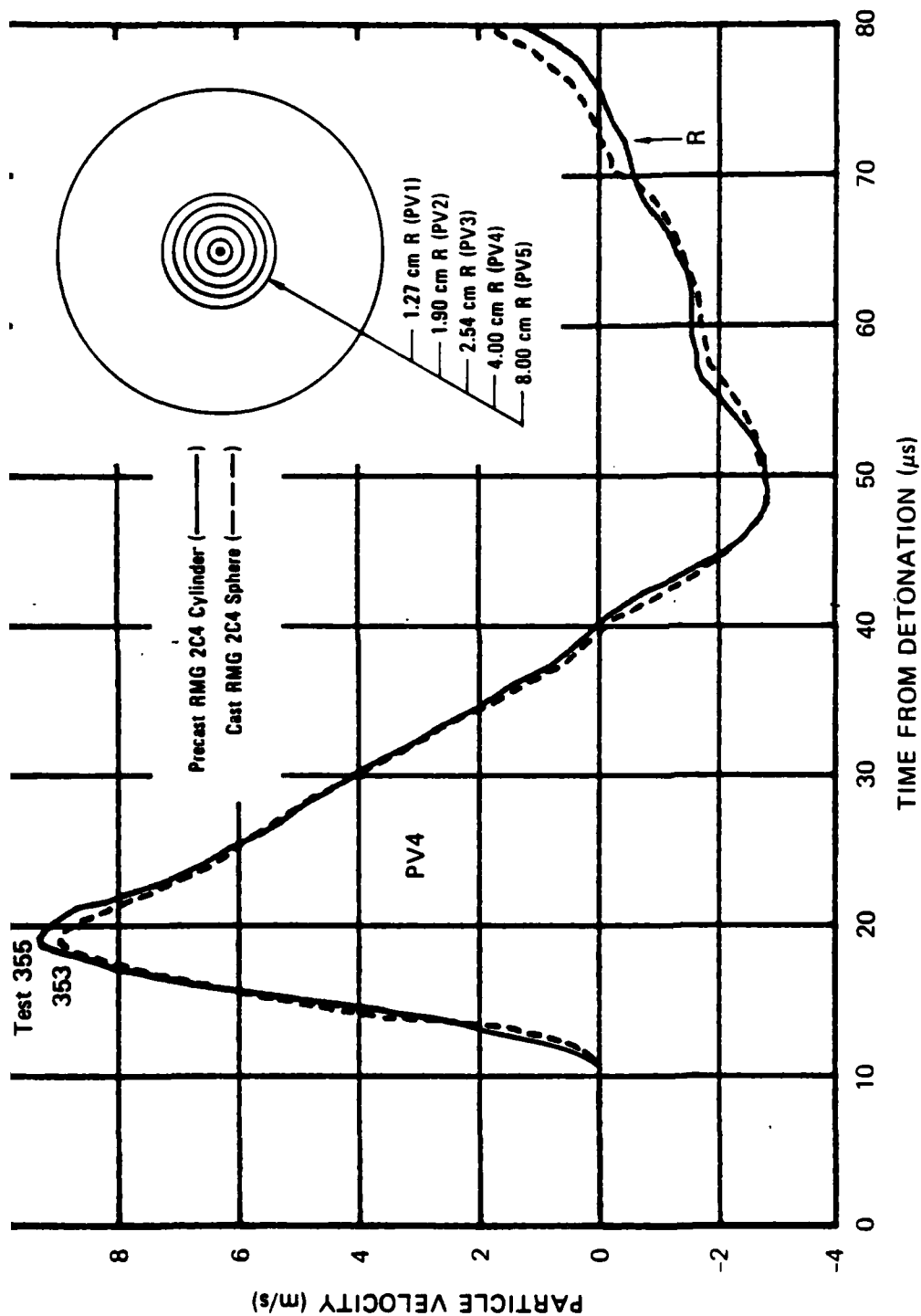
FIGURE 3.19 PARTICLE VELOCITY 4.00 cm FROM THE CENTER OF COUPLED EXPLOSIONS IN RMG 2C4 — CAST VERSUS PRECAST WITH WIDE GROOVES, ALUMINUM GAGE WIRE

JA-5372-74

76

FIGURE 3.18   PARTICLE VELOCITY 2.54 cm FROM THE CENTER OF COUPLED EXPLOSIONS IN RMG 2C4 — CAST VERSUS PRECAST WITH WIDE GROOVES, ALUMINUM GAGE WIRE

JA-5372-73

75

FIGURE 3.17 PARTICLE VELOCITY 1.90 cm FROM THE CENTER OF COUPLED EXPLOSIONS IN RMG 2C4 — CAST VERSUS PRECAST WITH WIDE GROOVES, ALUMINUM GAGE WIRE

JA-5372-72

Figure axis labels and legend content:

PARTICLE VELOCITY (m/s)

TIME FROM DETONATION (μs)

Test 355

353

PV1

Precast RMG 2C4 Cylinder (———)

Cast RMG 2C4 Sphere (— — —)

1.27 cm R (PV1)
1.90 cm R (PV2)
2.54 cm R (PV3)
4.00 cm R (PV4)
8.00 cm R (PV5)

JA-5372-71

FIGURE 3.16   PARTICLE VELOCITY 1.27 cm FROM THE CENTER OF COUPLED EXPLOSIONS IN RMG 2C4 —
CAST VERSUS PRECAST WITH WIDE GROOVES, ALUMINUM GAGE WIRE

73

FIGURE 3.15 PARTICLE VELOCITY 4.00 cm FROM THE CENTER OF COUPLED EXPLOSIONS IN RMG 2C4 — CAST VERSUS PRECAST WITH WIDE GROOVES, COPPER GAGE WIRE

72

FIGURE 3.14   PARTICLE VELOCITY 2.54 cm FROM THE CENTER OF COUPLED EXPLOSIONS IN RMG 2C4 – CAST VERSUS PRECAST WITH WIDE GROOVES, COPPER GAGE WIRE

FIGURE 3.13   PARTICLE VELOCITY 1.90 cm FROM THE CENTER OF COUPLED EXPLOSIONS IN RMG 2C4 —
CAST VERSUS PRECAST WITH WIDE GROOVES, COPPER GAGE WIRE

JA-5372-77

70

FIGURE 3.12 PARTICLE VELOCITY 1.27 cm FROM THE CENTER OF COUPLED EXPLOSIONS IN RMG 2C4 — CAST VERSUS PRECAST WITH WIDE GROOVES, COPPER GAGE WIRE

69
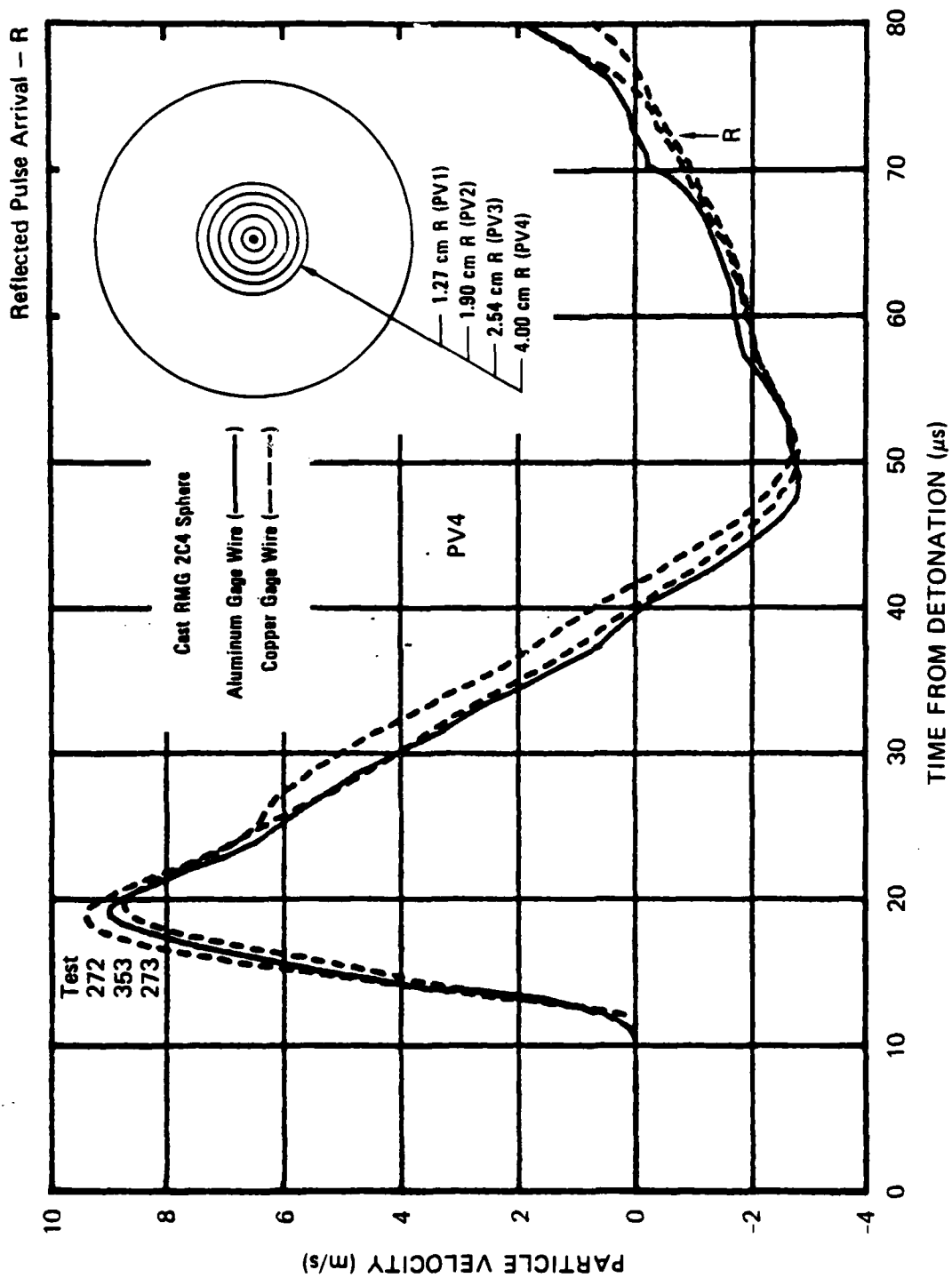
FIGURE 3.11 PARTICLE VELOCITY 4.00 cm FROM THE CENTER OF COUPLED EXPLOSIONS IN CAST RMG 2C4 — ALUMINUM VERSUS COPPER GAGE WIRE

68
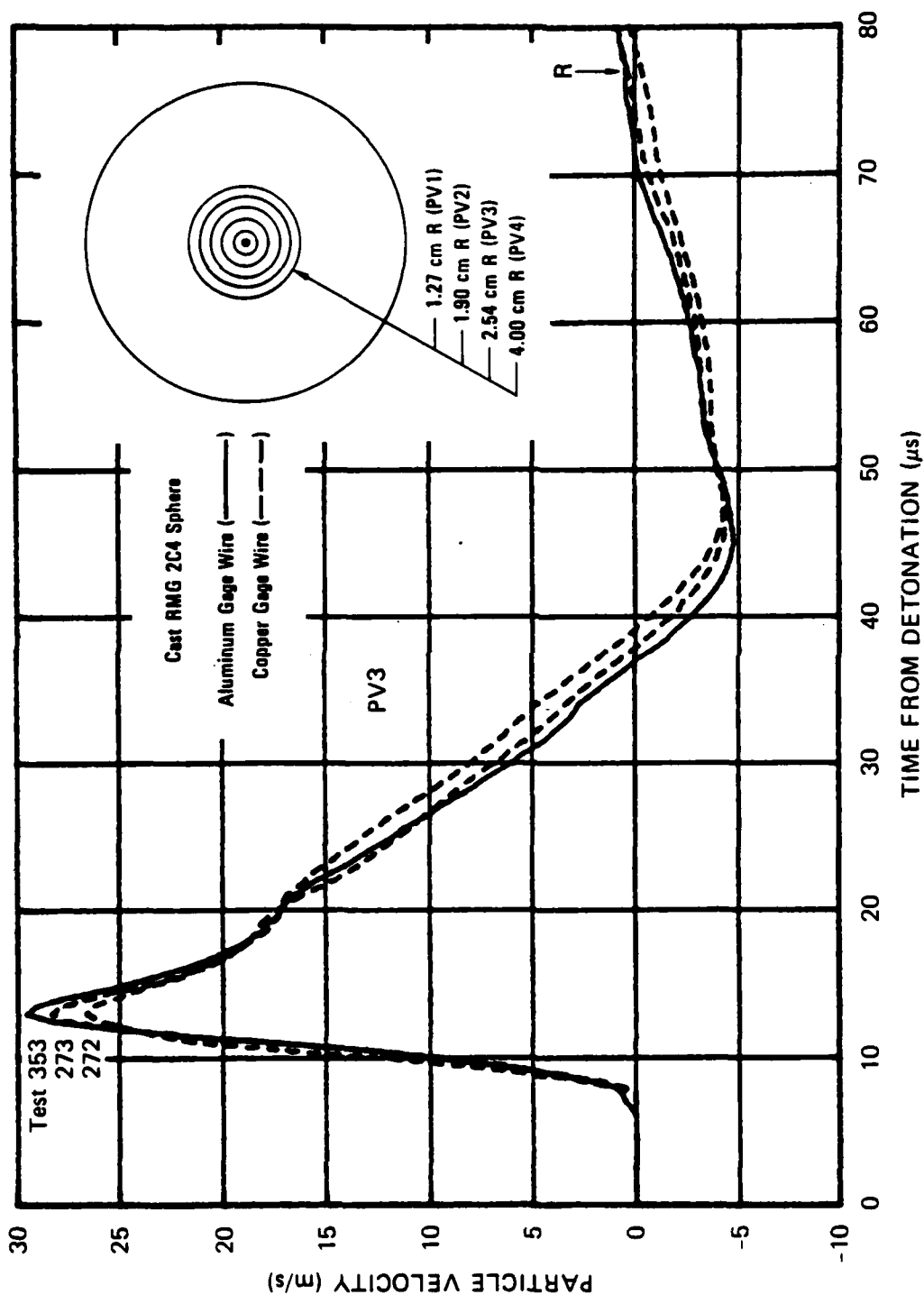
FIGURE 3.10 PARTICLE VELOCITY 2.54 cm FROM THE CENTER OF COUPLED EXPLOSIONS IN CAST RMG 2C4 — ALUMINUM VERSUS COPPER GAGE WIRE

67
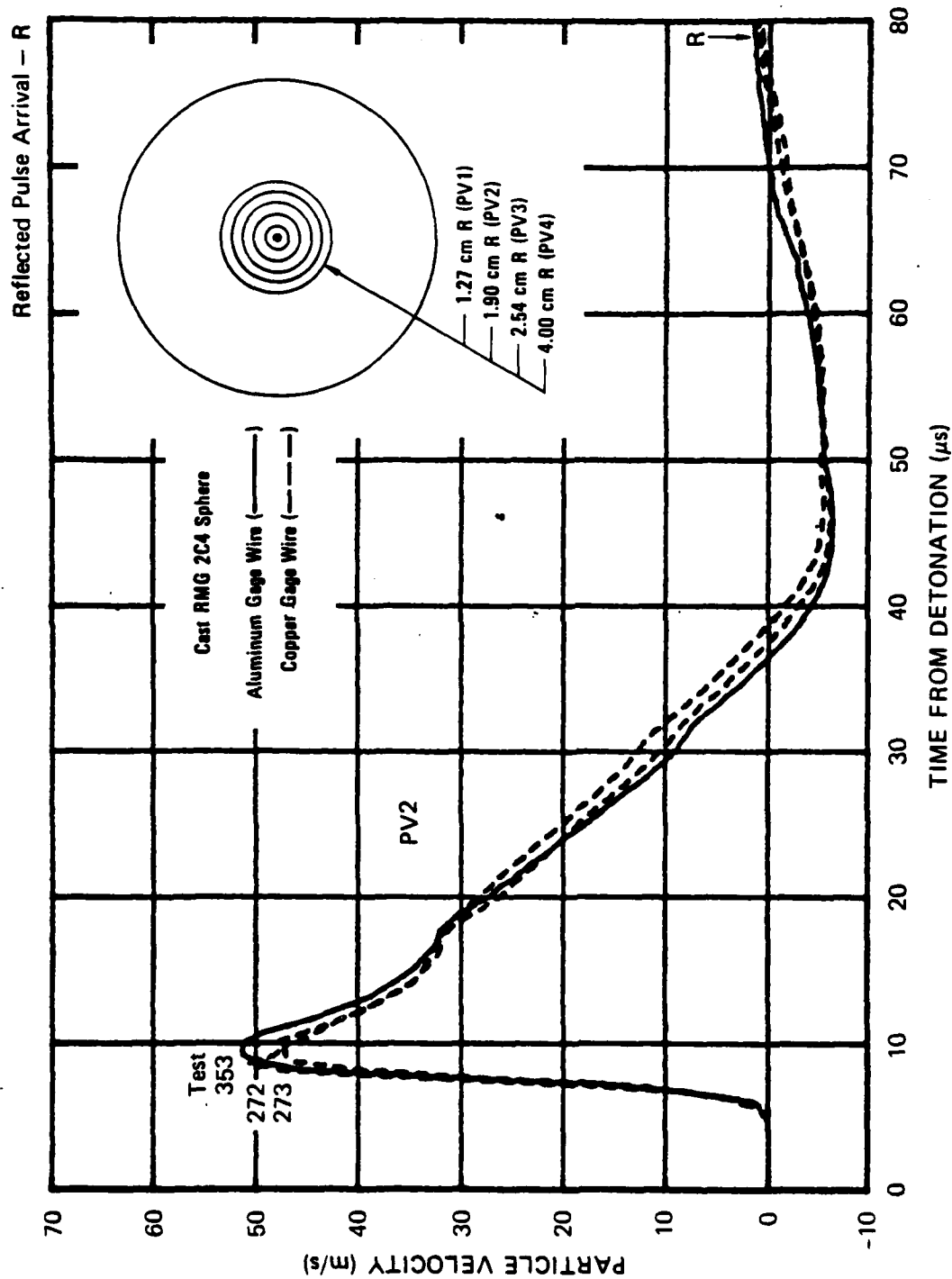
FIGURE 3.9   PARTICLE VELOCITY 1.90 cm FROM THE CENTER OF COUPLED EXPLOSIONS IN CAST RMG 2C4 —
ALUMINUM VERSUS COPPER GAGE WIRE
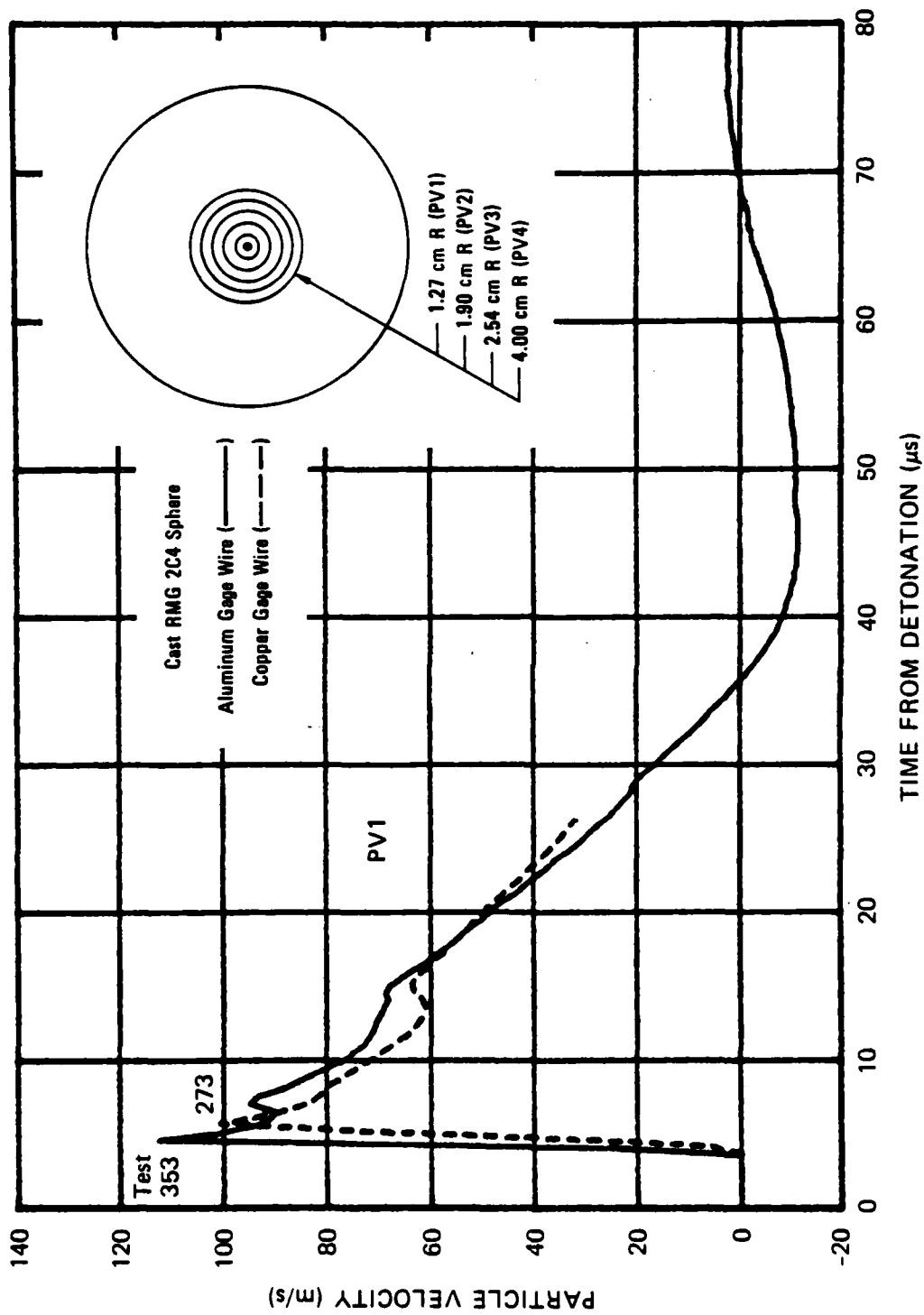
FIGURE 3.8 PARTICLE VELOCITY 1.27 cm FROM THE CENTER OF COUPLED EXPLOSIONS IN CAST RMG 2C4 — ALUMINUM VERSUS COPPER GAGE WIRE

65

(density 2.2 g/cm^3). In test 353, aluminum wire loops were cast in a sphere of RMG 2C4 at four radial locations (1.27, 1.90, 2.54, and 4.00 cm). The aluminum wire was 5 mils (0.127 mm) in diameter, the same as the copper wire. Figures 3.8 through 3.11 show the resulting particle velocity records. For comparison, results of previous tests[6] (272 and 273), in which copper wire loops were used, are included. The good agreement among the results from each location indicates that the inertial effects are small. In particular, agreement is excellent just behind the wave front where particle accelerations, and hence inertial forces, are at a maximum. The slightly shorter duration of outward motion associated with the aluminum wire is considered to be within the limits of experimental reproducibility.

Pressure pulses in the overburden fluid obtained from quartz gage measurements are shown in Figure B.2. Reproducibility of these pulses is consistent with the reproducibility of the particle velocity records.

Test type 2 considered the effects of gage installation technique on the particle velocity records. In test 354, circular grooves 40 mils (1.02 mm) wide were machined in a precast RMG cylinder at four radial locations (1.27, 1.90, 2.54, and 4.00 cm). Copper wire 5 mils (0.127 mm) in diameter was epoxied in the grooves. Figures 3.12 through 3.15 show the resulting particle velocity records. For comparison, results of a similar previous test[6] (293) are shown. Also shown for comparison are the results of tests 272 and 273, in which gages were cast in the grout. The generally good agreement among the results at each location indicates that the technique for installing gages in precast cylinders, and hence in cores of geologic material, is adequate.

The configuration for test type 3 was similar to that of test type 2 except that aluminum wire replaced the copper wire. Hence, the effects of gage installation technique on the particle velocity records were further assessed. Figures 3.16 through 3.20 show the resulting particle velocity records for test 355. For comparison, results of test 353, in which aluminum wire gages were cast in the grout are also shown. The excellent agreement between the records at each gage location

64

confirms that the gage installation technique required for cores of geologic material is suitable.

Test type 4 considered the effects of groove width on the particle velocity records. In test 356, circular grooves 9 mils (0.229 mm) wide were machined in a precast RMG cylinder at four radial locations (1.27, 1.90, 2.54, and 4.00 cm). Aluminum wire 5 mils (0.127 mm) in diameter was epoxied in the grooves. Figures 3.21 through 3.24 show the resulting particle velocity records. For comparison, results of test 353, in which aluminum wire loops were cast in RMG, are also shown. Agreement between the records is excellent at PV1 (Figure 3.21) and satisfactory at PV2 (Figure 3.22). However, agreement is not satisfactory at PV3 (Figure 3.23) and PV4 (Figure 3.24), where particle acceleration behind the wave front in test 356 is erratic. One possible cause of this response is seen in Figure B.3, where pressure pulses in the overburden fluid from similar tests (354, 355, and 356) are shown. The lower peak pressure in test 356 suggests that an attenuating mechanism, such as air voids, was present in the grout. The narrow grooves used in test 356 are a technique refinement that should be incorporated in future tests.

Particle displacements obtained from an integration of the particle velocity records for the above tests are shown in Figures A.1 through A.4. The displacements for Test 353 (Figure A.1) were used to generate the volumetric strain profile shown in Figure 3.25. The procedure for generating volume strain from particle displacement is presented in Appendix D. As shown in Figure 3.25, permanent compressive volumetric strain is induced in RMG 2C4 as the material is crushed by the outgoing spherical wave. This result is consistent with the measured exploded cavity diameter for tests in RMG 2C4 [0.808 inch (2.05 cm)]. That is, when the displacement records are combined with an assumption of incompressibility, the calculated exploded cavity diameter [0.739 inch (1.88 cm)] is less than the measured value. Hence, permanent volumetric compression is required for agreement between calculated and measured values.
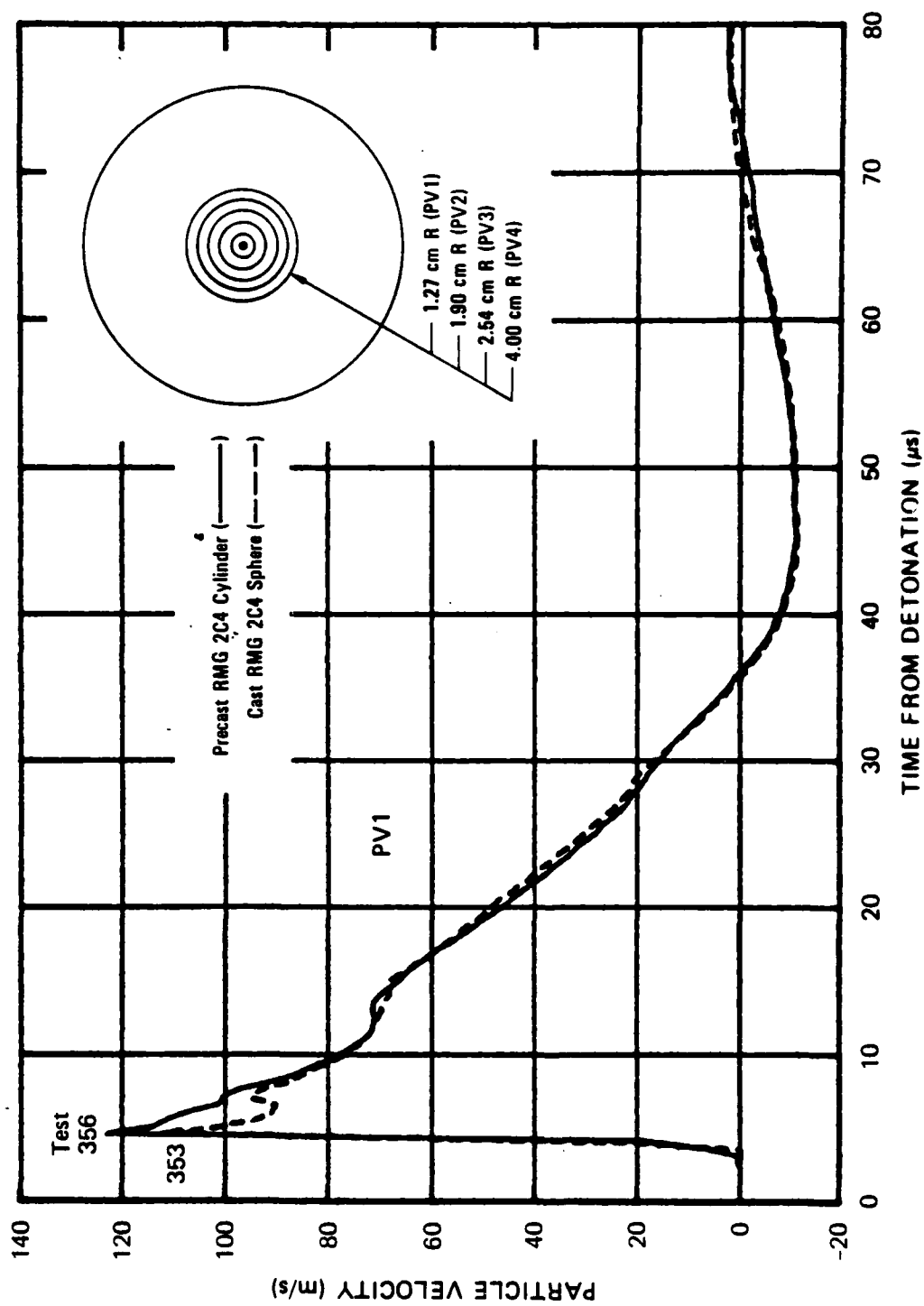
FIGURE 3.21 PARTICLE VELOCITY 1.27 cm FROM THE CENTER OF COUPLED EXPLOSIONS IN RMG 2C4 — CAST VERSUS PRECAST WITH NARROW GROOVES ALUMINUM GAGE WIRE
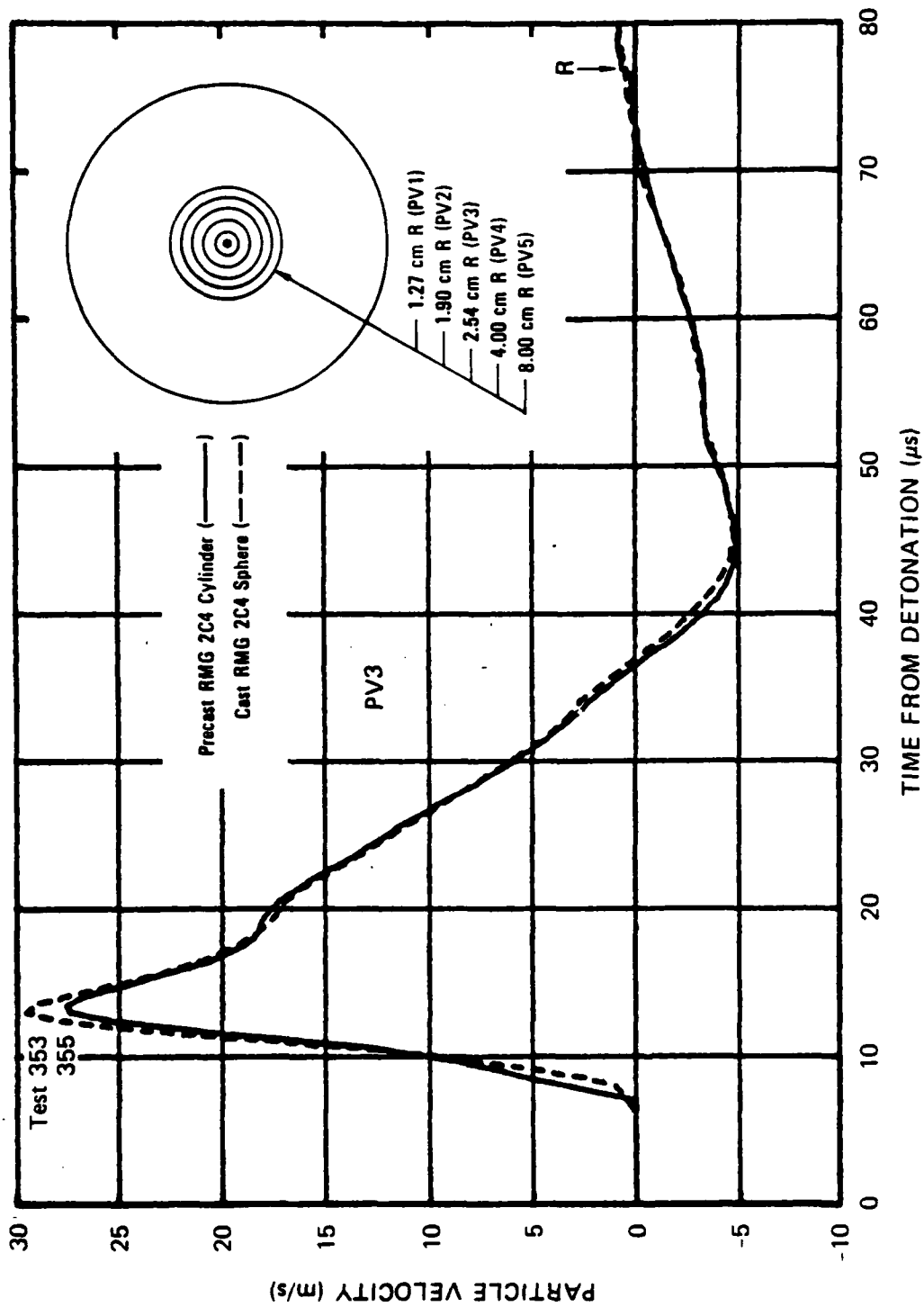
JA-5372-79

79
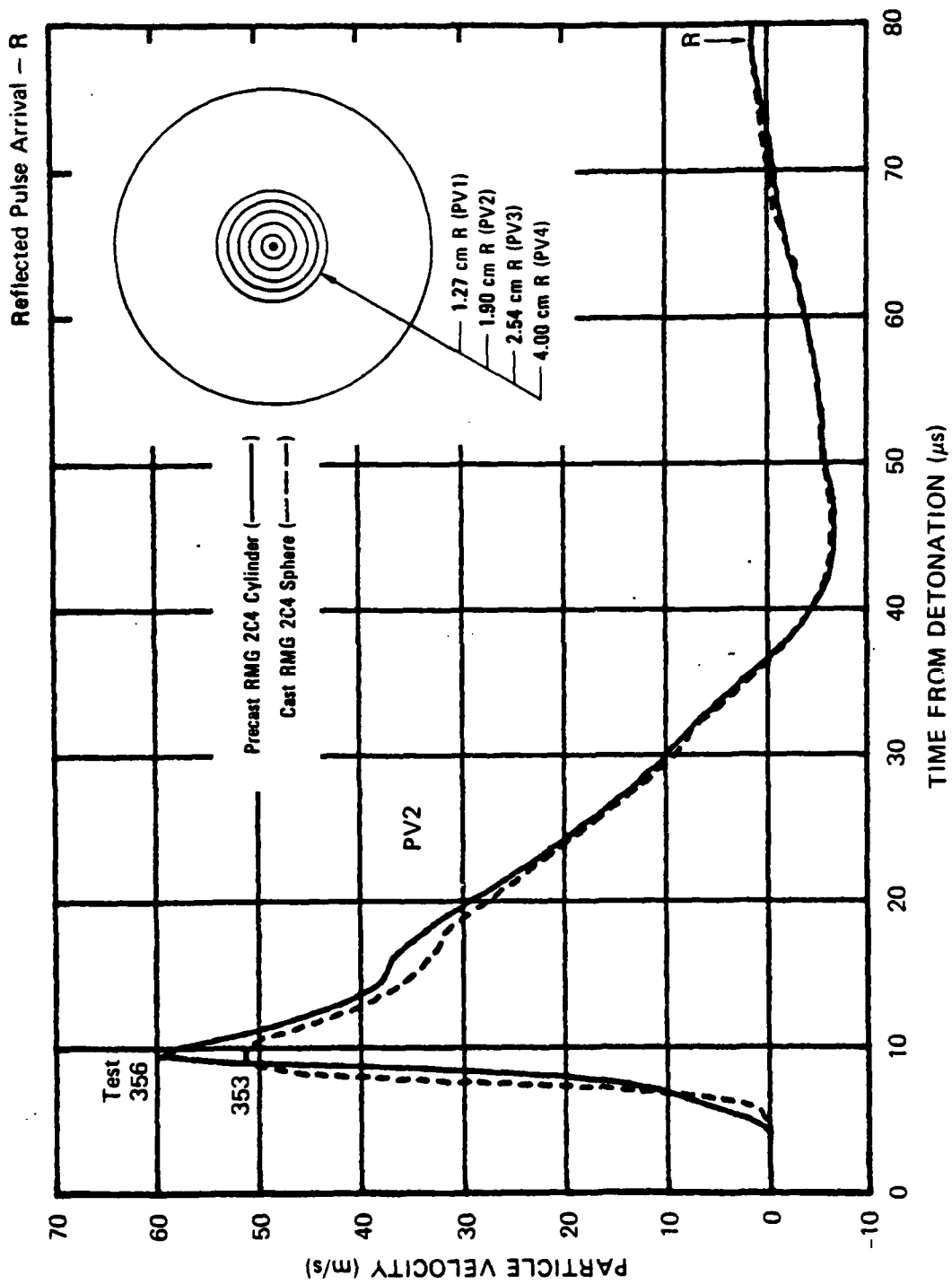
FIGURE 3.22 PARTICLE VELOCITY 1.90 cm FROM THE CENTER OF COUPLED EXPLOSIONS IN RMG 2C4 — CAST VERSUS PRECAST WITH NARROW GROOVES, ALUMINUM GAGE WIRE
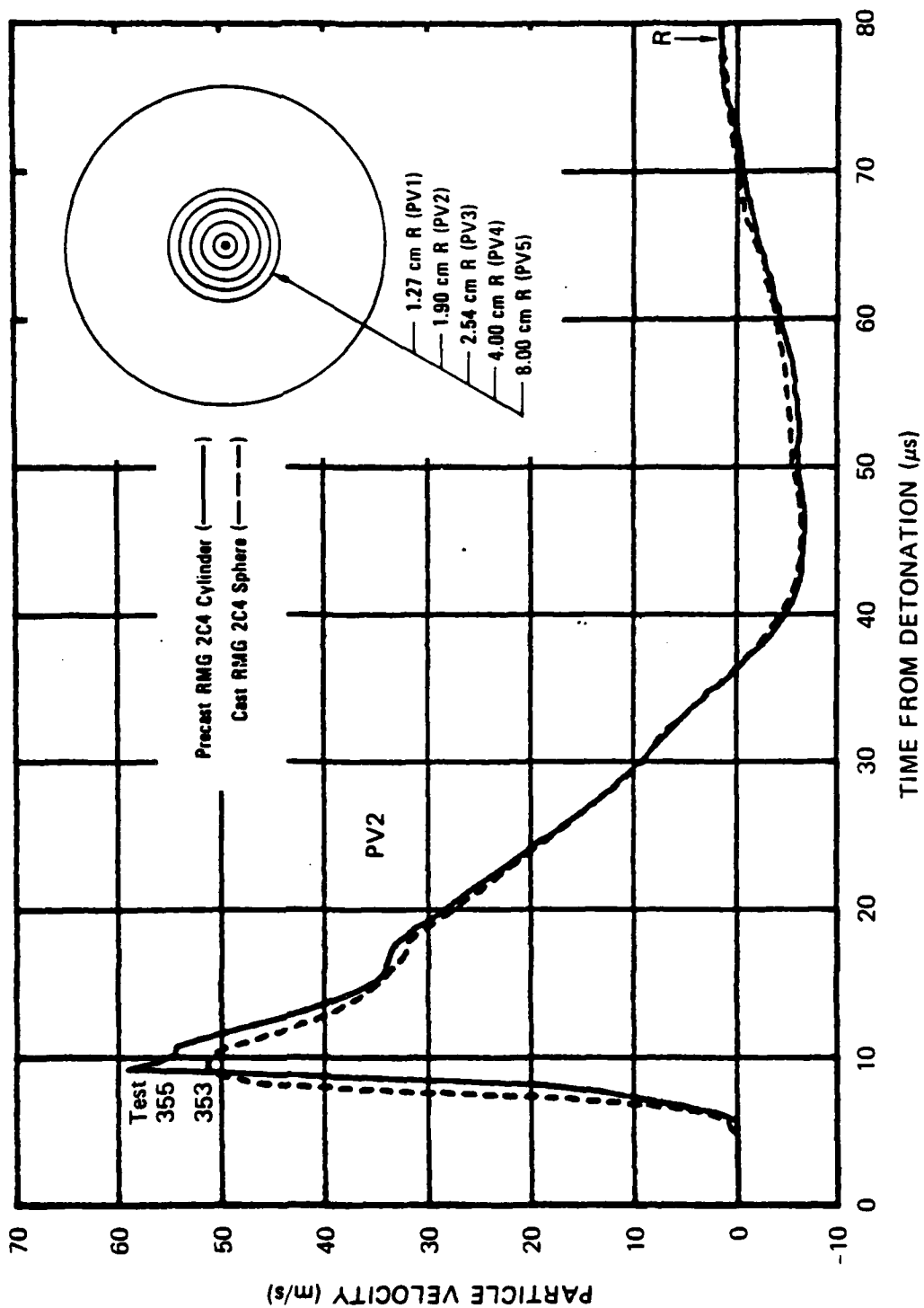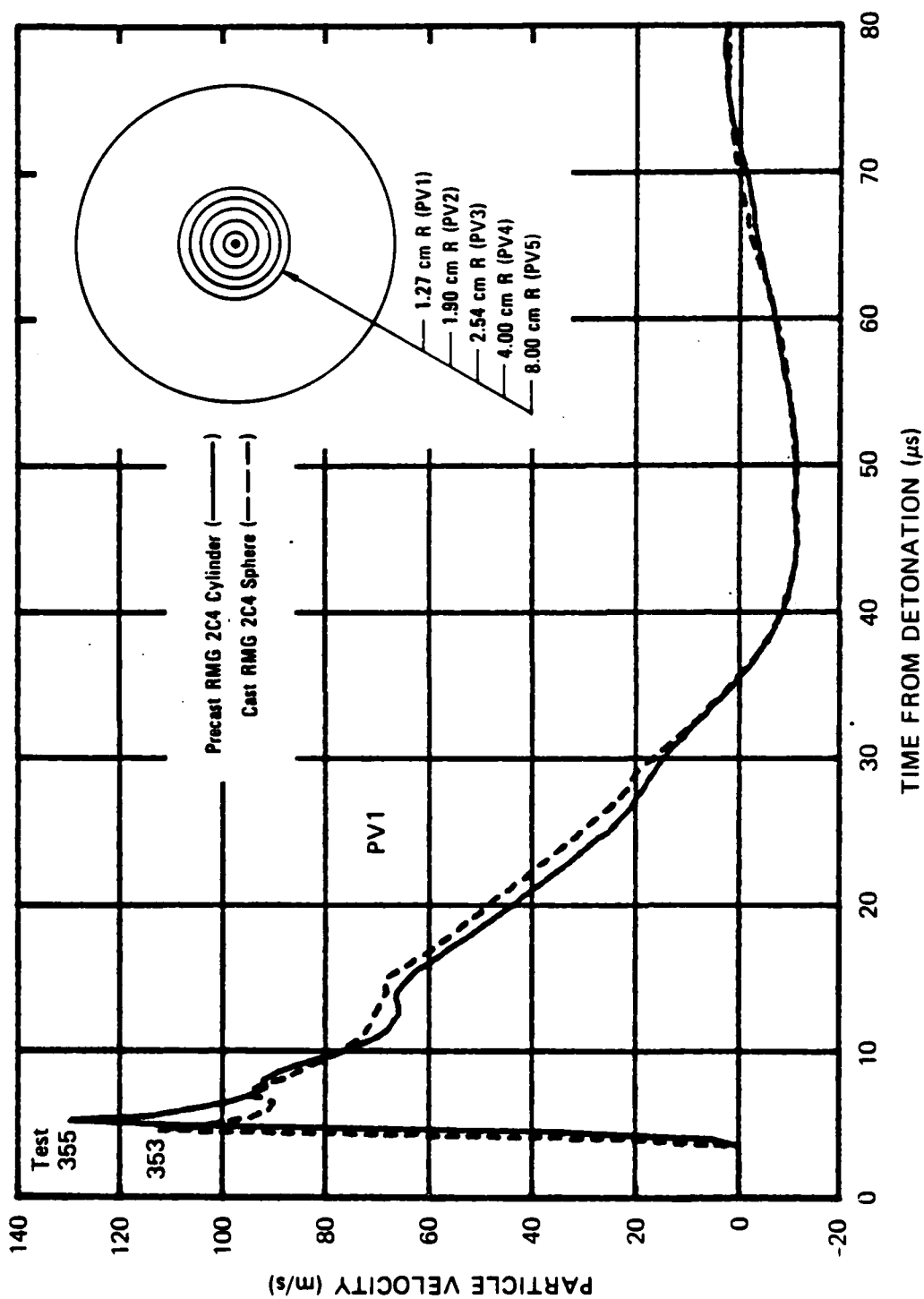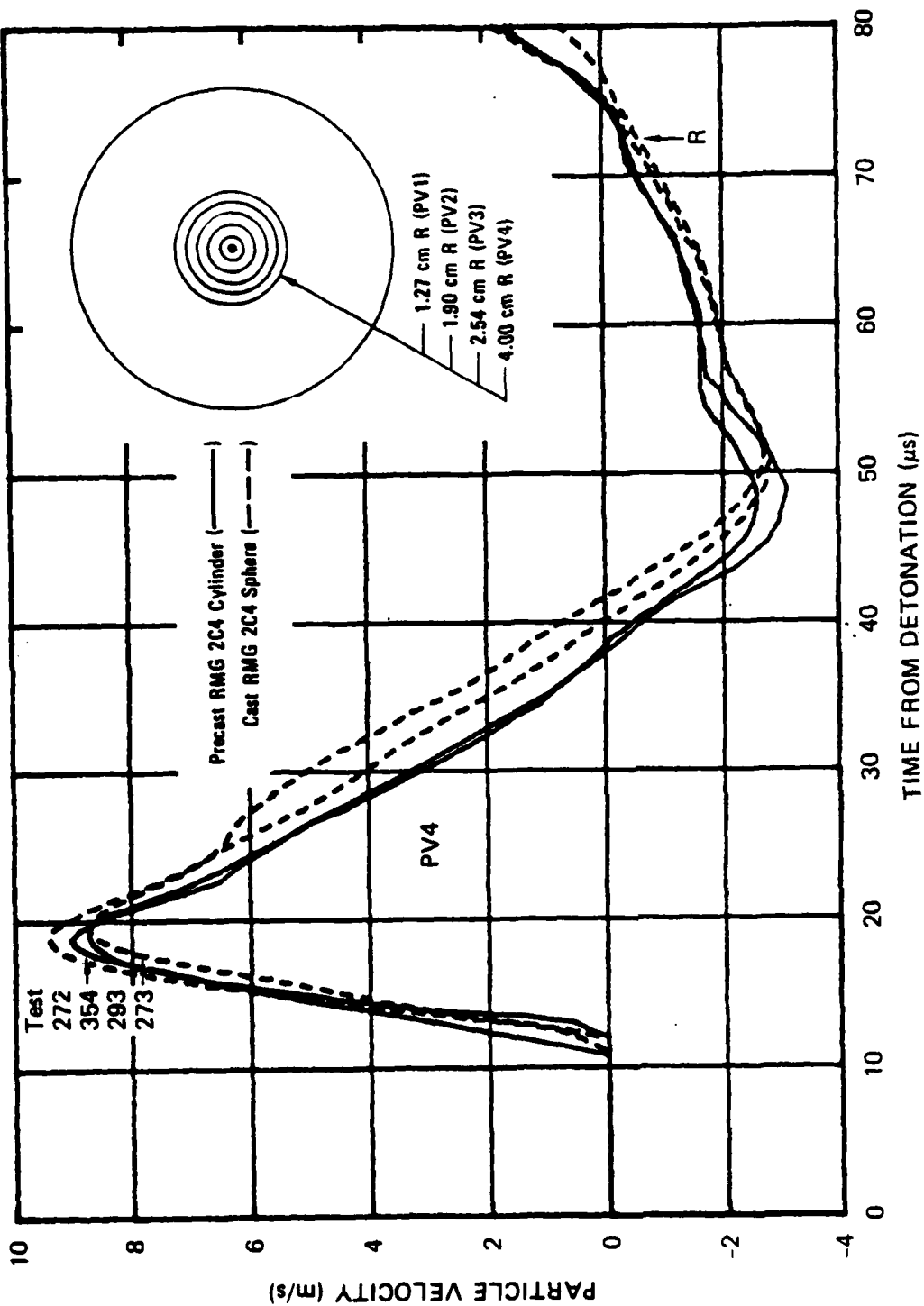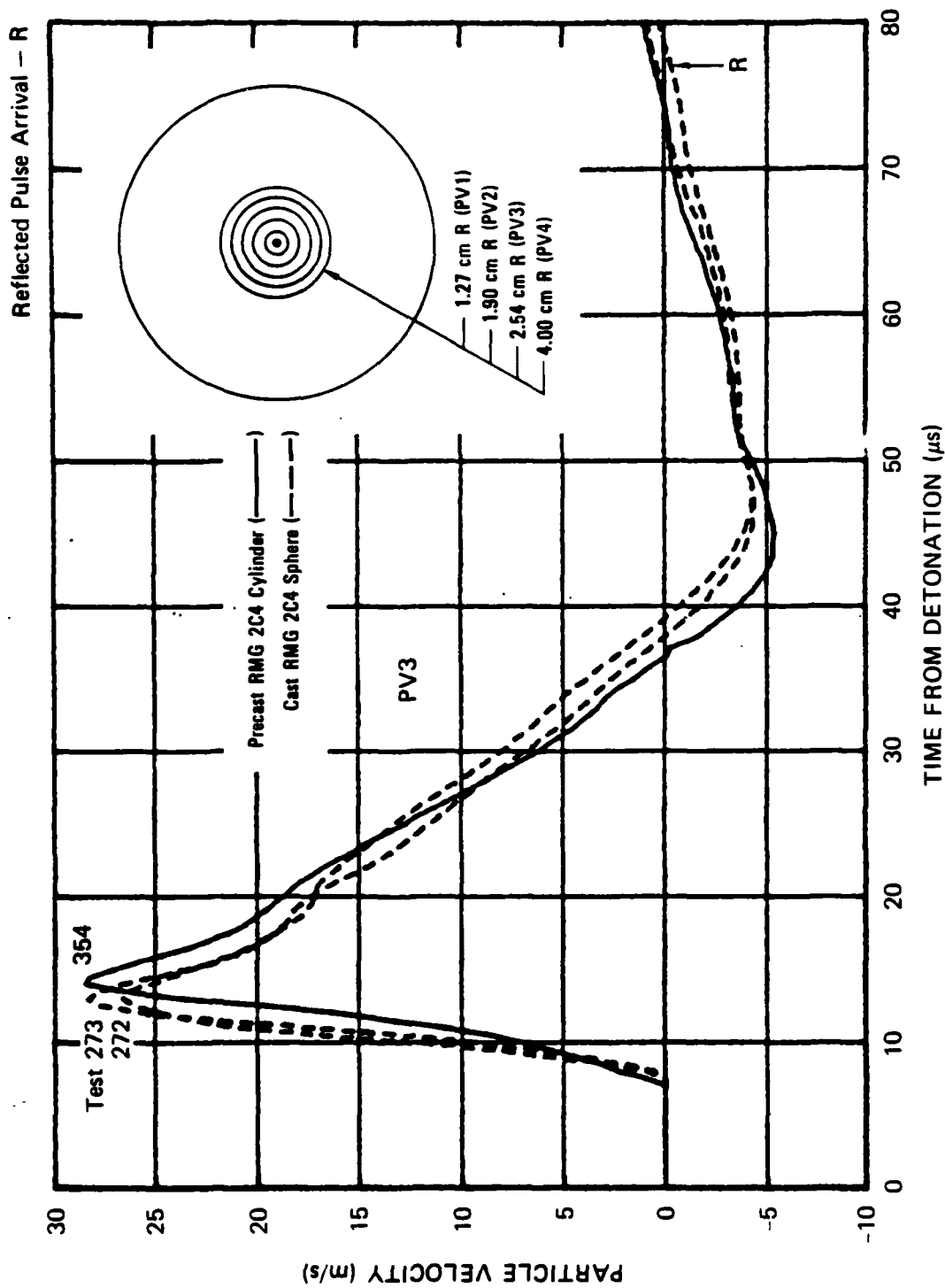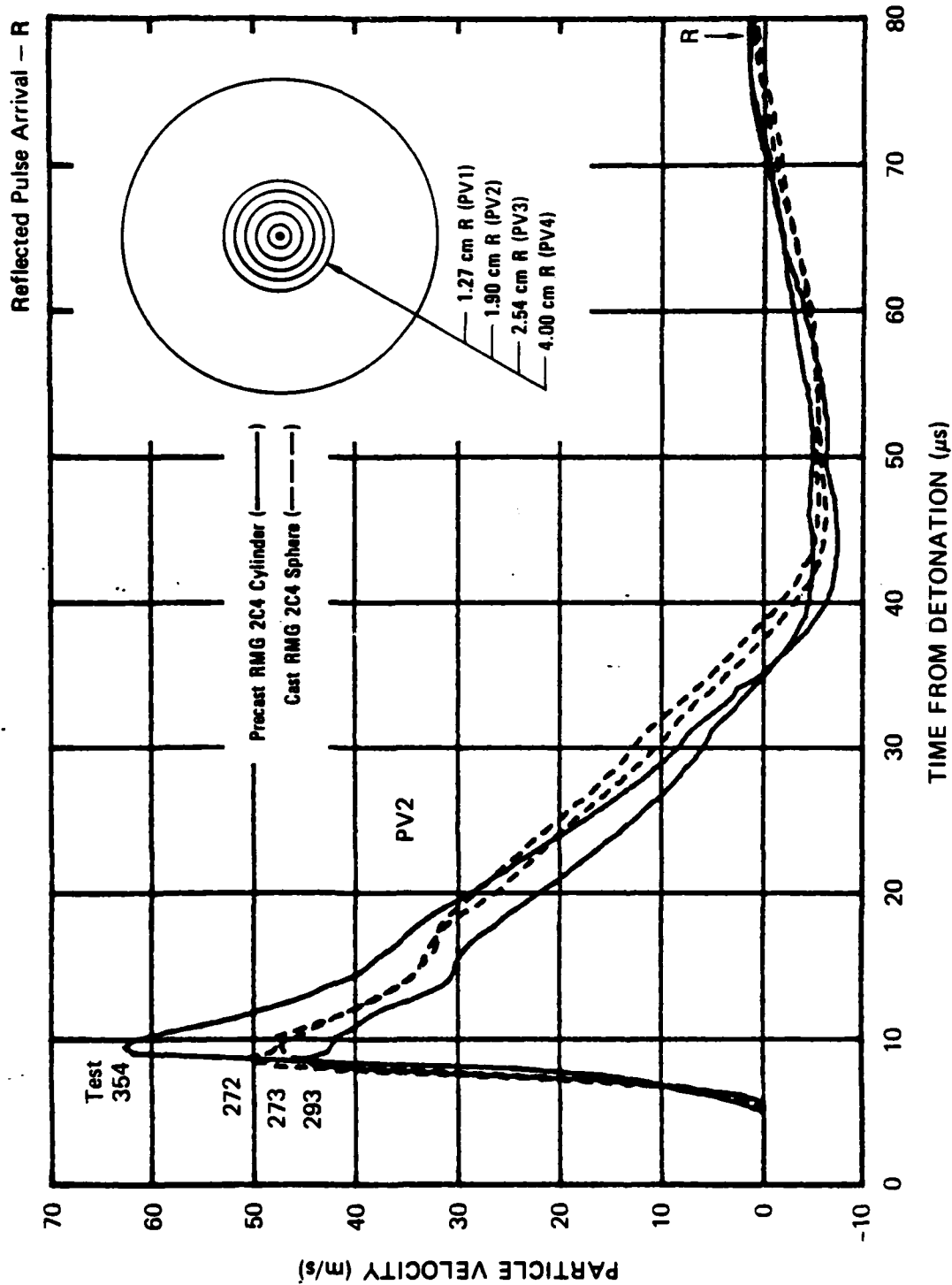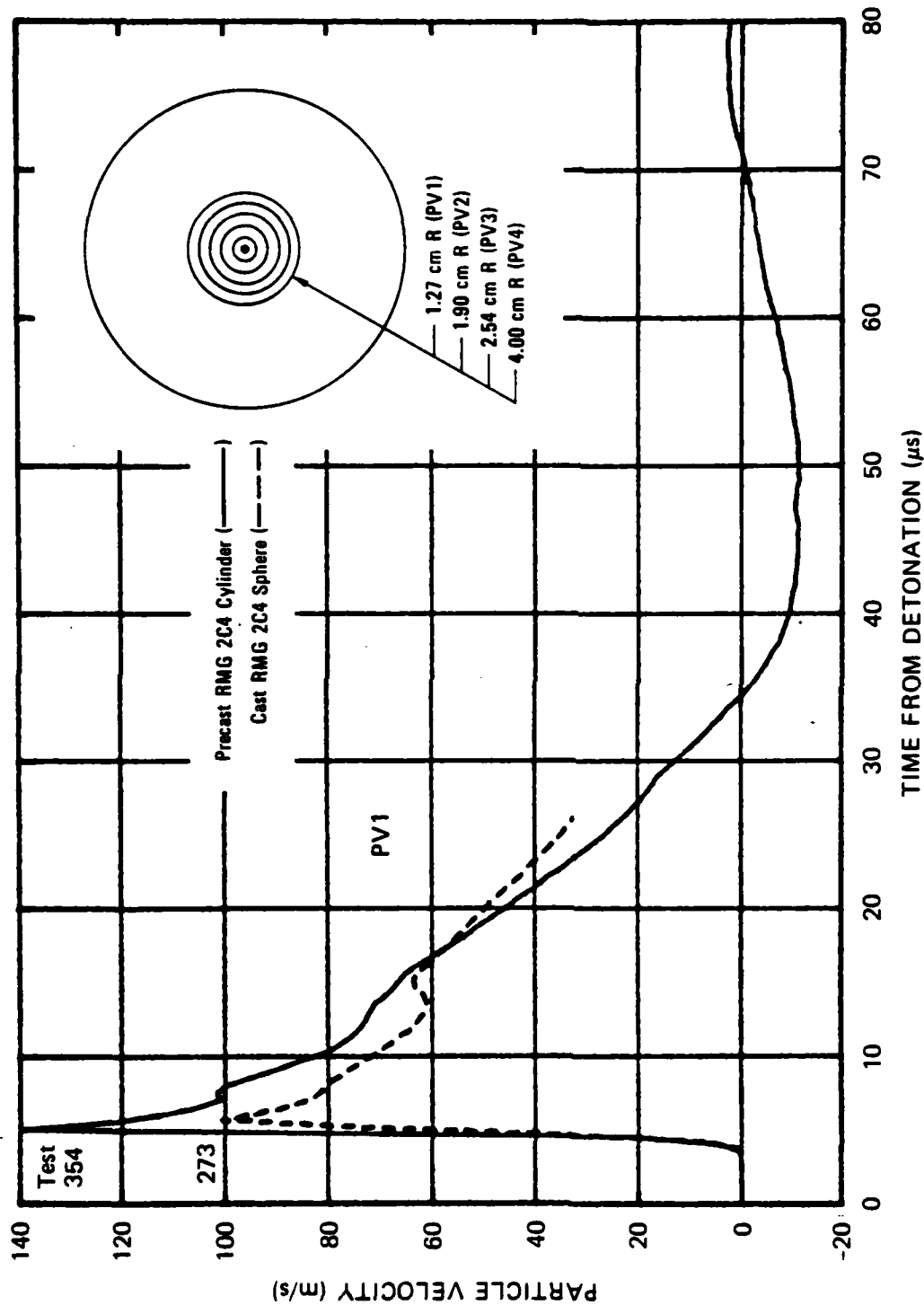
80
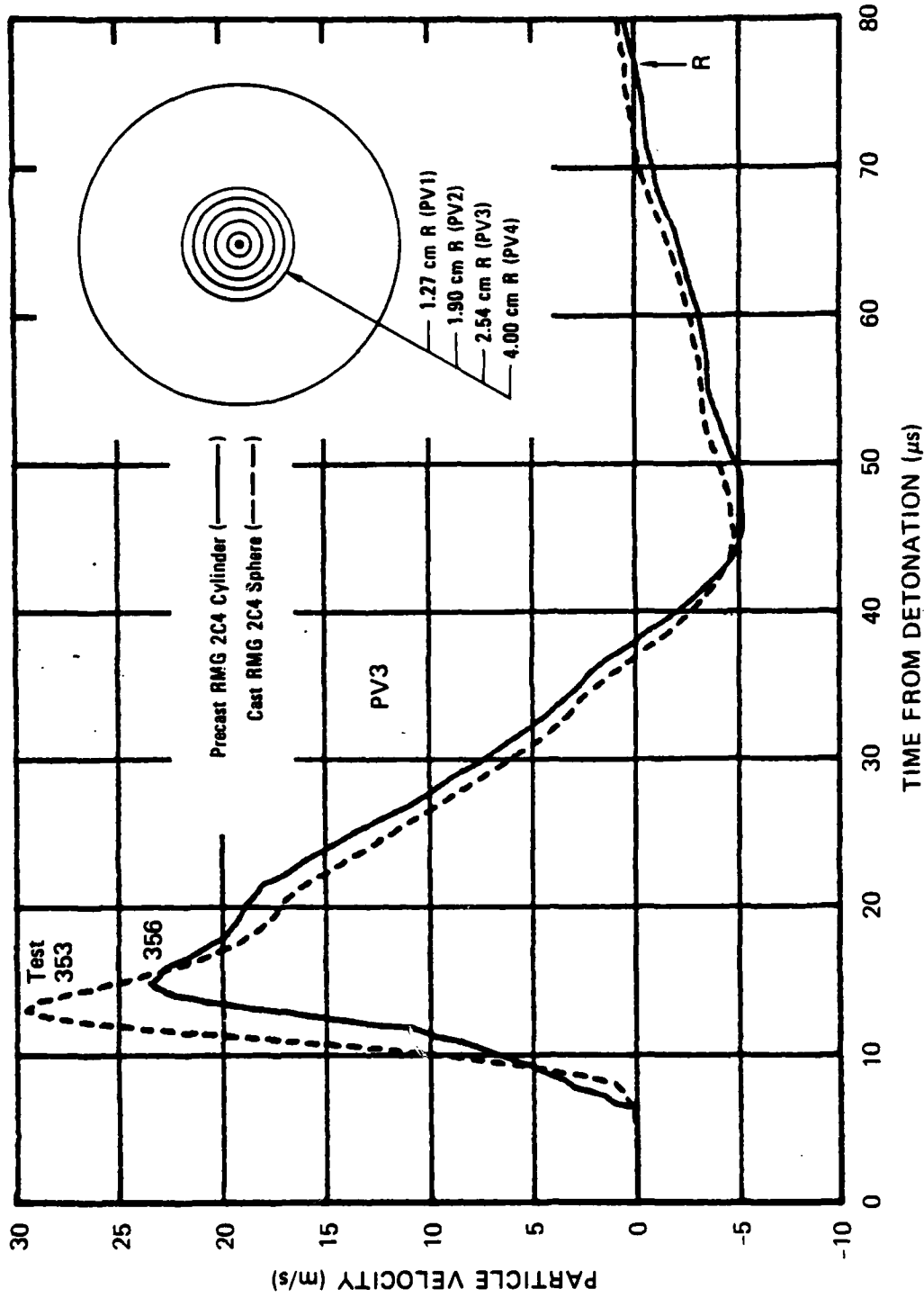
FIGURE 3.23 PARTICLE VELOCITY 2.54 cm FROM THE CENTER OF COUPLED EXPLOSIONS IN RMG 2C4 — CAST VERSUS PRECAST WITH NARROW GROOVES. ALUMINUM GAGE WIRE

81
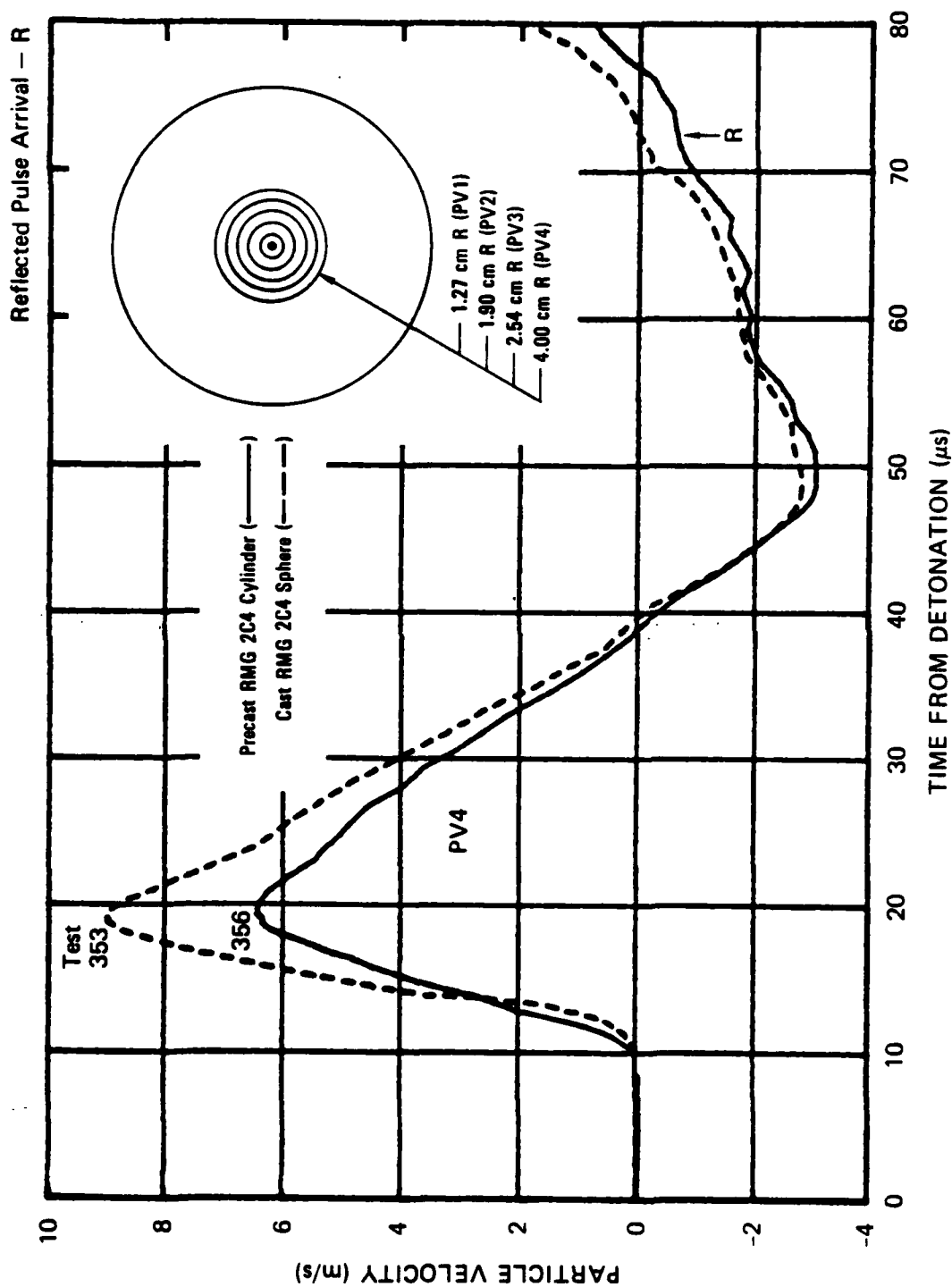
FIGURE 3.24 PARTICLE VELOCITY 4.00 cm FROM THE CENTER OF COUPLED EXPLOSIONS IN RMG 2C4 — CAST VERSUS PRECAST WITH NARROW GROOVES, ALUMINUM GAGE WIRE
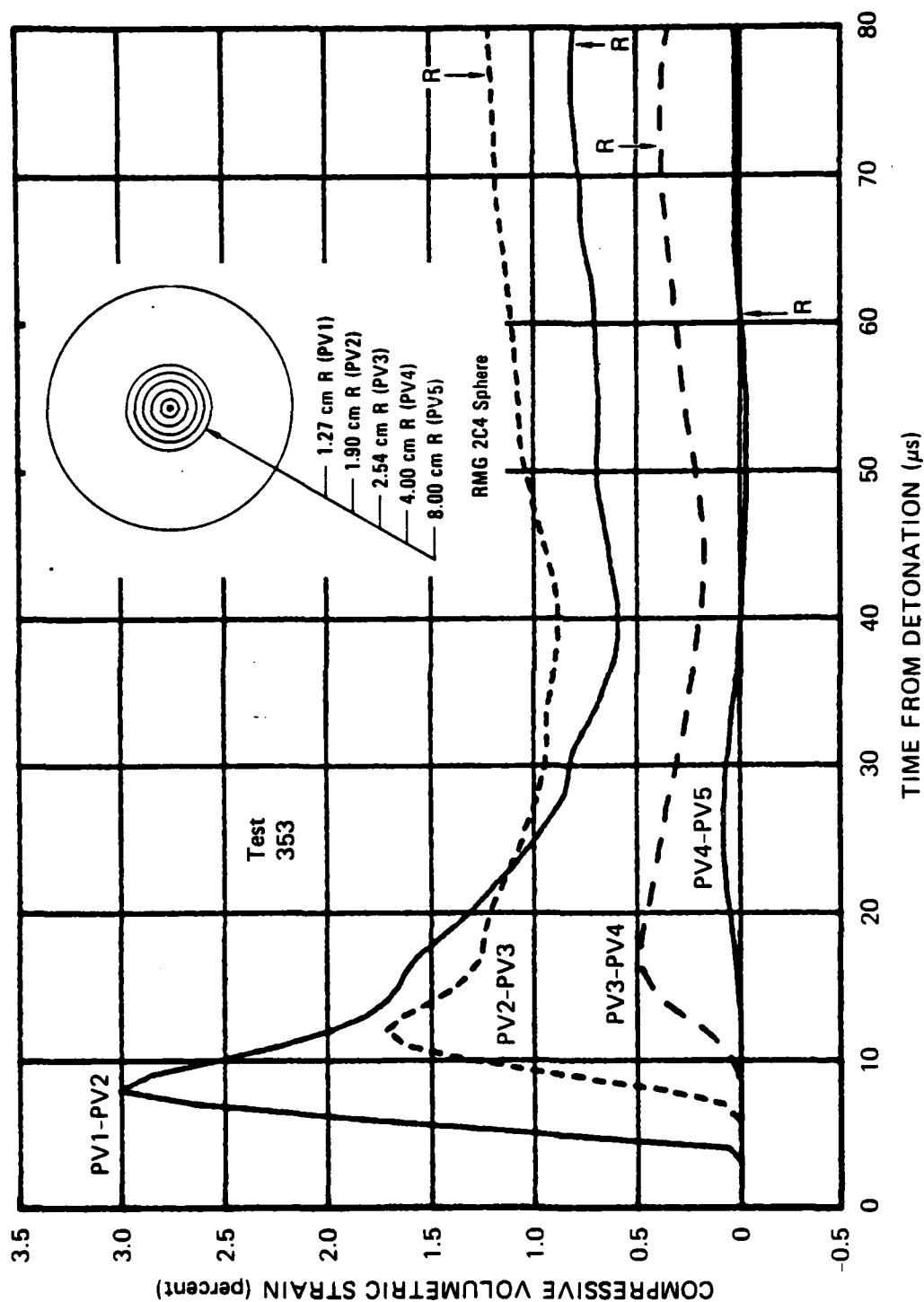
FIGURE 3.25   VOLUMETRIC STRAIN OBTAINED FROM A PARTICLE VELOCITY TEST IN RMG 2C4

JA-5372-140

83

Attenuation of peak particle velocity with range for RMG 2C4 is shown in Figure 3.26. The same attenuation curve applies to cast and precast material. Wavefront propagation distance versus time from detonation for RMG 2C4 is shown in Figure 3.27. A constant wave speed of 3.29 mm/µs applies over the range of the gages.

Series 5: Scaling Effects in RMG 2C4

Strain rate effects in RMG 2C4 were assessed by performing two particle velocity tests in which a nominal 3-g charge replaced the standard 3/8-g charge. The corresponding linear scale factor of 2.00 [i.e., $(3/0.375)^{1/3}$] was applied to the 3/8-g configuration to determine charge dimensions and gage locations for the 3-g tests. All tests were performed in 11-inch-diameter (27.94-cm) spheres.

The actual weight of explosive in the 3-g and 3/8-g charges was 3.14 g and 0.35 g, respectively. Hence, the corresponding linear scale factor of 2.08 [i.e., $(3.14/0.35)^{1/3}$] applies. To compare the 3-g and 3/8-g results, we first scaled the 3-g results in range and then in time. That is, if R represents the radius of a gage in the 3/8-g tests, then 2R represents the radius in the 3-g tests. However, the actual gage location should have been 2.08R in the 3-g tests. Hence, the particle velocity amplitudes at the 2R location were modified according to the attenuation for 2C4, as shown in Figure 3.26. The time in the 3-g tests was then scaled by a factor of 2.08.

Results of the 3-g tests (335 and 336), scaled to those of previous 3/8-g tests (272, 273, and 293), are shown in Figures 3.28 through 3.32. Hence, the gage locations shown (PV1 through PV5) are those in the 3/8-g tests. The attenuation factors used to scale the range in the 3-g tests were 0.936 (for gages PV1 and PV2) and 0.911 (for gages PV3, PV4, and PV5). In general, the 3-g and 3/8-g records show good agreement, indicating that the results may be scaled over the small range considered in these tests. One significant difference in the results is that the 3-g charge produces more displacement than the 3/8-g charge at gages PV3 (1.90 cm) and PV4 (2.54 cm), as shown in Figure A.5. However,
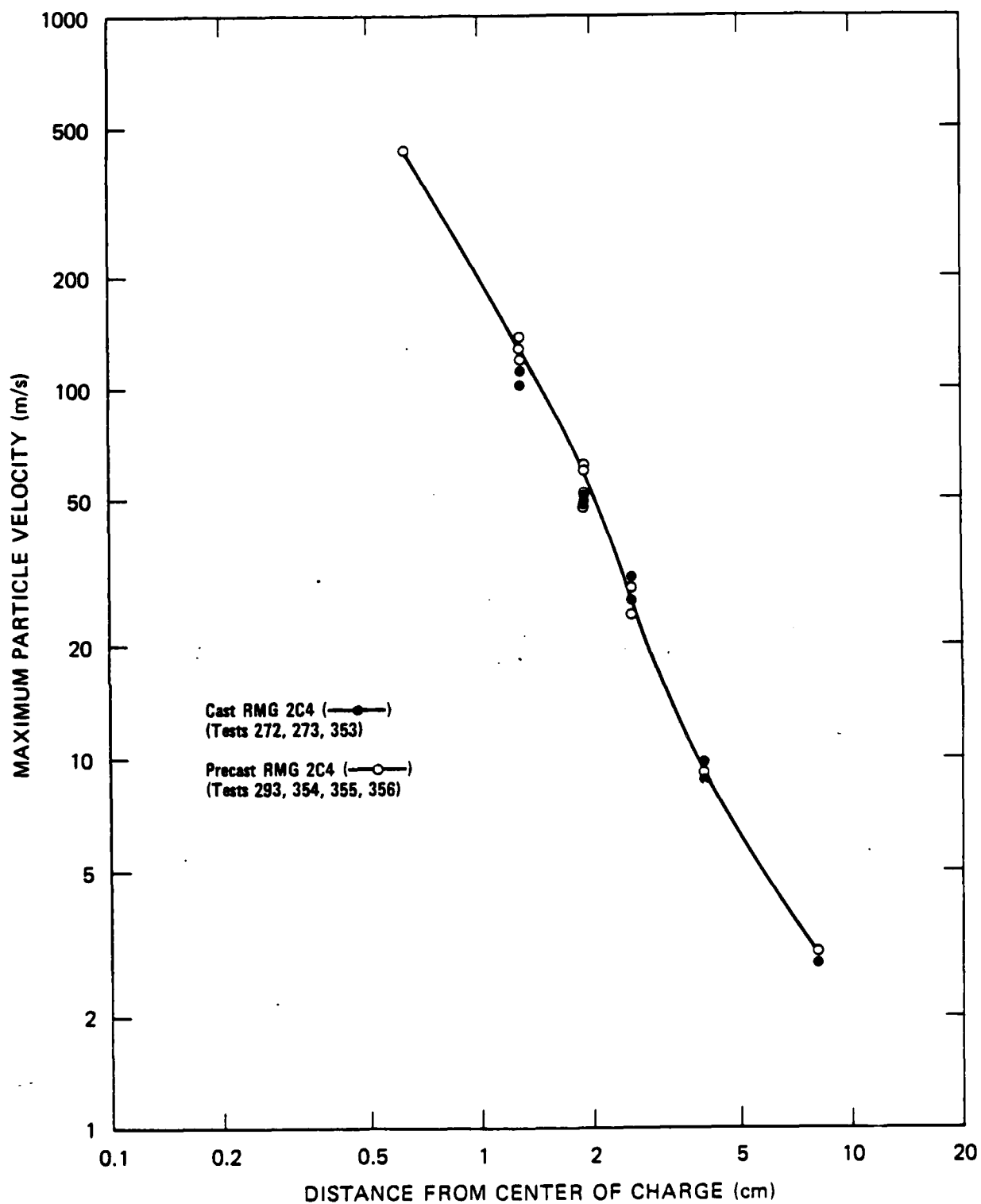
FIGURE 3.26   MAXIMUM PARTICLE VELOCITY VERSUS DISTANCE FROM CENTER OF CHARGE
FOR CAST AND PRECAST RMG 2C4
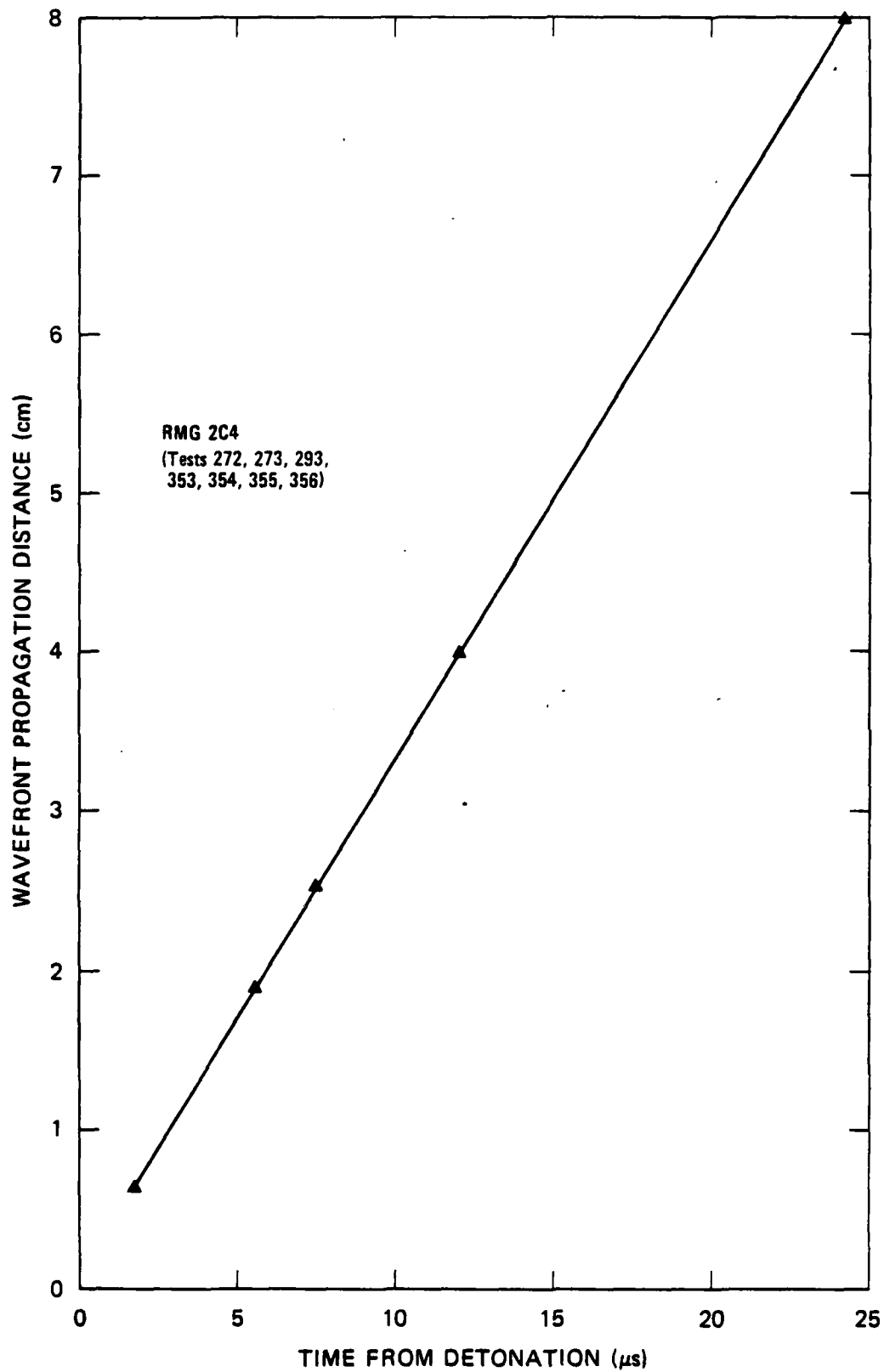
FIGURE 3.27   WAVEFRONT PROPAGATION DISTANCE VERSUS TIME FROM DETONATION
FOR RMG 2C4

JA-5372-102A

86
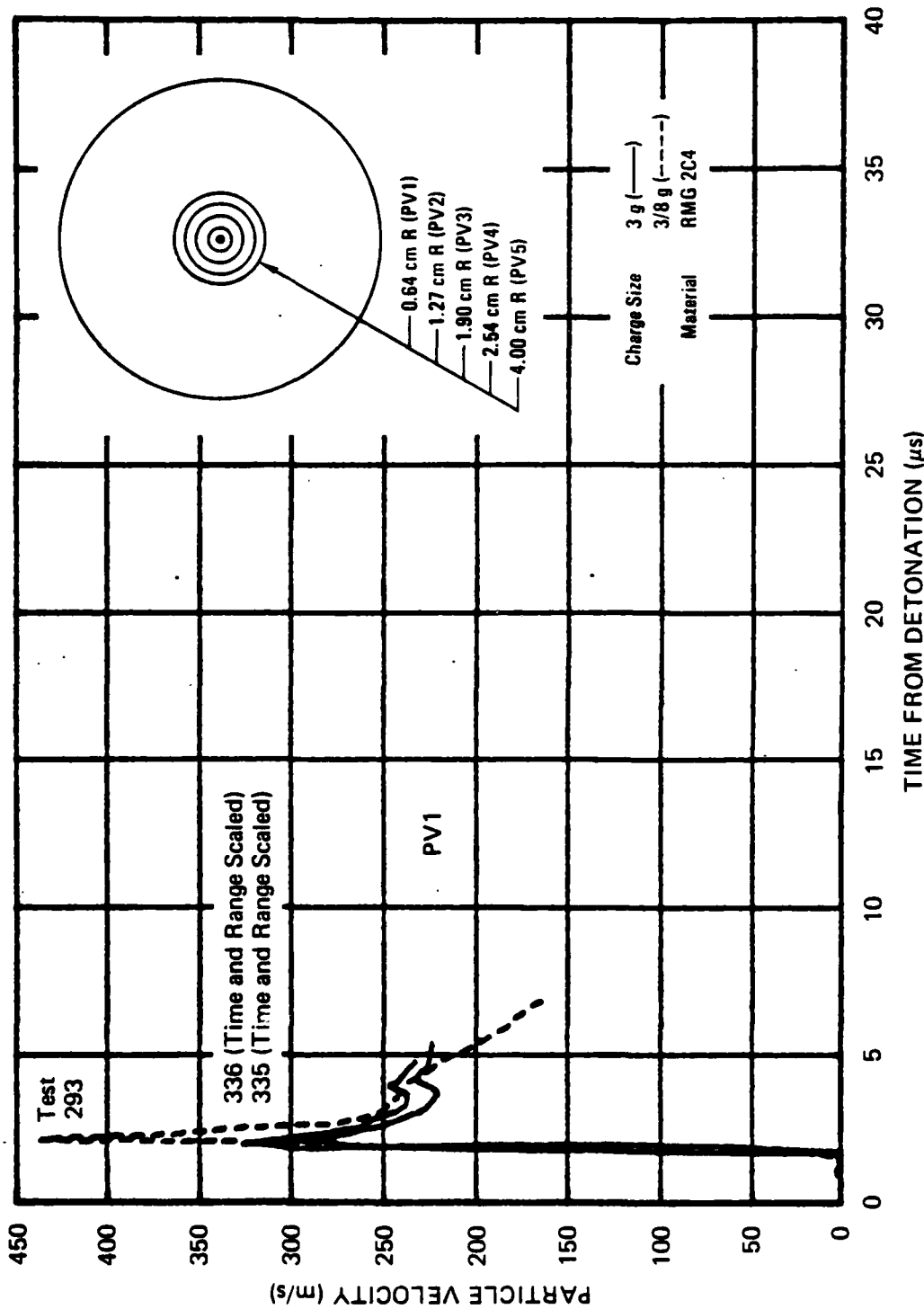
FIGURE 3.28 PARTICLE VELOCITY 0.64 cm FROM THE CENTER OF COUPLED EXPLOSIONS
IN RMG 2C4 – SCALING EFFECT (3 g PETN VERSUS 3/8 g PETN)

87
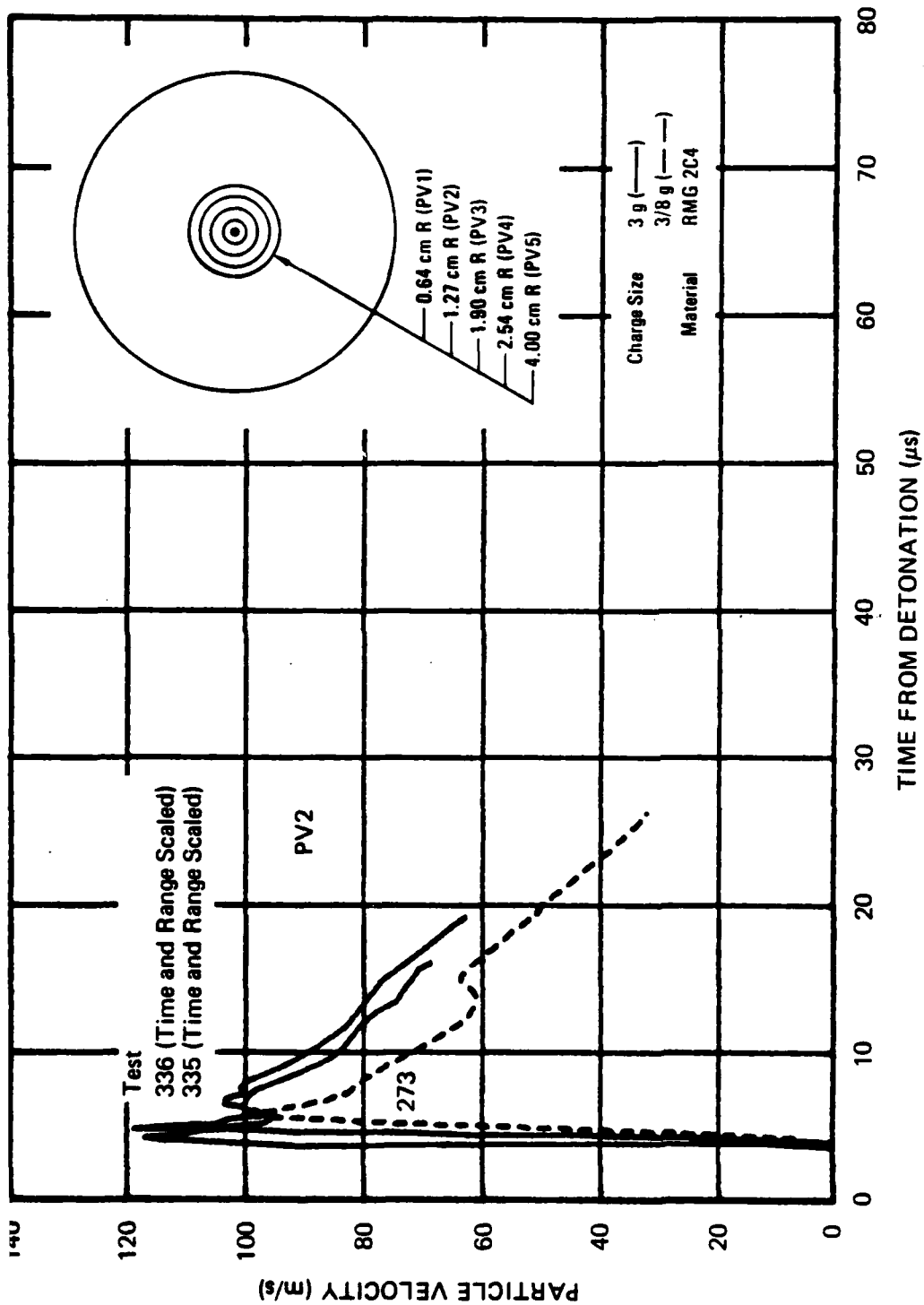
FIGURE 3.29 PARTICLE VELOCITY 1.27 cm FROM THE CENTER OF COUPLED EXPLOSIONS IN RMG 2C4 — SCALING EFFECT (3 g PETN VERSUS 3/8 g PETN)

88
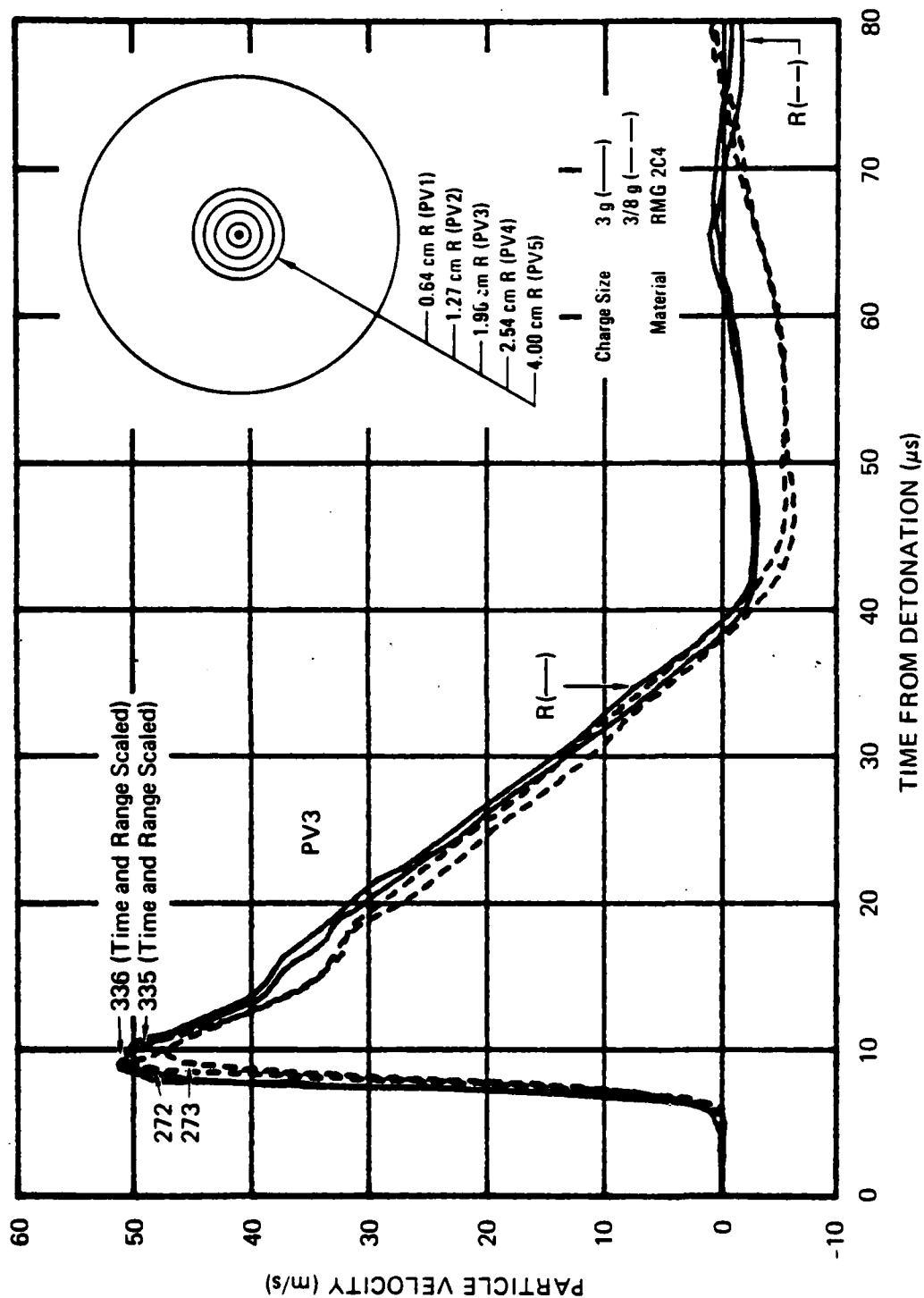
FIGURE 3.30 PARTICLE VELOCITY 1.90 cm FROM THE CENTER OF COUPLED EXPLOSIONS
IN RMG 2C4 — SCALING EFFECT (3 g PETN VERSUS 3/8 g PETN)
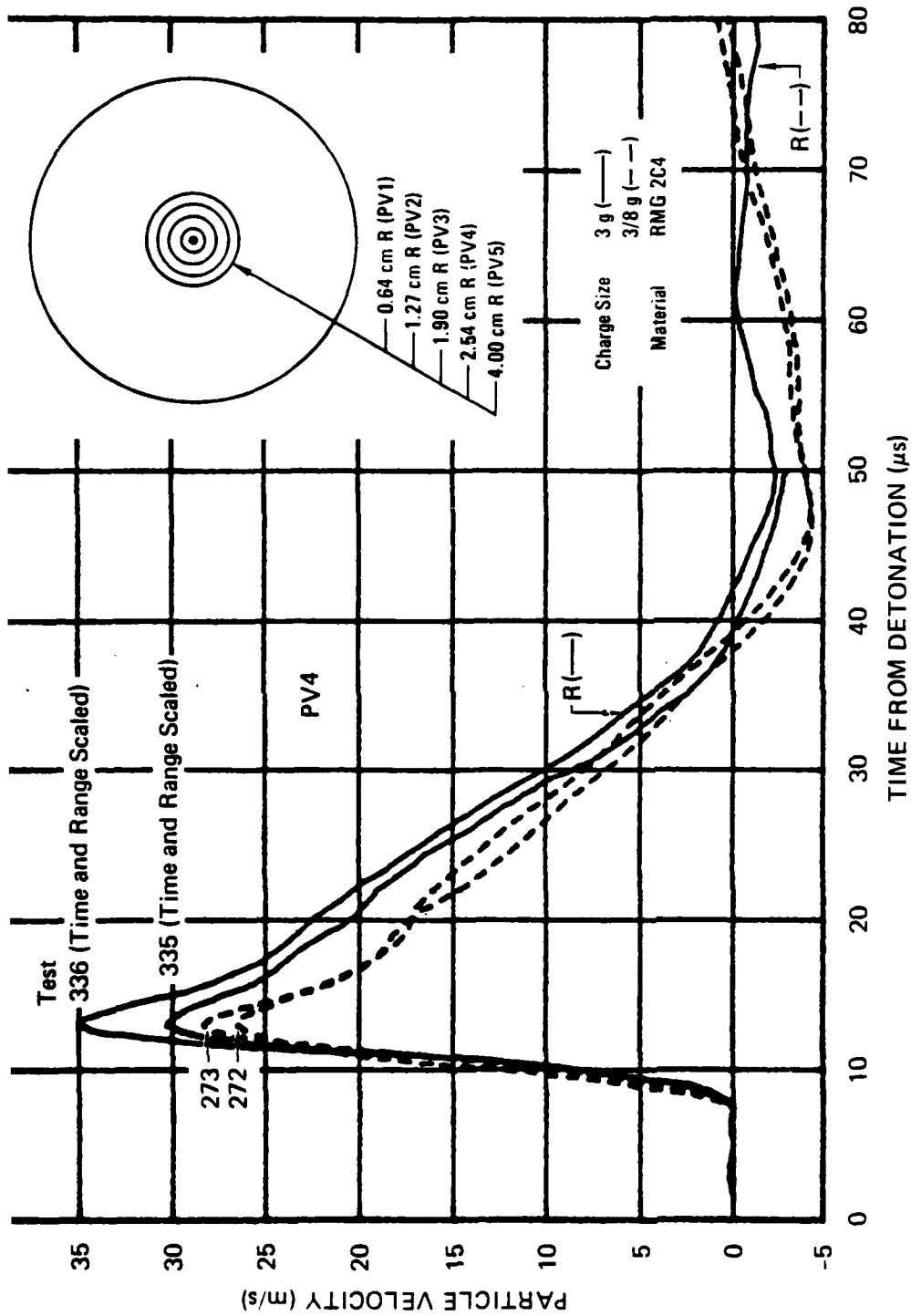
FIGURE 3.31   PARTICLE VELOCITY 2.54 cm FROM THE CENTER OF COUPLED EXPLOSIONS
IN RMG 2C4 – SCALING EFFECT (3 g PETN VERSUS 3/8 g PETN)

90
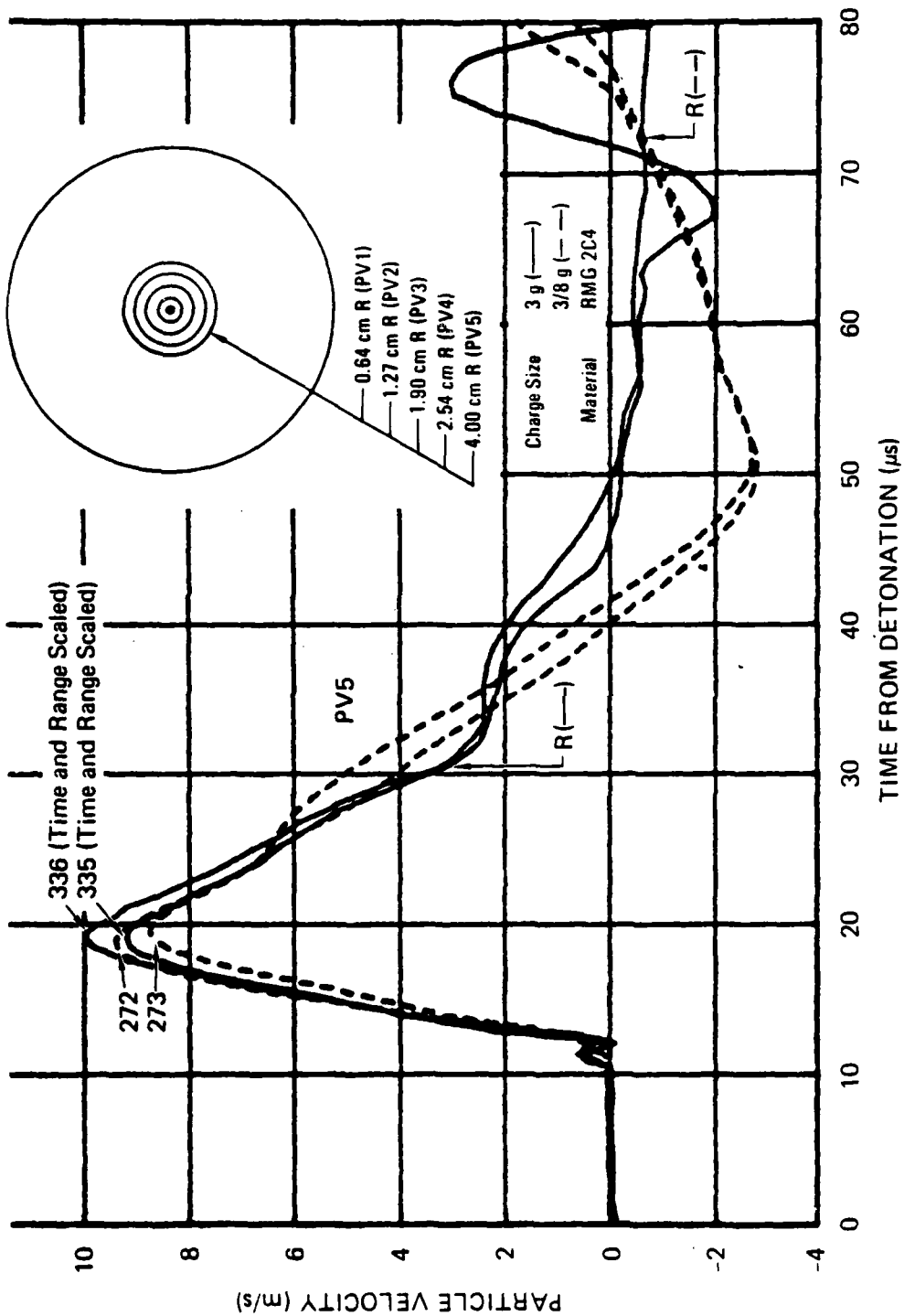
FIGURE 3.32 PARTICLE VELOCITY 4.00 cm FROM THE CENTER OF COUPLED EXPLOSIONS
IN RMG 2C4 — SCALING EFFECT (3 g PETN VERSUS 3/8 g PETN)
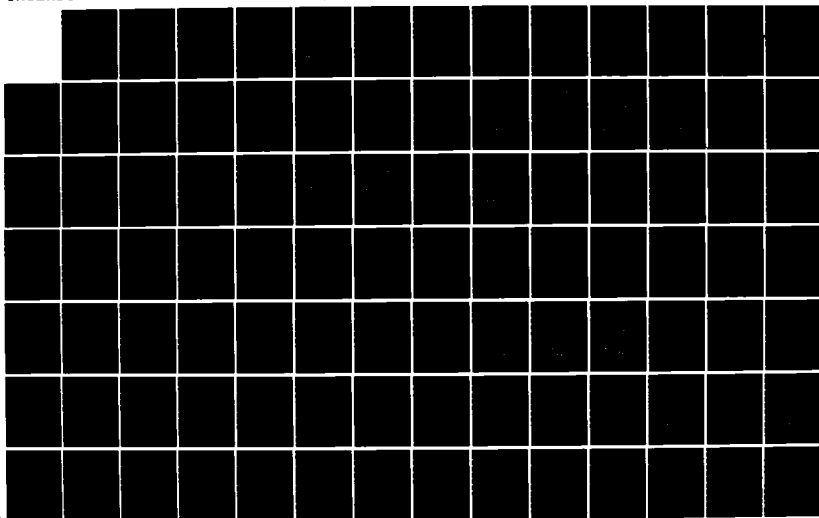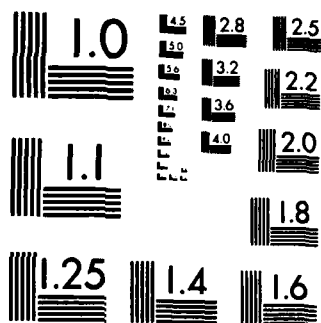
corresponding exploded cavity diameters were 1.656 inches (4.21 cm) and
0.808 inch (2.05 cm), and the resulting ratio (2.05) is in good agree-
ment with the scale factor (2.08). This is further evidence that the
results may be scaled.

Series 6: Material Property (SNLA G-Tunnel Tuff)

Cylindrical cores of G-tunnel tuff taken from near the working
point of a proposed SNLA 1-ton high explosives test were received from
the test site. The samples, which were 9.5 inches (24.13 cm) in
diameter, were cut to a length of 11 inches (27.94 cm) so that particle
velocity tests could be performed. The charge and gage installation
technique previously developed for geologic materials[10] was applied.
Gages were embedded at six radial locations (0.64, 1.27, 1.90, 2.54,
4.00, and 8.00 cm). Figures 3.33 through 3.38 show the resulting
particle velocity profiles for tests 340 and 341. For comparison,
results of previous tests (272, 273, and 293) on 11-inch-diameter
(27.94-cm) RMG 2C4 spheres or cylinders are included.

The particle velocity records for the tuff and RMG 2C4 are similar
during both outward and rebound phases of the motion. This result
indicates that the initial residual stress field surrounding exploded
cavities in these materials may be similar. However, estimates of
exploded cavity diameter based on integrated particle velocity records
(Figures A.1 and A.6) and an assumption of incompressibility yield
0.705 inch (1.79 cm) for the tuff and 0.739 inch (1.88 cm) for RMG 2C4.
Posttest measurements yield a smaller diameter of 0.688 inch (1.75 cm)
for the tuff but a larger diameter of 0.808 inch (2.05 cm) for RMG 2C4,
indicating permanent volumetric dilatation in the tuff and compression
in the RMG 2C4. Figure 3.39 shows permanent dilatation for tuff in the
region between gages PV1 and PV2. The smaller cavity in tuff results in
a higher cavity pressure, which increases the potential for cracking.
In fact, posttest examination revealed cracking along the plane of the
gages in test 341; however, no cracking was detected in test 340.
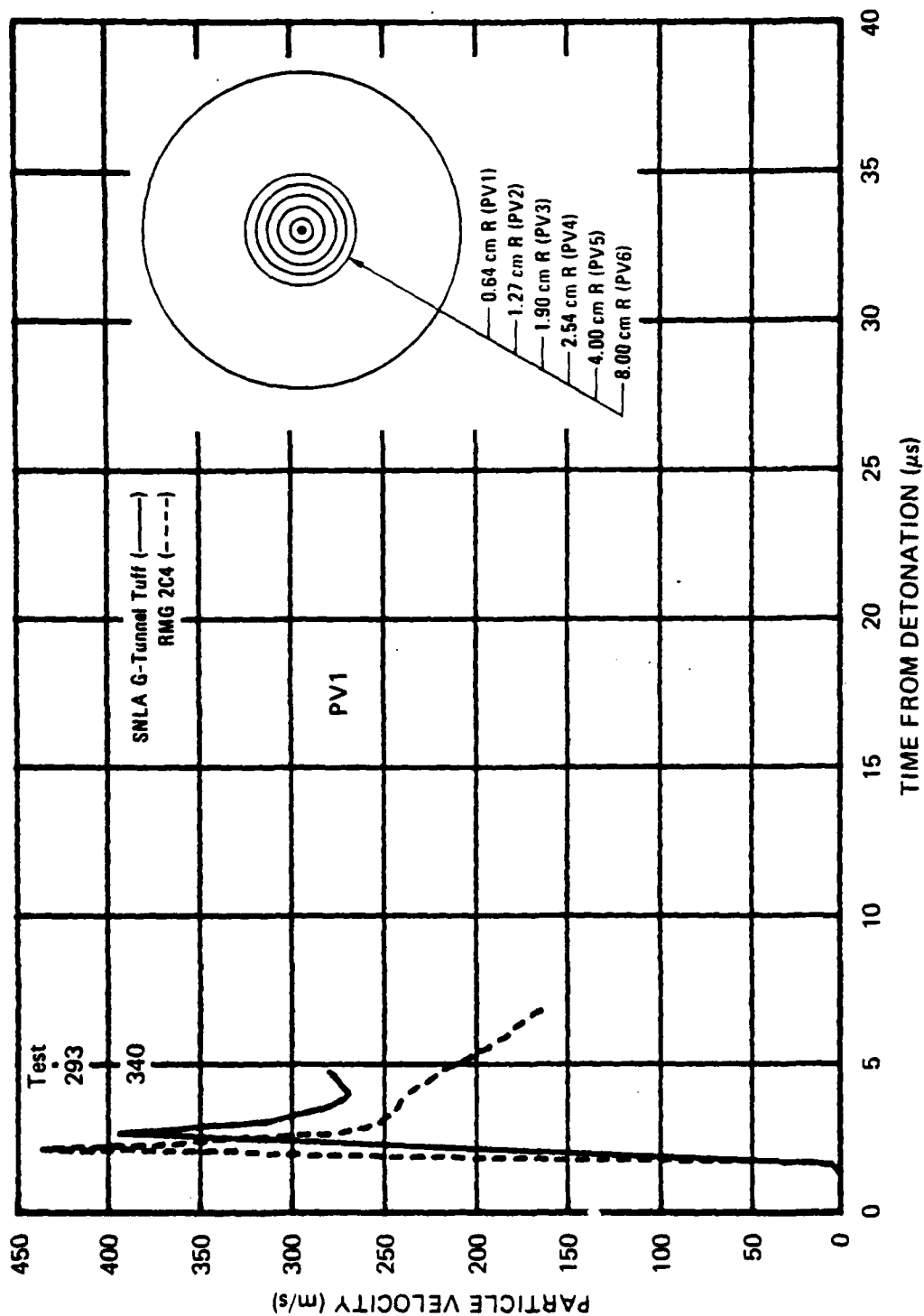
92

FIGURE 3.33   PARTICLE VELOCITY 0.64 cm FROM THE CENTER OF COUPLED EXPLOSIONS
IN SNLA G-TUNNEL TUFF AND RMG 2C4
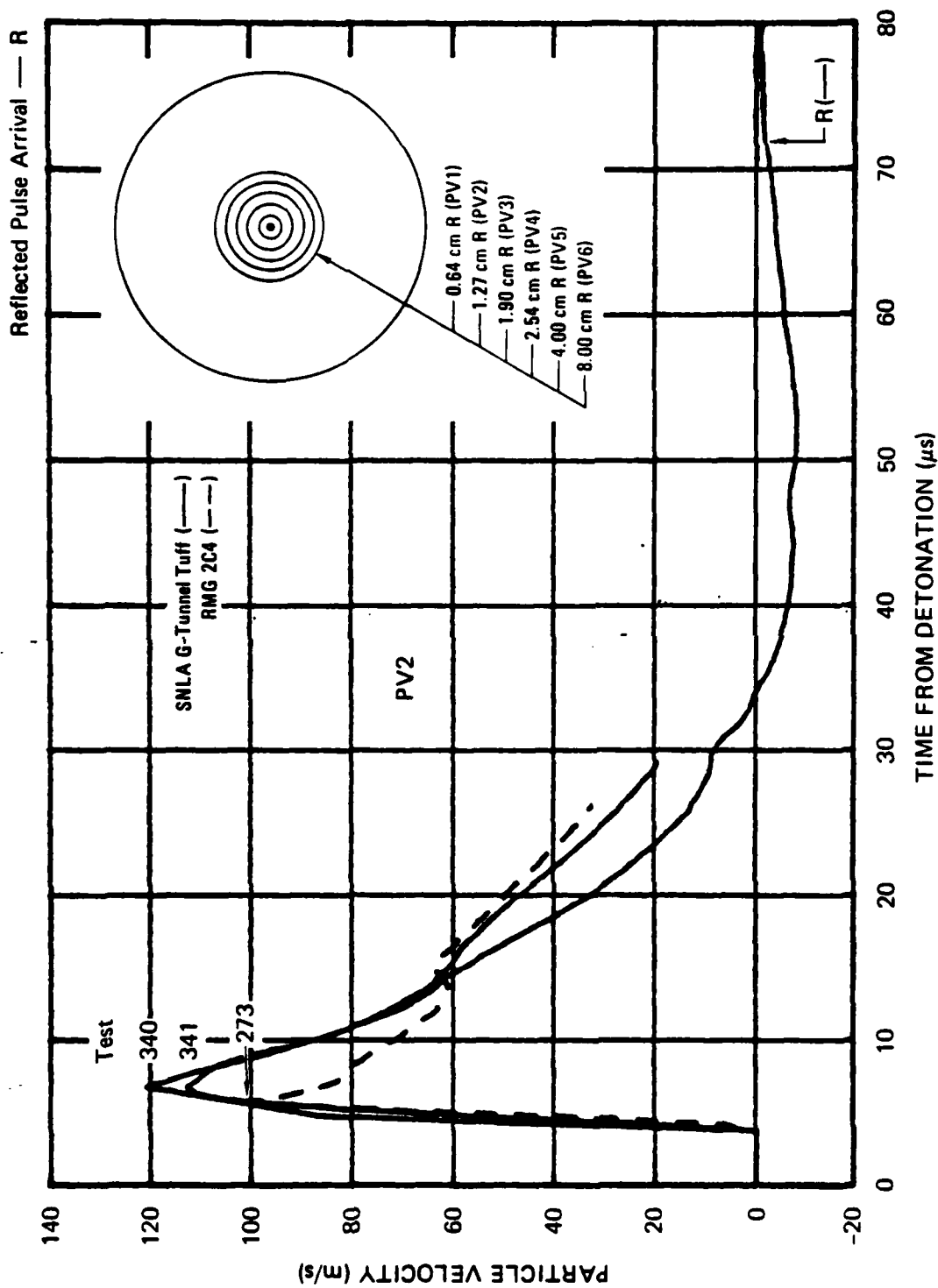
93

FIGURE 3.34   PARTICLE VELOCITY 1.27 cm FROM THE CENTER OF COUPLED EXPLOSIONS
IN SNLA G-TUNNEL TUFF AND RMG 2C4

JA-5372-13

94

FIGURE 3.35 PARTICLE VELOCITY 1.90 cm FROM THE CENTER OF COUPLED EXPLOSIONS IN SNLA G-TUNNEL TUFF AND RMG 2C4

95

FIGURE 3.36   PARTICLE VELOCITY 2.54 cm FROM THE CENTER OF COUPLED EXPLOSIONS
IN SNLA G-TUNNEL TUFF AND RMG 2C4

96

FIGURE 3.37   PARTICLE VELOCITY 4.00 cm FROM THE CENTER OF COUPLED EXPLOSIONS
IN SNLA G-TUNNEL TUFF AND RMG 2C4

JA-5372-16

97

FIGURE 3.38   PARTICLE VELOCITY 8.00 cm FROM THE CENTER OF COUPLED EXPLOSIONS
IN SNLA G-TUNNEL TUFF

98
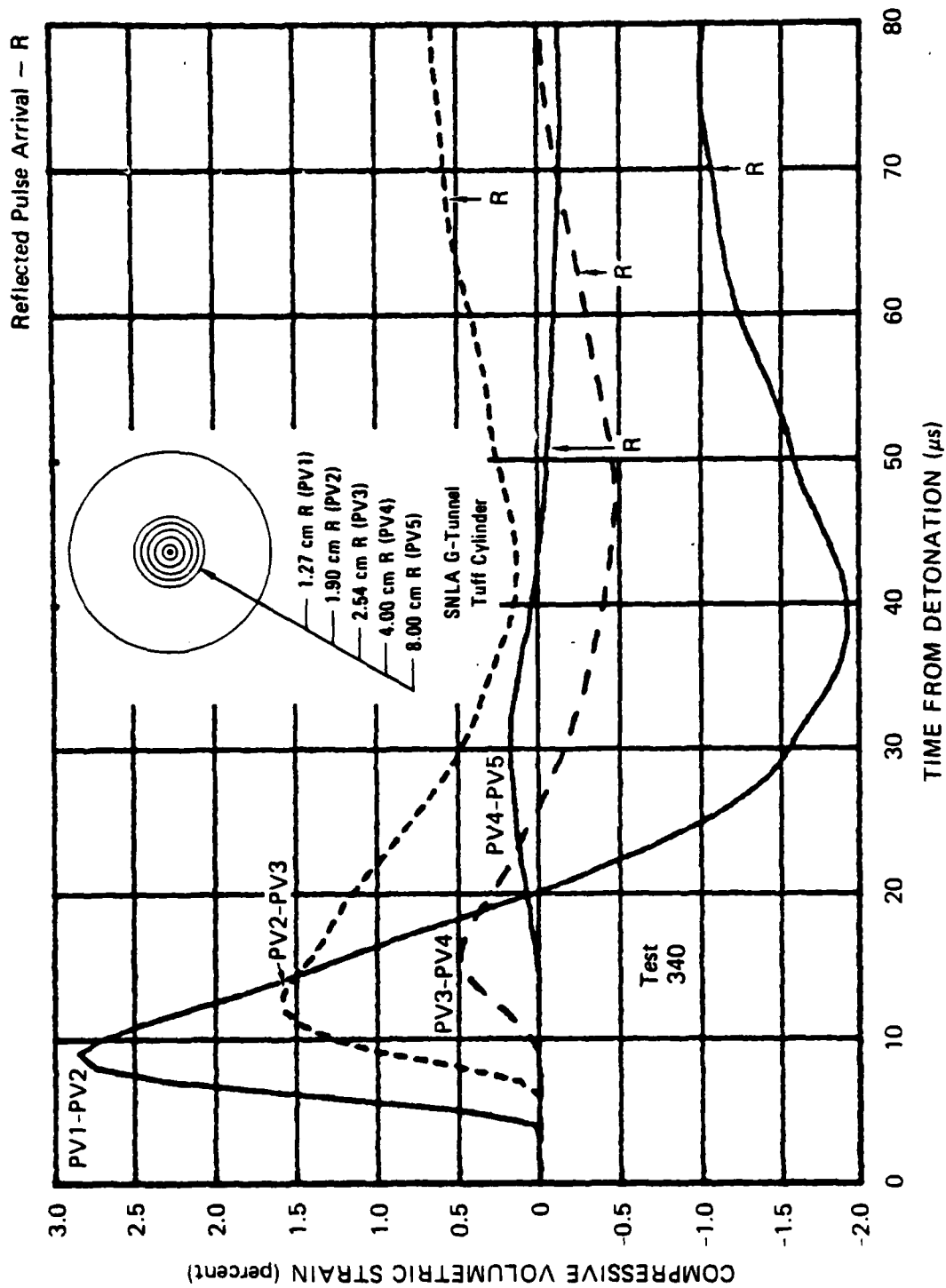
FIGURE 3.39 VOLUMETRIC STRAIN OBTAINED FROM A PARTICLE VELOCITY TEST IN SNLA G-TUNNEL TUFF

JA-5372-139

99

Because the records for these two tests are similar, cracking apparently had negligible influence on the dynamic response.

The absence of rebound at gage PV3 (Figure 3.35) in test 341 is attributed to a possible break in the gage at the end of the outward motion.

As shown in Figure 3.40, attenuations of peak velocity for the tuff and RMG 2C4 are similar over most of the range covered by the gages. Figure 3.41 shows the time of arrival of the wave front at each gage location. A constant wave speed of 3.16 mm/μs for the tuff and 3.29 mm/μs for RMG 2C4 applies over the range of the gages.

Pressure records in the overburden fluid obtained from quartz gage measurements are shown in Figure B.4. The similarity in pressure pulses of the tuff and RMG 2C4 is consistent with the similarity of the particle velocity records.

Series 7: Material Property (P-Tunnel Tuff)

One 12-inch-diameter (30.48-cm) cylindrical core of P-tunnel tuff received from the test site was recored to a diameter of 9-5/8 inches (24.45 cm) and cut to a length of 11 inches (27.94 cm) so that a particle velocity test could be performed. The charge and gage installation technique previously developed for geologic materials[10] was applied. Gages were embedded at five radial locations (1.27, 1.90, 2.54, 4.00, and 8.00 cm). Figures 3.42 through 3.46 show the resulting particle velocity profiles for test 350. For comparison, results of previous tests (340 and 341, Series 6) on 9-1/2-inch-diameter (24.13-cm) SNLA G-tunnel tuff tuff cylinders are included.

Peak velocity and duration of outward motion are greater for the P-tunnel tuff, but the rebound velocity is comparable for the two materials. These results are consistent with the measured exploded cavity diameter of 0.844 inch (2.14 cm) for P-tunnel tuff and 0.688 inch (1.75 cm) for G-tunnel tuff. An estimate of exploded cavity diameter for P-tunnel tuff based on the integrated particle velocity record of

100
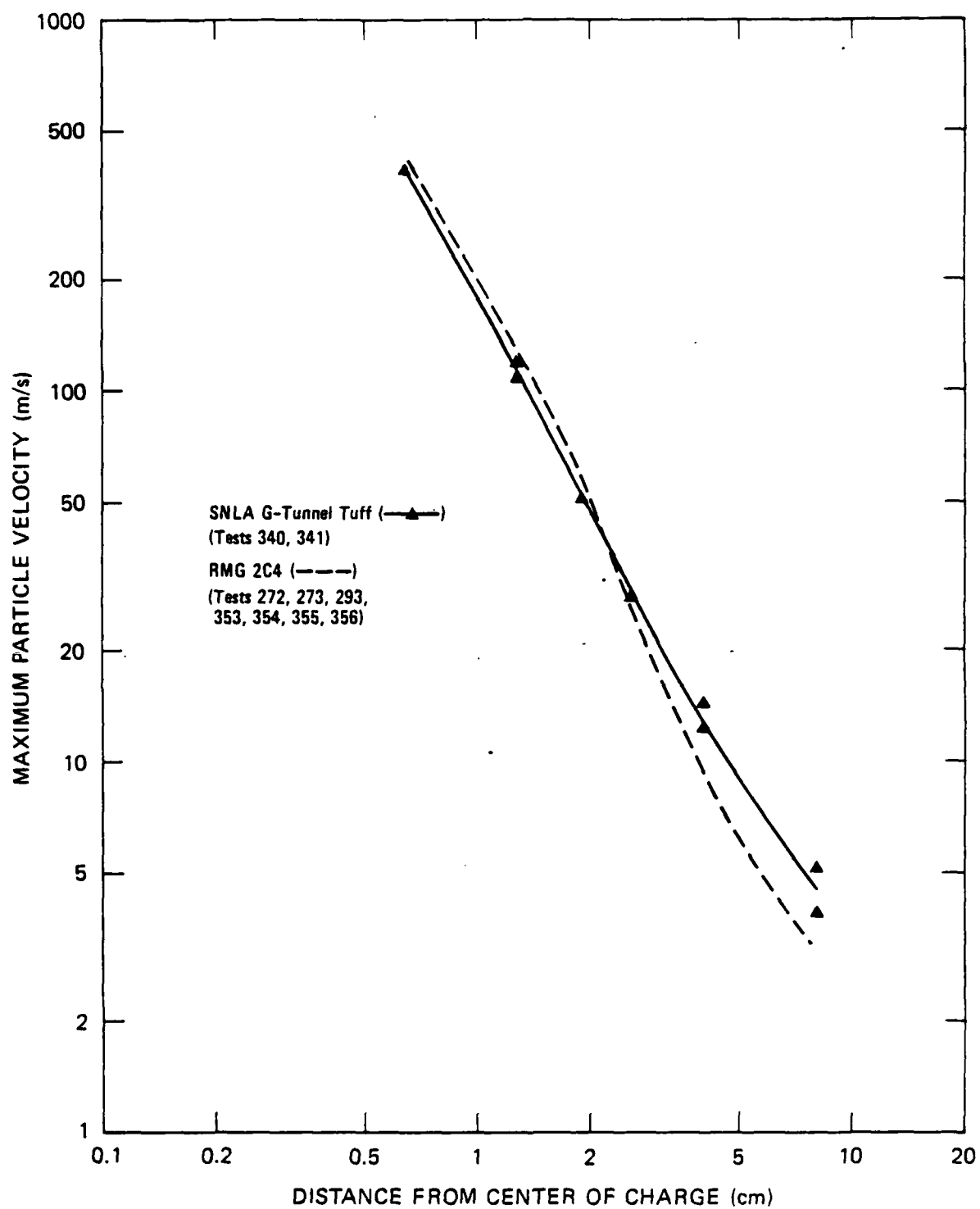
FIGURE 3.40   MAXIMUM PARTICLE VELOCITY VERSUS DISTANCE FROM CENTER
OF CHARGE FOR SNLA G-TUNNEL TUFF AND RMG 2C4

JA-3876-95A
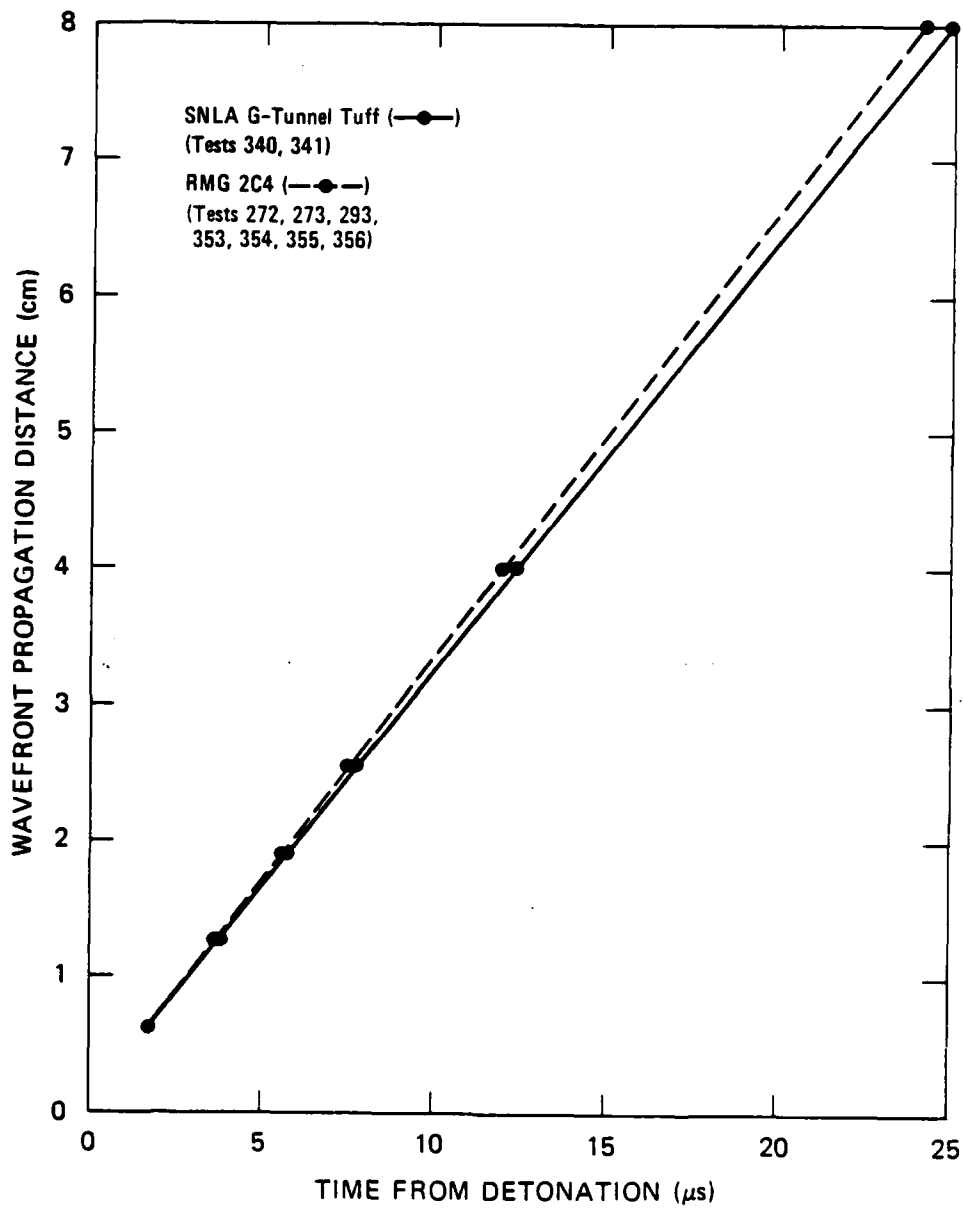
FIGURE 3.41   WAVEFRONT PROPAGATION DISTANCE VERSUS TIME FROM DETONATION
FOR RMG 2C4 AND SNLA G-TUNNEL TUFF

JA-5372-43

102
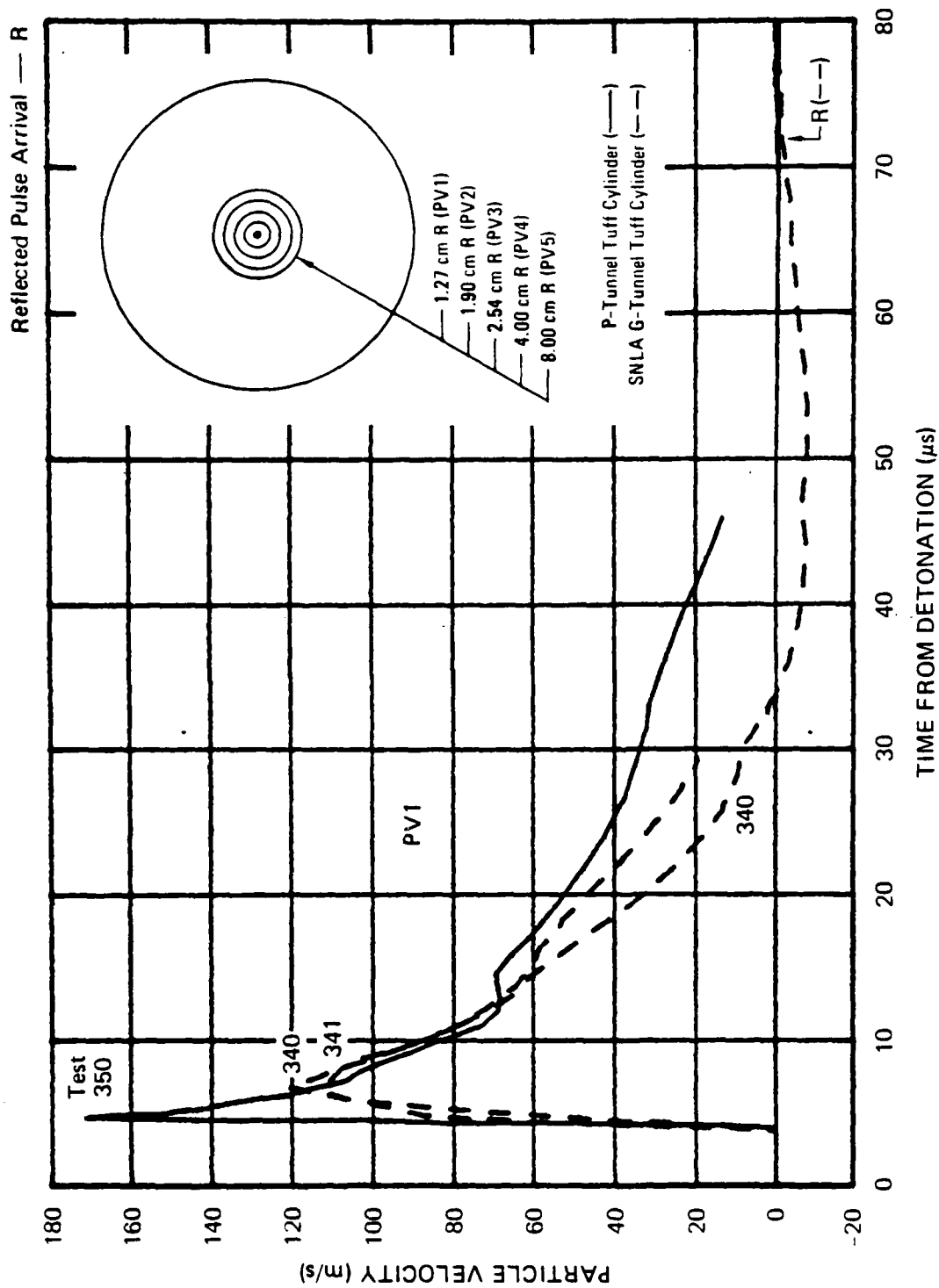
FIGURE 3.42 PARTICLE VELOCITY 1.27 cm FROM THE CENTER OF COUPLED EXPLOSIONS IN TUFF (P-TUNNEL AND SNLA G-TUNNEL)

JA-5372-24

103
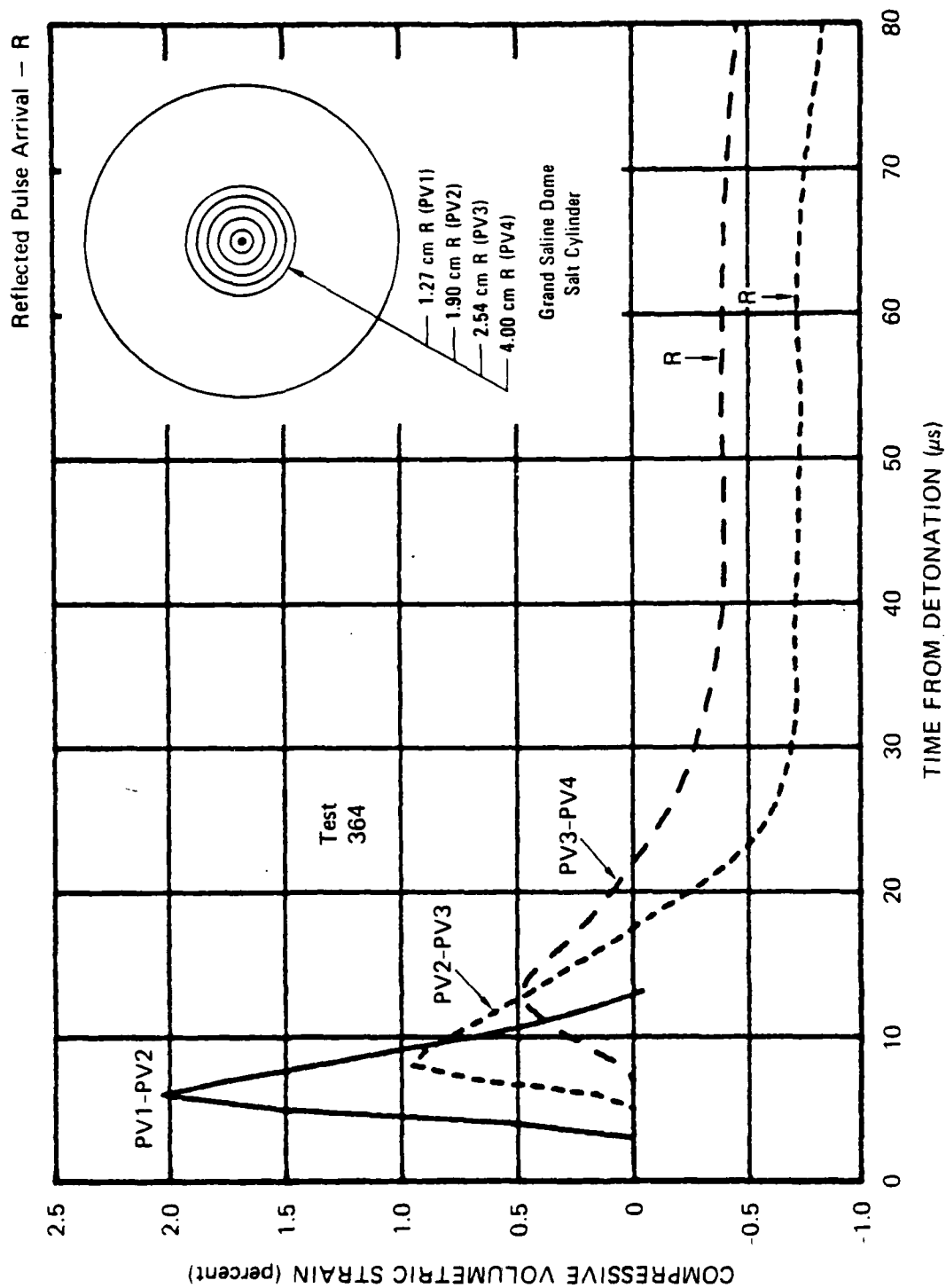
FIGURE 3.54 VOLUMETRIC STRAIN OBTAINED FROM A PARTICLE VELOCITY TEST IN SALT

JA-5372-141

117

velocity for salt. This lack of rebound is attributed to the dynamic radial cracks that reduce the restoring circumferential component of stress. Posttest examination of the salt cylinders revealed blackened fracture surfaces (three in test 364 and four in test 365) extending about 2 inches (5.08 cm) from the cavity.

An estimate of exploded cavity diameter for salt is 0.699 inch (1.78 cm), based on the integrated particle velocity record of PV2 (Figure A.8) and an assumption of incompressibility. The measured value is 0.625 inch (1.59 cm). A calculated diameter larger than the measured value implies an apparent dilatancy of the material behind the wavefront. This dilatancy is shown in Figure 3.54 and is attributed to the observed dynamic cracking.

Figure 3.55 shows the decay of peak velocity with range for salt and RMG 2C4. Near the charge, the rate of attenuation for these materials is comparable. As the distance from the charge increases, however, attenuation becomes more pronounced in RMG because of the greater energy absorbed in closing pores.

Figure 3.56 shows the time of arrival of the wavefront at each gage location for salt and RMG. A constant wave speed of 3.56 mm/μs for salt and 3.29 mm/μs for RMG applies over the range of the gages. Note, however, that a shock wave speed of 4.40 mm/μs applies to salt between the charge and gage PV1.

Series 9A: Technique Improvements for Hard Rock (Granite)

Three 1-foot cubes of California grey/white granite were cored to a diameter of 9-5/8 inches (24.45 cm) so that particle velocity tests could be performed. The standard charge and gage installation technique previously developed for geologic materials[10] was applied. Gages were epoxied in grooves 40 mils (1.02 mm) wide and 40 mils (1.02 mm) deep at five radial locations (1.27, 1.90, 2.54, 4.00, and 8.00 cm). Figures 3.57 through 3.61 show the resulting particle velocity profiles for tests 349, 351, and 352.

116
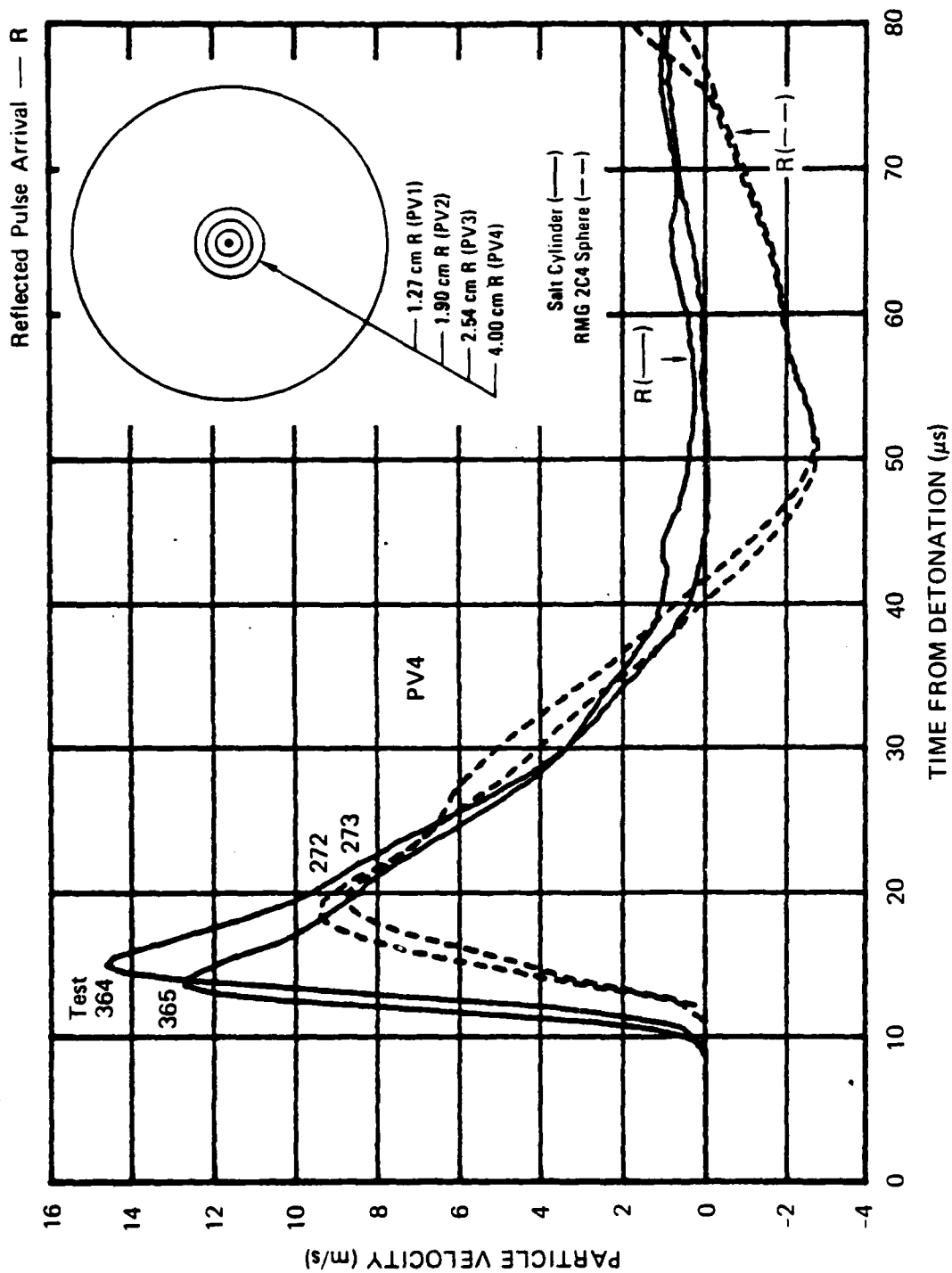
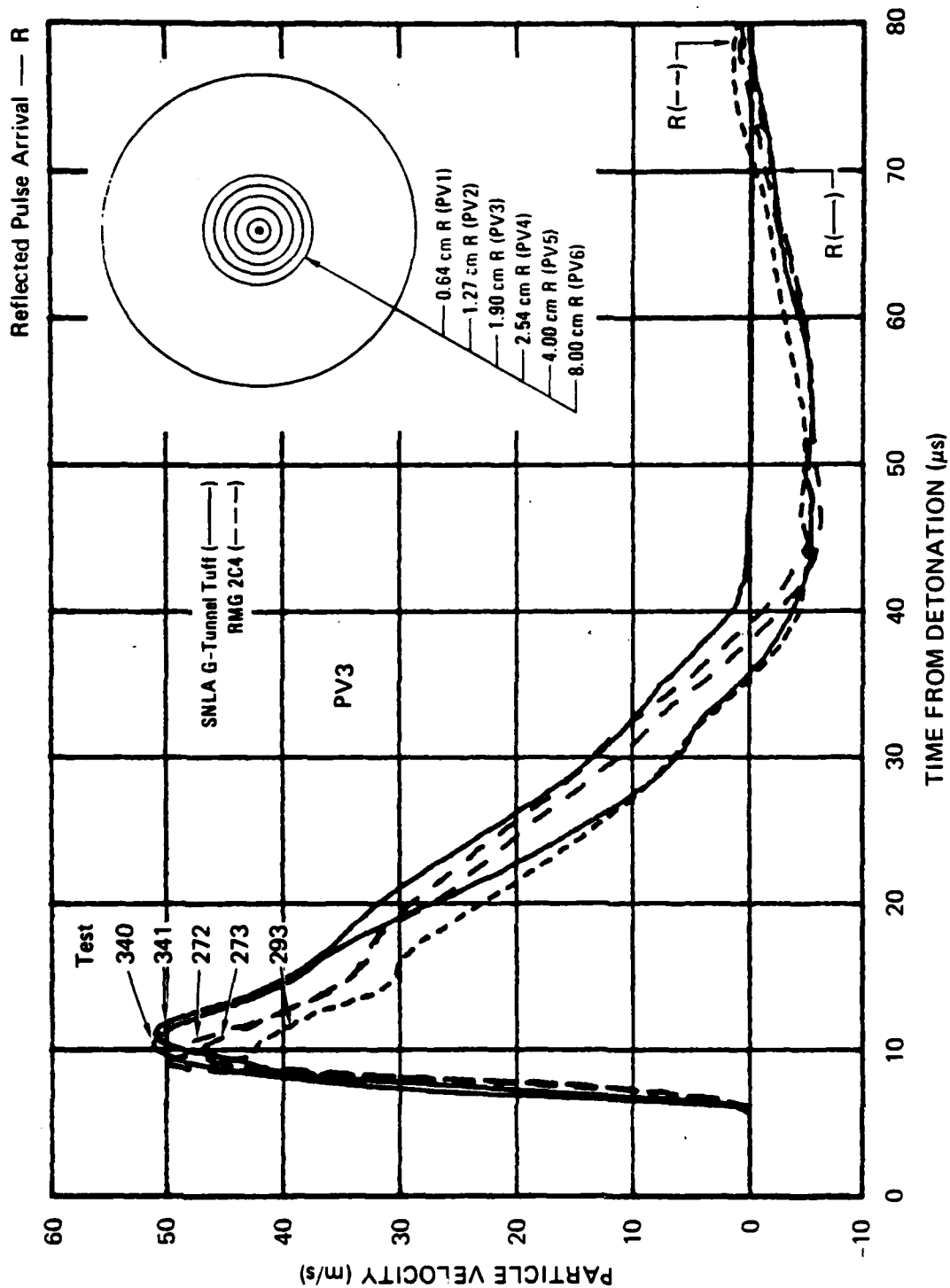FIGURE 3.53 PARTICLE VELOCITY 4.00 cm FROM THE CENTER OF COUPLED EXPLOSIONS IN SALT AND RMG 2C4

JA-5372-33

115
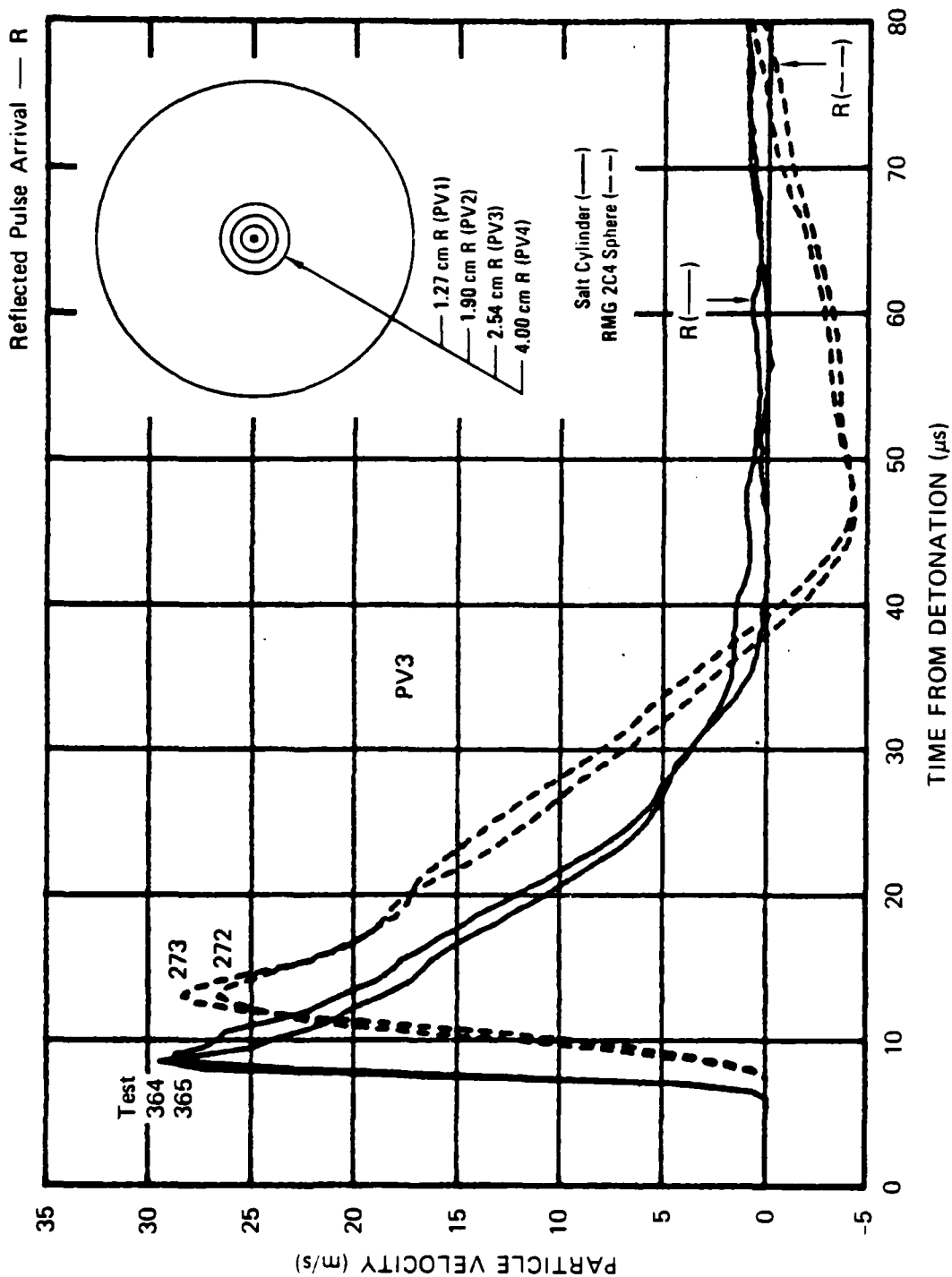
FIGURE 3.52 PARTICLE VELOCITY 2.54 cm FROM THE CENTER OF COUPLED EXPLOSIONS
IN SALT AND RMG 2C4

JA-5372-32

114
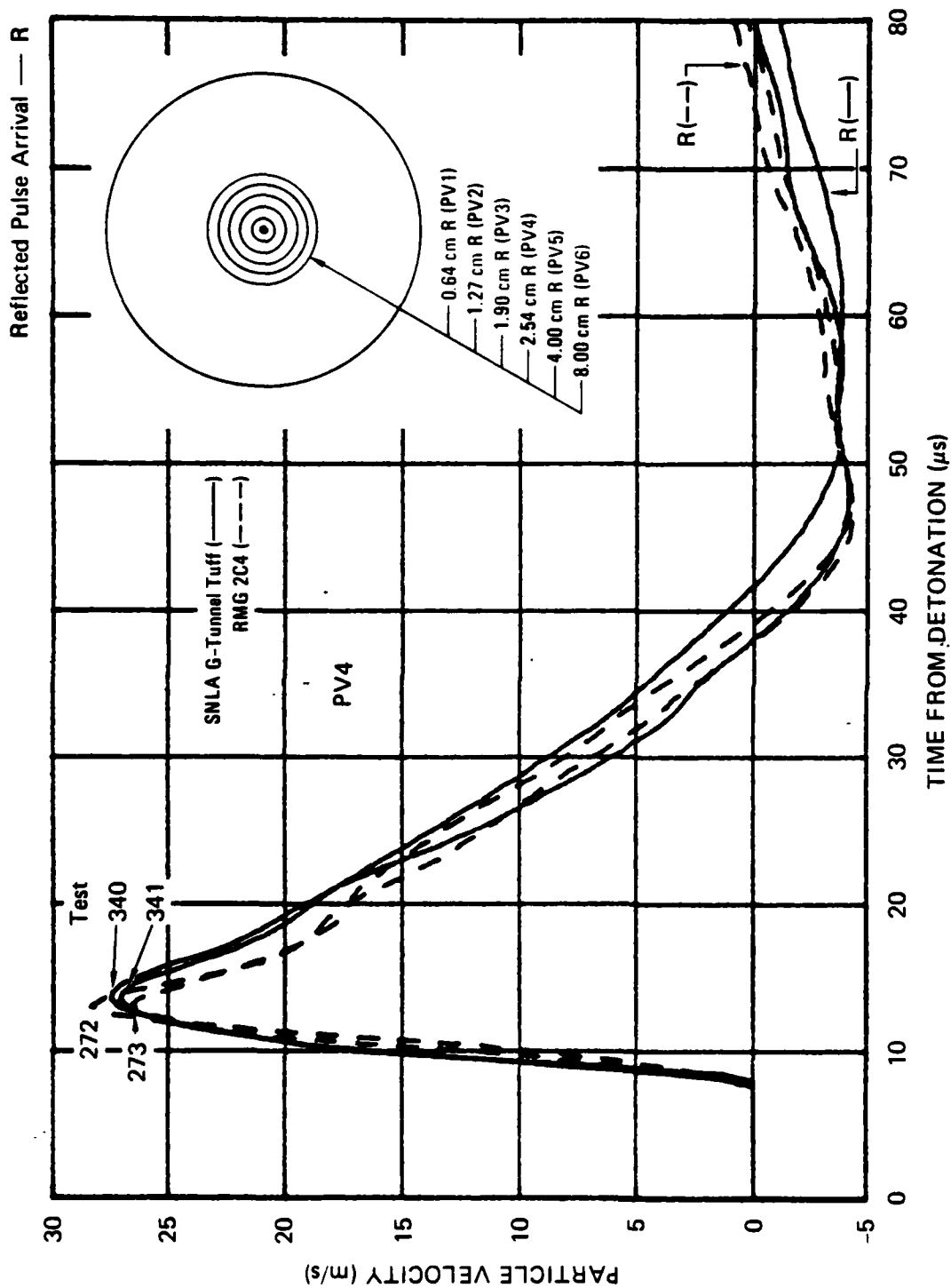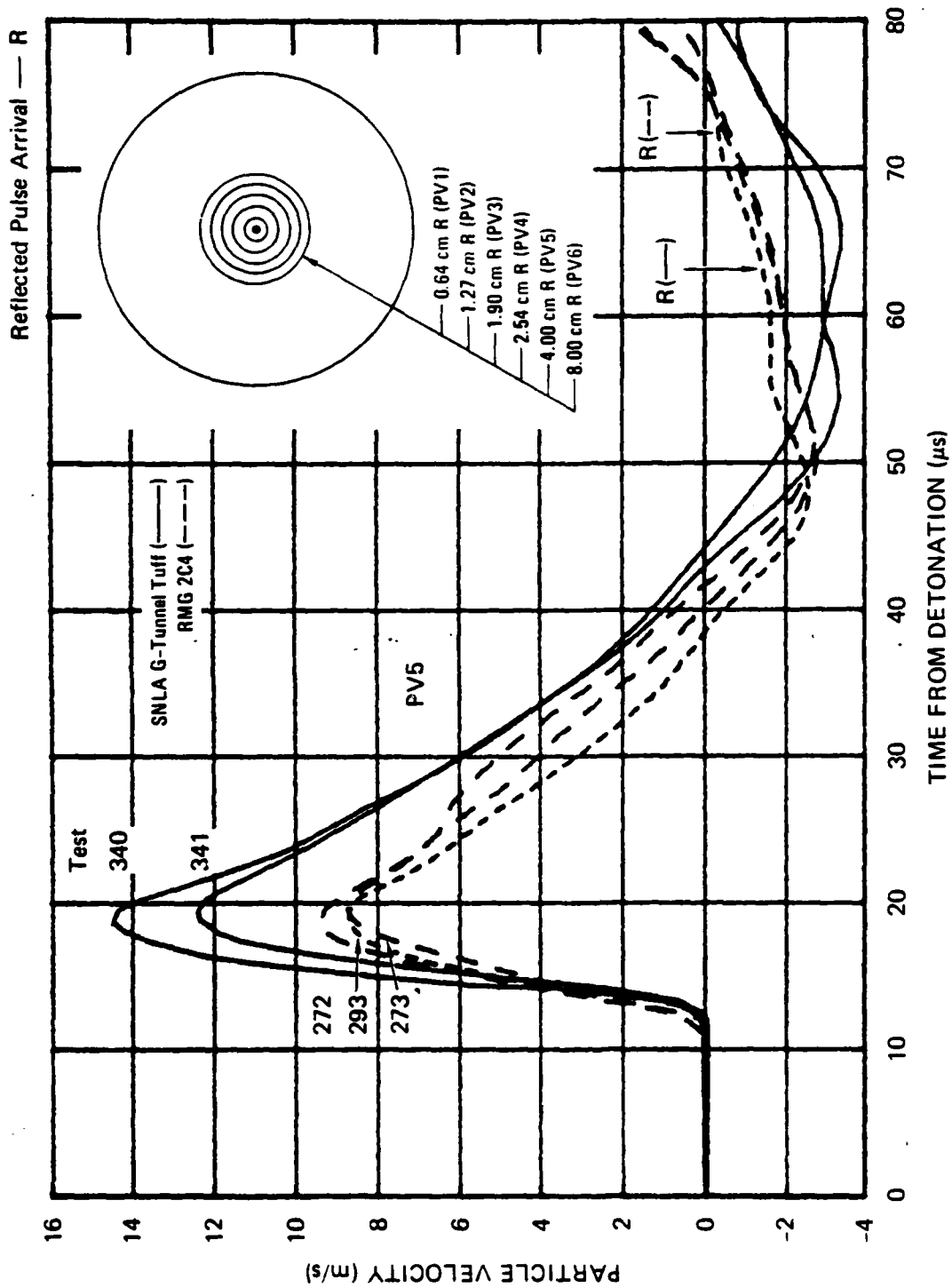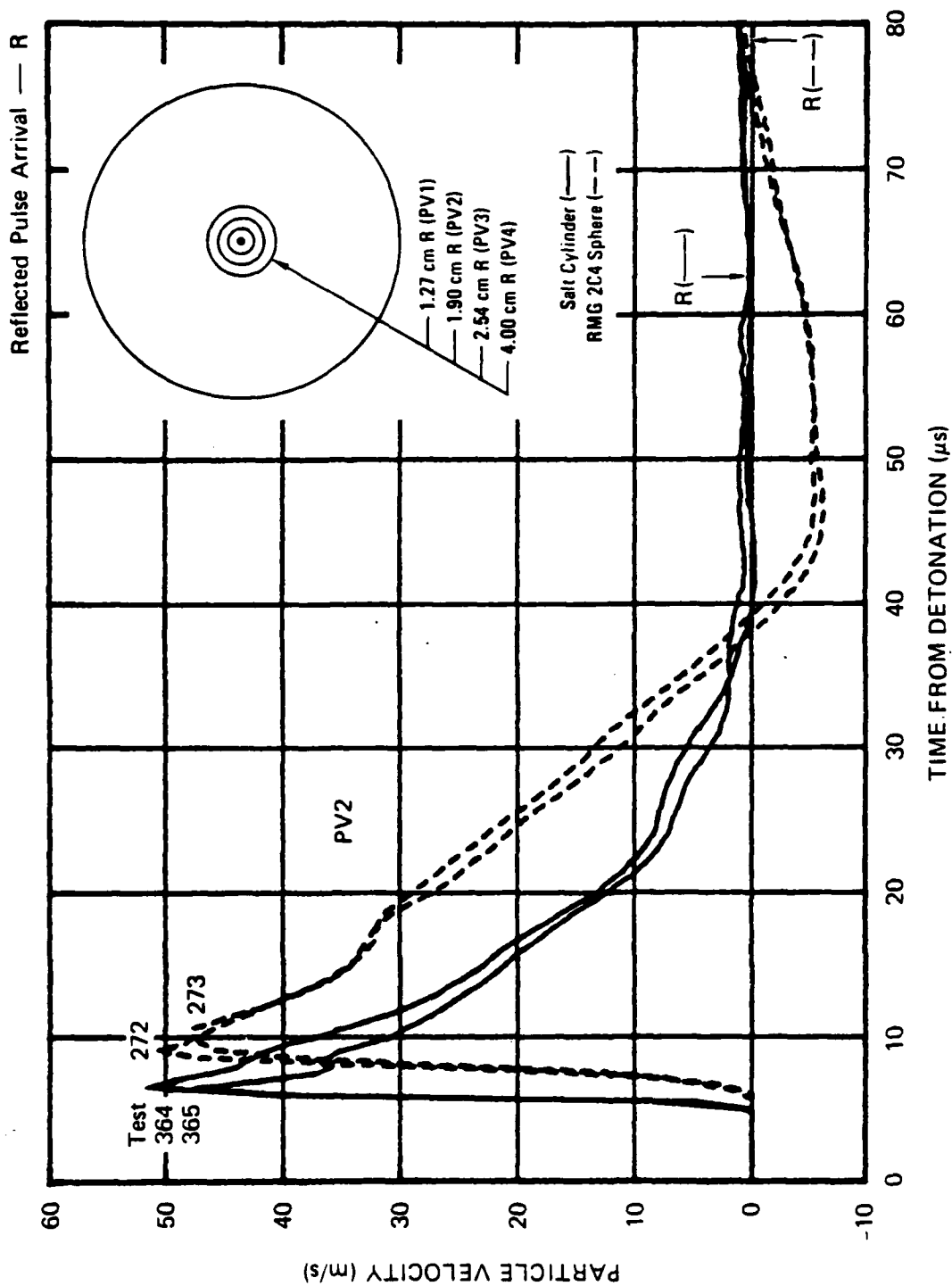
FIGURE 3.51 PARTICLE VELOCITY 1.90 cm FROM THE CENTER OF COUPLED EXPLOSIONS IN SALT AND RMG 2C4

JA-5372-31

113

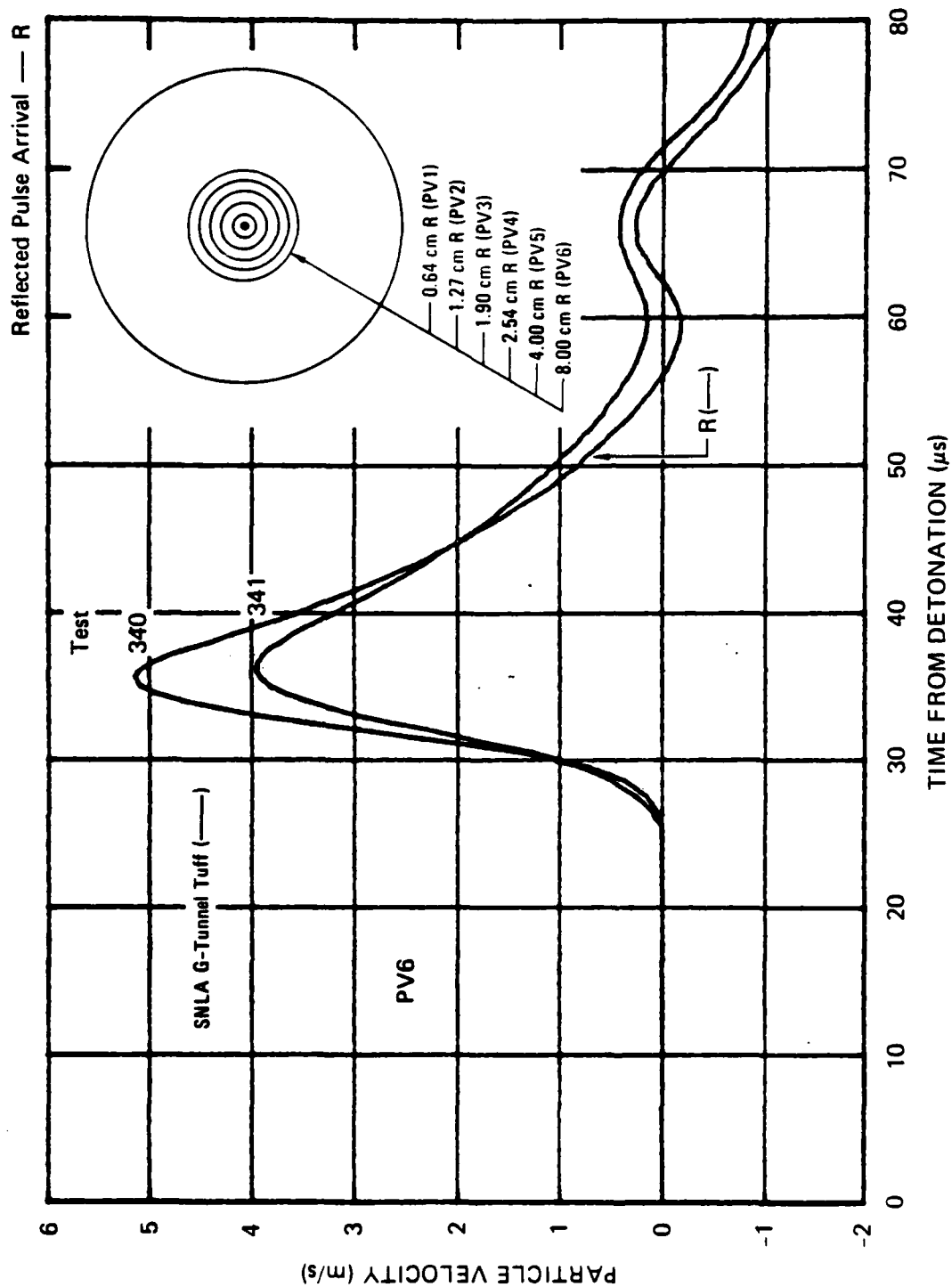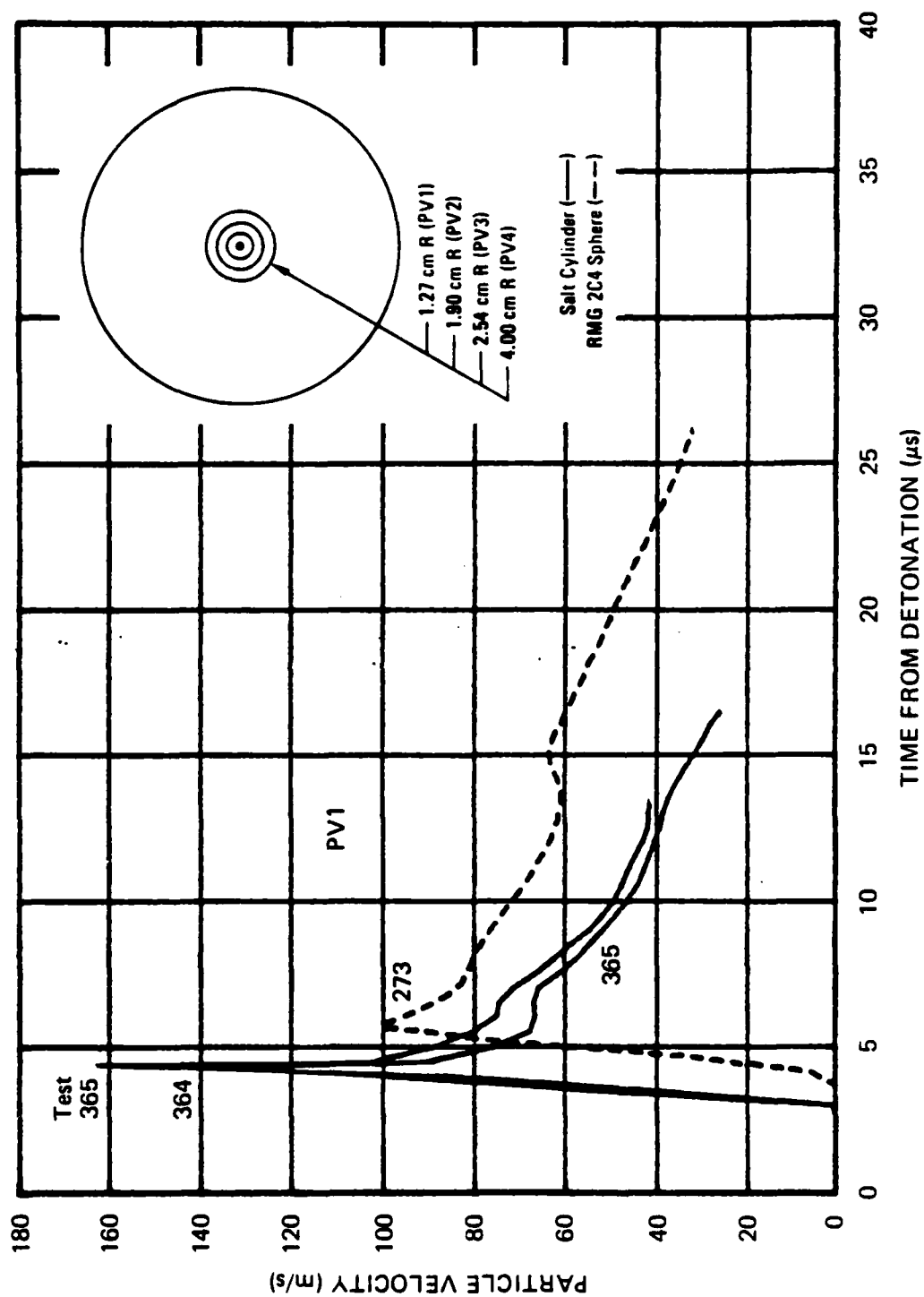FIGURE 3.50 PARTICLE VELOCITY 1.27 cm FROM THE CENTER OF COUPLED EXPLOSIONS IN SALT AND RMG 2C4

112
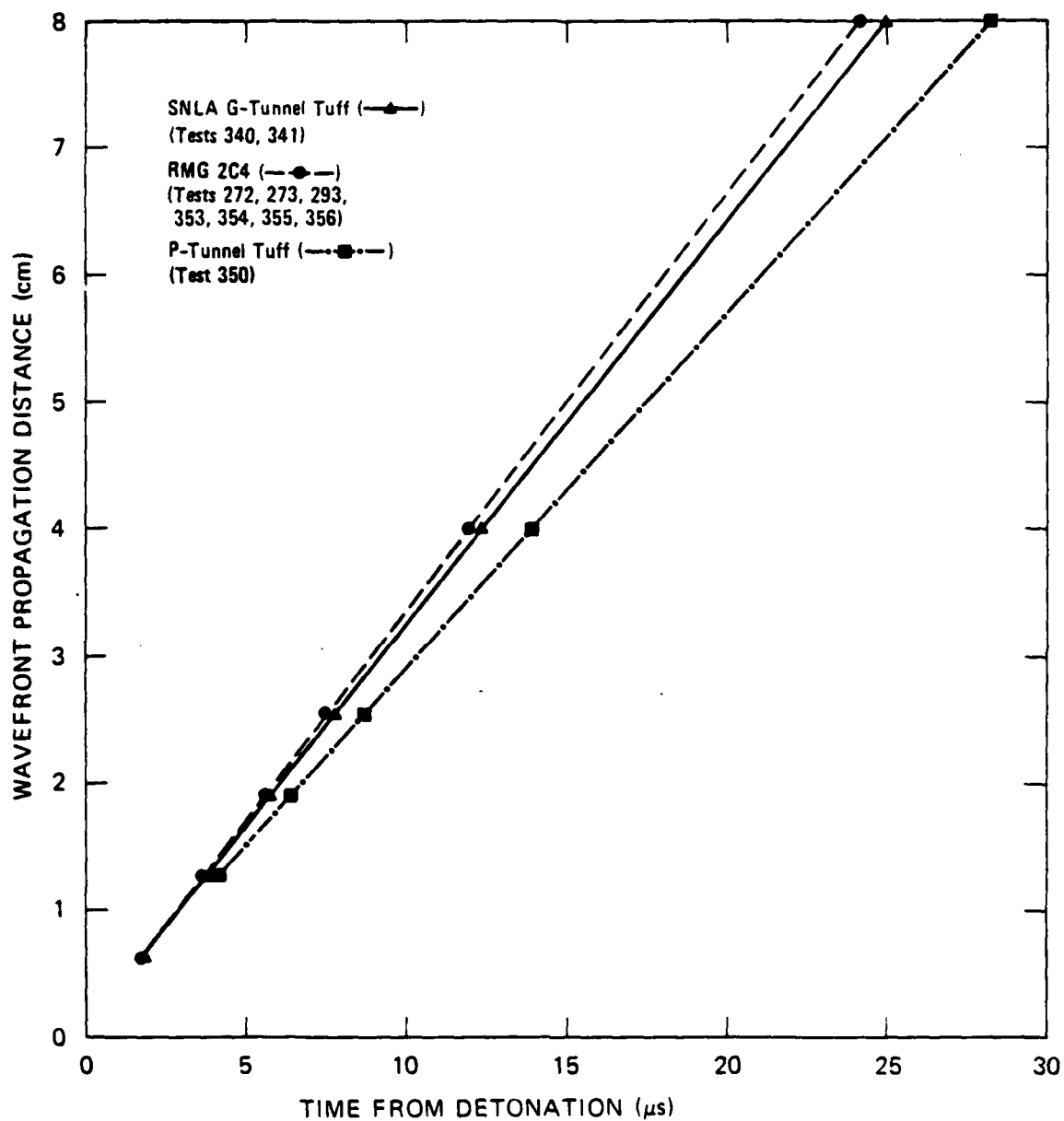
FIGURE 3.49 WAVEFRONT PROPAGATION DISTANCE VERSUS TIME FROM DETONATION
FOR RMG 2C4, SNLA G-TUNNEL TUFF, AND P-TUNNEL TUFF

111
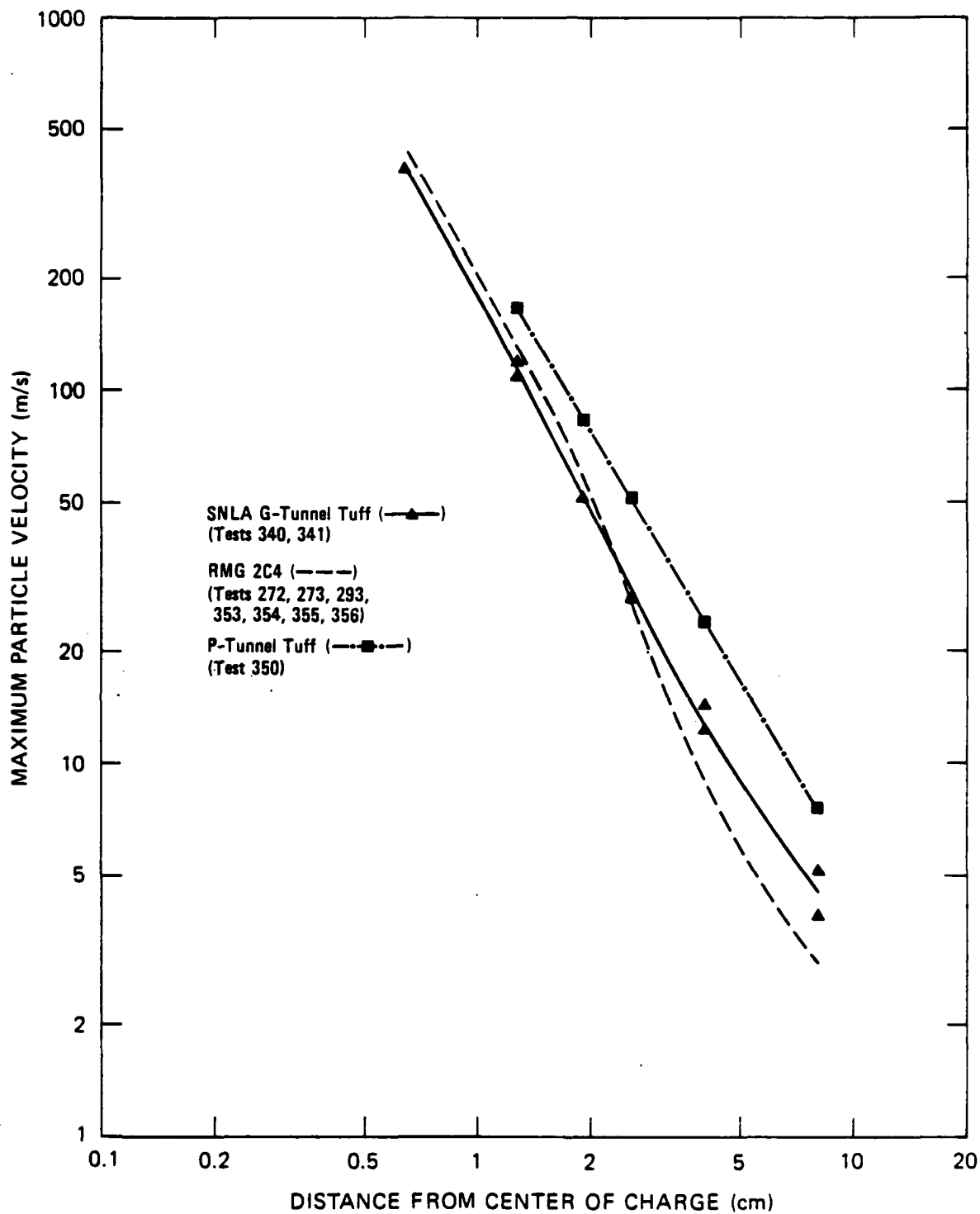
FIGURE 3.48   MAXIMUM PARTICLE VELOCITY VERSUS DISTANCE FROM CENTER
OF CHARGE FOR RMG 2C4, SNLA G-TUNNEL TUFF,
AND P-TUNNEL TUFF
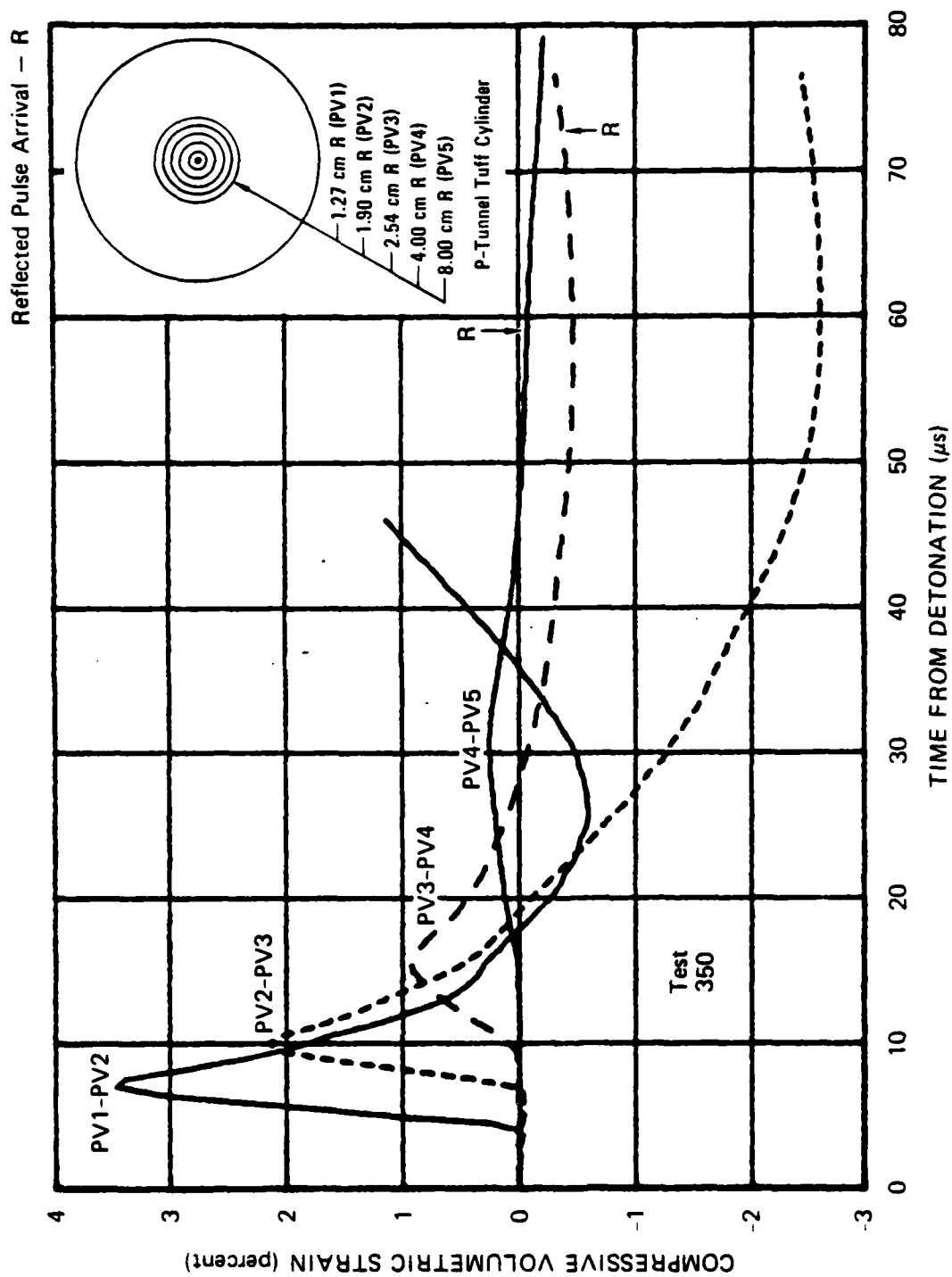
110

FIGURE 3.47 VOLUMETRIC STRAIN OBTAINED FROM A PARTICLE VELOCITY TEST IN P-TUNNEL TUFF

JA-5372-170

109

PV2 (Figure A.7) and an assumption of incompressibility yields 0.800 inch (2.03 cm). Crushing of the P-tunnel tuff appears to contribute to the formation of the larger exploded cavity. Figure 3.47 shows permanent compaction in the region between gages PV1 and PV2. The larger cavity results in lower cavity pressure, which decreases the potential for cracking. Posttest examination of the cylinder revealed no evidence of cracking even along the bonded plane of the gages.

Figure 3.48 shows the decay of peak velocity with range for P-tunnel tuff, SNLA G-tunnel tuff, and RMG 2C4. Overall, the rate of attenuation for these three materials is comparable. Figure 3.49 shows the time of arrival of the wavefront at each gage location for the same materials. A constant wave speed of 2.78 mm/μs for P-tunnel tuff, 3.16 mm/μs for G-tunnel tuff, and 3.29 mm/μs for RMG 2C4 applies over the range of the gages.

Pressure records in the overburden fluid obtained from quartz gage measurements for P-tunnel tuff and G-tunnel tuff are shown in Figure B.5. The higher pressure for the P-tunnel tuff is consistent with the particle velocity results.

Series 8: Material Property (Grand Saline Dome Salt)

A 500-lb (227-kg) block of salt wrapped in plastic was received from the mine in Grand Saline, Texas. Two 1-foot (0.3-m) cubes were cut from the block and cored (without the use of water) to a diameter of 9-5/8 inches (24.45 cm) so that particle velocity tests could be performed. The standard charge and gage installation technique previously developed for geologic materials[10] was applied. Aluminum wire gages were epoxied in grooves 9 mils (0.23 mm) wide and 25 mils (0.64 mm) deep at four radial locations (1.27, 1.90, 2.54, and 4.00 cm). Figures 3.50 through 3.53 show the resulting particle velocity profiles for tests 364 and 365. For comparison, results of previous tests[6] (272 and 273) on 11-inch-diameter (27.94-cm) RMG 2C4 spheres are included.

The pulse shapes for salt and RMG are similar during outward motion but differ during the rebound phase because of the lack of rebound
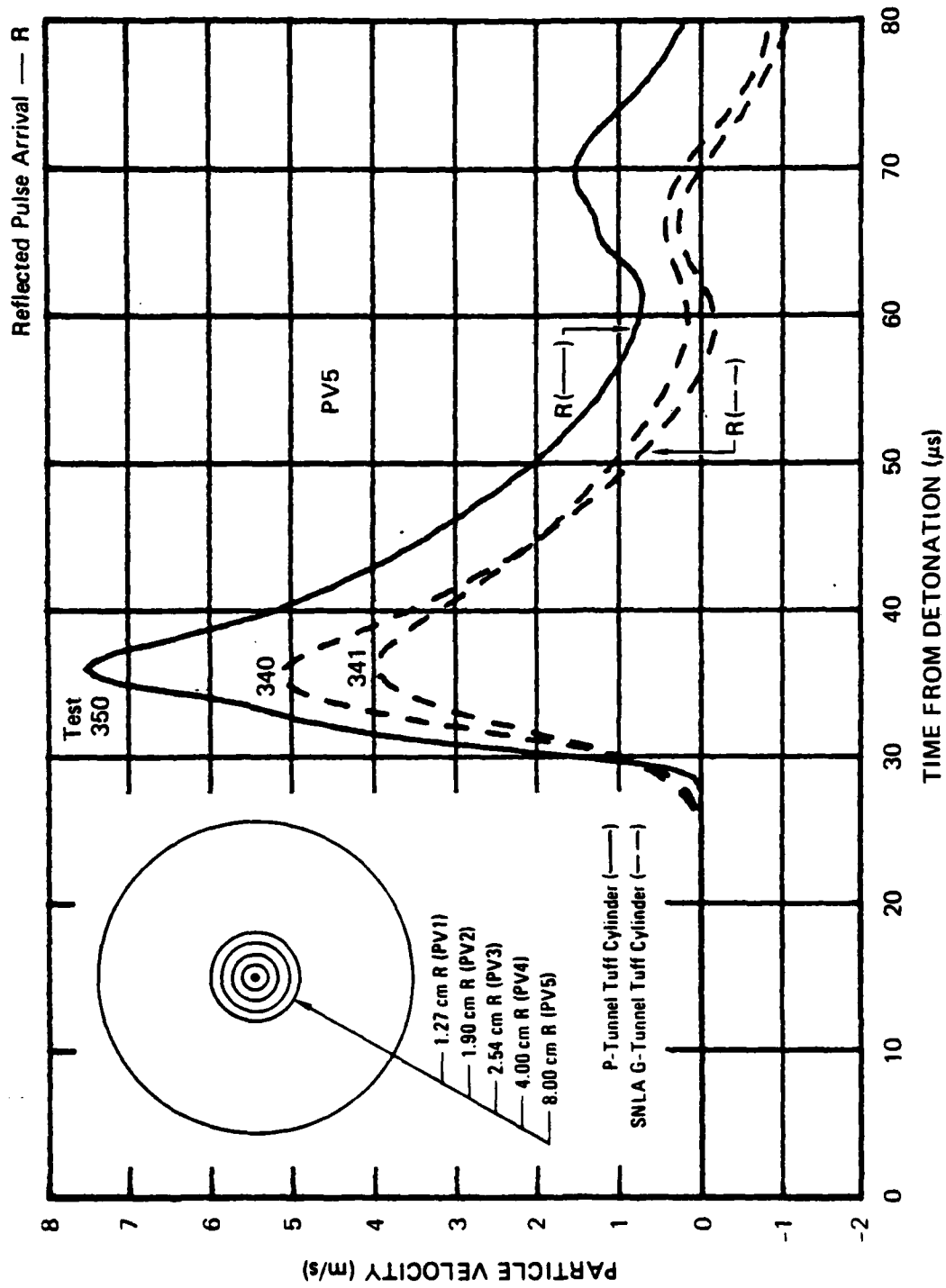
108

FIGURE 3.46 PARTICLE VELOCITY 8.00 cm FROM THE CENTER OF COUPLED EXPLOSIONS
IN TUFF (P-TUNNEL AND SNLA G-TUNNEL)
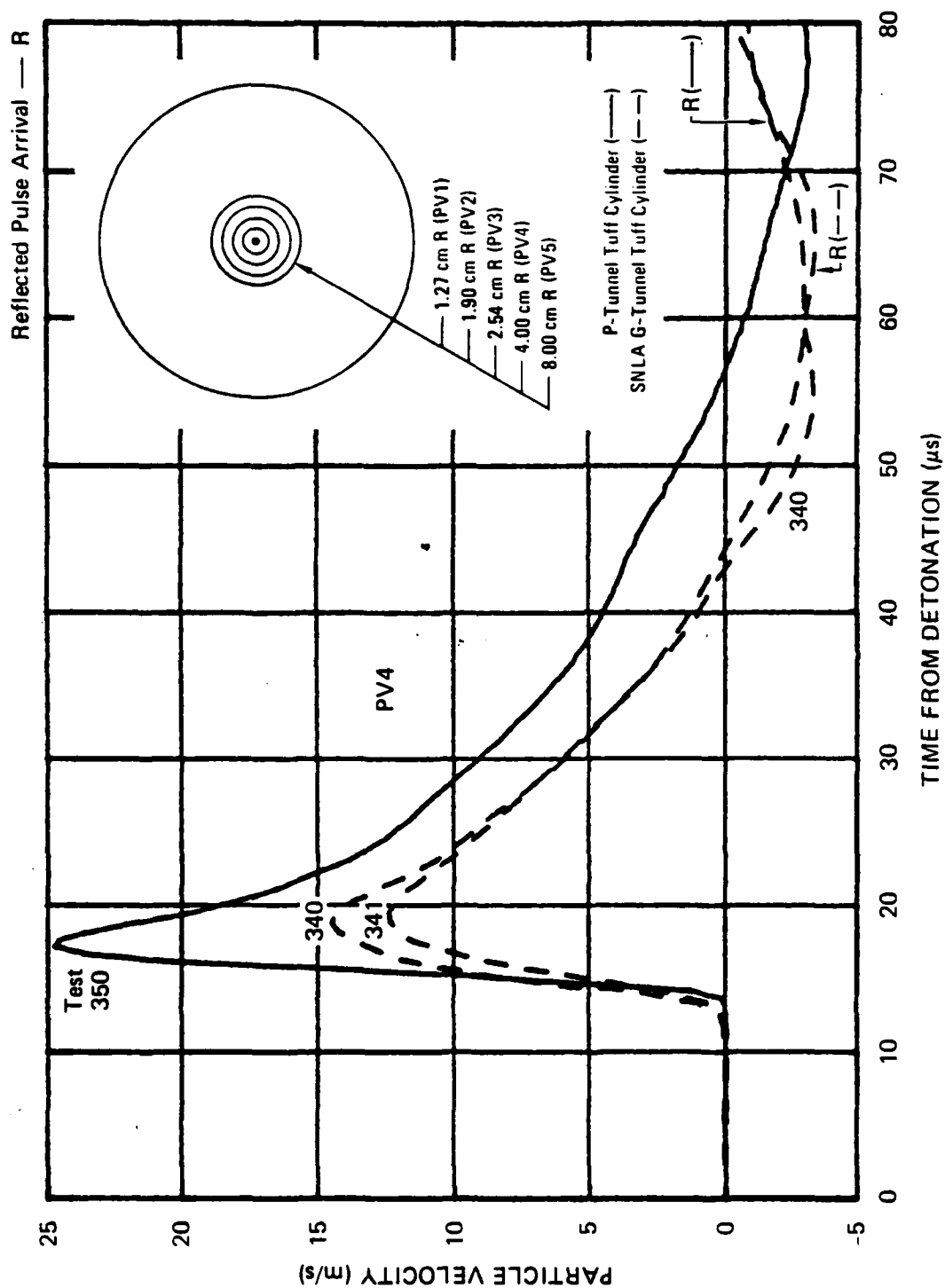
FIGURE 3.45 PARTICLE VELOCITY 4.00 cm FROM THE CENTER OF COUPLED EXPLOSIONS IN TUFF (P-TUNNEL AND SNLA G-TUNNEL)
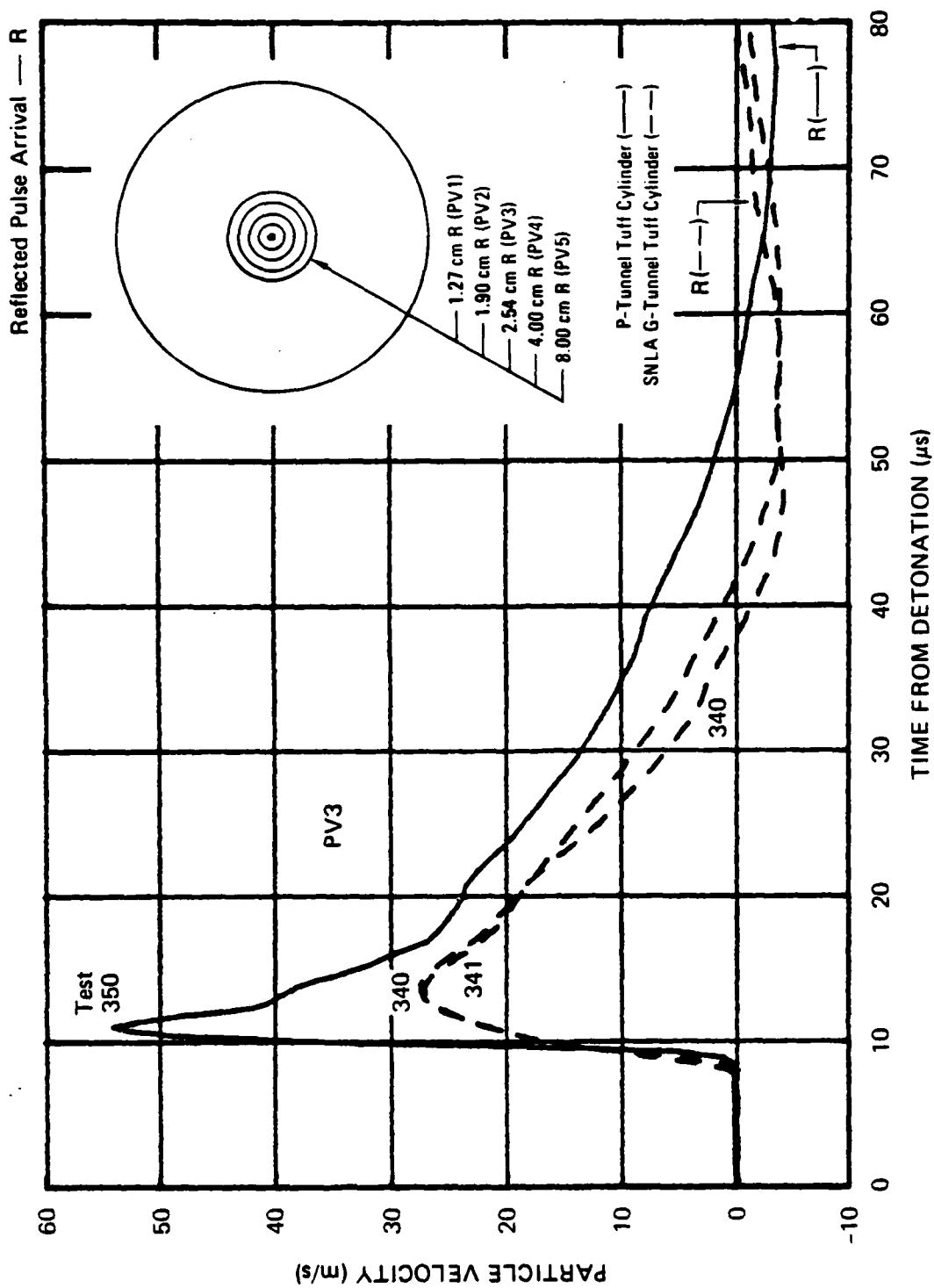
106

FIGURE 3.44 PARTICLE VELOCITY 2.54 cm FROM THE CENTER OF COUPLED EXPLOSIONS
IN TUFF (P-TUNNEL AND SNLA G-TUNNEL)
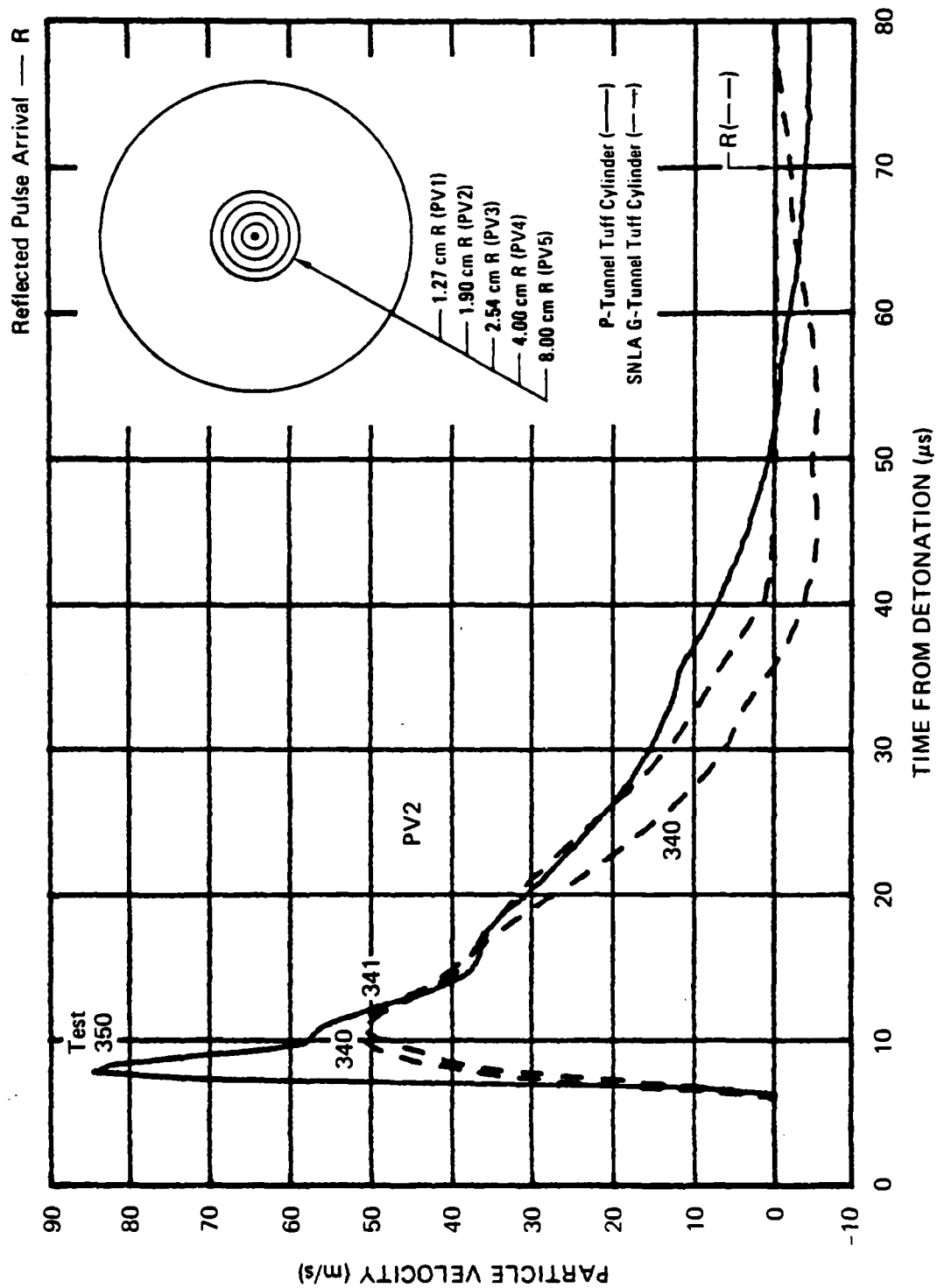
105

FIGURE 3.43   PARTICLE VELOCITY 1.90 cm FROM THE CENTER OF COUPLED EXPLOSIONS
IN TUFF (P-TUNNEL AND SNLA G-TUNNEL)

104
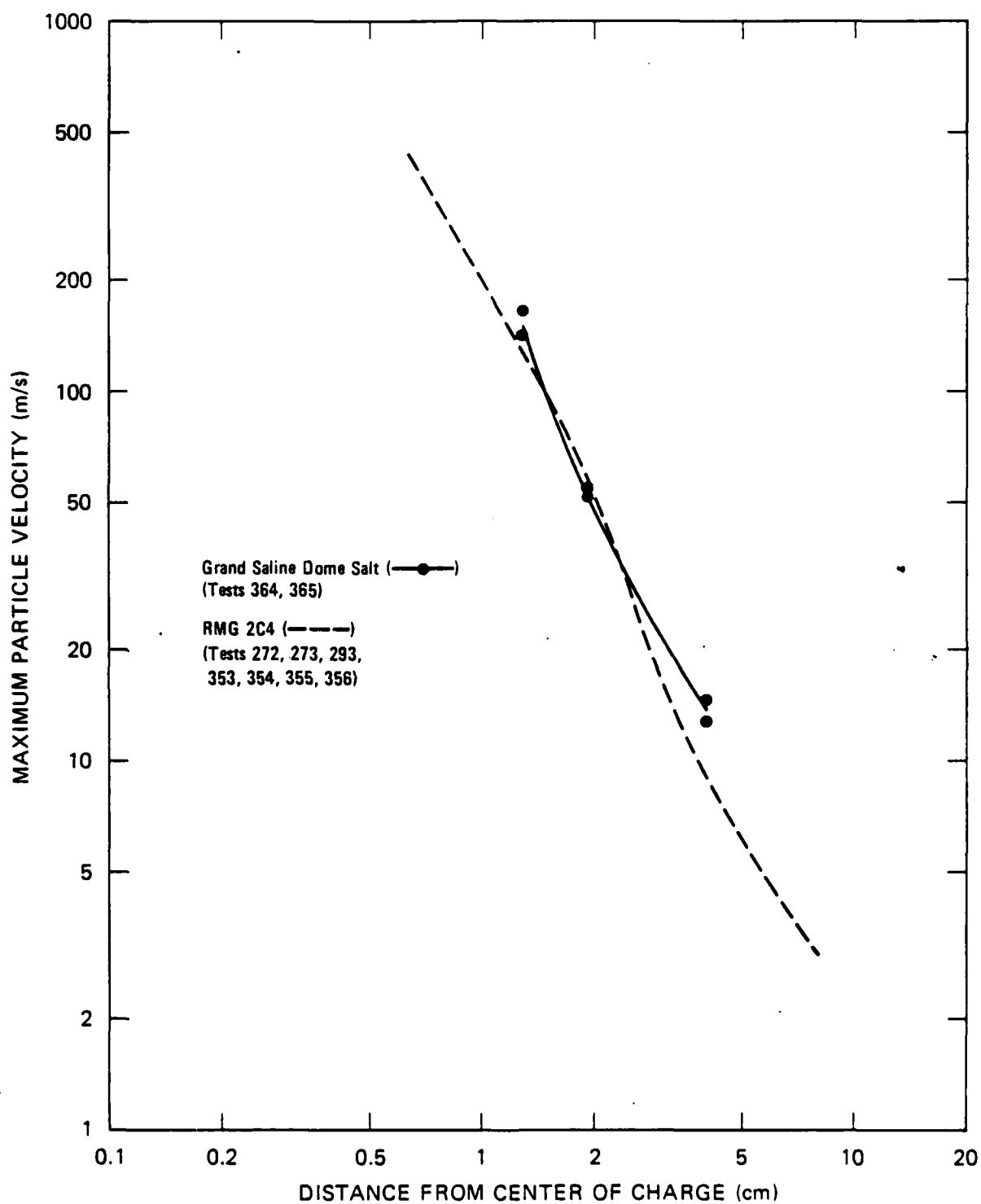
FIGURE 3.55   MAXIMUM PARTICLE VELOCITY VERSUS DISTANCE FROM CENTER OF CHARGE
FOR SALT AND RMG 2C4
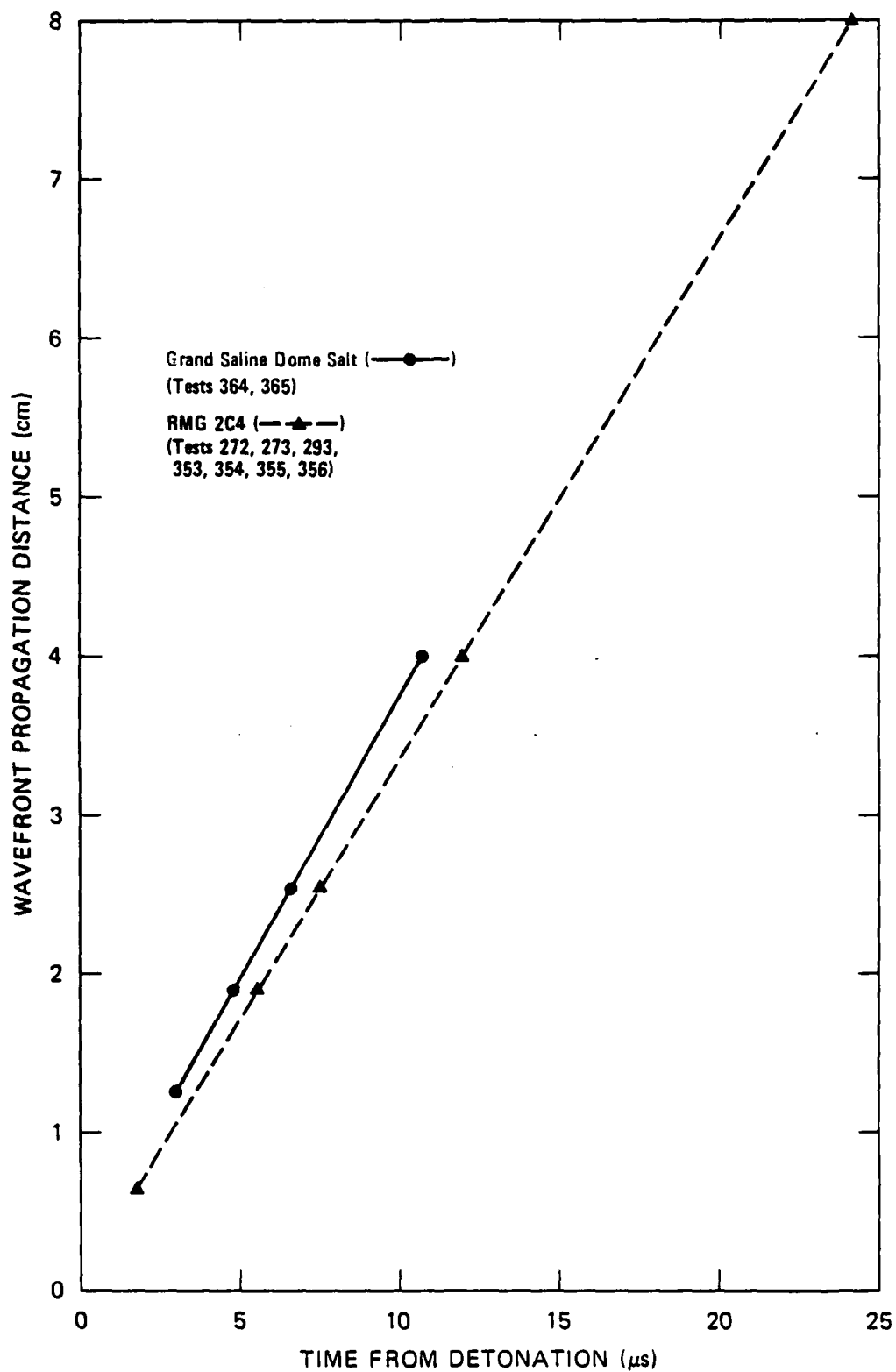
FIGURE 3.56   WAVEFRONT PROPAGATION DISTANCE VERSUS TIME FROM DETONATION
FOR SALT AND RMG 2C4
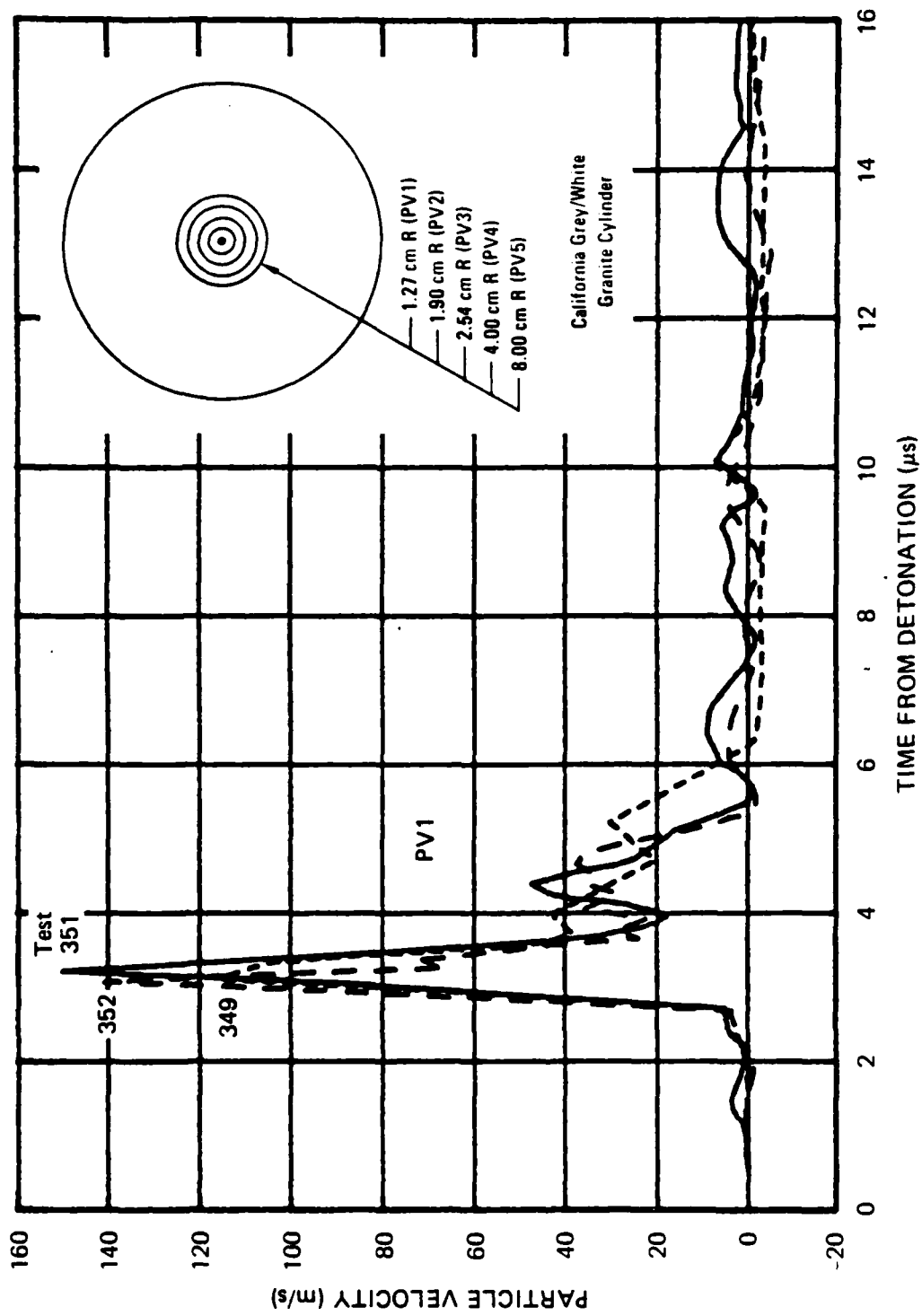
119

FIGURE 3.57 PARTICLE VELOCITY 1.27 cm FROM THE CENTER OF COUPLED EXPLOSIONS
IN GRANITE — TECHNIQUE DEVELOPMENT
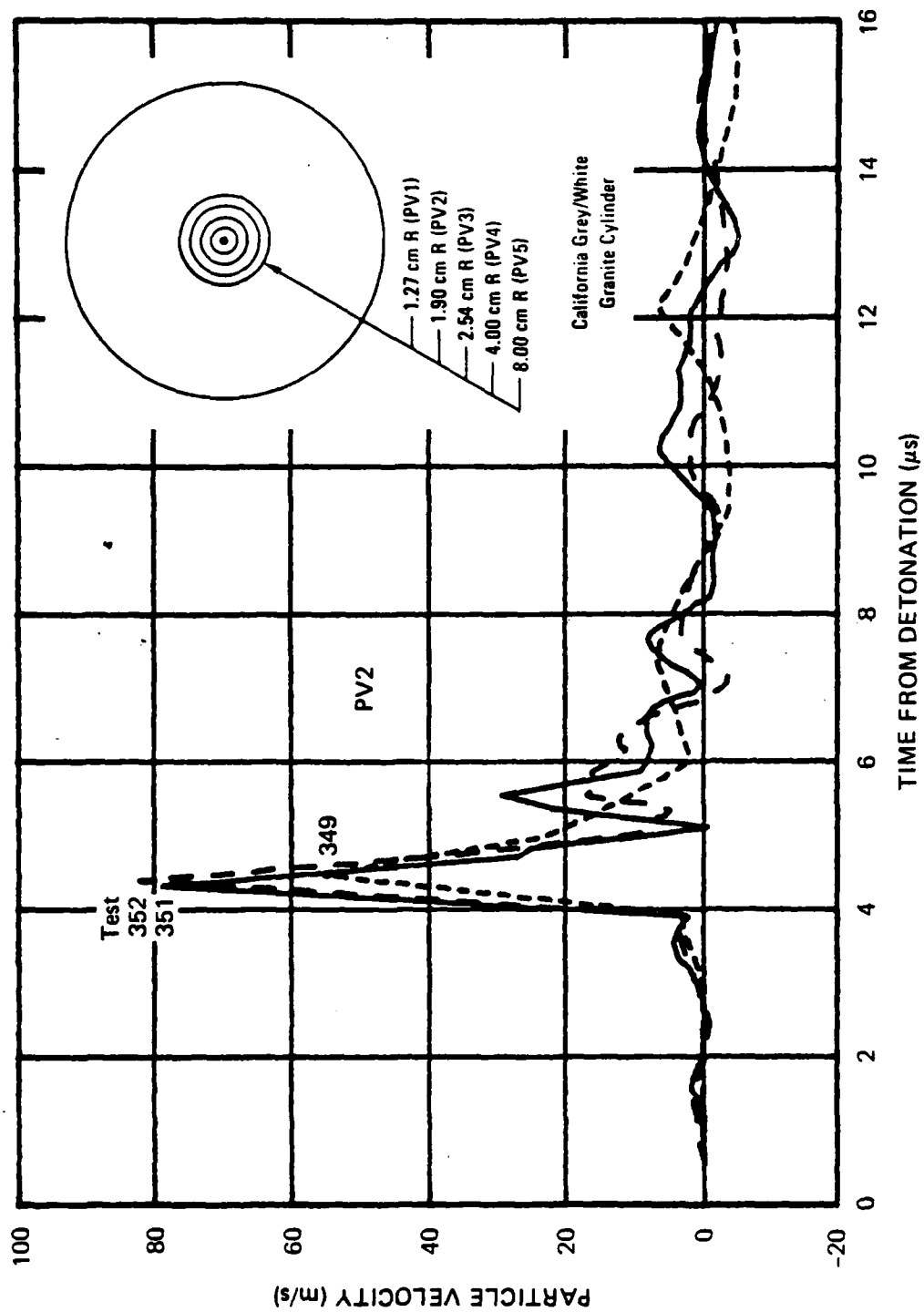
120

FIGURE 3.58 PARTICLE VELOCITY 1.90 cm FROM THE CENTER OF COUPLED EXPLOSIONS IN GRANITE — TECHNIQUE DEVELOPMENT
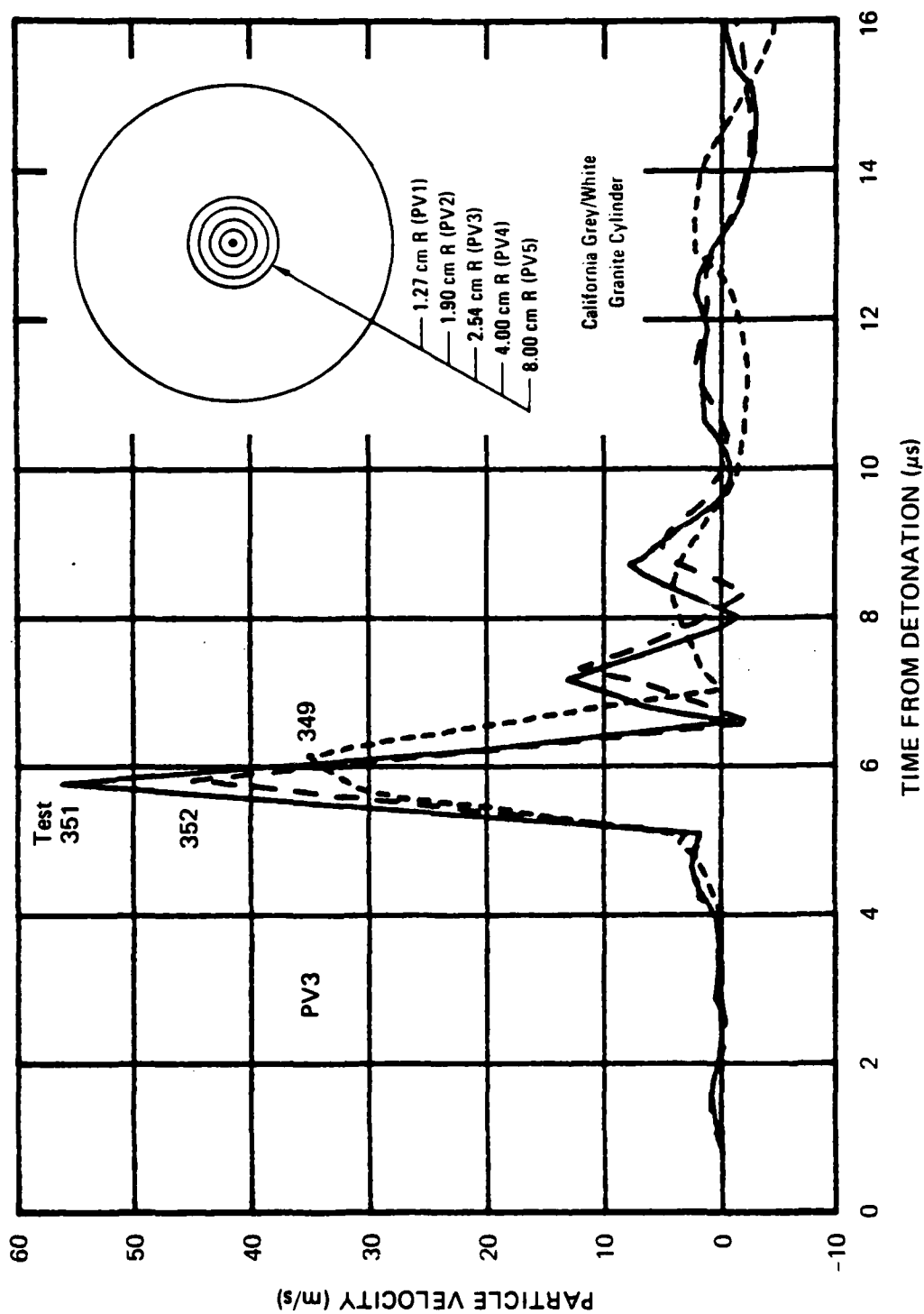
121

FIGURE 3.59   PARTICLE VELOCITY 2.54 cm FROM THE CENTER OF COUPLED EXPLOSIONS IN GRANITE –
TECHNIQUE DEVELOPMENT
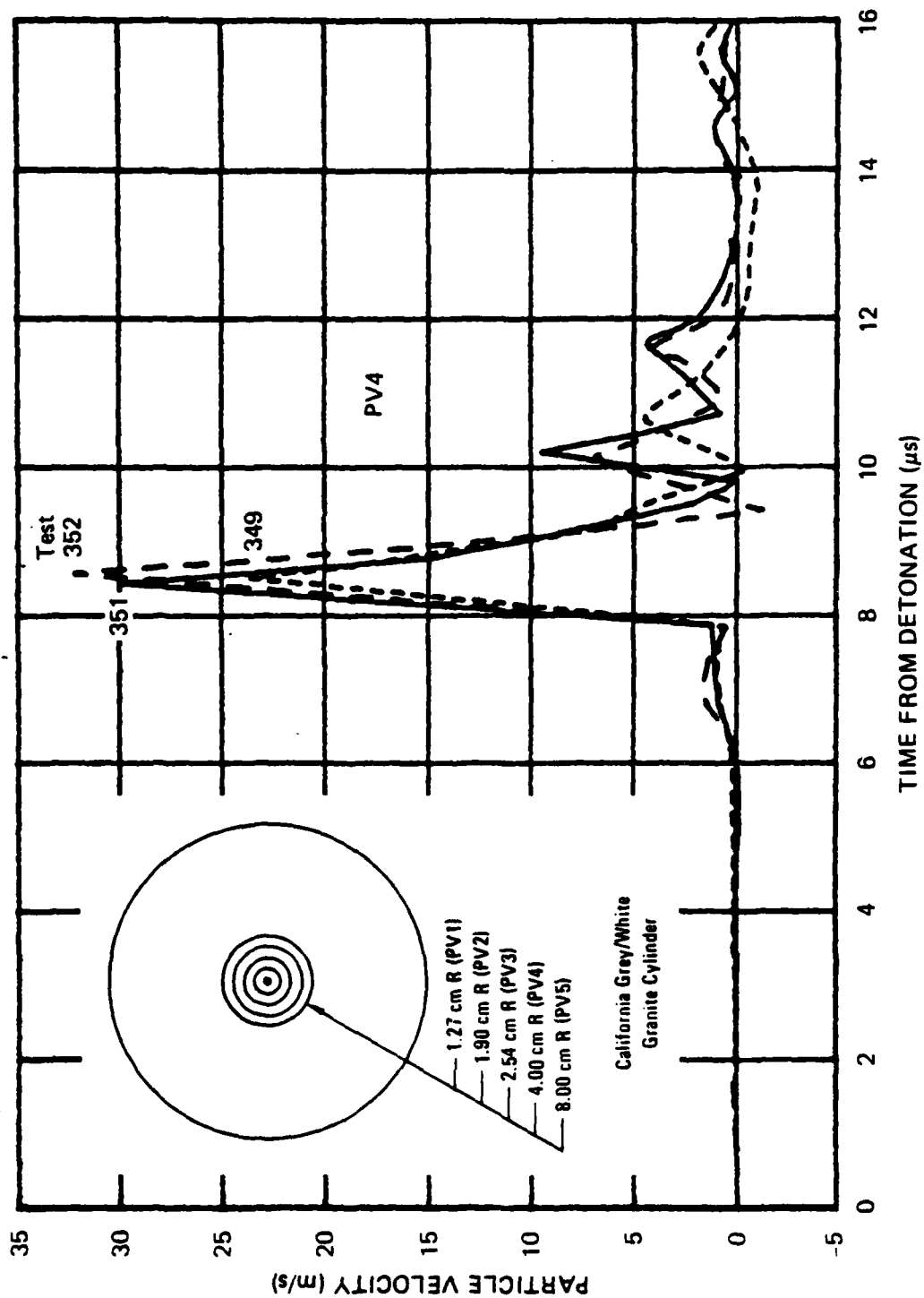
JA-5372-21

122

FIGURE 3.60   PARTICLE VELOCITY 4.00 cm FROM THE CENTER OF COUPLED EXPLOSIONS IN GRANITE – TECHNIQUE DEVELOPMENT
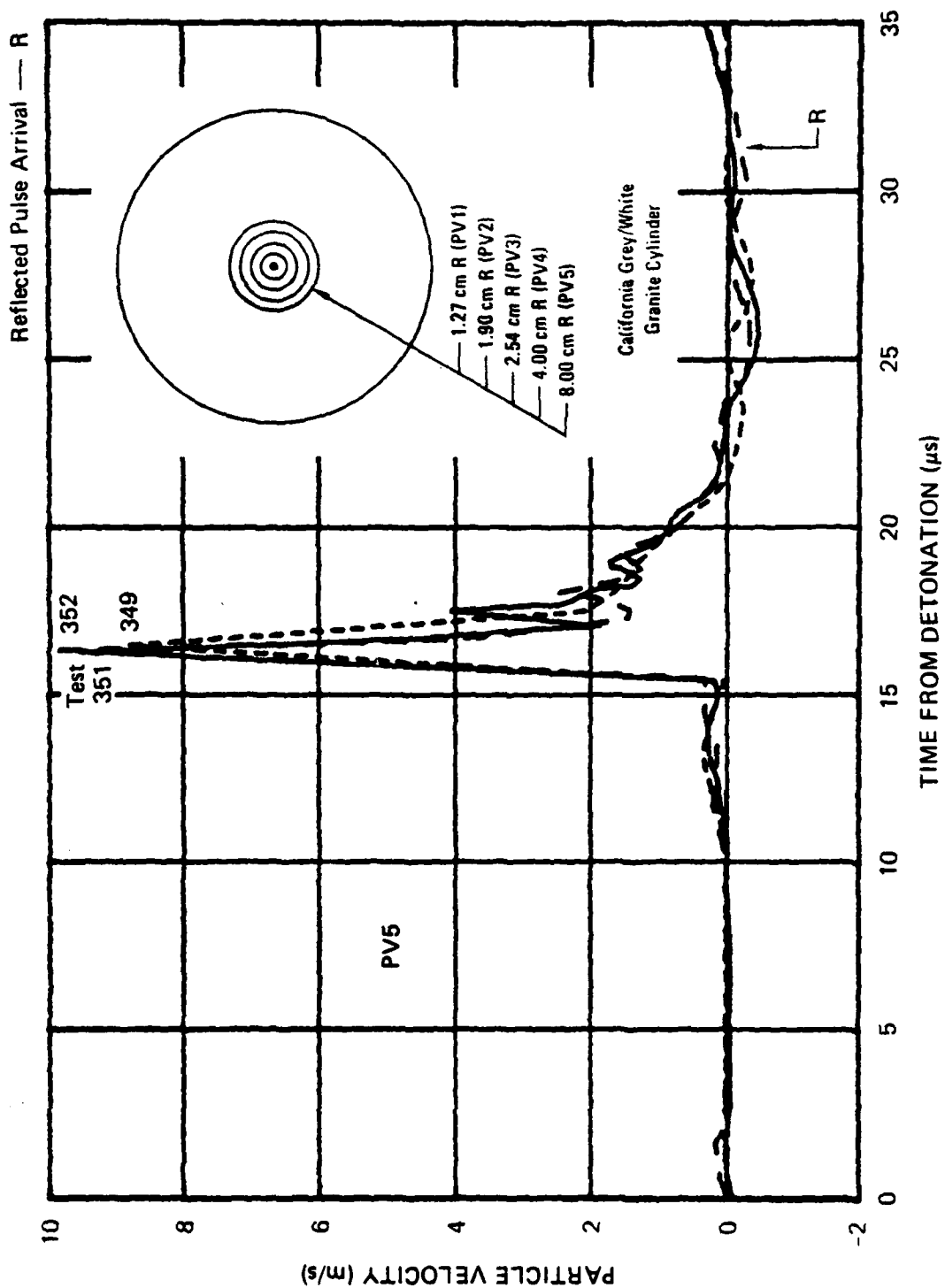
123

FIGURE 3.61   PARTICLE VELOCITY 8.00 cm FROM THE CENTER OF COUPLED EXPLOSIONS IN GRANITE –
TECHNIQUE DEVELOPMENT

124

The pulse at each gage location is characterized by a sharp peak, short duration of outward motion, and negligible rebound. The resulting small displacements produce an exploded cavity diameter of 0.460 inch (1.17 cm). The small cavity results in high cavity pressure, which represents a potential for cracking. In fact, posttest examination of the granite cylinders revealed evidence of dynamic cracking along the bonded plane of the gages in test 349. Although no similar evidence was detected in tests 351 and 352, the high calculated pressure suggests that cracking probably occurred.

Because particle velocities are influenced by cracking, techniques were developed to (1) monitor crack arrival and (2) prevent cracking along the particle velocity gage plane.

Two 1-foot (0.3-m) cubes of California grey/white granite were cored to a diameter of 9-5/8 inches (24.45 cm) so that combination particle velocity/crack arrival tests could be performed. The standard charge and particle velocity gage installation technique previously developed for geologic materials[10] was applied. Gages were epoxied in grooves 9 mils (0.23 mm) wide and 25 mils (0.64 mm) deep at two radial locations (1.27 and 2.54 cm). In addition, two fracture gages (see Section 2.3) were installed in axial holes on opposite sides of the charge to monitor crack arrival along the bonded interface. These gages were located at a radius of 1.90 cm. Figures 3.62 and 3.63 show the resulting particle velocity profiles and the time of crack arrival for tests 366 and 367.

The earliest crack detection was at 8.82 µs (test 366). Assuming that cracking started when the detonation wave in the explosive reached the granite (1.32 µs) and propagated from the cavity at a constant rate, we arrive at a crack velocity of 1.84 mm/µs, which is 35% of the 5.29 mm/µs compressional wave speed. Hence, crack arrival at PV1 (1.27 cm) and PV2 (2.54 cm) would occur at 5.39 and 12.29 µs, respectively. Particle velocity response before these times, which includes peak velocities, may be unaffected.
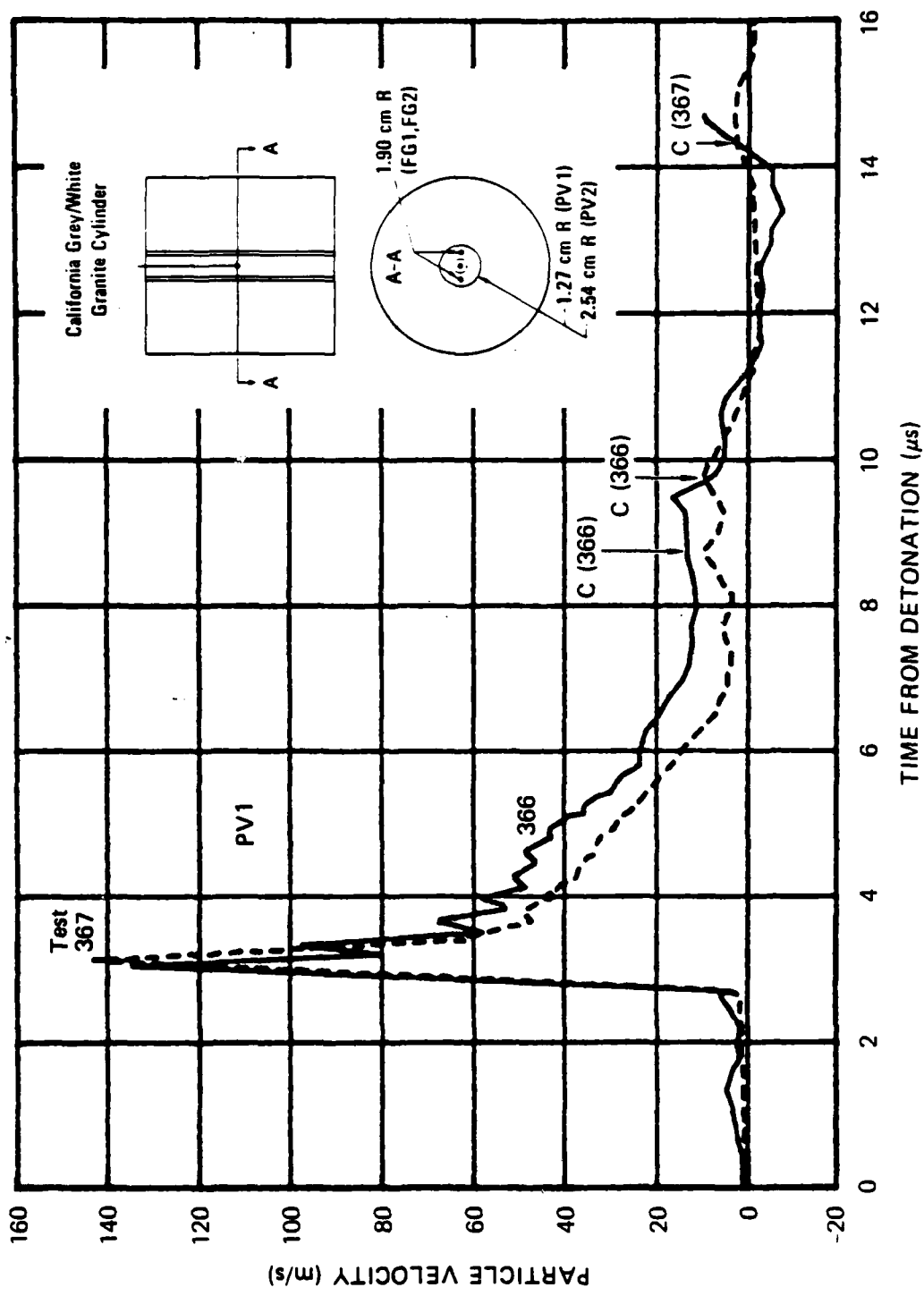
FIGURE 3.62   PARTICLE VELOCITY 1.27 cm FROM THE CENTER OF COUPLED EXPLOSIONS IN GRANITE – FRACTURE DETECTION

126
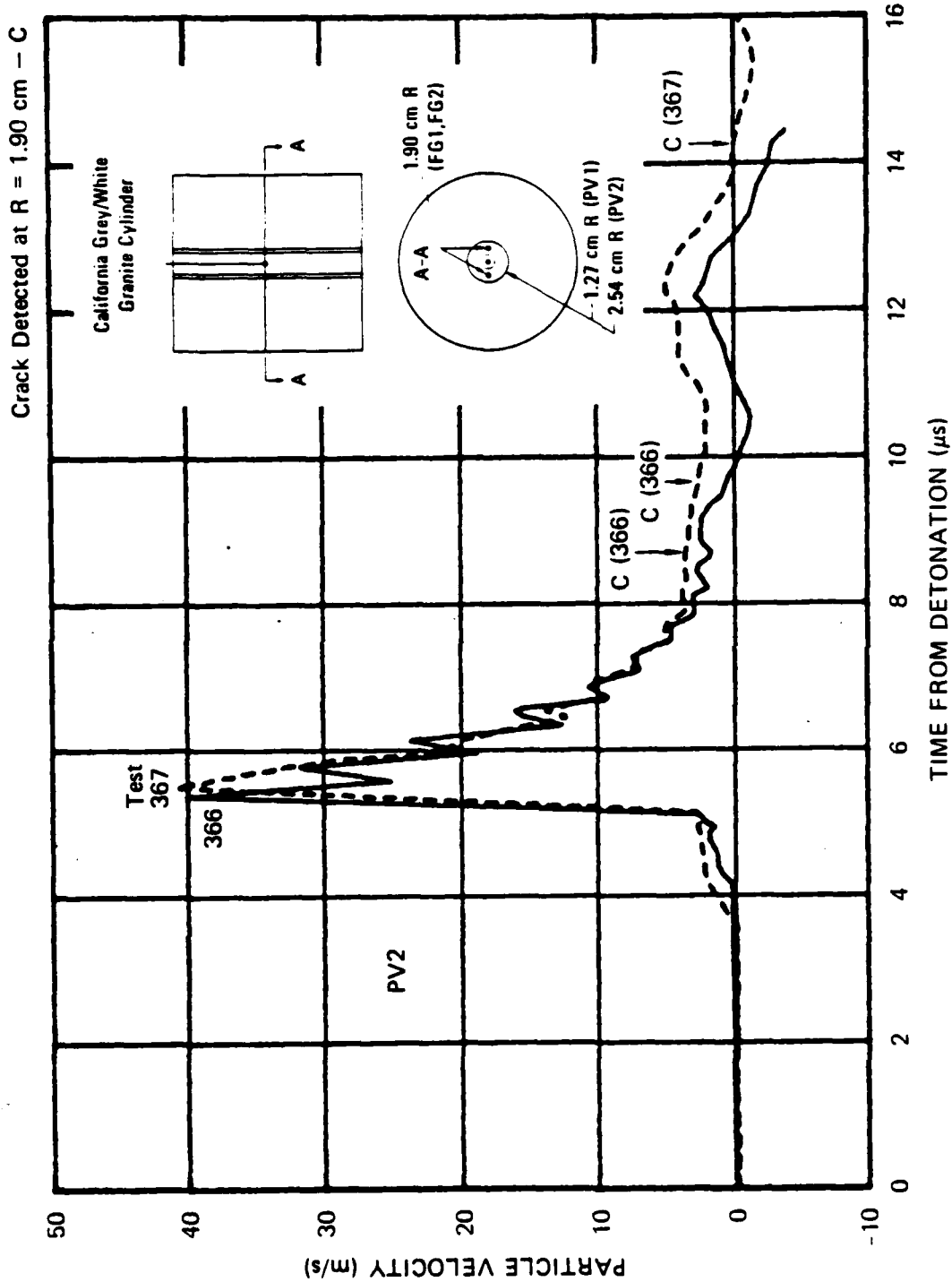
FIGURE 3.63   PARTICLE VELOCITY 2.54 cm FROM THE CENTER OF COUPLED EXPLOSIONS IN GRANITE – FRACTURE DETECTION

127

Posttest examination of the granite cylinders in tests 366 and 367 confirmed that dynamic cracking occurred along the bonded plane of the gages. Evidence of cracking was visible to a radius of 2 inches (5.08 cm).

Figure 3.64 shows the decay of peak velocity with range for granite and RMG 2C4. The lower rate of attenuation in granite is consistent with the negligible energy lost to crushing of voids.

Figure 3.65 shows the time of arrival of the particle velocity pulse at each gage location for granite. A constant wave speed of 5.29 mm/μs applies over the range of the gages.

Unconfined crush strength determined from one test on a granite cylinder 2 inches (5.08 cm) in diameter and 4 inches (10.16 cm) long is 20,660 psi (142.45 MPa). Splitting tensile strength determined from one test on a similar cylinder is 3240 psi (22.34 MPa).

Two additional 1-foot (0.3-m) cubes of granite were cored to a diameter of 9-5/8 inches (24.45 cm) so that a technique to prevent cracking along the plane of particle velocity gages could be tested. In the new configuration, an axial hole was drilled to the center of the cylinder so that the charge and access tube could be grouted in place with granite simulant GS4, as shown in Figure 2.7 (Section 2.2). However, the cylinder was then cut and bonded along a plane 1/2 inch (1.27 cm) below the center of the charge. Circular loop gages were epoxied in grooves 9 mils (0.23 mm) wide and 25 mils (0.64 mm) deep at four cylindrically radial locations (1.27, 1.90, 2.54, and 4.00 cm) on the charge side of the interface.

Figures 3.66 through 3.69 show the particle velocity profiles for tests 369 and 370. The results shown are total velocities obtained from the cylindrically radial components measured by the gages. Overall pulse shapes are similar to those described above. Peak velocities are not well-defined, however, because of reflected pulses at the bonded interface. Maximum particle displacements normal to the interface, obtained from the particle velocity records, ranged from 4.2 mils

128
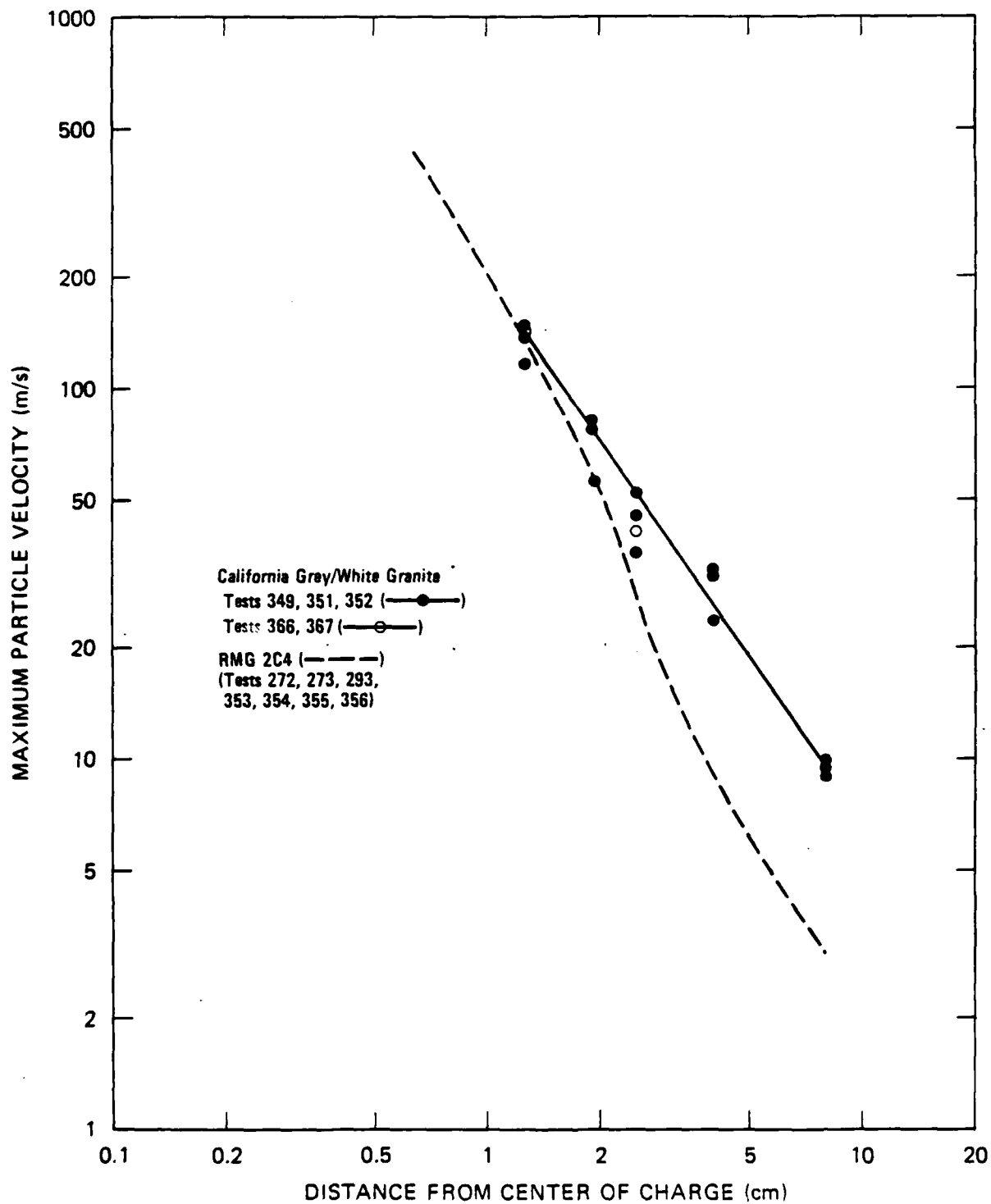
FIGURE 3.64   MAXIMUM PARTICLE VELOCITY VERSUS DISTANCE FROM CENTER OF CHARGE
FOR GRANITE AND RMG 2C4

129
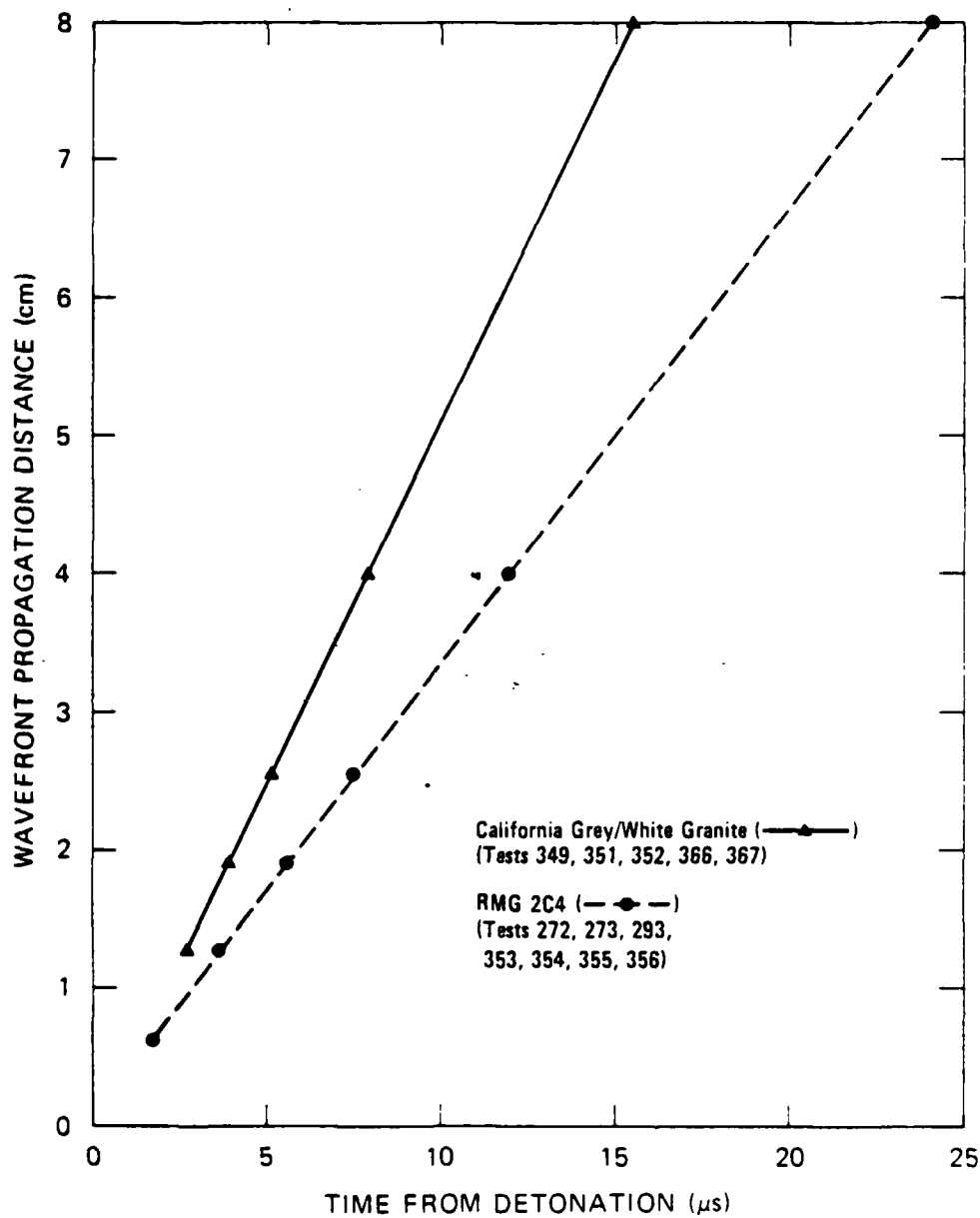
FIGURE 3.65   WAVEFRONT PROPAGATION DISTANCE VERSUS TIME FROM DETONATION
FOR GRANITE AND RMG 2C4
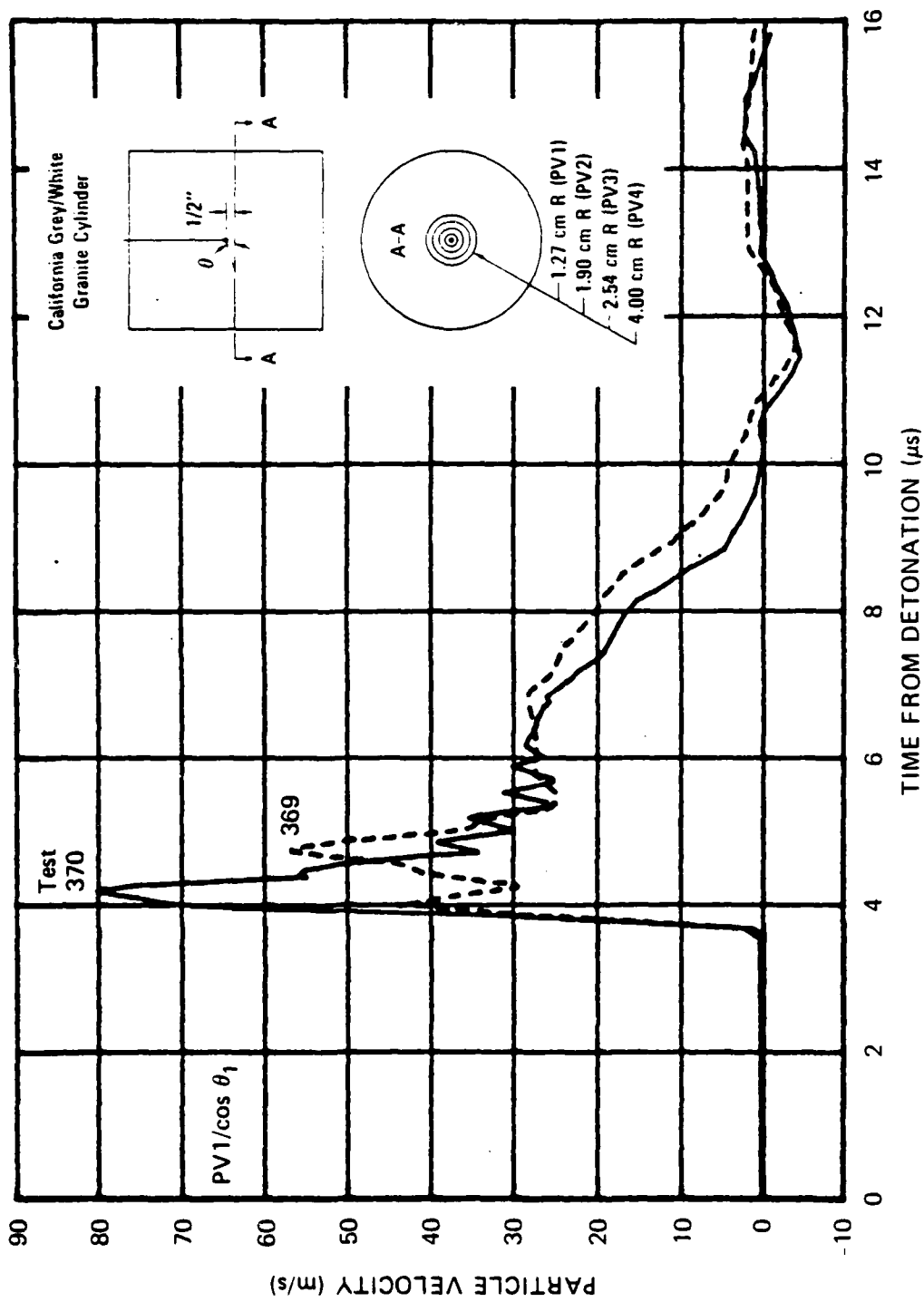
130

FIGURE 3.66 PARTICLE VELOCITY 1.76 cm FROM THE CENTER OF COUPLED EXPLOSIONS IN GRANITE – GAGE PLANE BELOW CHARGE

131
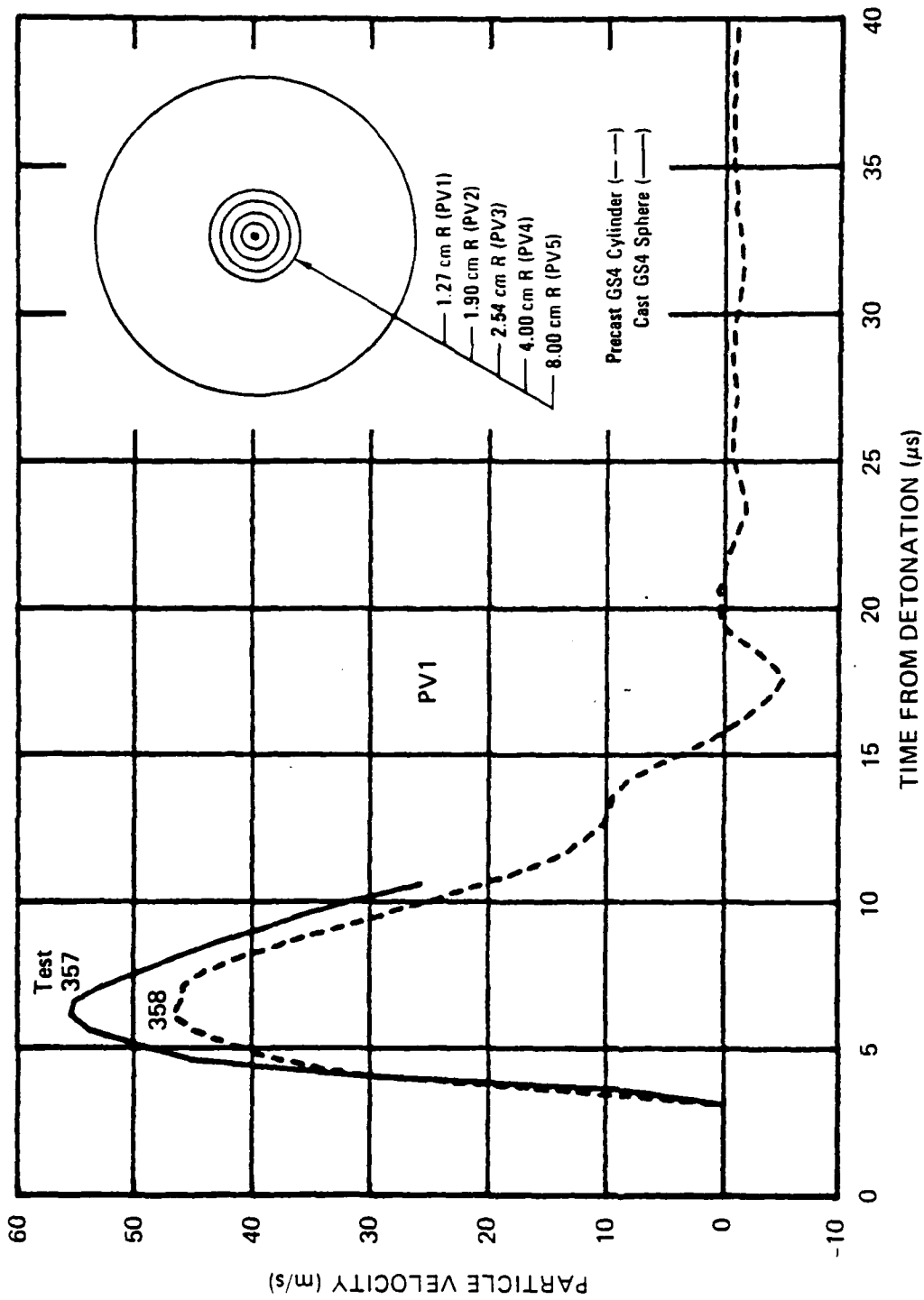
FIGURE 3.77 PARTICLE VELOCITY 1.27 cm FROM THE CENTER OF COUPLED EXPLOSIONS IN GS4
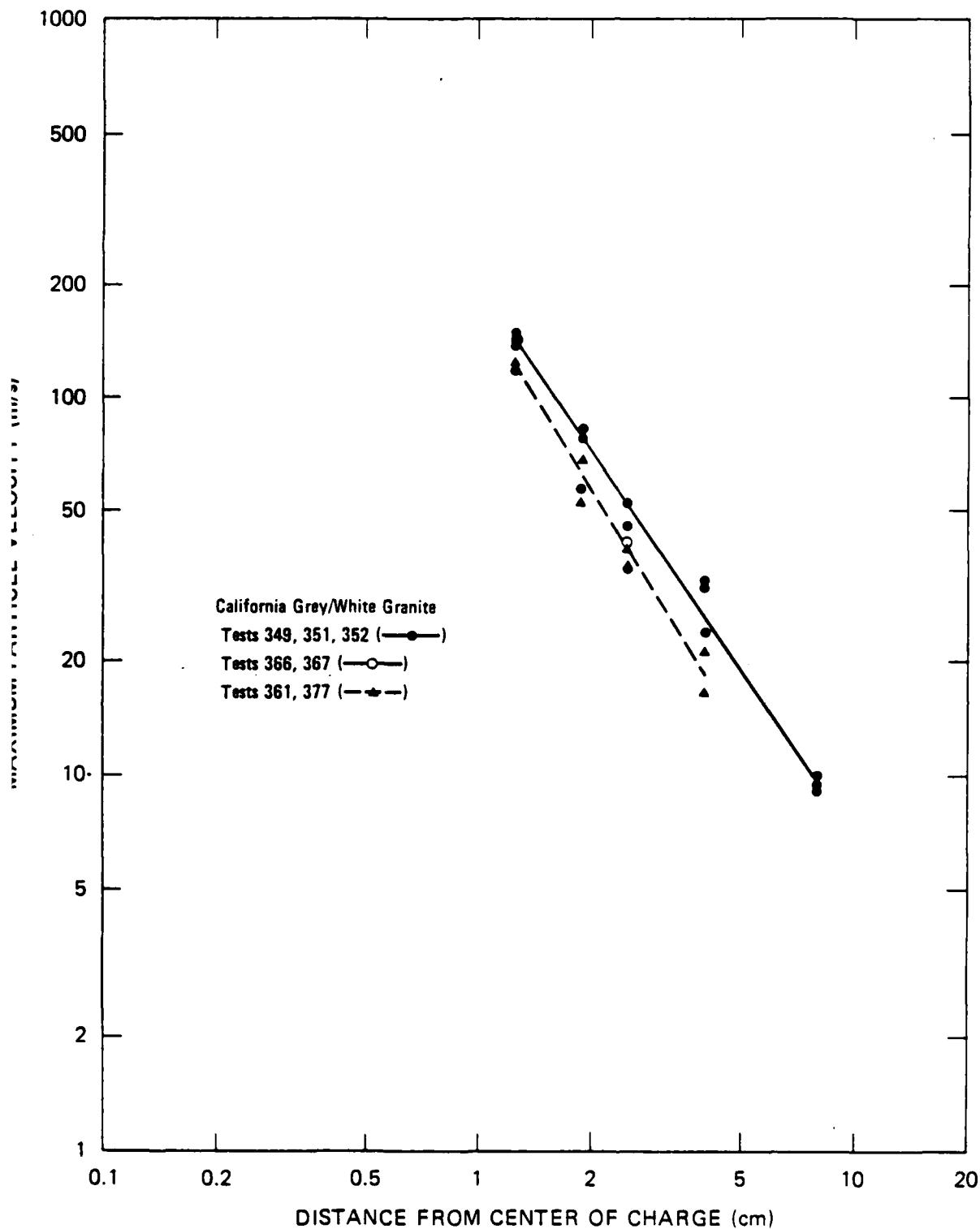
JA-5372-37A

FIGURE 3.76   MAXIMUM PARTICLE VELOCITY VERSUS DISTANCE FROM CENTER OF CHARGE
FOR GRANITE

144
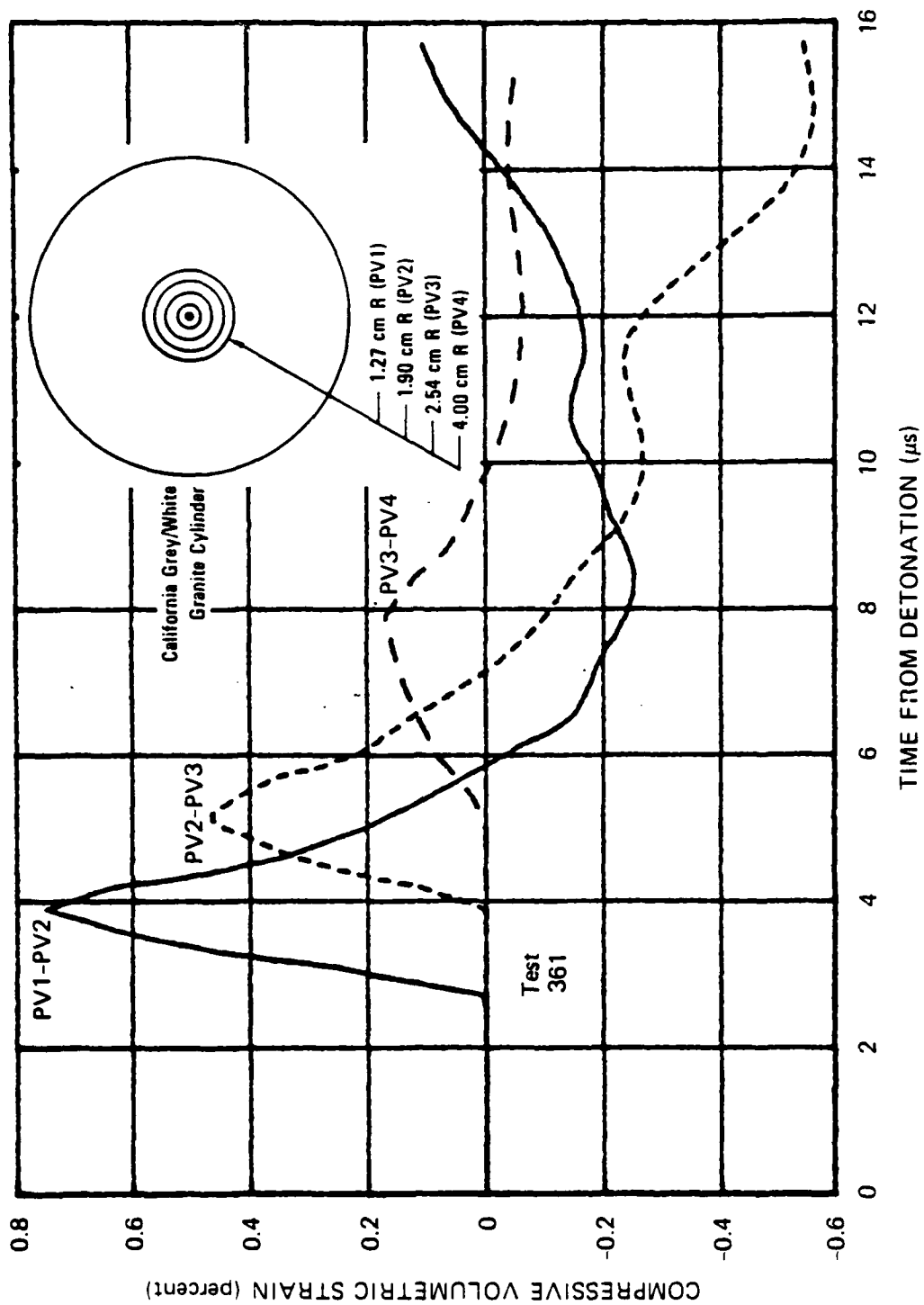
FIGURE 3.75 VOLUMETRIC STRAIN OBTAINED FROM A PARTICLE VELOCITY TEST IN GRANITE

143

as well as gage wire material and overburden pressure may have only a small influence on the particle velocity records. Posttest examination of the cylinder revealed cracking along the gage plane in both tests. The crack in test 377 extended through the plug.

The measured exploded cavity diameter in tests 361 and 377 was 0.460 inch (1.17 cm). An estimate of exploded cavity diameter based on the integrated particle velocity record for gage PV1, Test 361 (Figure A.9) and an assumption of incompressibility yields 0.461 inch (1.17 cm). Hence, there is no apparent crushing of the granite. Figure 3.75 shows that negligible permanent volume strain is produced in the region between gages PV1 and PV2.

A summary of peak particle velocity attenuation for tests in granite is shown in Figure 3.76. Although scatter exists at a given range, the rate of attenuation is generally consistent from test to test.

Series 10: Material Property (Granite Simulant GS4)

Two particle velocity experiments were performed in granite simulant GS4 to validate the basic technique for obtaining results in a hard rock simulant. Aluminum wire 5 mils (0.127 mm) in diameter was the gage material. Test 357 was performed to generate standard results for gages cast in place. Circular loops of wire were cast in a sphere of GS4 at five radial locations (1.27, 1.90, 2.54, 4.00, and 8.00 cm). Test 358 was performed to consider the effects of the gage installation technique on the particle velocity records. Narrow circular grooves 9 mils (0.229 cm) wide were machined in a precast GS4 cylinder at four radial locations (1.27, 1.90, 2.54, and 4.00 cm), and the aluminum wire was epoxied in the grooves. Figures 3.77 through 3.81 show the resulting particle velocity records for tests 357 and 358. [Note that gage PV2 (Figure 3.78) in test 357 broke before the test.]

Complete records for tests 357 and 358 are available at two locations [PV3 (Figure 3.79) and PV4 (Figure 3.80)]. These records show good agreement during the outward phase of motion but reveal significant

142
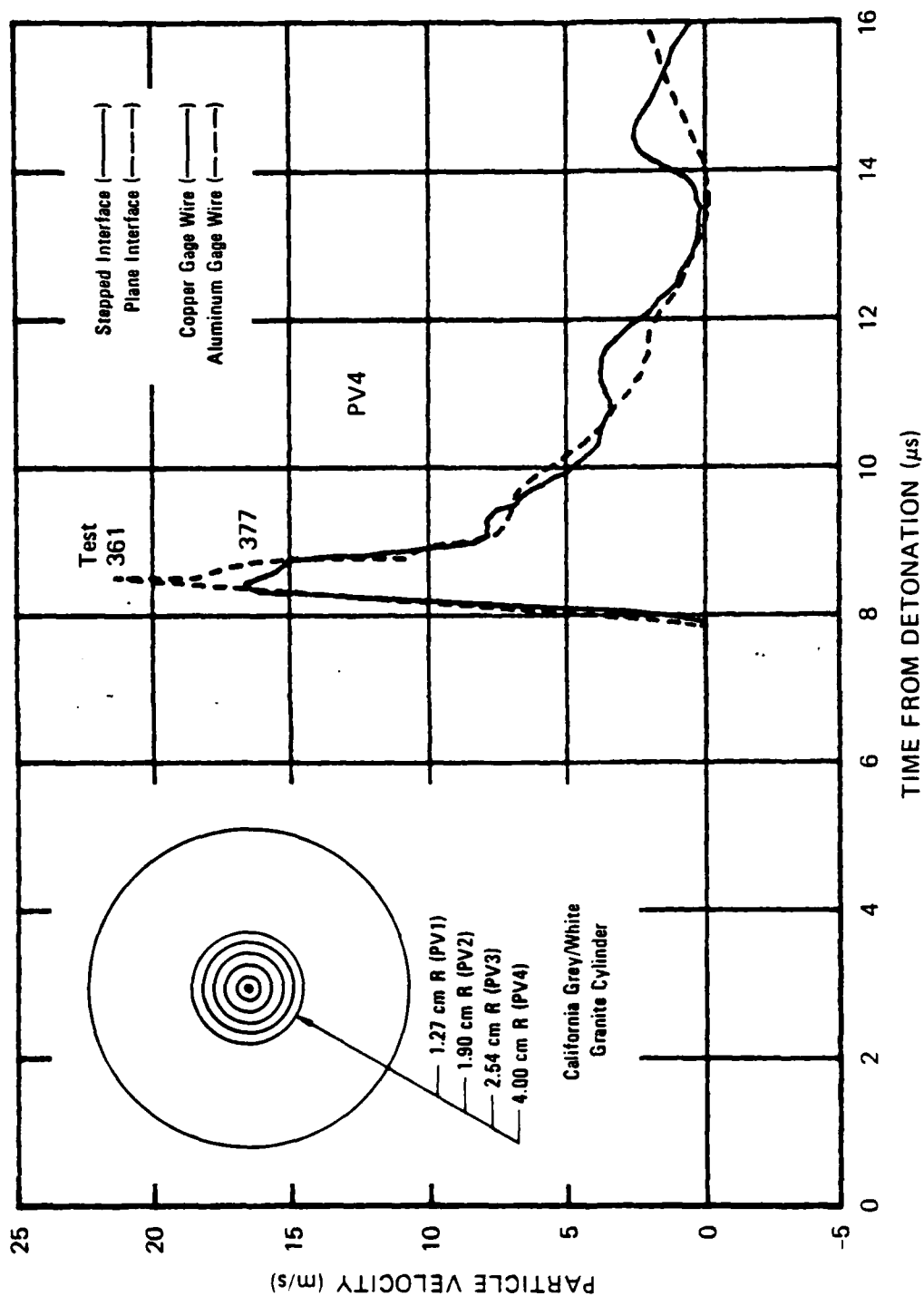
FIGURE 3.74   PARTICLE VELOCITY 4.00 cm FROM THE CENTER OF COUPLED EXPLOSIONS IN GRANITE —
MATERIAL PROPERTY

JA-5372-108

141
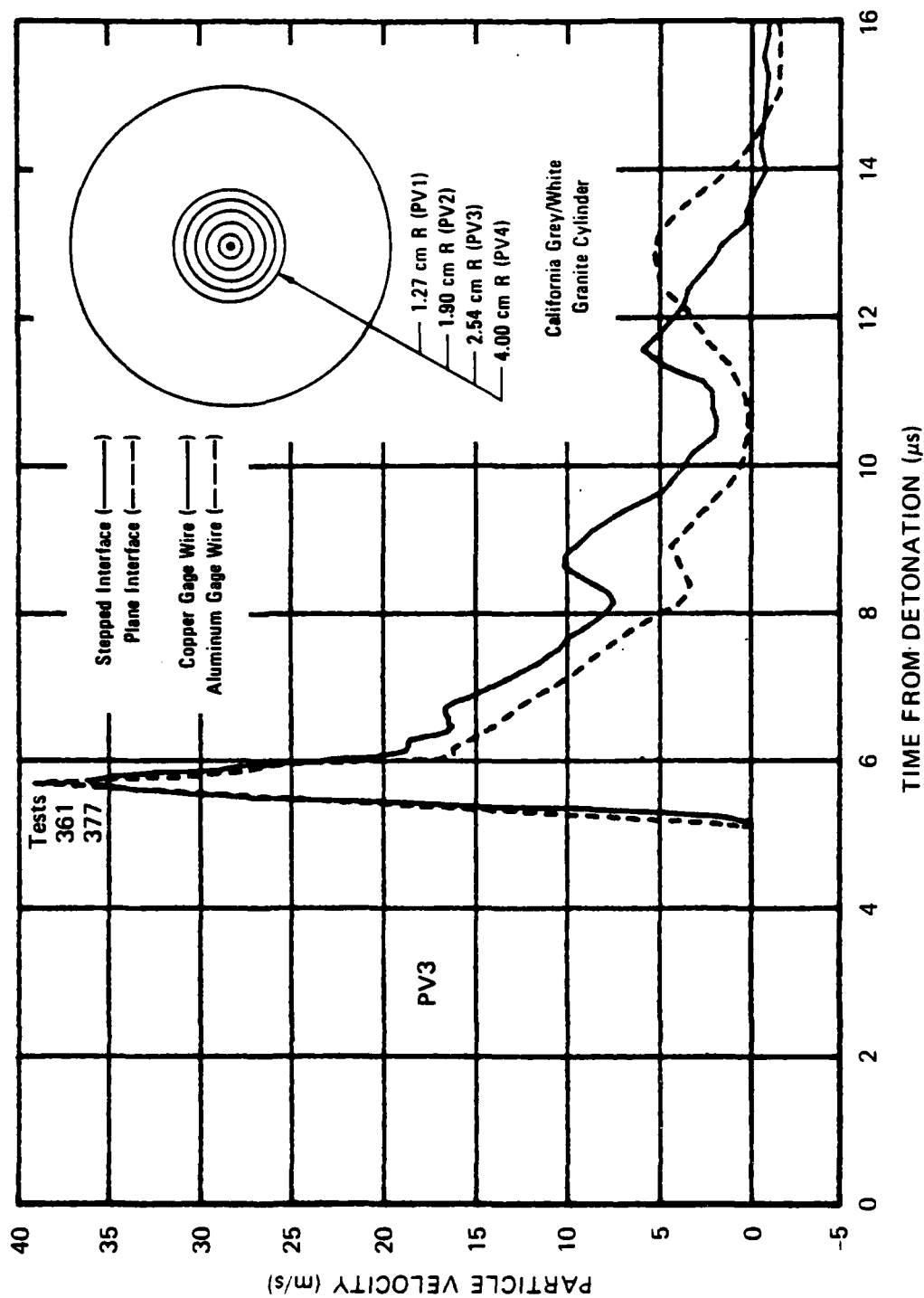
FIGURE 3.73 PARTICLE VELOCITY 2.54 cm FROM THE CENTER OF COUPLED EXPLOSIONS IN GRANITE —
MATERIAL PROPERTY
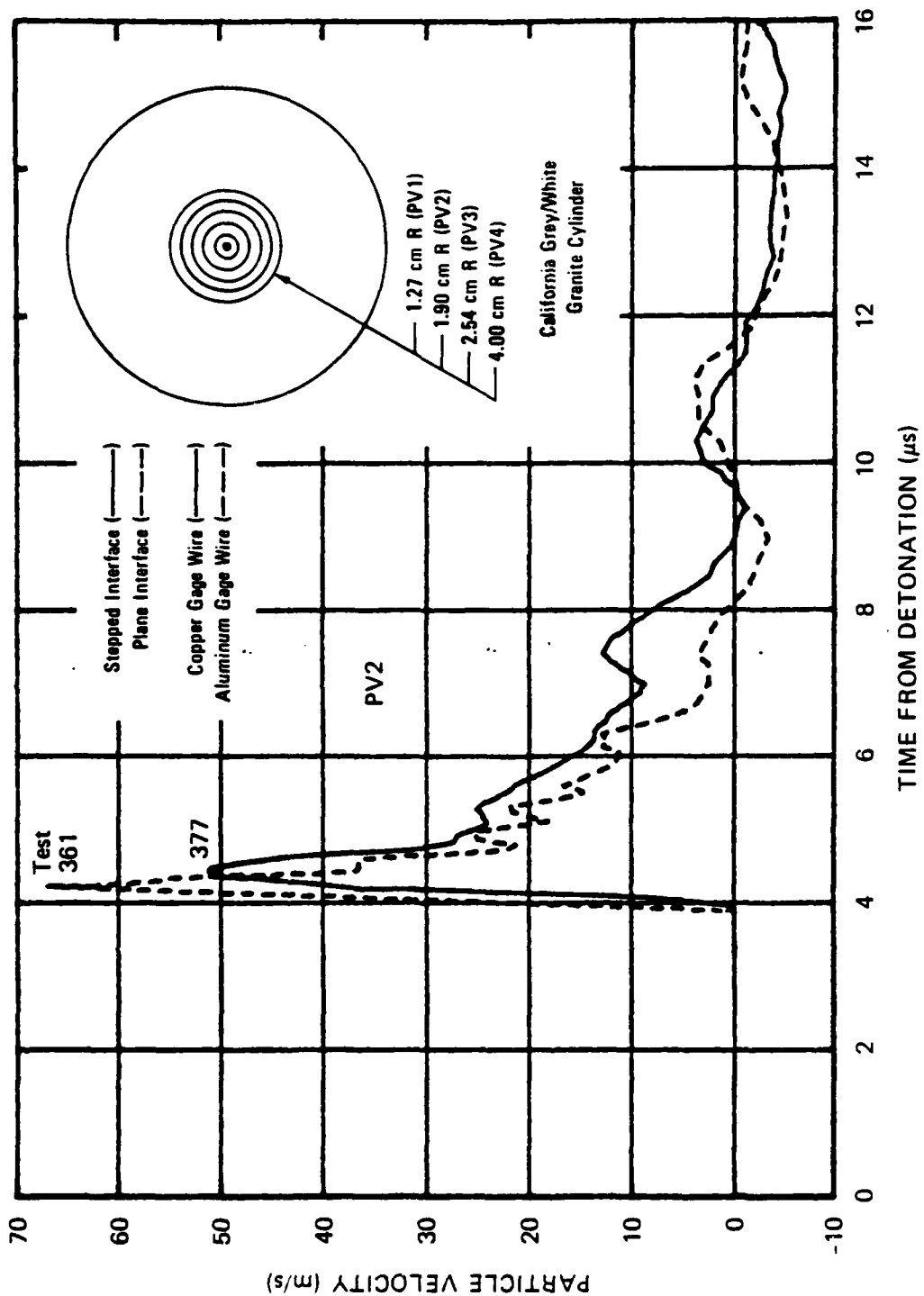
FIGURE 3.72 PARTICLE VELOCITY 1.90 cm FROM THE CENTER OF COUPLED EXPLOSIONS IN GRANITE – MATERIAL PROPERTY
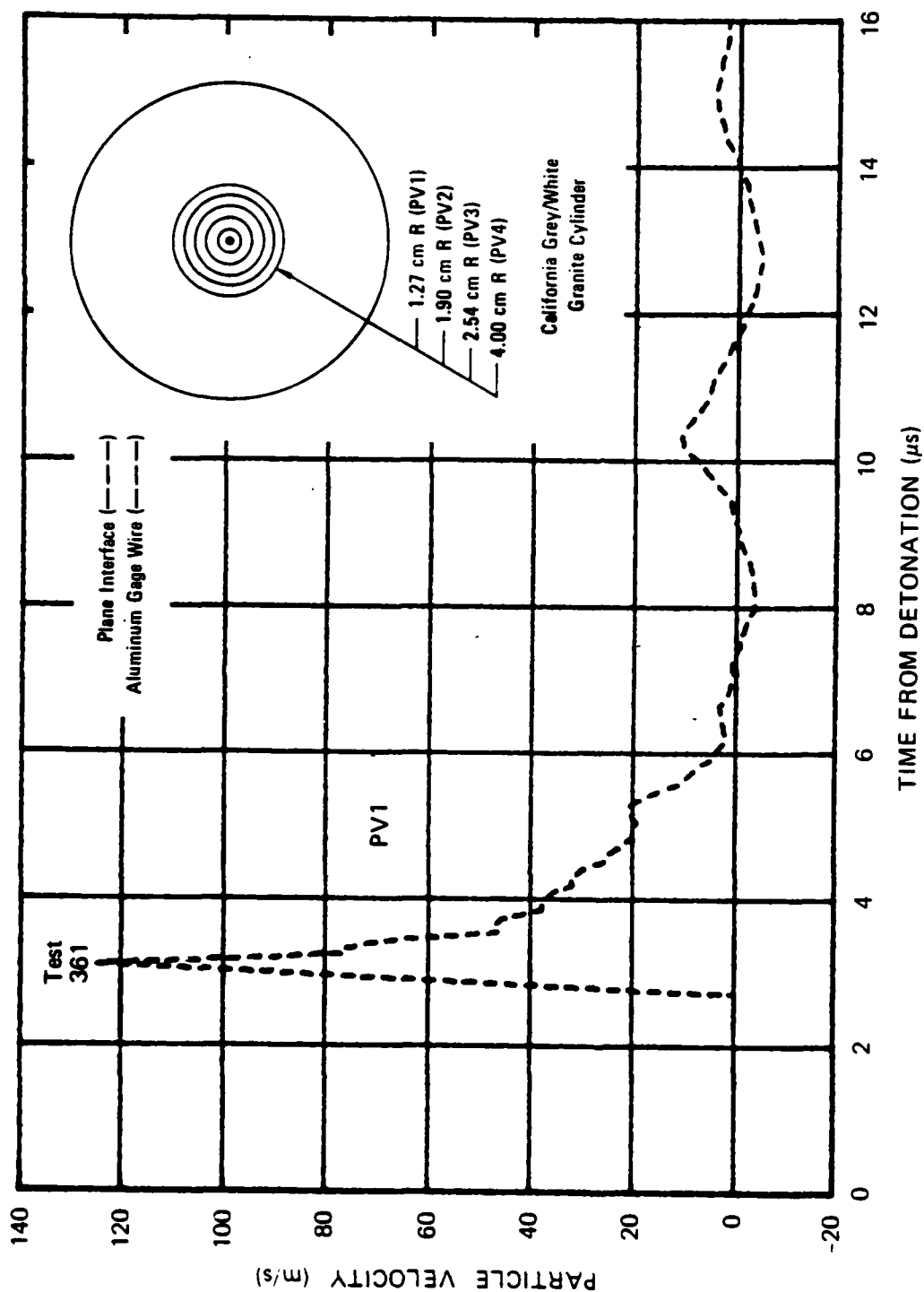
FIGURE 3.71 PARTICLE VELOCITY 1.27 cm FROM THE CENTER OF COUPLED EXPLOSION IN GRANITE – MATERIAL PROPERTY

138

vertical planes. After each cut, dyed water was pumped down the access tube and into the cavity to determine if the cut had intersected a fracture. This process showed that in both tests, a dynamic vertical fracture extending 2 inches (5.08 cm) from the cavity had formed as a result of charge detonation. Hence, dynamic cracking has been shown to be an inherent feature of particle velocity tests in California grey/white granite.

Pressure pulses in the overburden fluid from quartz gage measurements for tests 375 and 376 are shown in Figure B.8. The results are similar to measurements made during previous particle velocity tests (Series 9A).

An additional 1-foot (0.3-m) cube of granite was cored to a diameter of 9-5/8 inches (24.45 cm) so that a technique to prevent cracking along the particle velocity gage plane could be assessed. The configuration is shown in Figure 2.12 (Section 2.3). A hole and plug were precision ground in matching faces of a sectioned granite cylinder to provide a stepped interface. Circular grooves 9 mils (0.229 mm) wide were machined in the upper half of the cylinder at four radial locations (1.27, 1.90, 2.54, and 4.00 cm). Copper wire 5 mils (0.127 mm) in diameter was epoxied in the grooves, and the cylinder was epoxied along the plane of the gages. The charge was centered in the gage plane at the bottom of an axial hole. This configuration requires that a crack extending from the cavity propagate through granite before reaching the interface.

The configuration shown in Figure 2.12 was used in test 377, where the overburden pressure was 2300 psi (15.86 MPa). Figures 3.71 through 3.74 show the resulting particle velocity records. [Note that gage PV1 (Figure 3.71) broke before the test.] For comparison, results of test 361, in which a plane bonded interface extended through the charge as usual, are also shown. In test 361, the overburden pressure was 1000 psi (6.89 MPa) and aluminum wire 5 mils (0.127 mm) in diameter was epoxied in grooves 9 mils (0.229 mm) wide. The good agreement between the results for tests 361 and 377 indicates that the new configuration

137

Stainless Steel Access Tube
(0.250 in. OD, 0.180 in. ID)

Cylindrical Core
of Geologic Material

1 grain/ft MDF
Epoxied in Access
Tube

GS4
Stemming
Column

Explosive Charge
Epoxied to Access
Tube
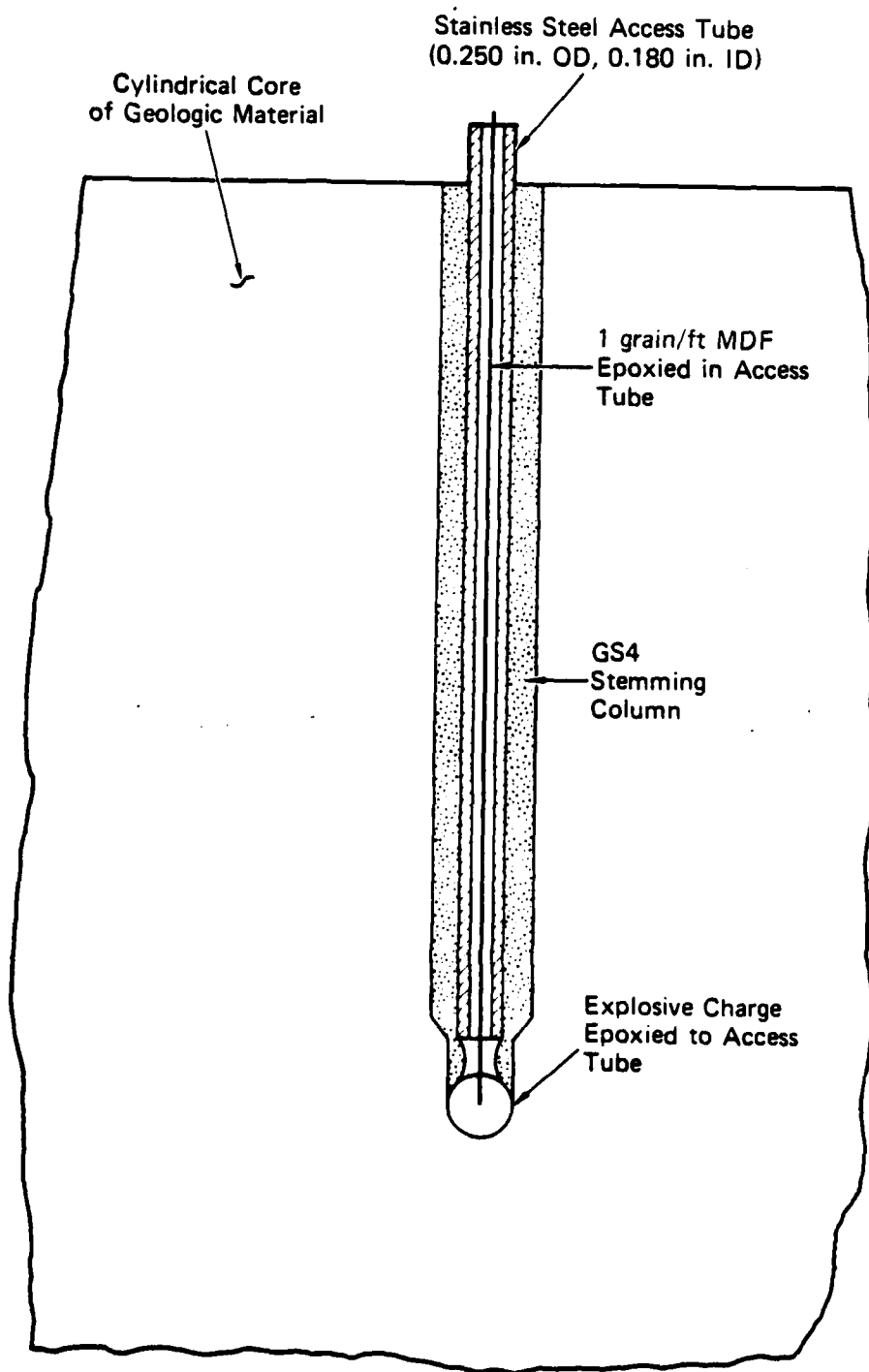
JA-5372-120

FIGURE 3.70   CONFIGURATION FOR EXPLODED CAVITY TEST IN CYLINDRICAL
CORE OF GEOLOGIC MATERIAL

136

(0.11 mm) at PV1 to 0.6 mil (0.02 cm) at PV4. The thickness of the epoxy layer at the interface was 10 mils (0.25 mm). One technique improvement would be to reduce or possibly eliminate the epoxy layer.

Pressure pulses in the overburden fluid obtained from quartz gage measurements for granite are shown in Figure B.6 (tests 366 and 367) and Figure B.7 (tests 369 and 370). In tests 369 and 370, the pulse crossed the bonded interface before reaching the quartz gage, and the impulse was reduced.

Series 9B: Material Property (California Grey/White Granite)

Particle velocity tests in granite cylinders have resulted in dynamic cracking along the bonded plane of the gages (Series 9A). Because particle velocity records are influenced by cracking, a series of tests was conducted to determine (1) if charge detonation in granite results in dynamic cracking even when the cylinder has not been sectioned and (2) if a technique could be developed to prevent cracking along the particle velocity gage plane.

Two 1-foot (0.3-m) cubes of California grey/white granite were cored to a diameter of 9-5/8 inches (24.45 cm) so that exploded cavity tests could be performed. Figure 3.70 shows the configuration developed for charge installation. A stepped axial hole is first drilled to the center of the cylinder. An access tube with attached explosive charge is then grouted into the hole. Granite simulant GS4 is used to stem the access hole in granite. The bottom of the hole is hemispherical and has a diameter equal to that of the charge to ensure coupling between the charge and surrounding material. The central charge is detonated by a strand of 1 gr/foot mild detonating fuse (MDF) epoxied in the access tube.

In tests 375 and 376, overburden pressure was increased from the standard 1000 psi (6.89 MPa) to 2300 psi (15.86 MPa) to reduce the potential for dynamic cracking. Following charge detonation, the cylinders were removed from the pressure vessel, the access tubes were drilled out, and the granite was sectioned along several horizontal and

135
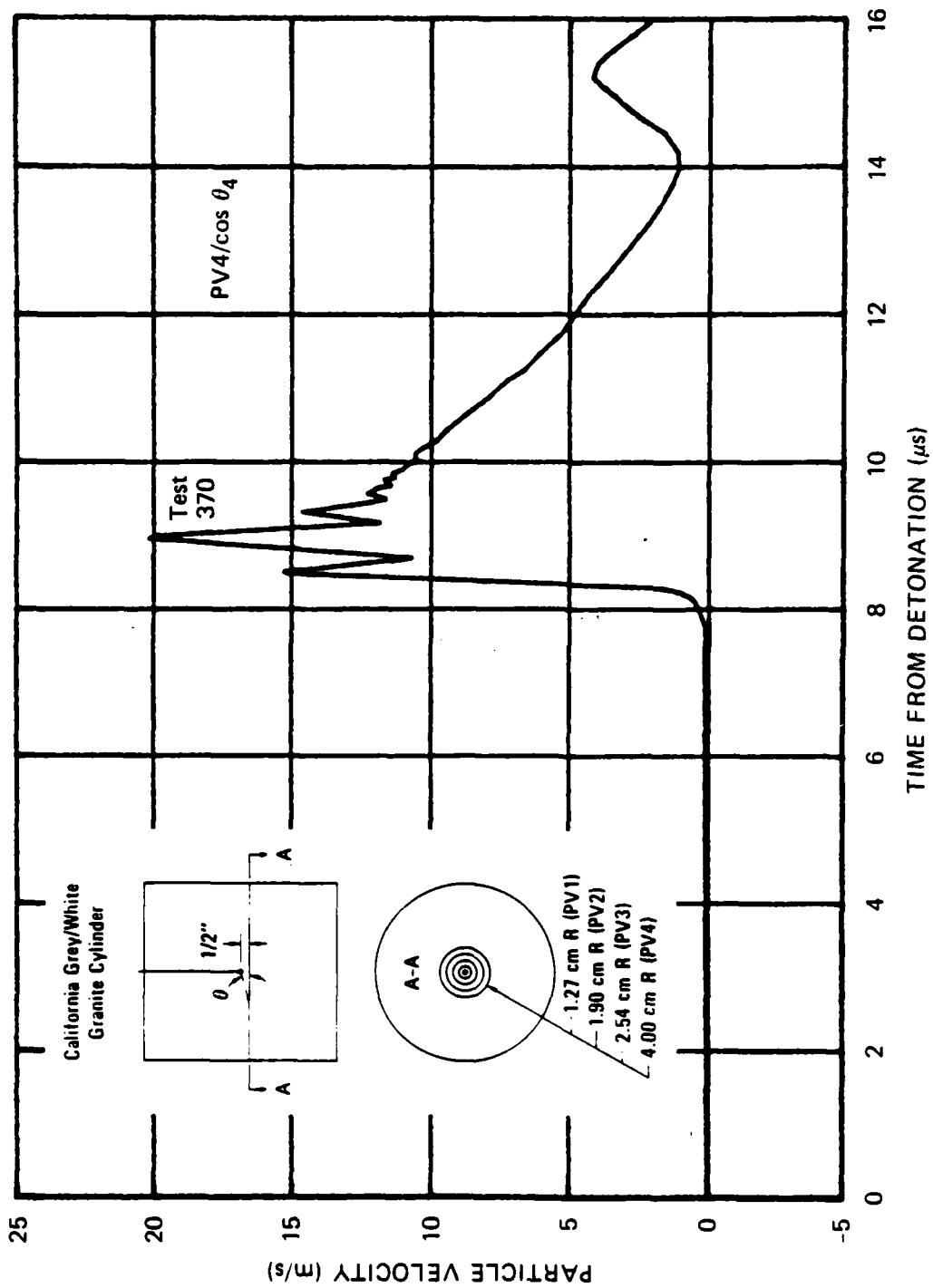
FIGURE 3.69   PARTICLE VELOCITY 4.18 cm FROM THE CENTER OF COUPLED EXPLOSION IN GRANITE — GAGE PLANE BELOW CHARGE

134
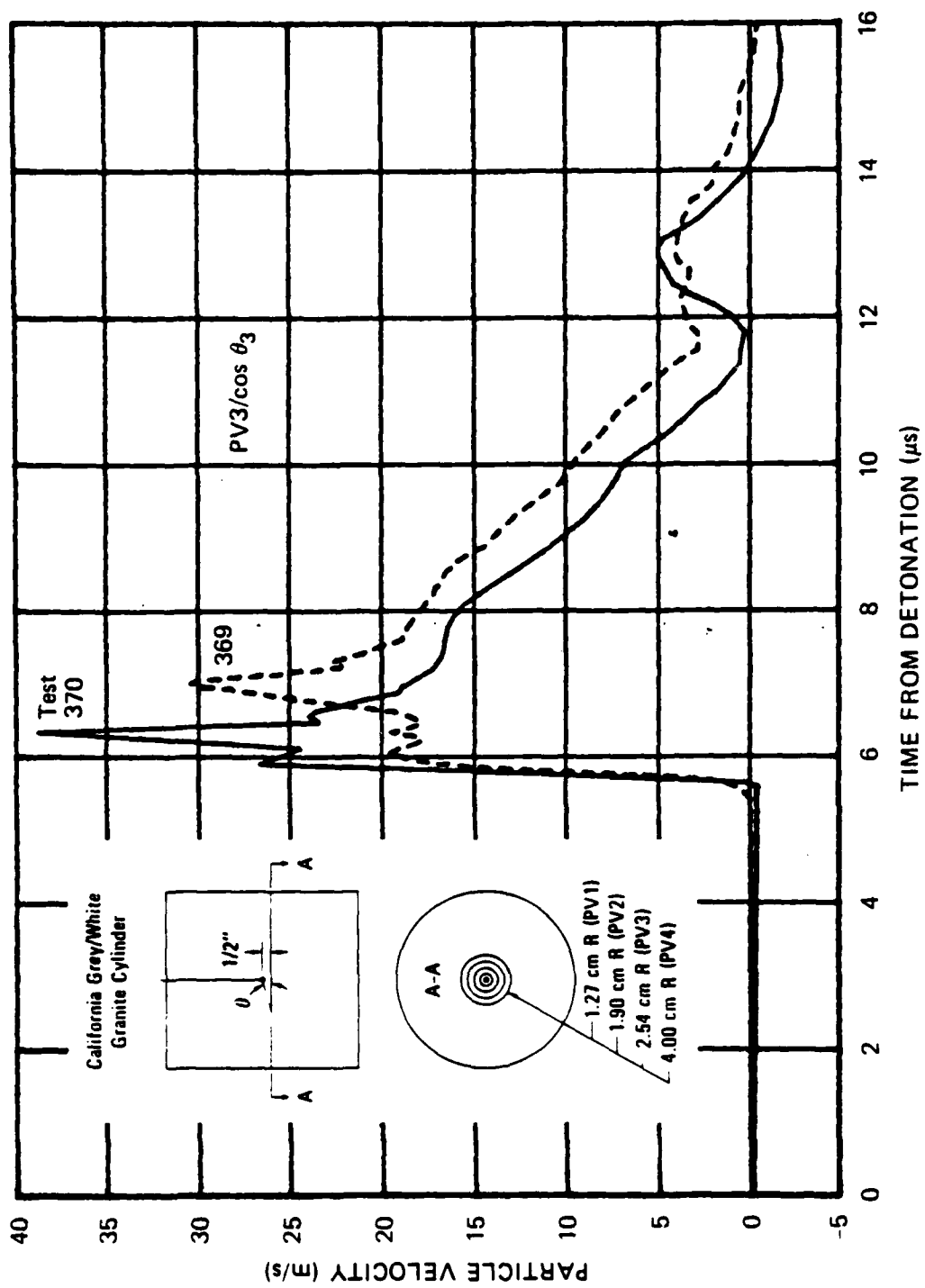
FIGURE 3.68 PARTICLE VELOCITY 2.82 cm FROM THE CENTER OF COUPLED EXPLOSIONS IN GRANITE – GAGE PLANE BELOW CHARGE

JA-5372-62

133
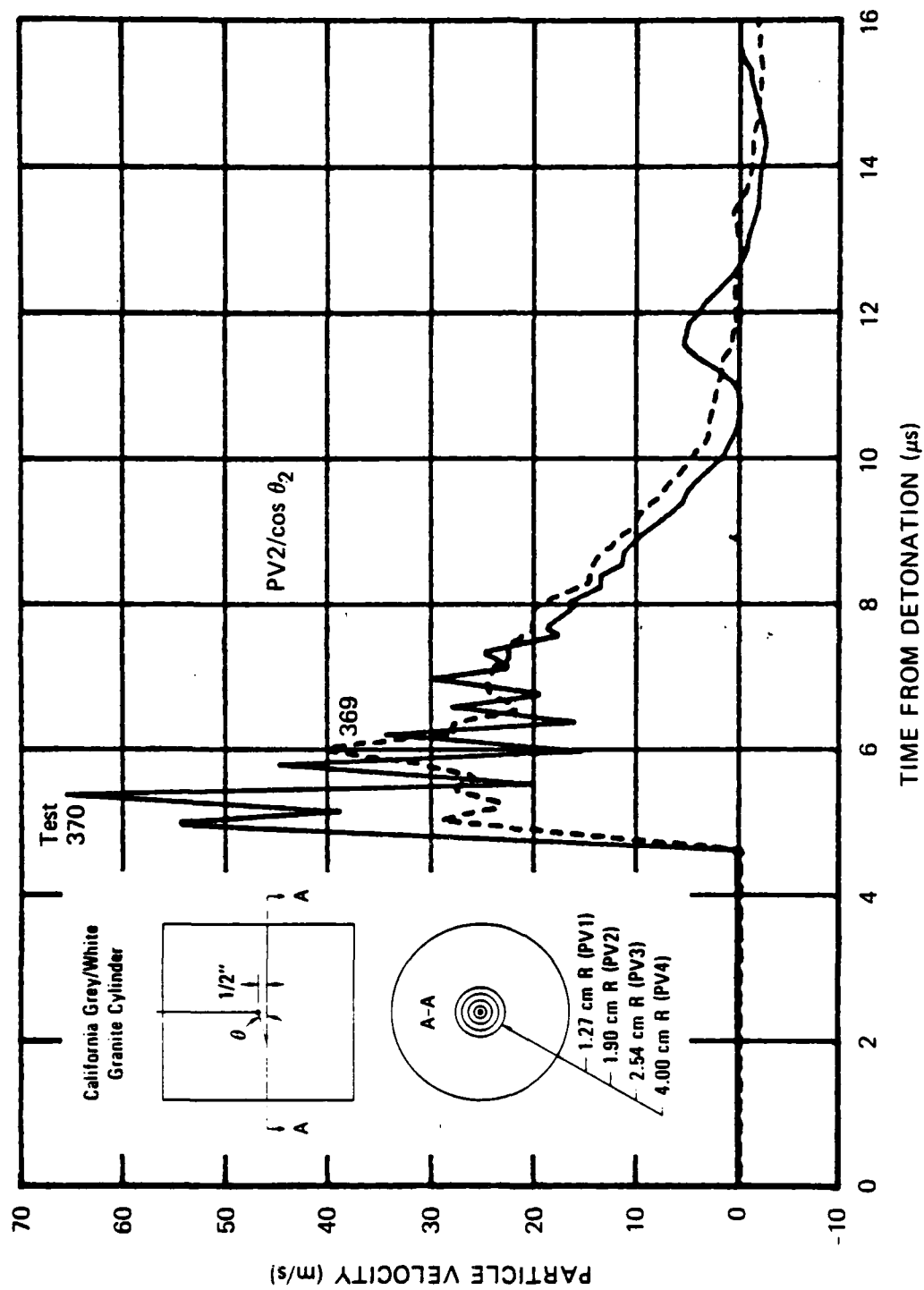
FIGURE 3.67   PARTICLE VELOCITY 2.26 cm FROM THE CENTER OF COUPLED EXPLOSIONS IN GRANITE —
GAGE PLANE BELOW CHARGE
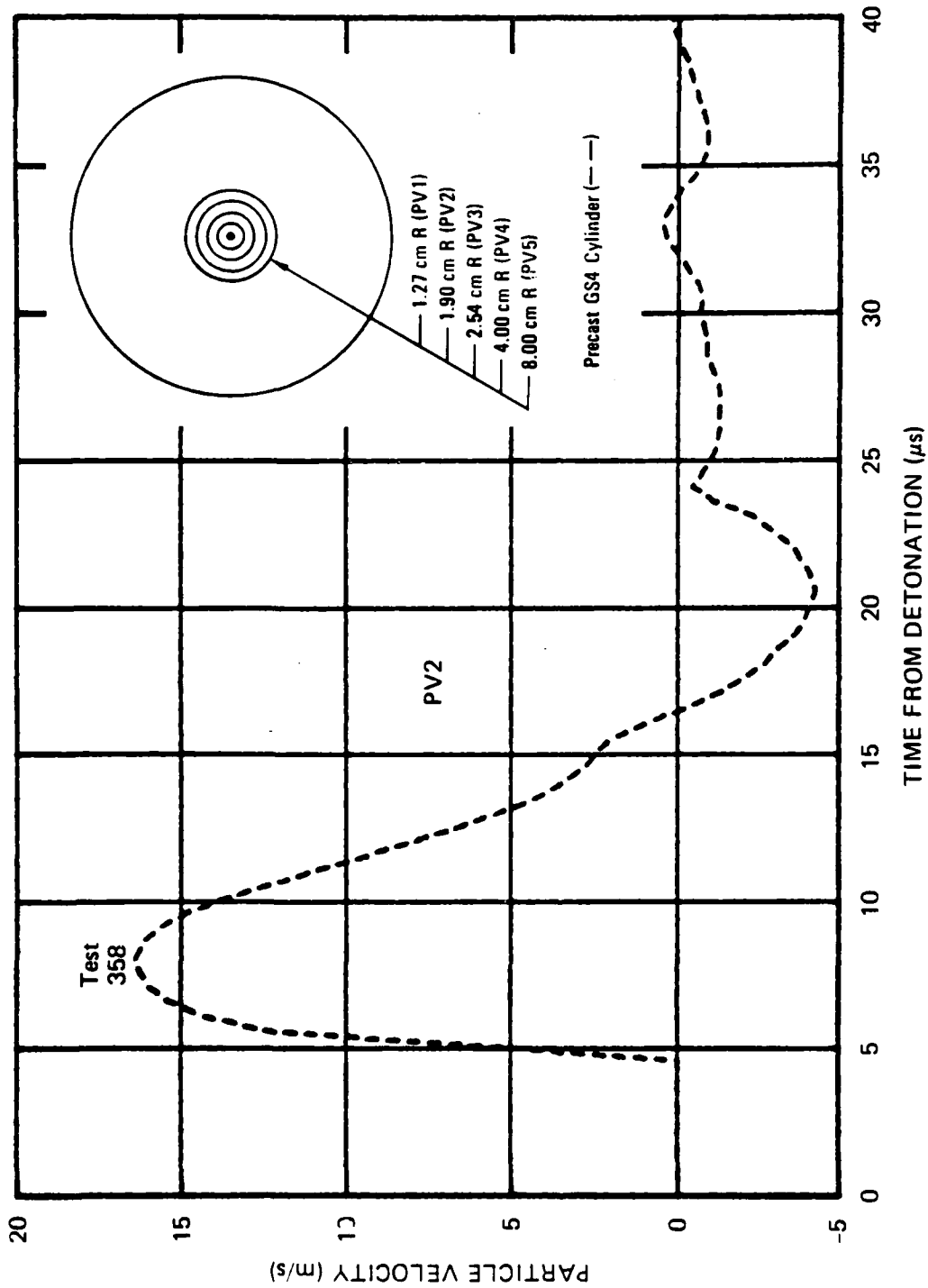
FIGURE 3.78   PARTICLE VELOCITY 1.90 cm FROM THE CENTER OF COUPLED EXPLOSION IN GS4

JA-5372-38A

146
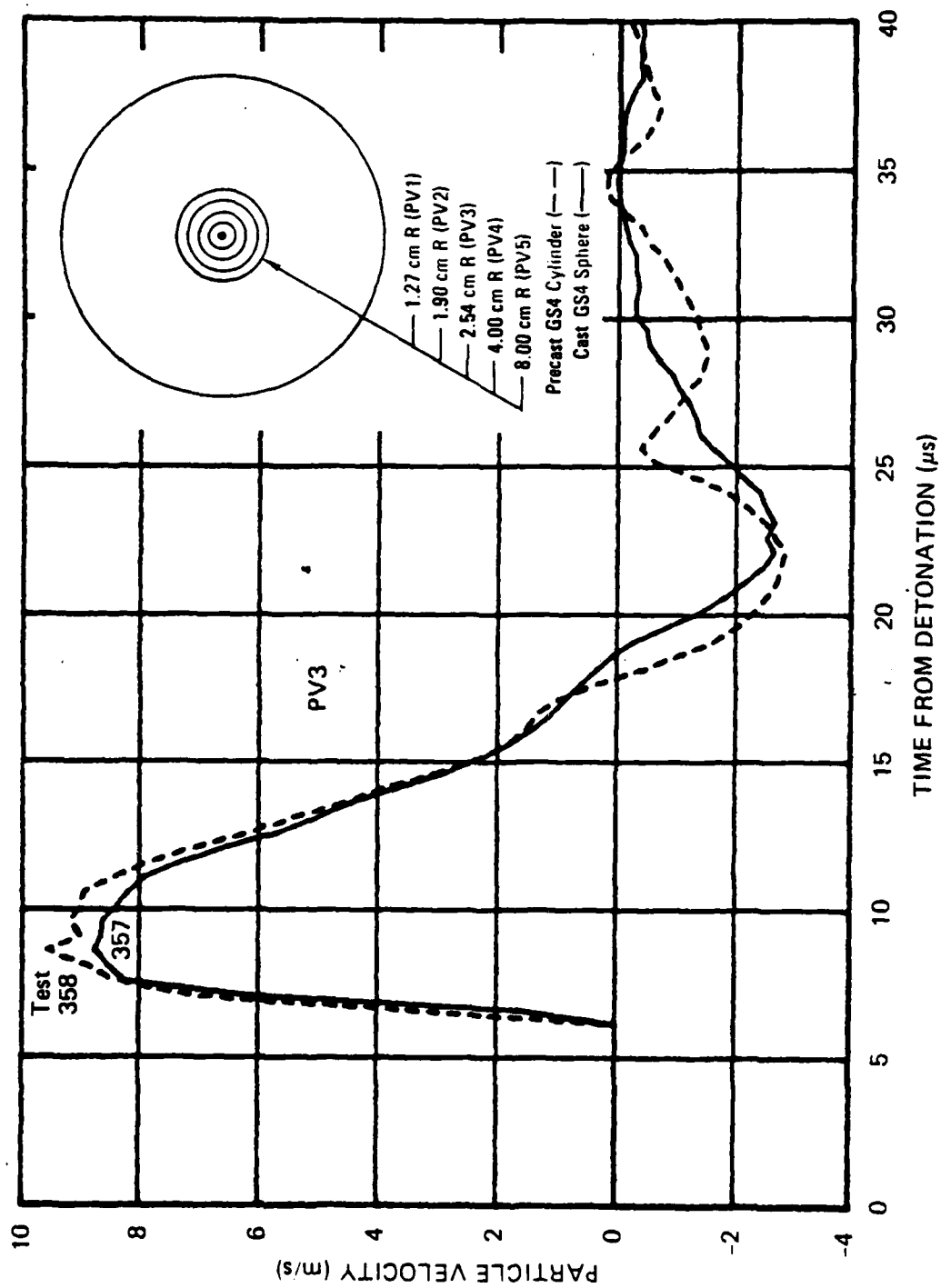
FIGURE 3.79 PARTICLE VELOCITY 2.54 cm FROM THE CENTER OF COUPLED EXPLOSIONS IN GS4

JA-5372-39

147
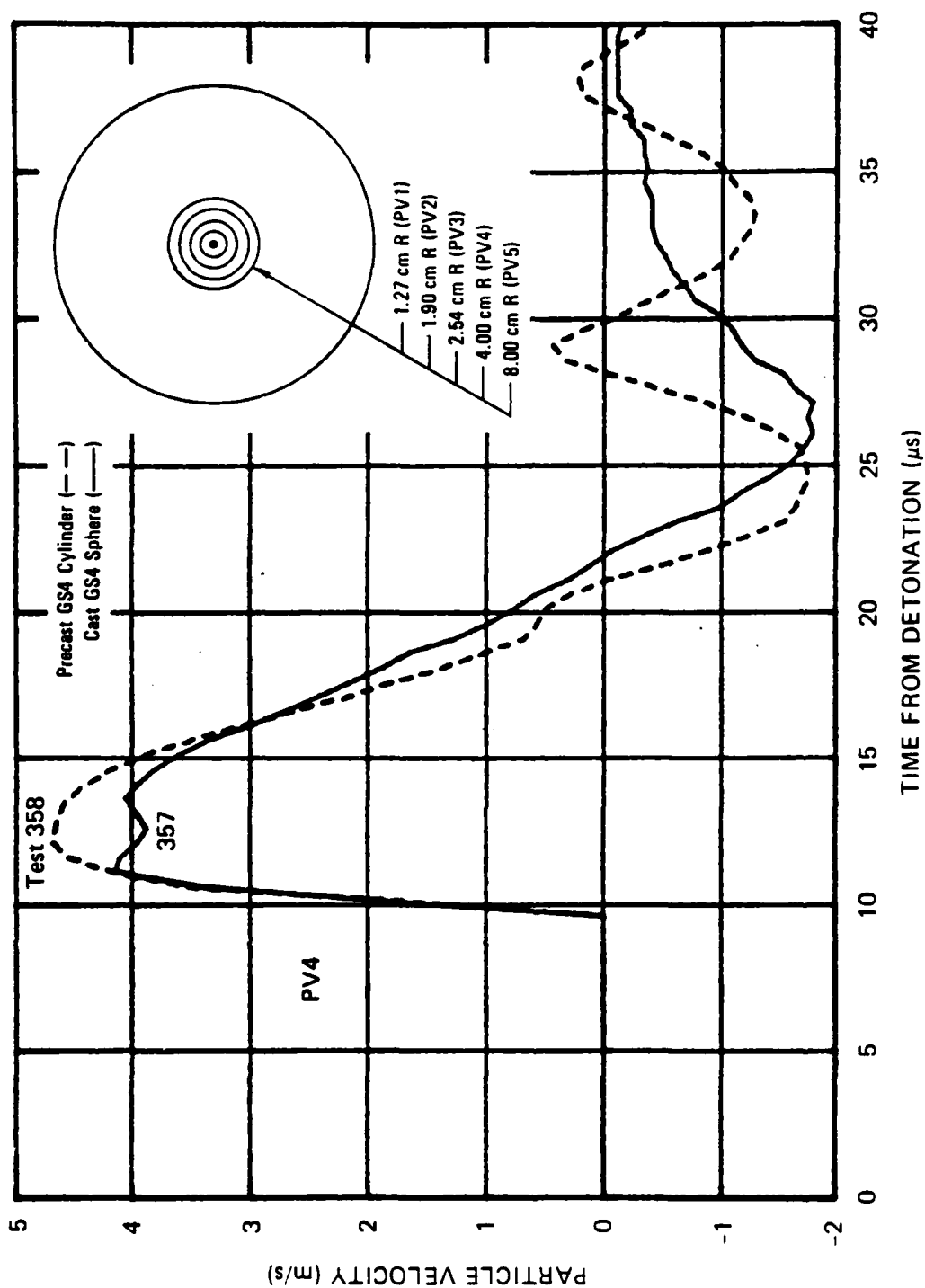
FIGURE 3.80   PARTICLE VELOCITY 4.00 cm FROM THE CENTER OF COUPLED EXPLOSIONS IN GS4

148
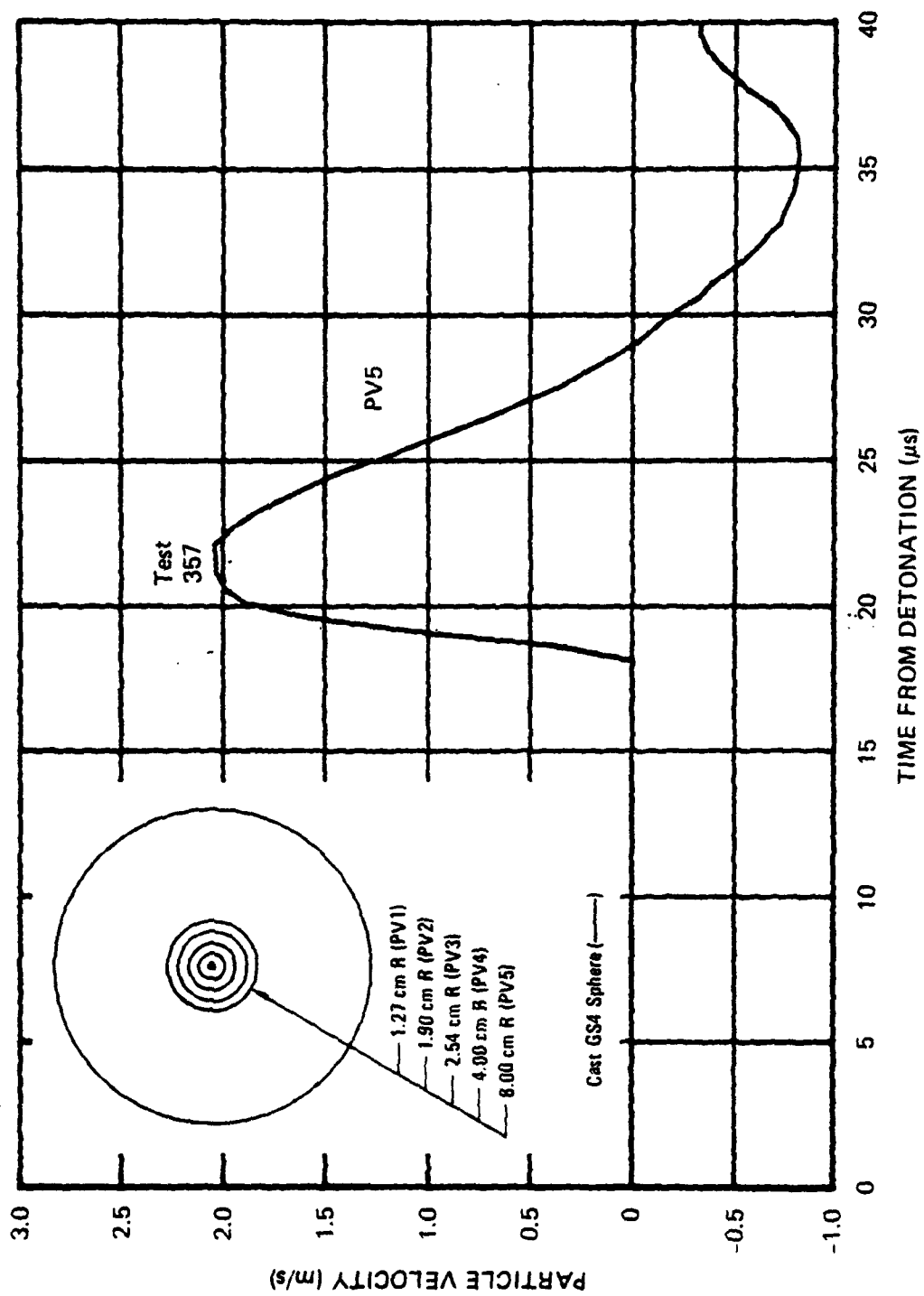
FIGURE 3.81 PARTICLE VELOCITY 8.00 cm FROM THE CENTER OF COUPLED EXPLOSION IN GS4

JA-6372-41A

149

differences during rebound. In test 357, rebound occurs smoothly. In test 358, however, rebound occurs erratically as a series of accelerating and decelerating motions. This erratic motion is attributed to dynamic cracking along the bonded plane of the gages. A crack extending 2 inches (5.08 cm) from the center of the cavity was detected during posttest examination of the cylinder. Hydrofracture of the sphere used in test 357, however, indicated that no dynamic fracture had occurred in that test.

In both GS4 tests, a 0.625-inch-diameter (1.59-cm) exploded cavity was formed. An estimate of exploded cavity diameter based on particle displacement (Test 358, PV1, Figure A.10) and an assumption of incompressibility yields 0.665 inch (1.69 cm). The larger calculated value indicates that the GS4 is permanently compacted near the cavity. The volume strain (Figure 3.82) shows permanent compression in the region between gages PV1 and PV2.

Attentuation of peak particle velocity with range for GS4, granite, and RMG 2C4 is shown in Figure 3.83. Figure 3.84 shows the time of arrival of the wavefront at each gage location for granite, GS4 and RMG. A constant wave speed of 4.20 mm/μs for GS4, 5.29 mm/μs for granite, and 3.29 mm/μs for RMG 2C4 applies over the range of the gages.

Pressure pulses in the overburden fluid obtained from quartz gage measurements are shown in Figure B.9. Similarity of the pulses indicates charge reproducibility and consistency in the material properties of GS4.

Series 11: Material Property (Reconstituted Alluvium with Zero Pore Pressure

The procedure described in Appendix E for measuring particle velocity in reconstituted alluvium was applied in six tests. The gage material was 10-mil-diameter (0.254-mm) copper wire insulated with a 5-mil-thick (0.127-mm) layer of Teflon. Overall gage density was 3.1 g/cm^3. Gages were embedded at five radial locations (1.27, 1.90, 2.54, 4.00, and 8.00 cm). Figures 3.85 through 3.89 show the resulting
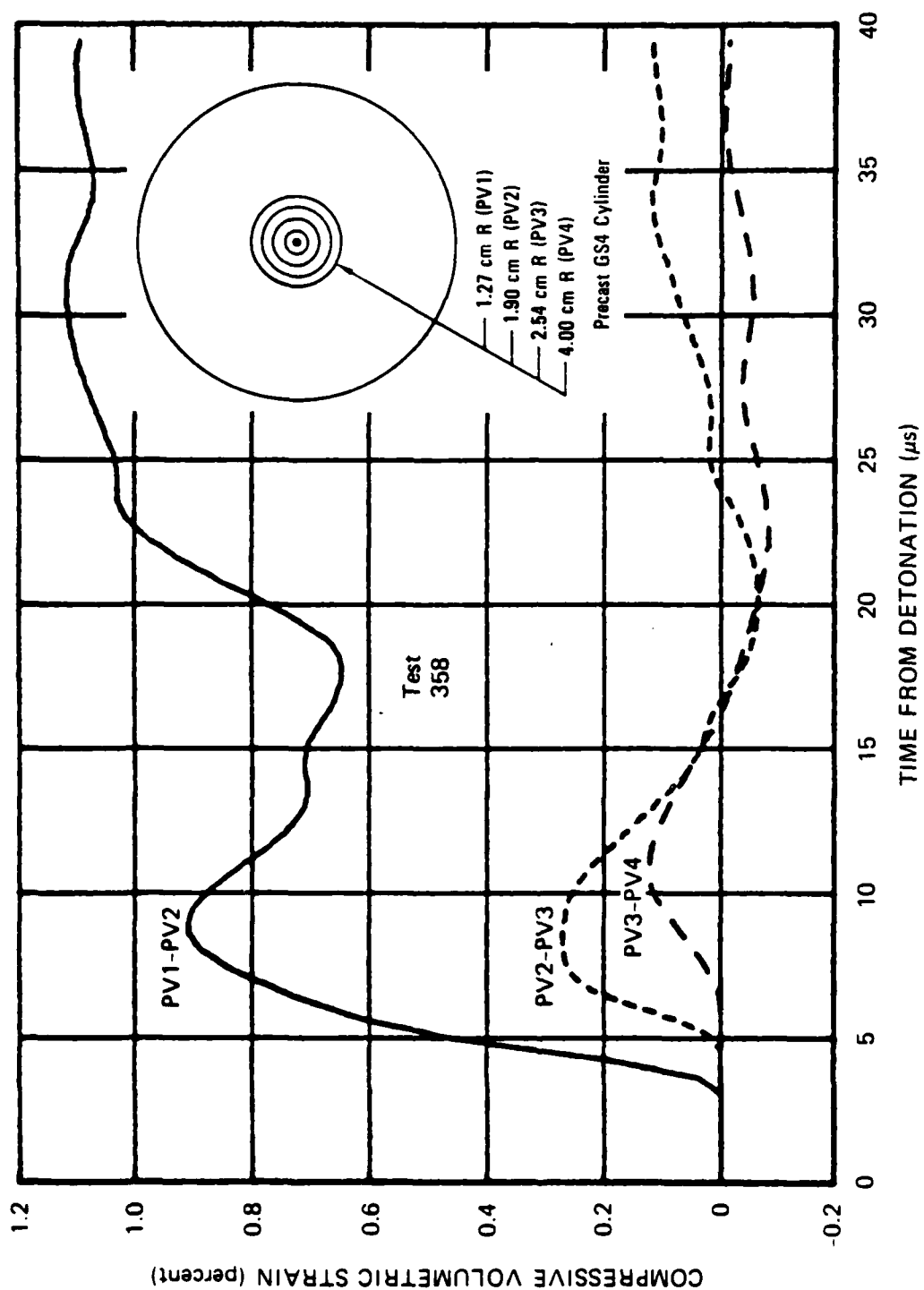
FIGURE 3.82   VOLUMETRIC STRAIN OBTAINED FROM A PARTICLE VELOCITY TEST IN GS4

151
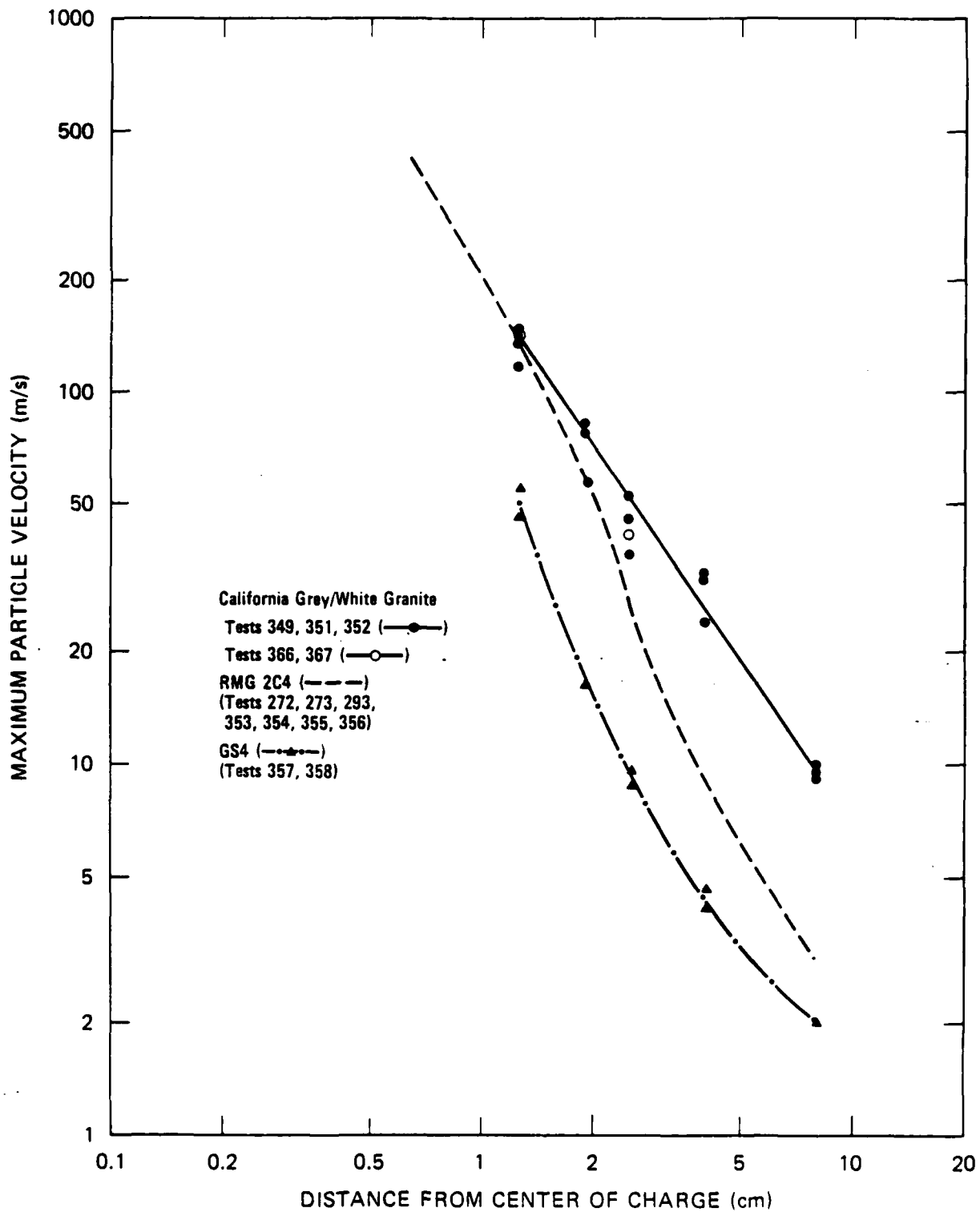
FIGURE 3.83 MAXIMUM PARTICLE VELOCITY VERSUS DISTANCE FROM CENTER OF CHARGE
FOR GS4, GRANITE, AND RMG 2C4

JA-5372-103B

152
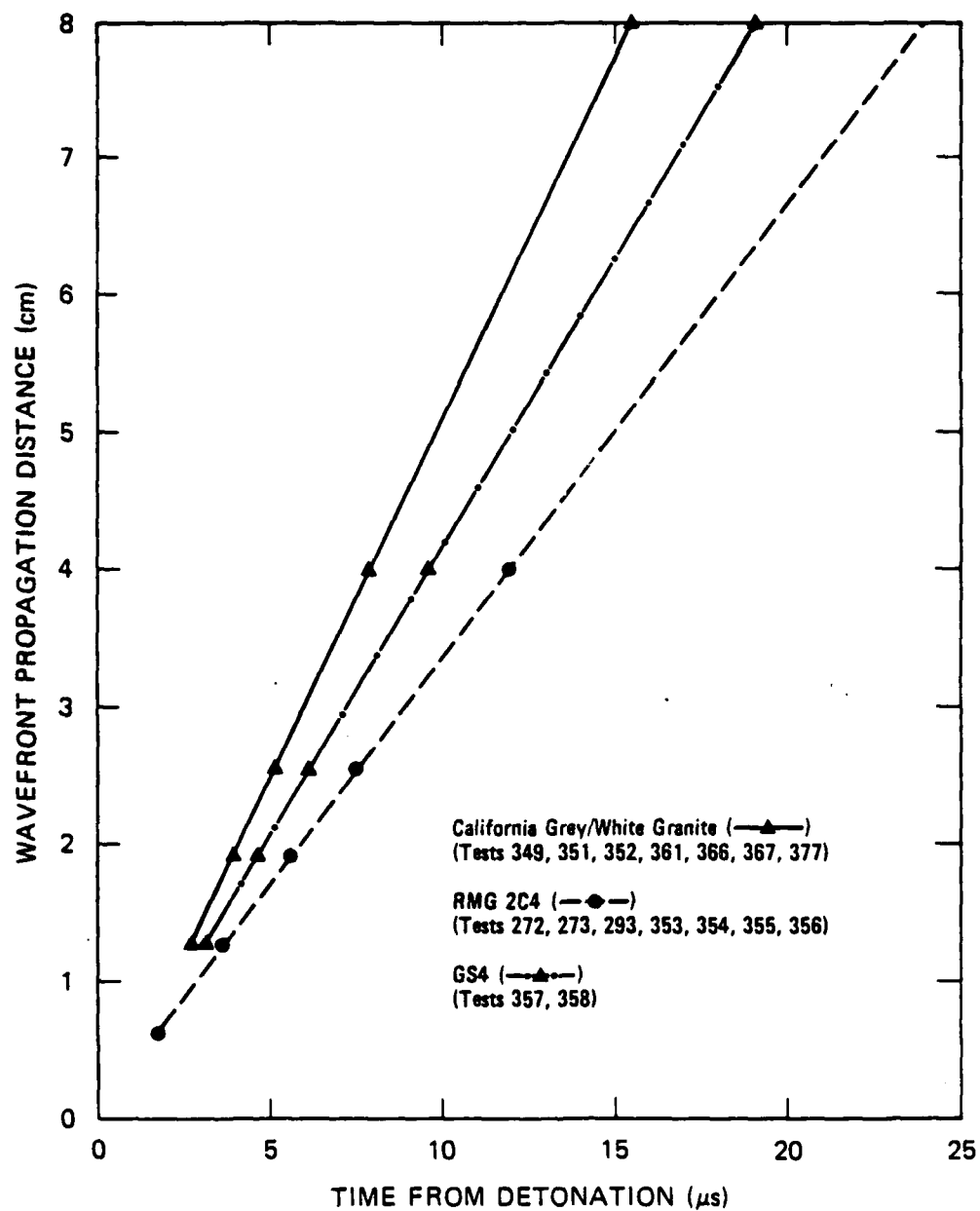
FIGURE 3.84 WAVEFRONT PROPAGATION DISTANCE VERSUS TIME FROM DETONATION
FOR GS4, GRANITE, AND RM6 2C4

153
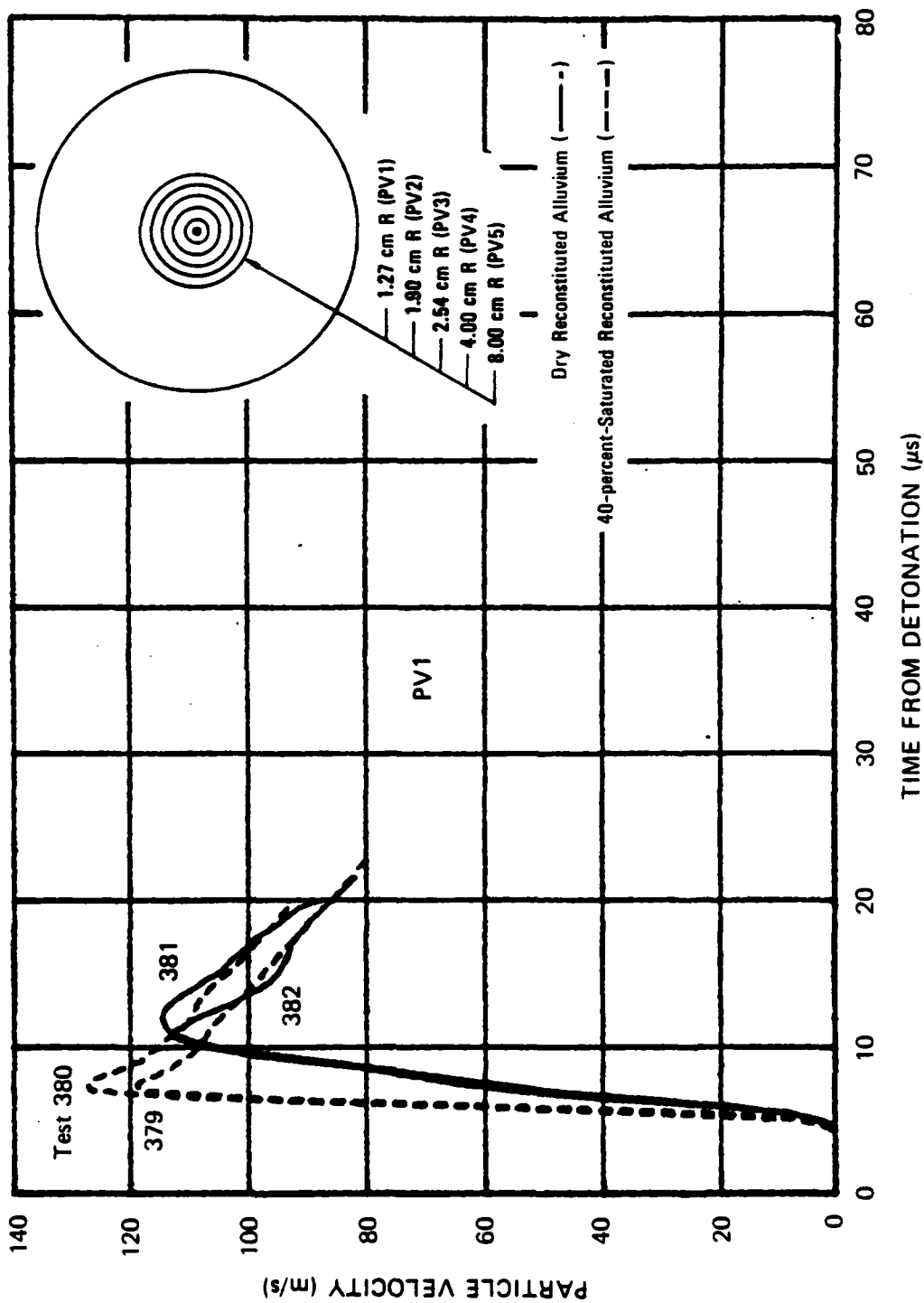
FIGURE 3.85 PARTICLE VELOCITY 1.27 cm FROM THE CENTER OF COUPLED EXPLOSIONS IN RECONSTITUTED ALLUVIUM – DRY VERSUS 40 percent SATURATED

JA-5372-122

154
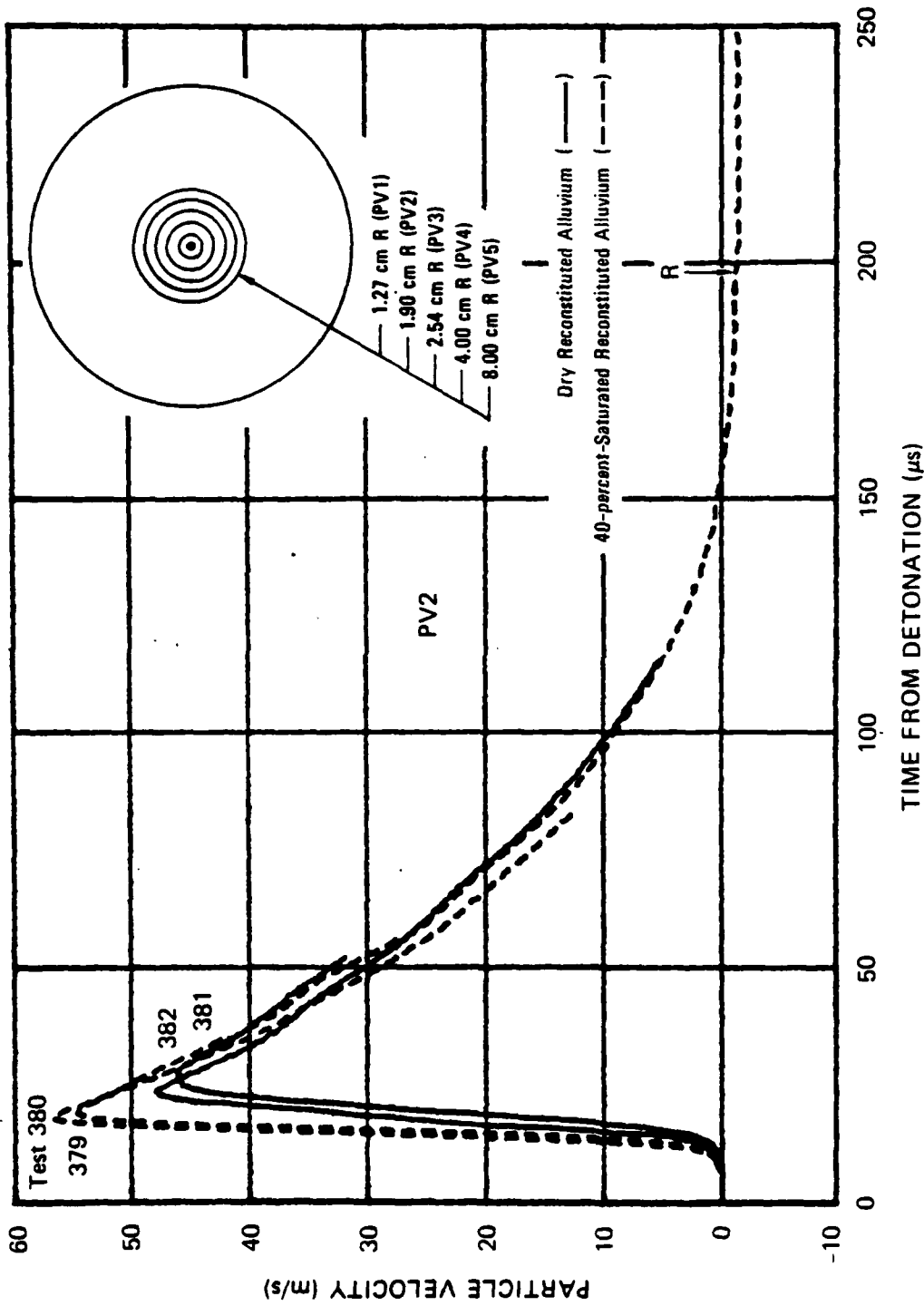
FIGURE 3.86 PARTICLE VELOCITY 1.90 cm FROM THE CENTER OF COUPLED EXPLOSIONS IN RECONSTITUTED ALLUVIUM – DRY VERSUS 40 percent SATURATED

JA-5372-123

155
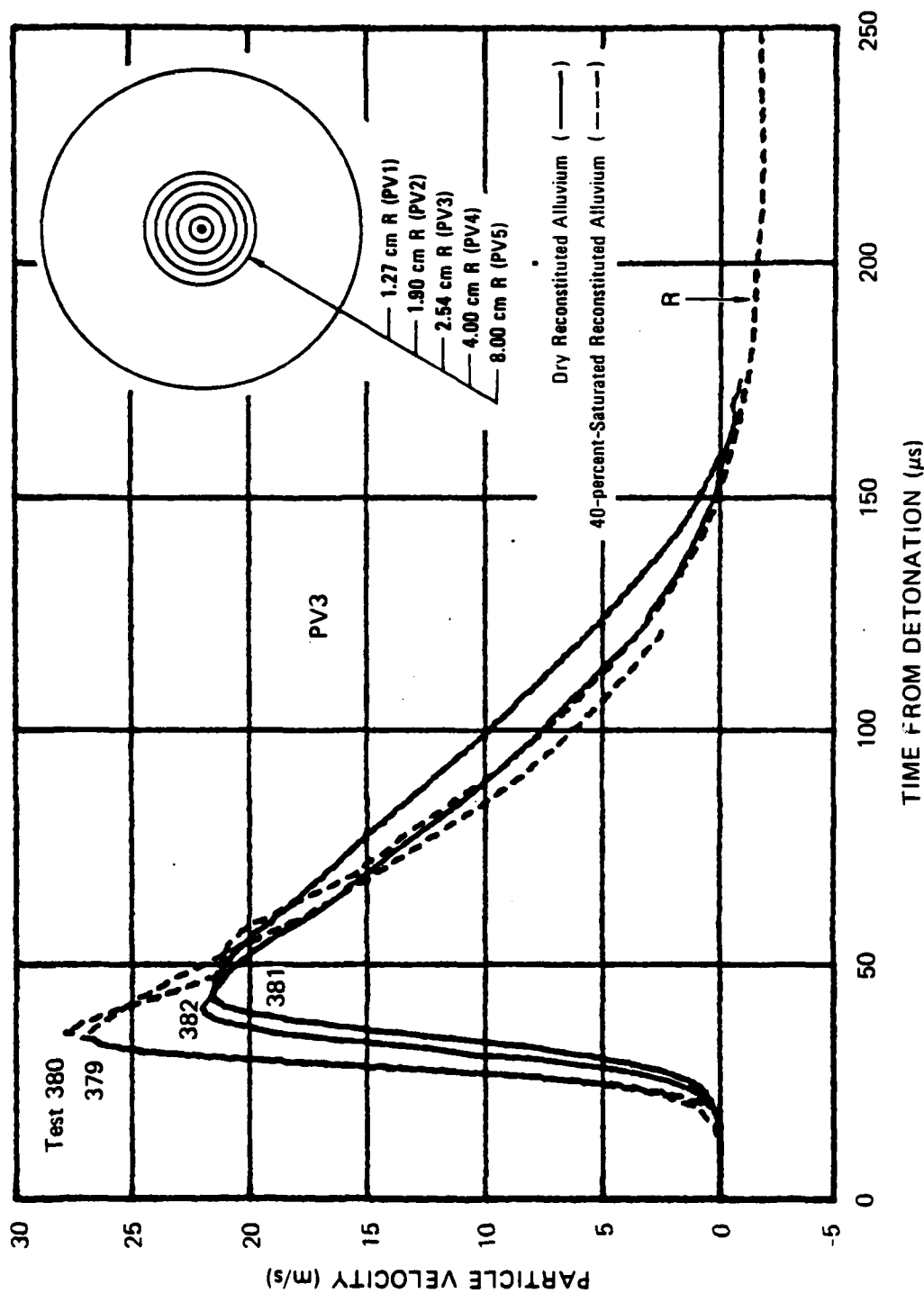
FIGURE 3.87 PARTICLE VELOCITY 2.54 cm FROM THE CENTER OF COUPLED EXPLOSIONS
IN RECONSTITUTED ALLUVIUM – DRY VERSUS 40 percent SATURATED

JA-5372-124

156
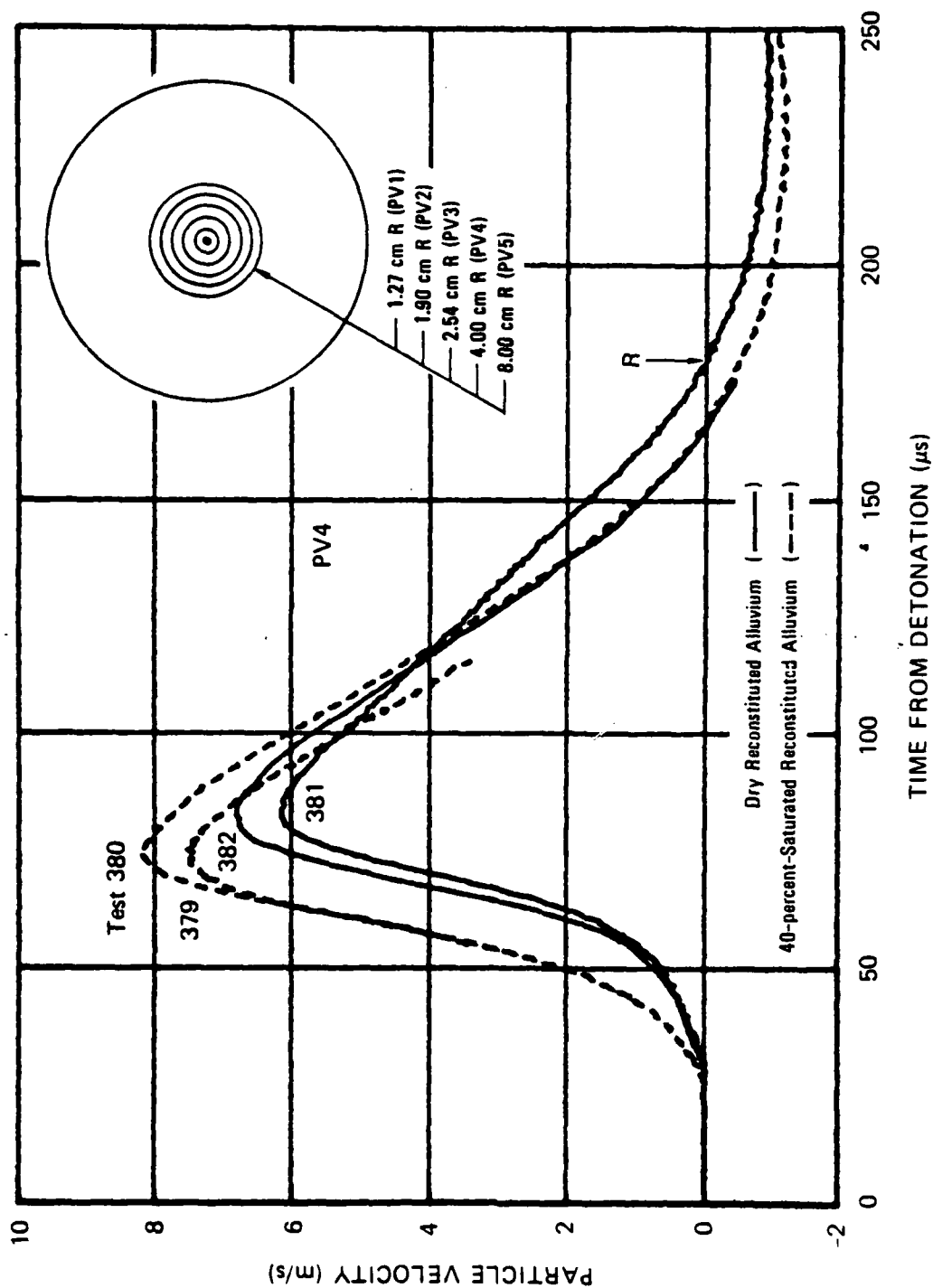
FIGURE 3.88 PARTICLE VELOCITY 4.00 cm FROM THE CENTER OF COUPLED EXPLOSIONS IN RECONSTITUTED ALLUVIUM – DRY VERSUS 40 percent SATURATED

157
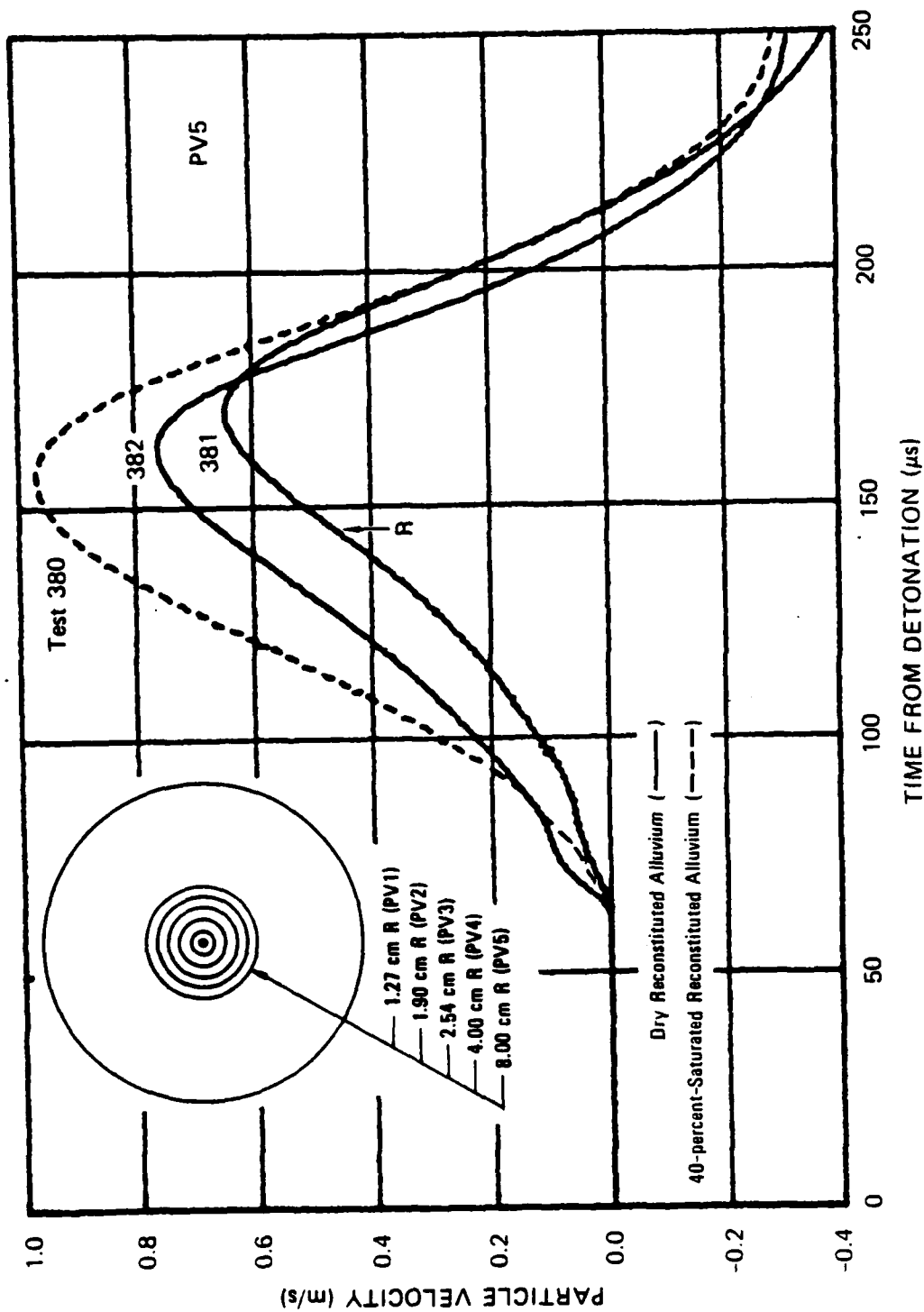
FIGURE 3.89 PARTICLE VELOCITY 8.00 cm FROM THE CENTER OF COUPLED EXPLOSIONS
IN RECONSTITUTED ALLUVIUM – DRY VERSUS 40 percent SATURATED

JA-5372-126

158

particle velocity profiles for dry alluvium (tests 381 and 382) and 40%-saturated alluvium (tests 379 and 380). Figures 3.90 through 3.94 show the corresponding profiles for 88%-saturated alluvium (tests 383 and 384).

The particle velocity records show predominantly outward motion. This result is consistent with the negligible tensile strength of the material. The records also show that accelerations at the wavefront are highest for the 88%-saturated alluvium and lowest for the dry desert fines. This result indicates that compaction of pores has a strong influence on the initial particle velocity response.

A measure of pore compaction in the reconstituted alluvium is obtained from the volumetric strain response of the material. Figures 3.95 through 3.97 show this response as derived from the particle velocity records. Similar volumetric strain response was obtained for dry alluvium (Figure 3.95) and 40%-saturated material (Figure 3.96). Compressive strain was produced over the entire region monitored by the particle velocity gages, and a maximum strain of 10% was measured. In contrast, if the reflected wave is weak and does not contribute to volume strain, then volume dilatation occurred for the 88%-saturated alluvium (Figure 3.97), and the maximum compressive strain measured was only 3%. These results suggest that pore fluid pressure develops in the 88%-saturated material as pores are compacted.

Note that for the 88%-saturated alluvium (Figure 3.98), volume strain in the region between gages PV1 and PV2 is less than the strain between gages PV2 and PV3. This result indicates that gage PV1 did not respond satisfactorily to peak particle velocity. The lack of a pronounced peak in the particle velocity record (Figure 3.91) also indicates the same result. A closer match between gage wire density and alluvium density may be required in regions of large particle acceleration.

Posttest examination of the alluvium revealed well-formed spherical exploded cavities with diameters of 3.0 cm for dry and 88%-saturated material and 2.5 cm for the 40%-saturated material. Hence tensile

159

FIGURE 3.102   PARTICLE VELOCITY 2.54 cm FROM THE CENTER OF COUPLED EXPLOSIONS IN RECONSTITUTED ALLUVIUM (WITH 2000-psi PORE PRESSURE) AND RMG 2C4

173

FIGURE 3.101   PARTICLE VELOCITY 1.90 cm FROM THE CENTER OF COUPLED EXPLOSIONS IN RECONSTITUTED
ALLUVIUM (WITH 2000-psi PORE PRESSURE) AND RMG 2C4

172

FIGURE 3.100 PARTICLE VELOCITY 1.27 cm FROM THE CENTER OF COUPLED EXPLOSIONS IN RECONSTITUTED ALLUVIUM (WITH 2000-psi PORE PRESSURE) AND RMG 2C4

JA-5372-53

171

FIGURE 3.99   WAVEFRONT PROPAGATION DISTANCE VERSUS TIME
FROM DETONATION FOR RECONSTITUTED ALLUVIUM

170

JA-5372-142

FIGURE 3.98 MAXIMUM PARTICLE VELOCITY VERSUS DISTANCE FROM CENTER
OF CHARGE FOR RECONSTITUTED ALLUVIUM

169

circumferential strains at the cavity were the same for dry and 88%-saturated material even though volume strains differed.

Figure 3.98 shows the attenuation of maximum particle velocity for the alluvium tested. In general, velocity at a given range increased with saturation. Figure 3.99 shows the time of arrival of the wavefront at each gage location. For dry and 40%-saturated alluvium, the wave speed was a constant 1.15 mm/μs over the range of the gages. For 88%-saturated alluvium, the wave speed decreased over the range of the gages from 2.12 to 1.31 mm/μs.

Series 12: Material Property (Reconstituted Alluvium with 2000-psi Pore Pressure

Three particle velocity tests were performed in reconstituted alluvium using an assembly technique different from that described in Appendix E. In these tests, alluvium was reconstituted in the laboratory by tamping water-saturated test site fines in a 10-inch-diameter (25.4-cm) and 10-inch-long (25.4-cm) cylindrical mold to a density of 1.99 g/cm^3. The fines were tamped in 1-inch (2.54-cm) layers to provide a uniform density. Particle velocity gages in the form of 10-mil-diameter (0.25-mm) Teflon-coated wire loops were embedded in the alluvium at the midheight of the cylinder. The gage radii were 1.27, 1.90, 2.54, 4.00, and 8.00 cm. An explosive charge epoxied to the end of the access tube was positioned at the center of the gages along the axis of the cylinder. The saturated alluvium was pressurized internally and externally to 2000 psi (13.79 MPa) by the same nitrogen source. Hence, the material was in an undrained state. Figures 3.100 through 3.104 show the resulting particle velocity profiles for tests 362, 363, and 368. For comparison, results of previous tests (272 and 273) on 11-inch-diameter spheres are included.

The particle velocity records for alluvium show outward motion only. This result is consistent with the negligible tensile strength of the material. The results for tests 362 and 368 are similar but differ noticably from those of test 363, particularly at the outermost gages.

168
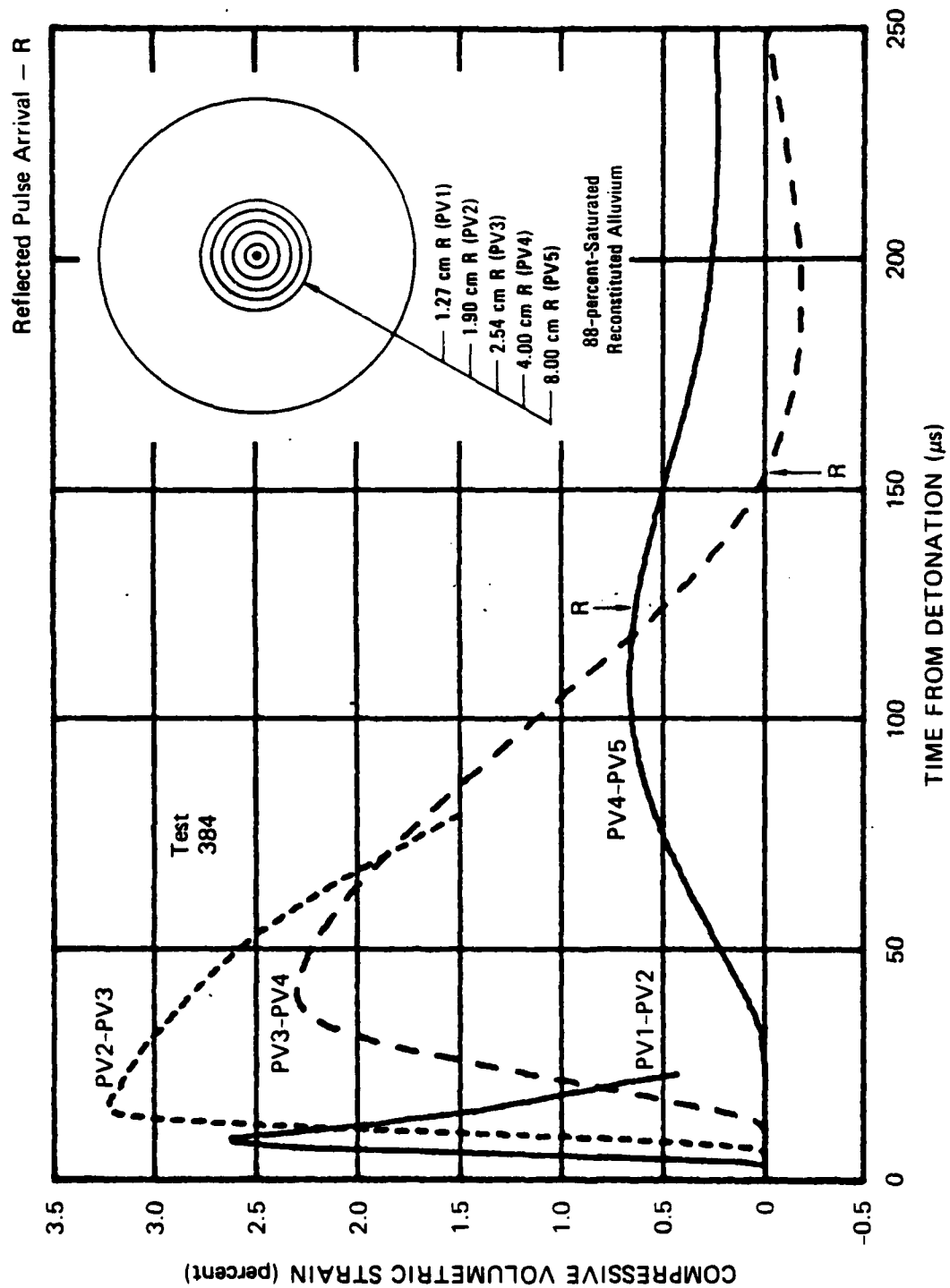
FIGURE 3.97   VOLUMETRIC STRAIN OBTAINED FROM A PARTICLE VELOCITY TEST
IN 88-percent-SATURATED RECONSTITUTED ALLUVIUM

JA-5372-163

167
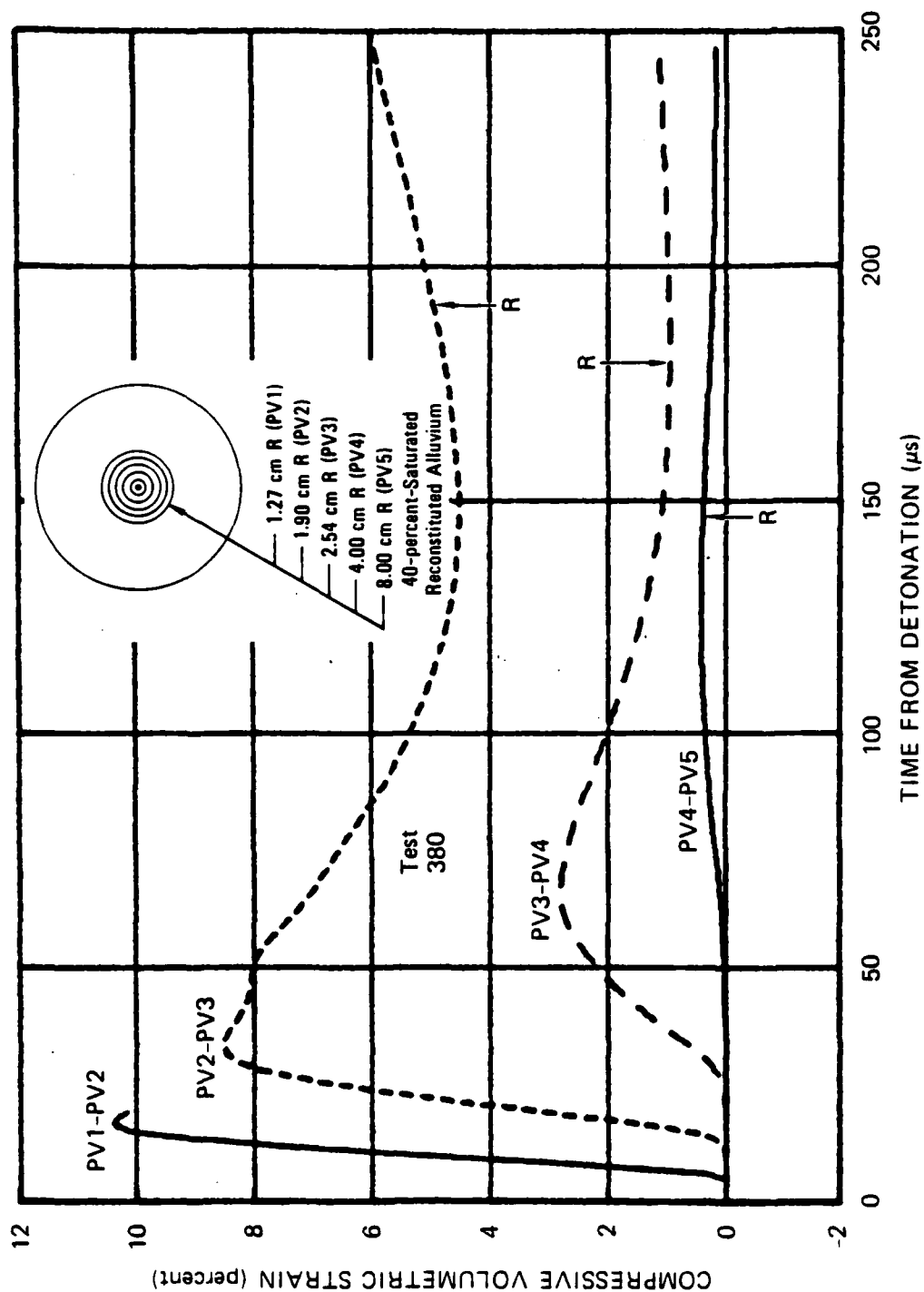
FIGURE 3.96   VOLUMETRIC STRAIN OBTAINED FROM A PARTICLE VELOCITY TEST
IN 40-percent-SATURATED RECONSTITUTED ALLUVIUM

166
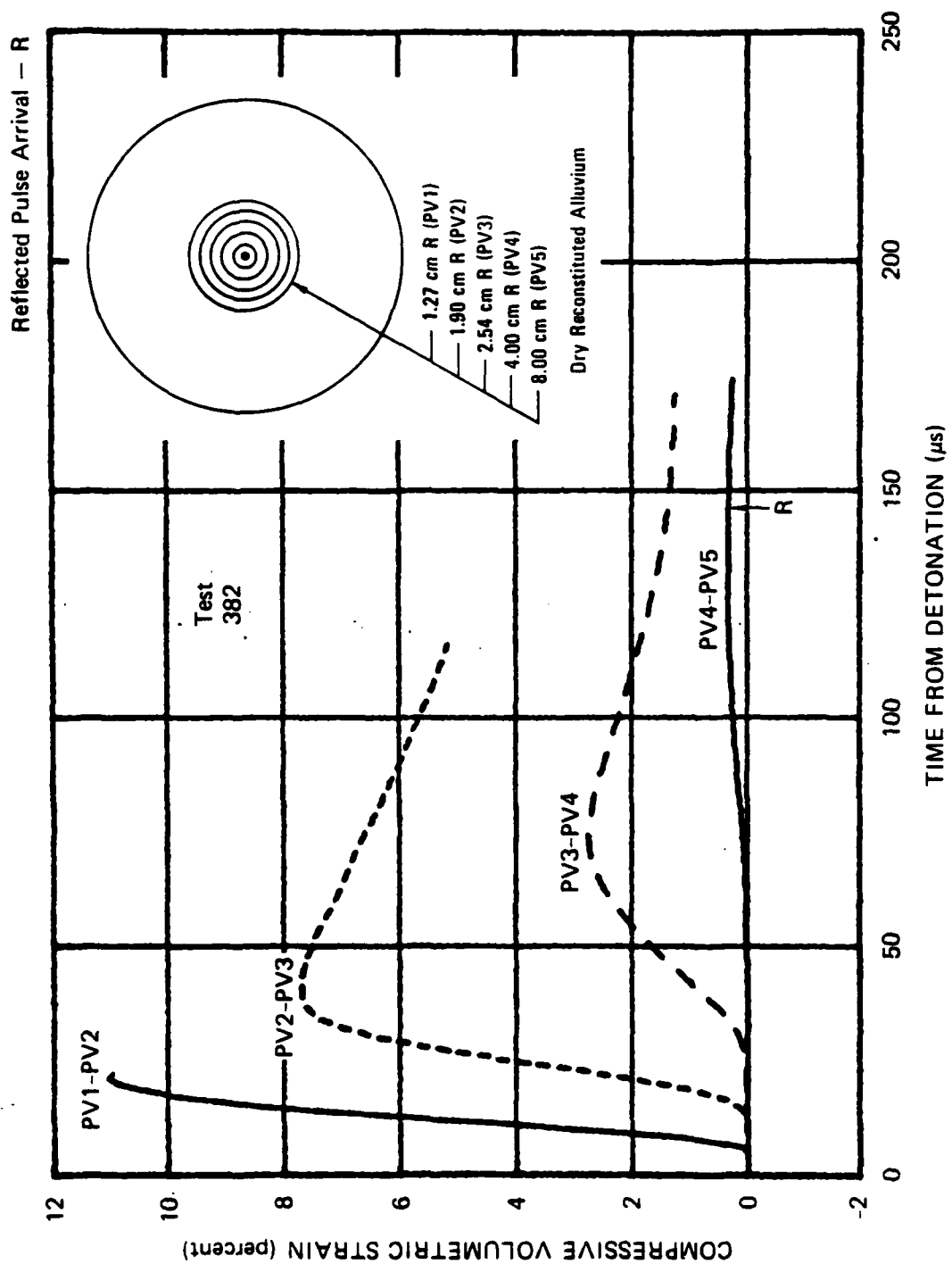
FIGURE 3.95 VOLUMETRIC STRAIN OBTAINED FROM A PARTICLE VELOCITY TEST IN DRY RECONSTITUTED ALLUVIUM

165
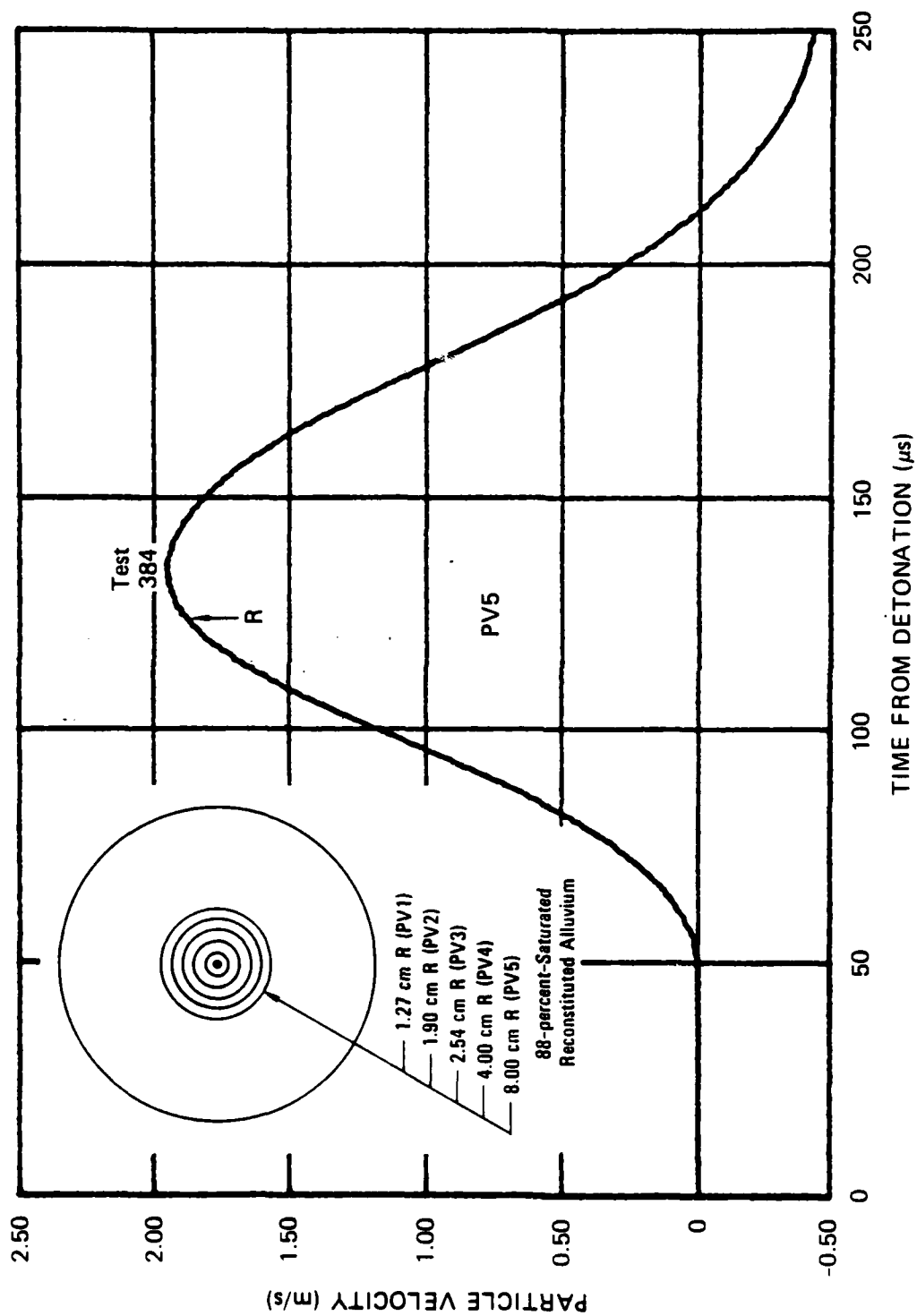
FIGURE 3.94   PARTICLE VELOCITY 8.00 cm FROM THE CENTER OF A COUPLED EXPLOSION IN 88-percent-SATURATED RECONSTITUTED ALLUVIUM

164
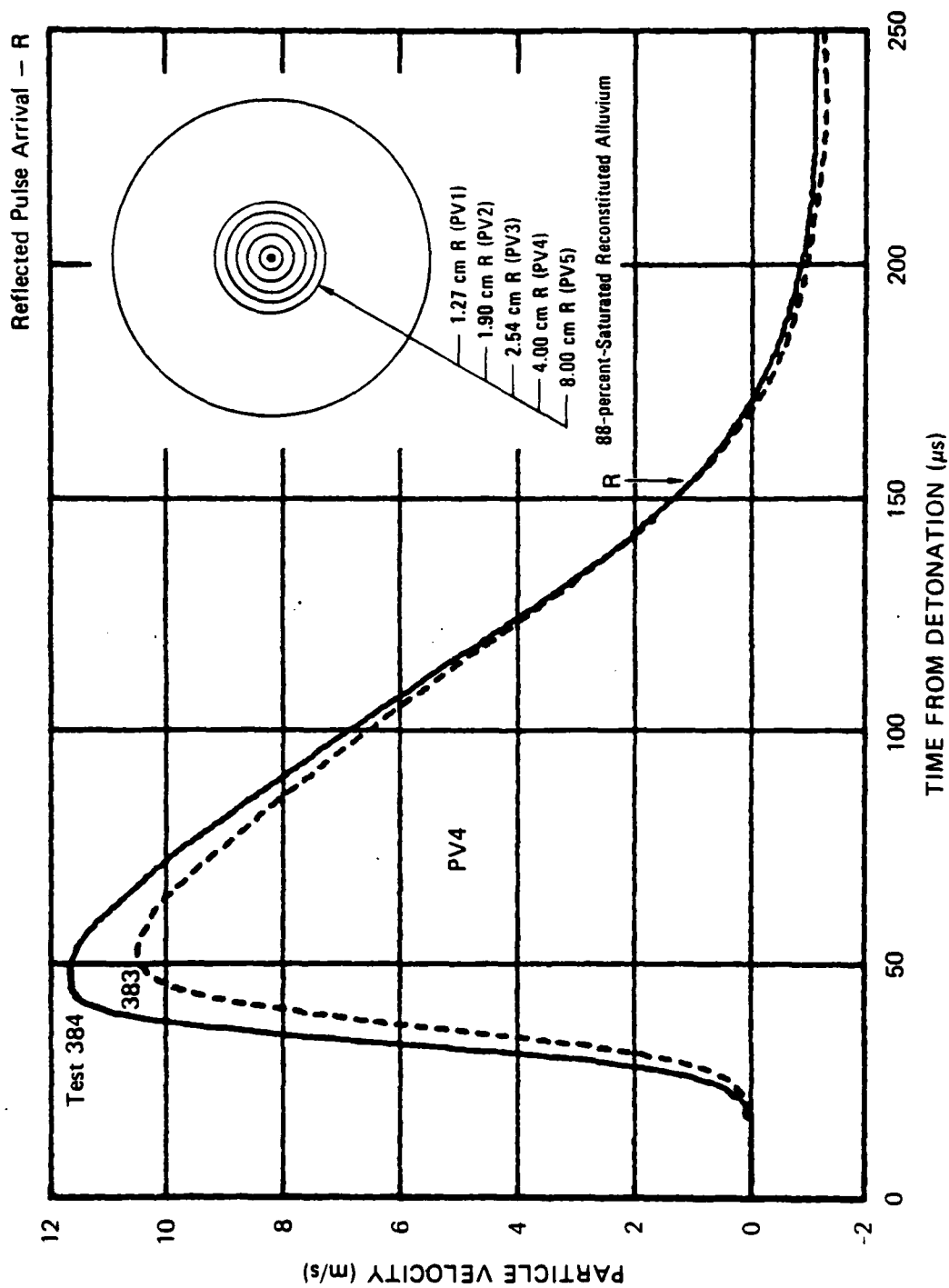
FIGURE 3.93   PARTICLE VELOCITY 4.00 cm FROM THE CENTER OF COUPLED EXPLOSIONS
IN 88-percent-SATURATED RECONSTITUTED ALLUVIUM

163
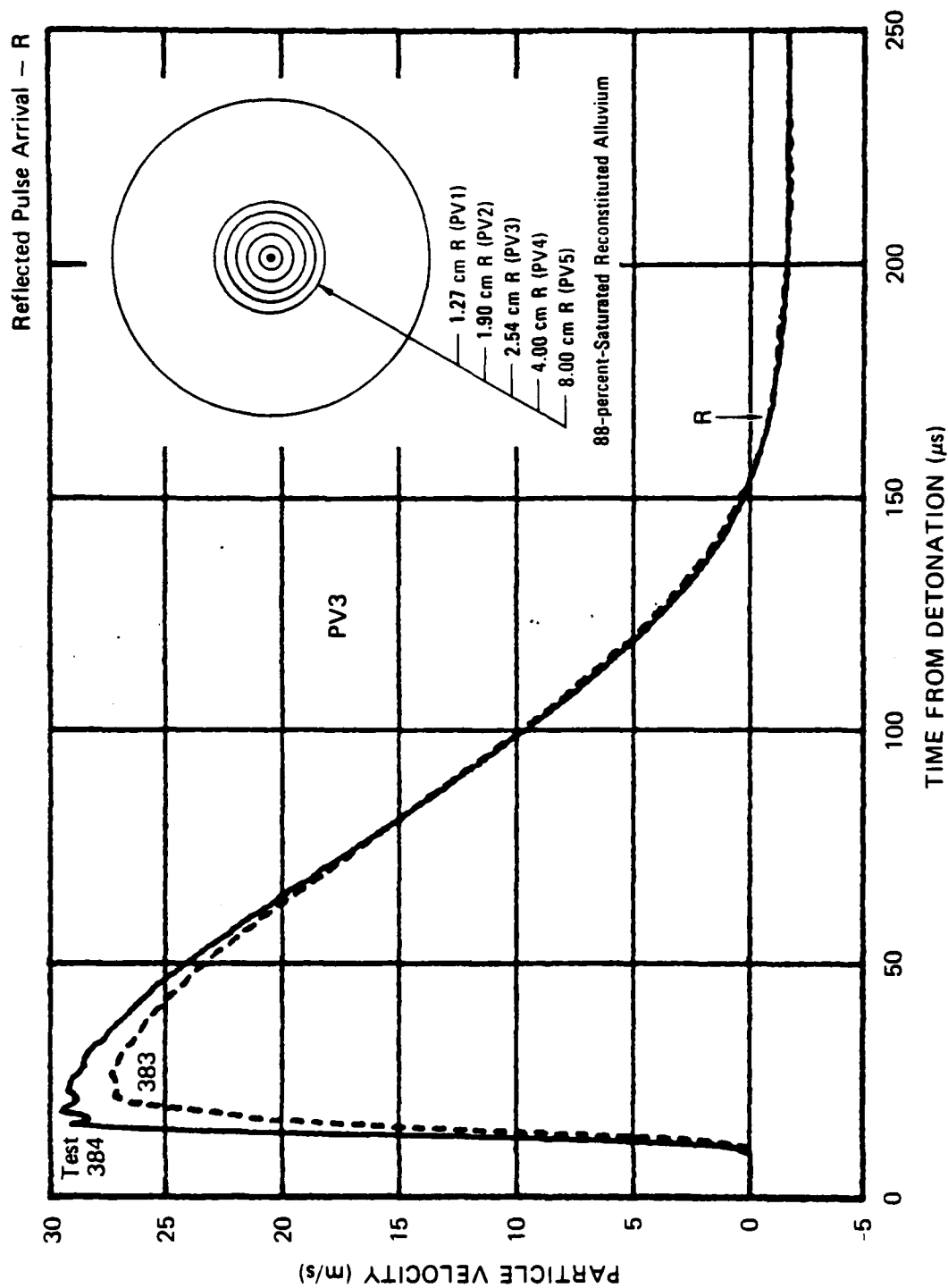
FIGURE 3.92 PARTICLE VELOCITY 2.54 cm FROM THE CENTER OF COUPLED EXPLOSIONS
IN 88-percent-SATURATED RECONSTITUTED ALLUVIUM

JA-5372-136

162
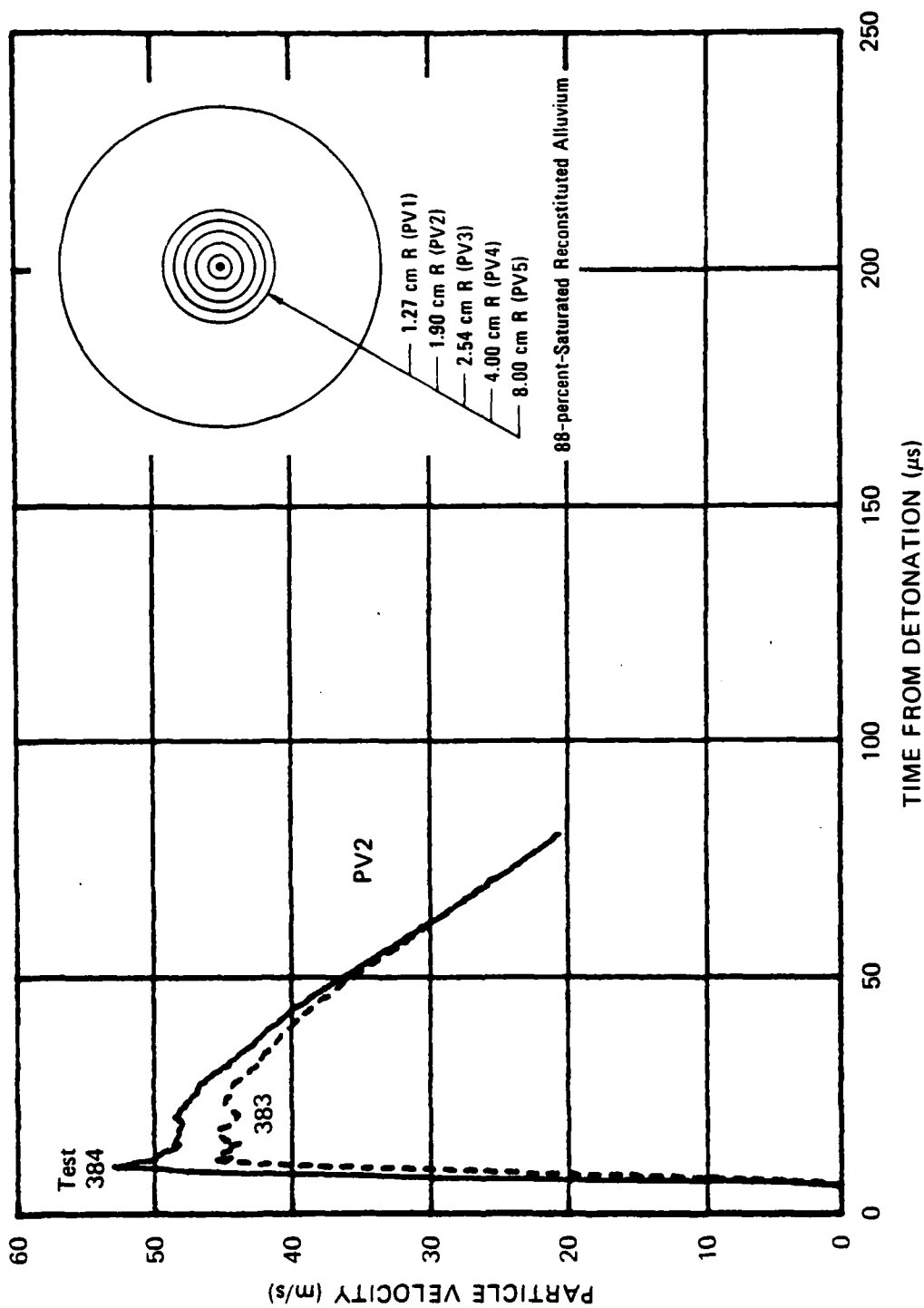
FIGURE 3.91 PARTICLE VELOCITY 1.90 cm FROM THE CENTER OF COUPLED EXPLOSIONS
IN 88-percent-SATURATED RECONSTITUTED ALLUVIUM

161
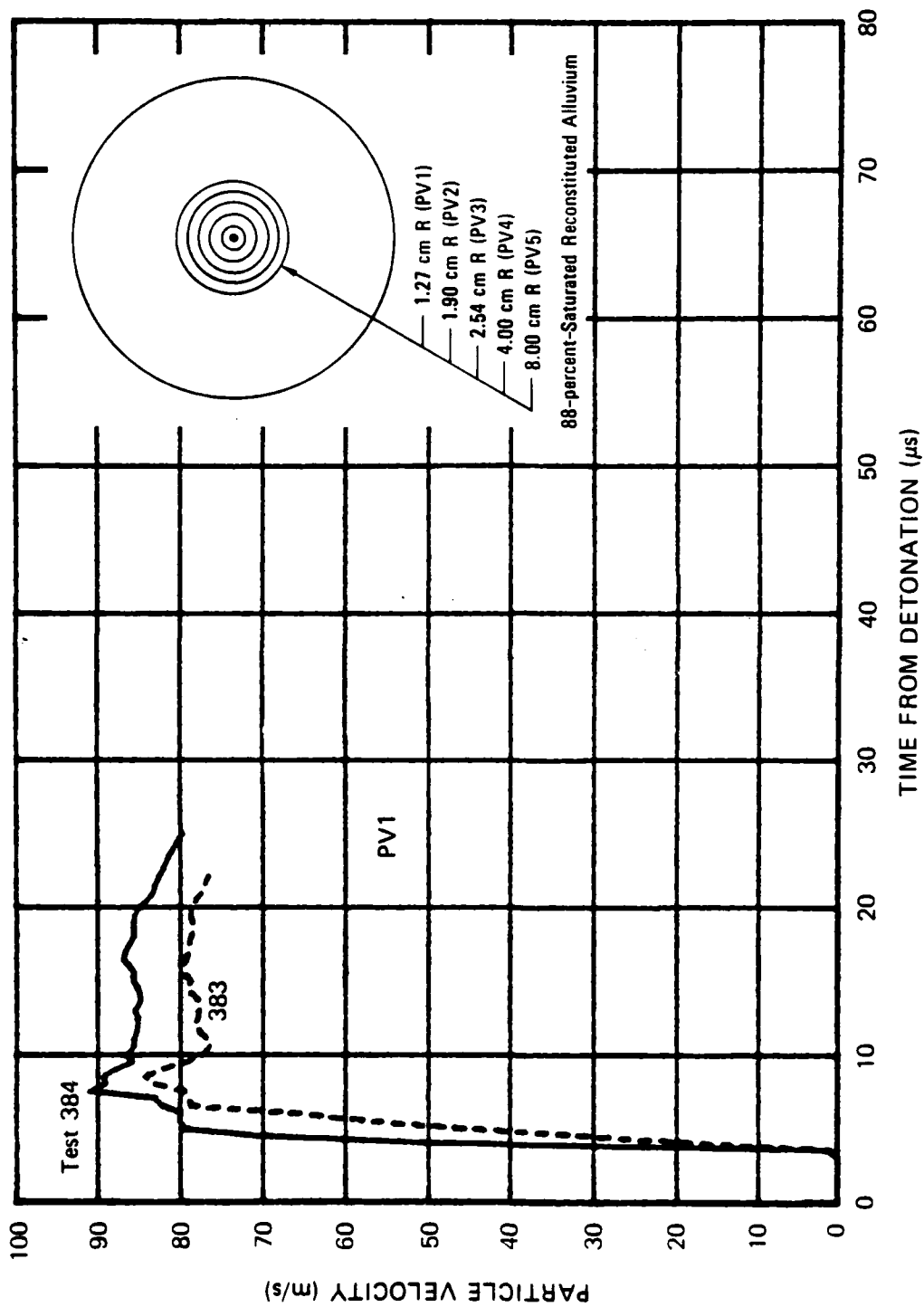
FIGURE 3.90 PARTICLE VELOCITY 1.27 cm FROM THE CENTER OF COUPLED EXPLOSIONS
IN 88-percent-SATURATED RECONSTITUTED ALLUVIUM
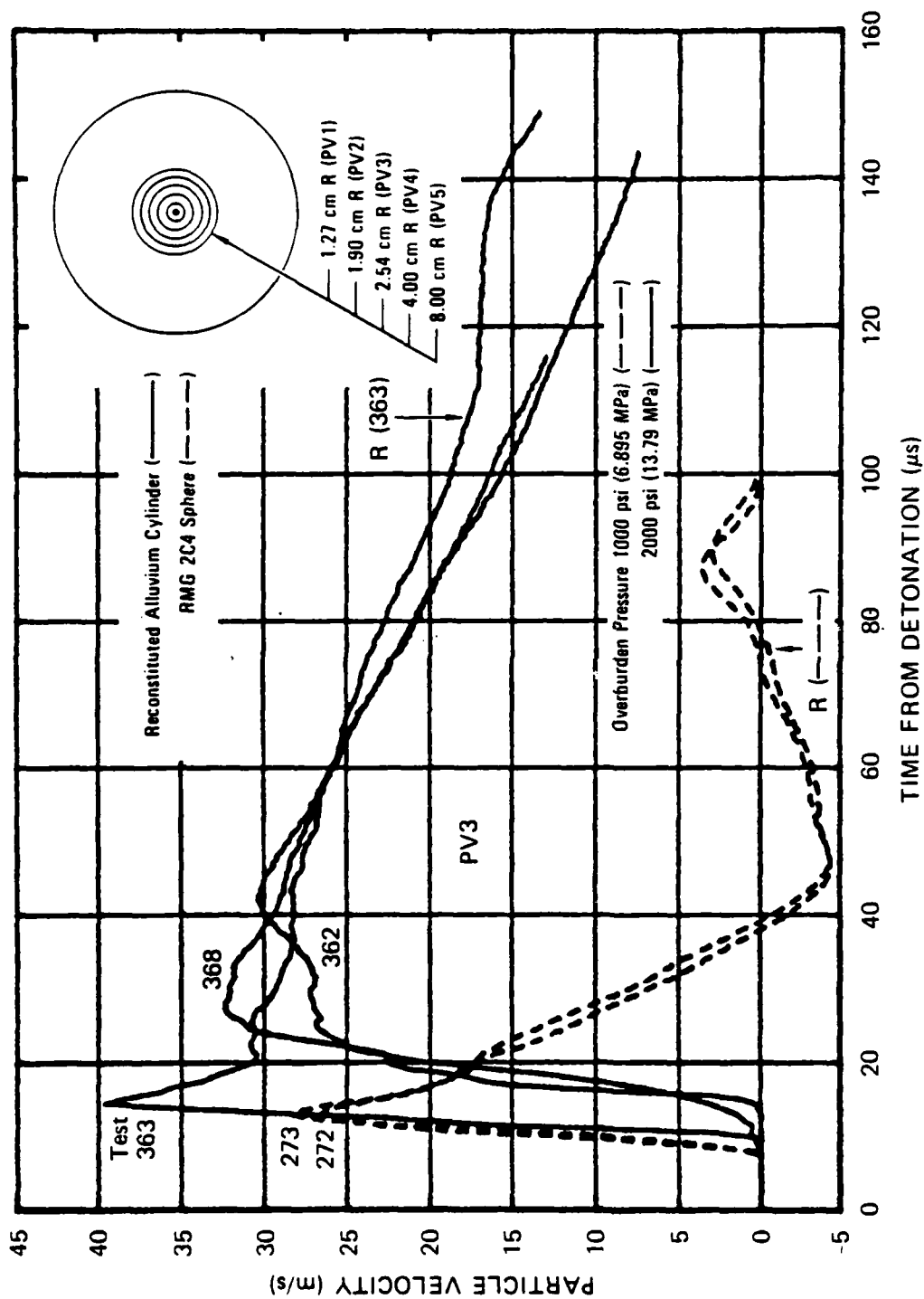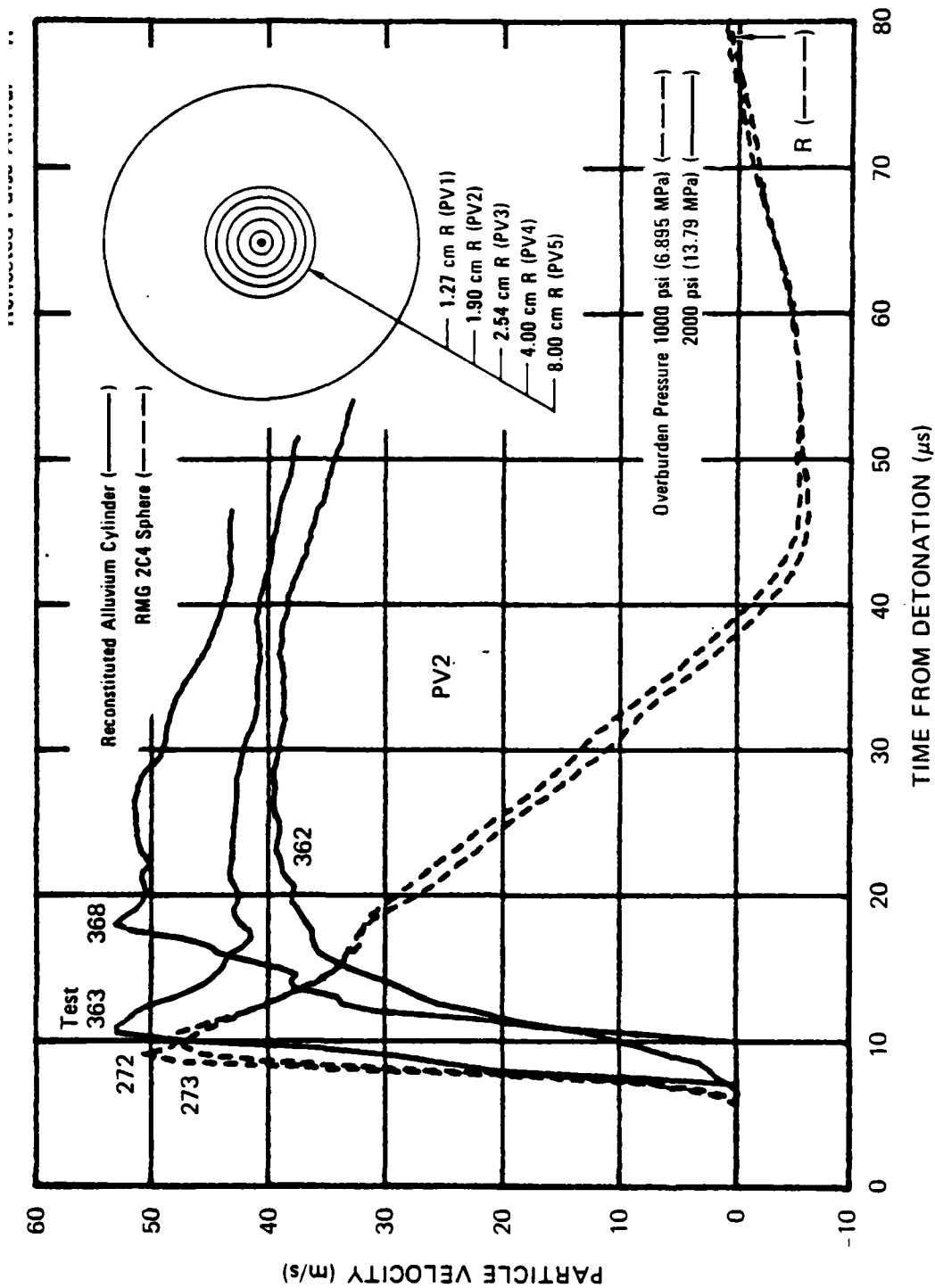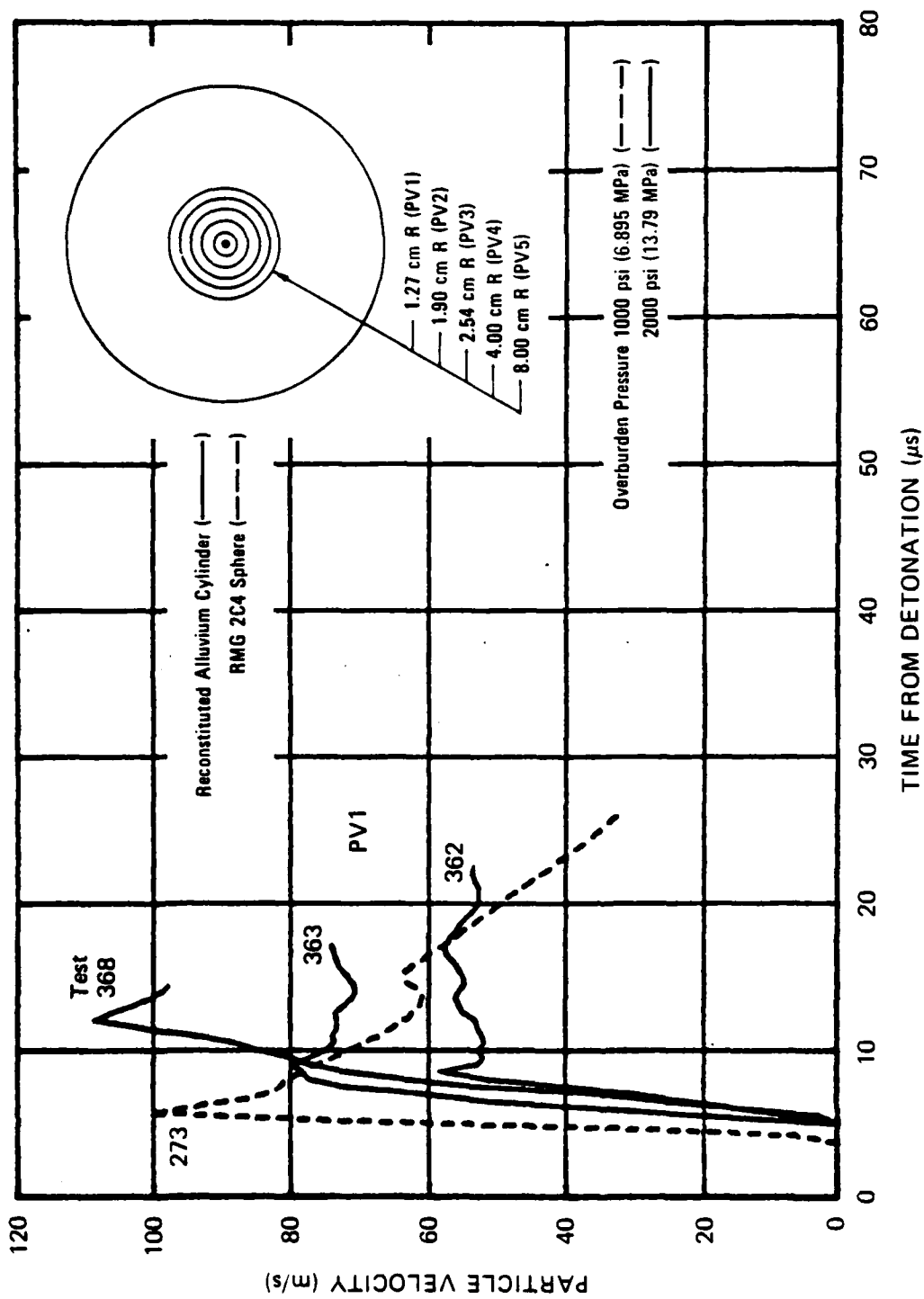
JA-5372-134

160
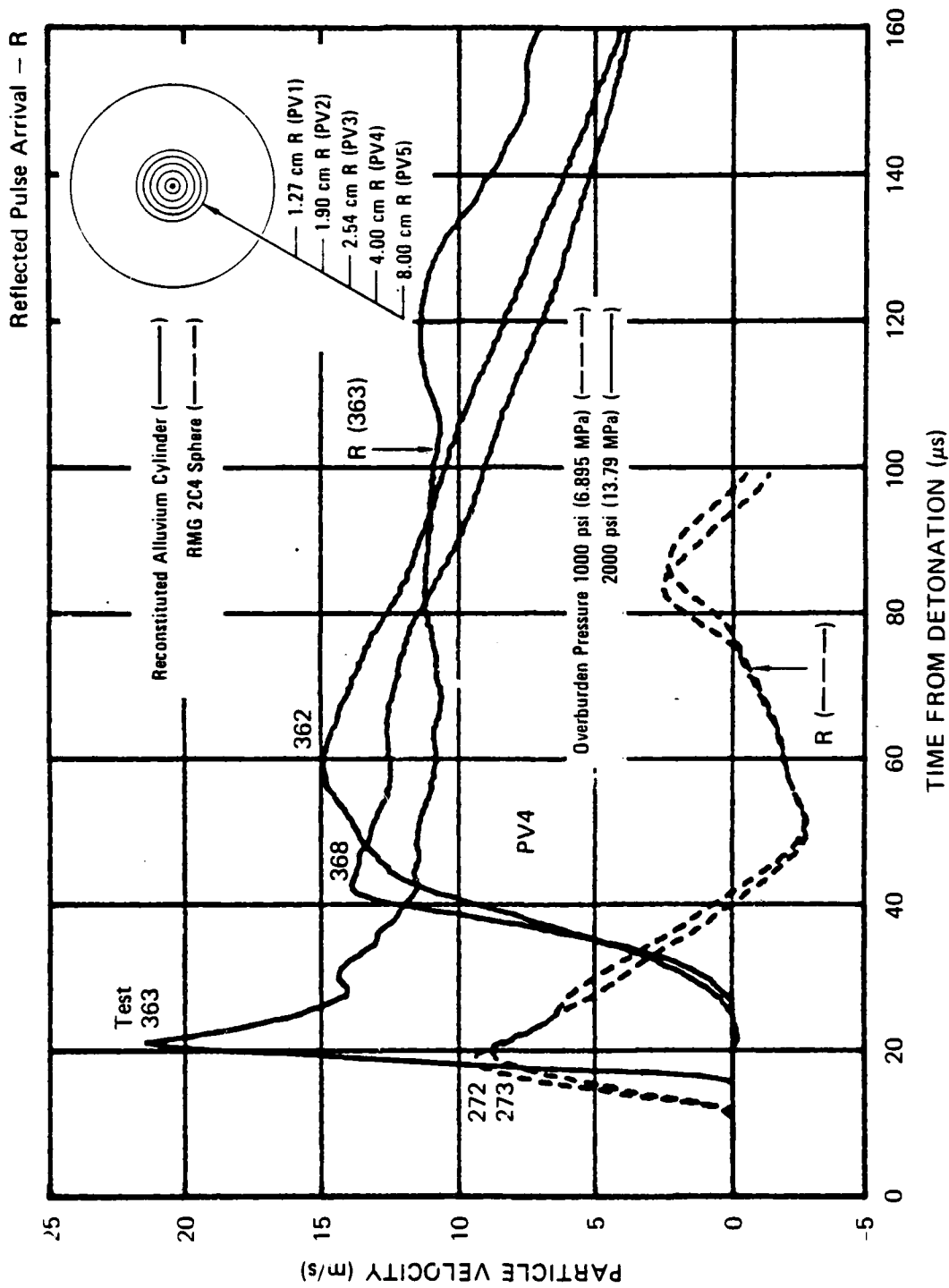
FIGURE 3.103   PARTICLE VELOCITY 4.00 cm FROM THE CENTER OF COUPLED EXPLOSIONS IN RECONSTITUTED ALLUVIUM (WITH 2000-psi PORE PRESSURE) AND RMG 2C4
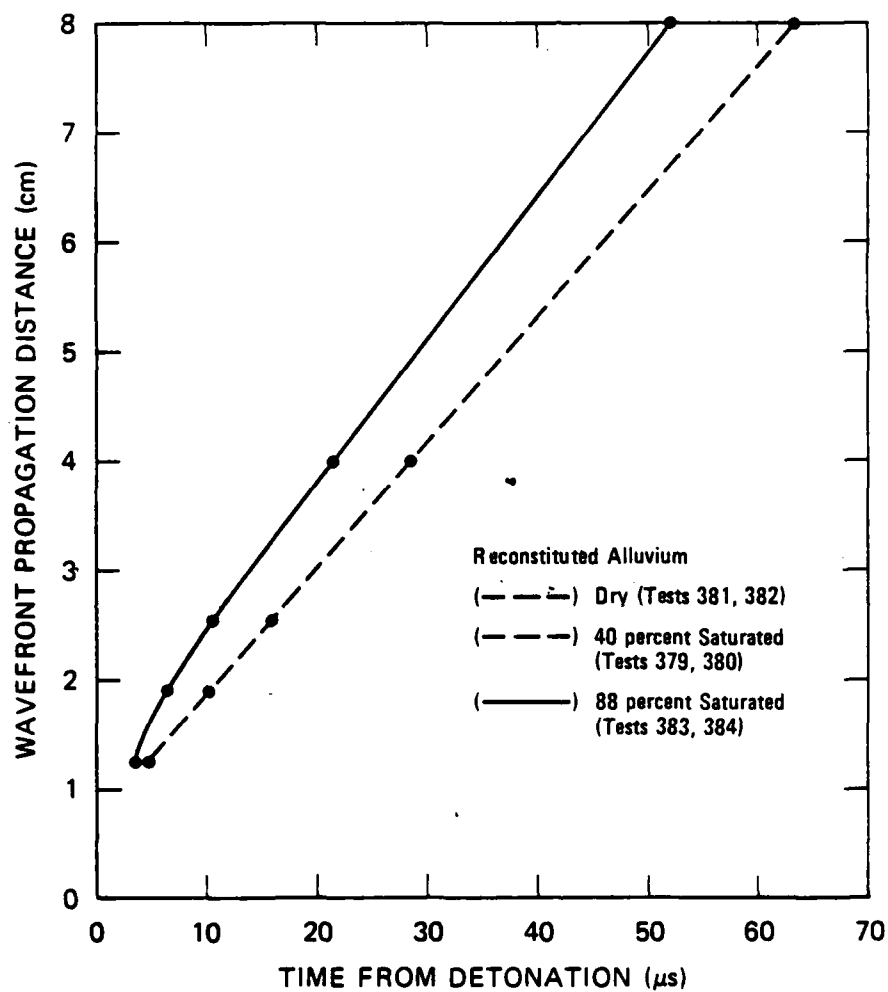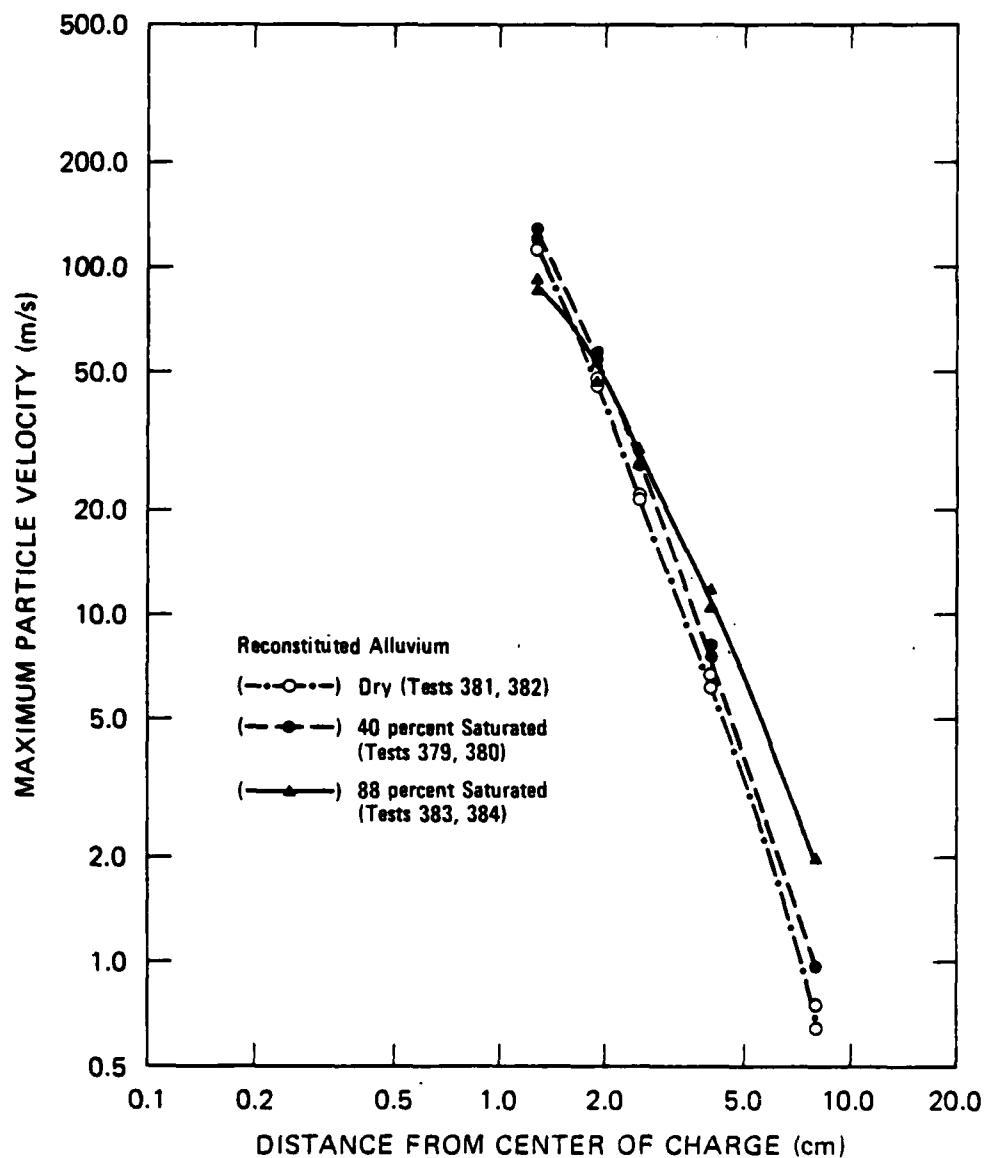
JA-5372-56

174
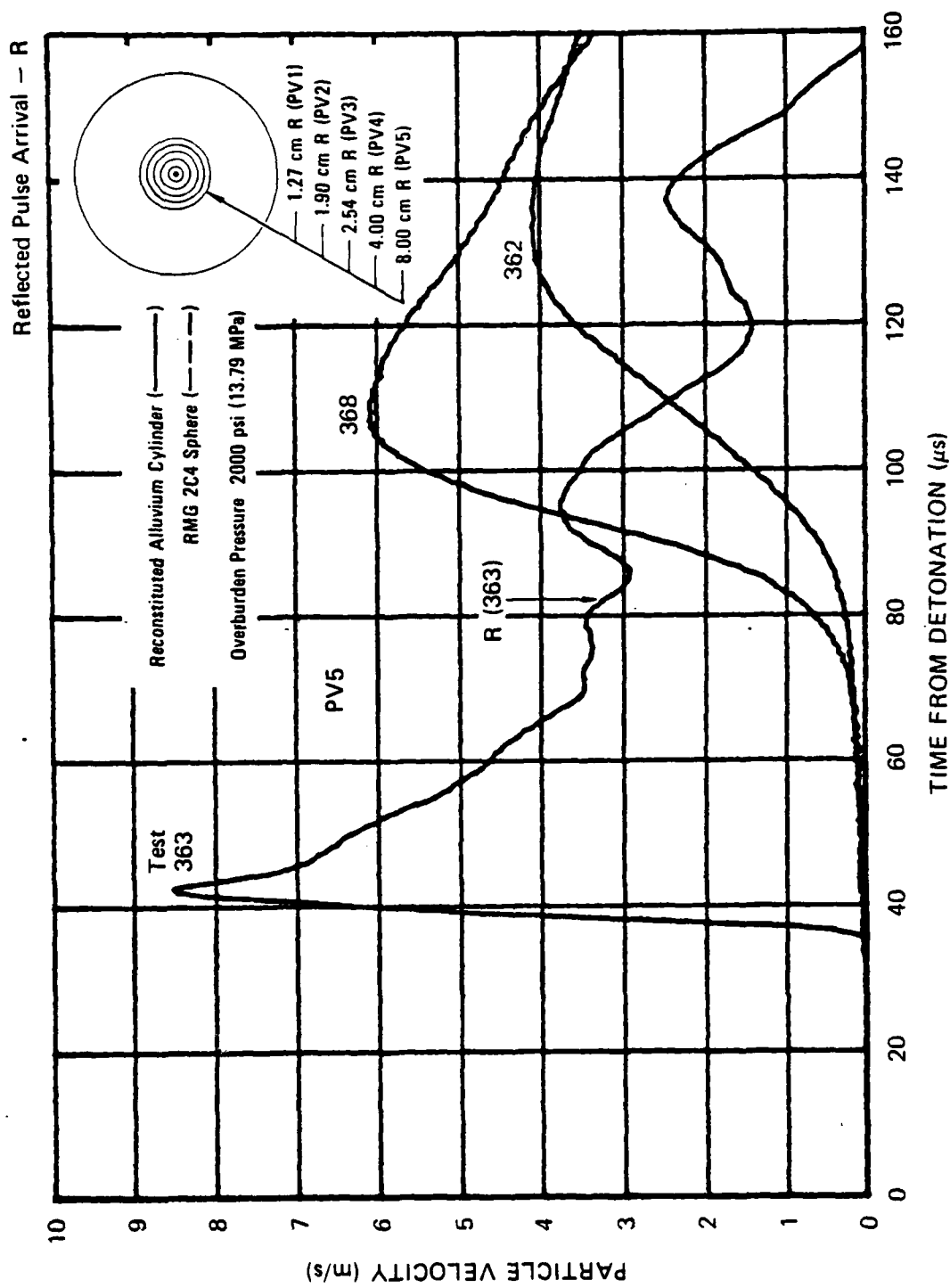
FIGURE 3.104   PARTICLE VELOCITY 8.00 cm FROM THE CENTER OF COUPLED EXPLOSIONS IN RECONSTITUTED ALLUVIUM (WITH 2000-psi PORE PRESSURE)

175

The different responses are attributed to slight differences in the degree of saturation. The material in tests 362 and 368 apparently retained more unfilled voids during saturation.

Volumetric strain response for tests 362, 363, and 368 is shown in Figures 3.105, 3.106, and 3.107, respectively. The generation of volume dilatation for these nearly saturated materials is consistent with the response of the 88%-saturated alluvium shown in Figure 3.97 (Series 11).

Figure 3.108 shows the attenuation of maximum particle velocity for the three tests in alluvium. Figure 3.109 shows the time of arrival of the wavefront at each gage location. In test 363, the wave speed decreased over the range of the gages from 2.93 to 2.00 mm/μs. In tests 362 and 368, the wave speed decreased from 1.55 to 0.93 mm/μs. Wave speeds in tests 362 and 368 that are lower than the 1.5-mm/μs wave speed in water indicate unfilled voids in the alluvium.

Series 13: Depth-of-Burial Failure Criterion Below an Air/RMG 2C4 Interface)

Depth-of-burial represents an important containment parameter affecting both the safety and economy of underground tests. A depth-of-burial study was conducted in exploded cavity RMG 2C4 cylinders by providing a free surface at one end in the form of a gas interface, varying the distance between the charge and the free surface, and varying the overburden pressure. Hydrofracture tests were performed (see Series 3) to determine a threshold of failure. Particle velocity tests were performed to further aid the development of a failure criterion.

The configuration for particle velocity tests 347 and 348 is shown in Figure 3.110. Although the intended depth-of-burial was 4 inches (10.16 cm), the actual depth was greater in each test as shown. Loop gages were embedded in the horizontal plane of the charge (PV1 and PV2), in a plane 2 inches (5.08 cm) above (PV3 and PV4), and in the free surface (PV5 and PV6). The overburden pressure was 500 psi (3.447 MPa) in test 347 and 250 psi (1.724 MPa) in test 348.

176
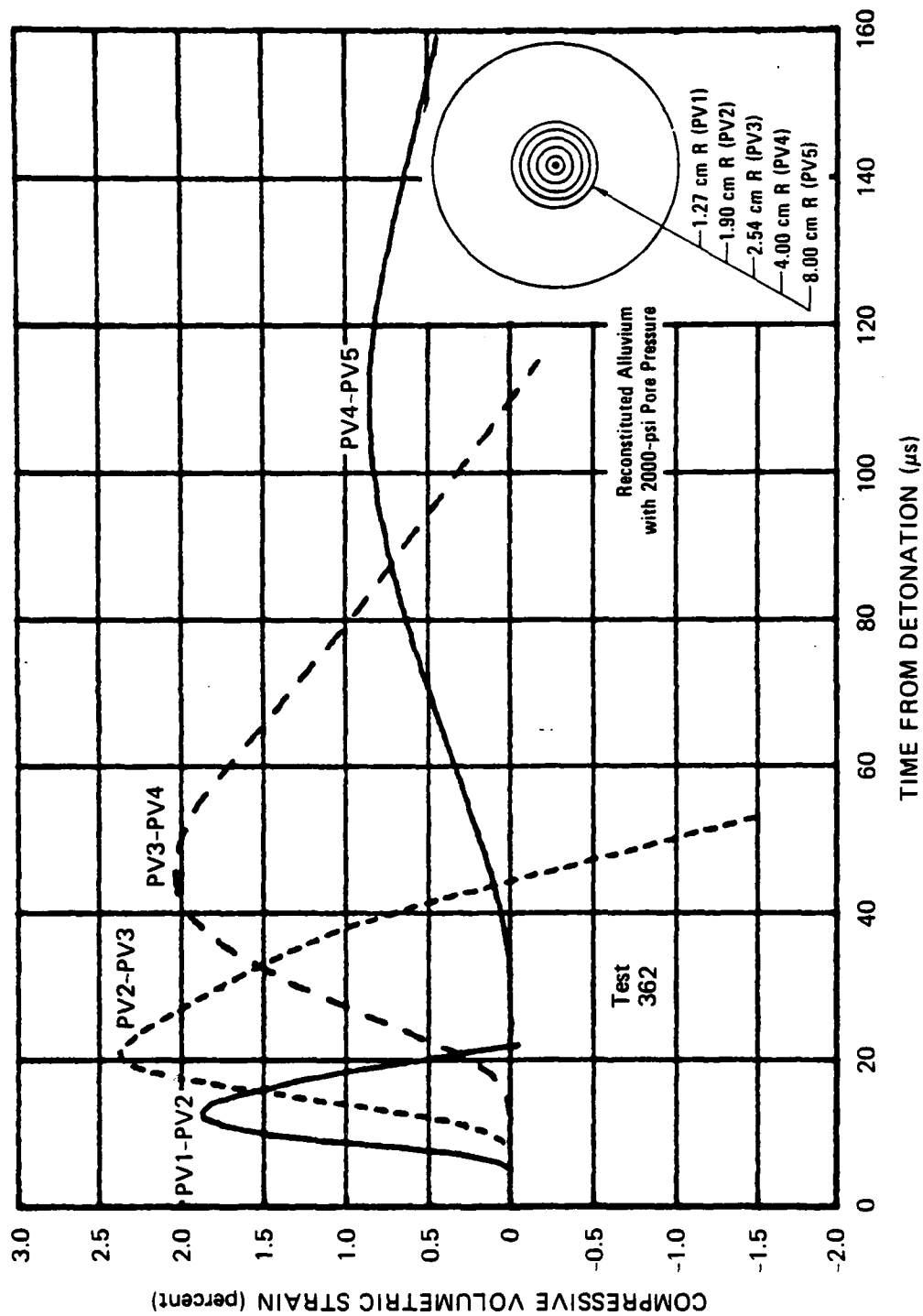
FIGURE 3.105 VOLUMETRIC STRAIN OBTAINED FROM PARTICLE VELOCITY TEST 362 IN RECONSTITUTED ALLUVIUM WITH 2000-psi PORE PRESSURE

JA-5372-167

177
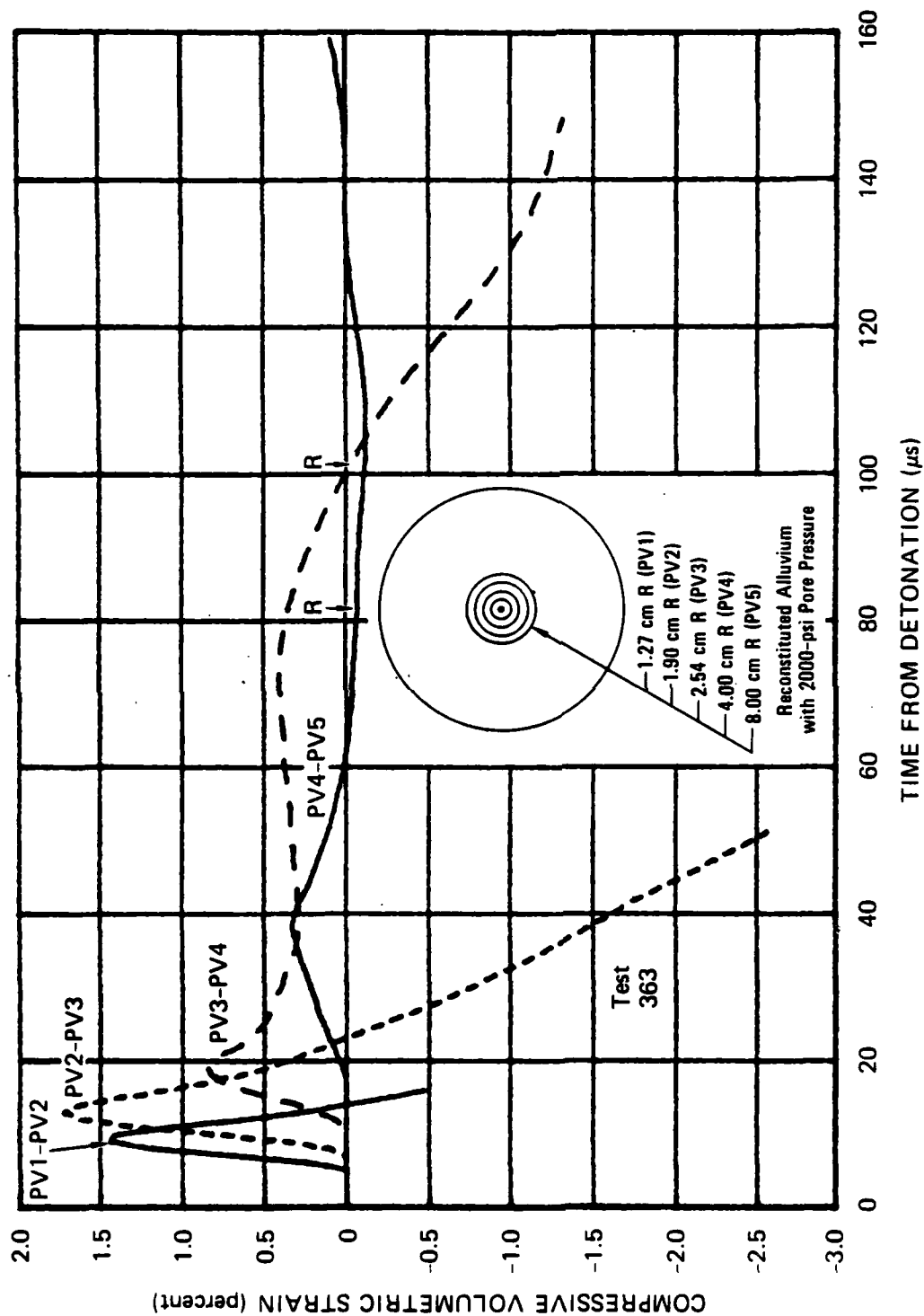
FIGURE 3.106   VOLUMETRIC STRAIN OBTAINED FROM PARTICLE VELOCITY TEST 363
IN RECONSTITUTED ALLUVIUM WITH 2000-psi PORE PRESSURE

178
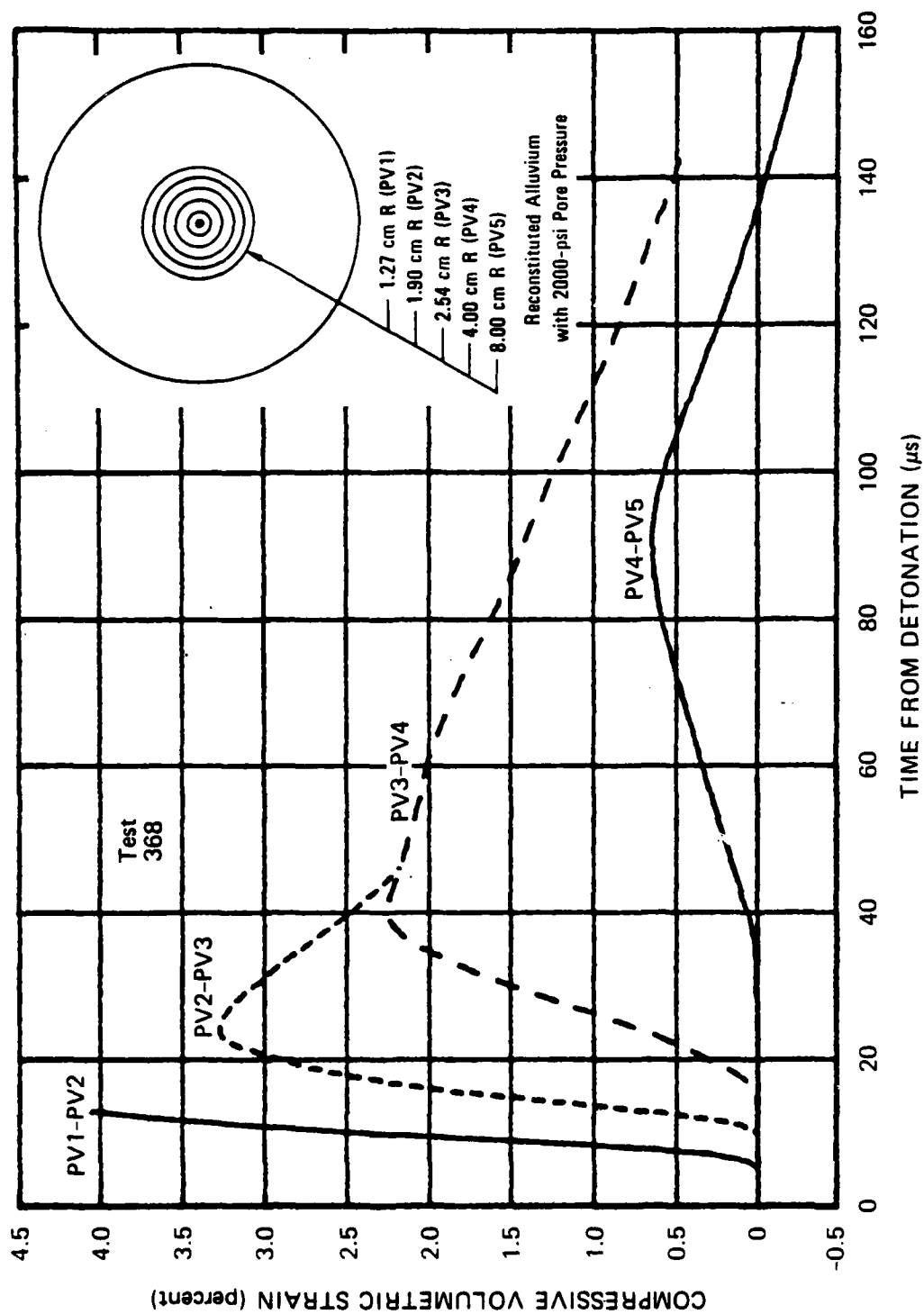
FIGURE 3.107   VOLUMETRIC STRAIN OBTAINED FROM PARTICLE VELOCITY TEST 368 IN RECONSTITUTED ALLUVIUM WITH 2000-psi PORE PRESSURE
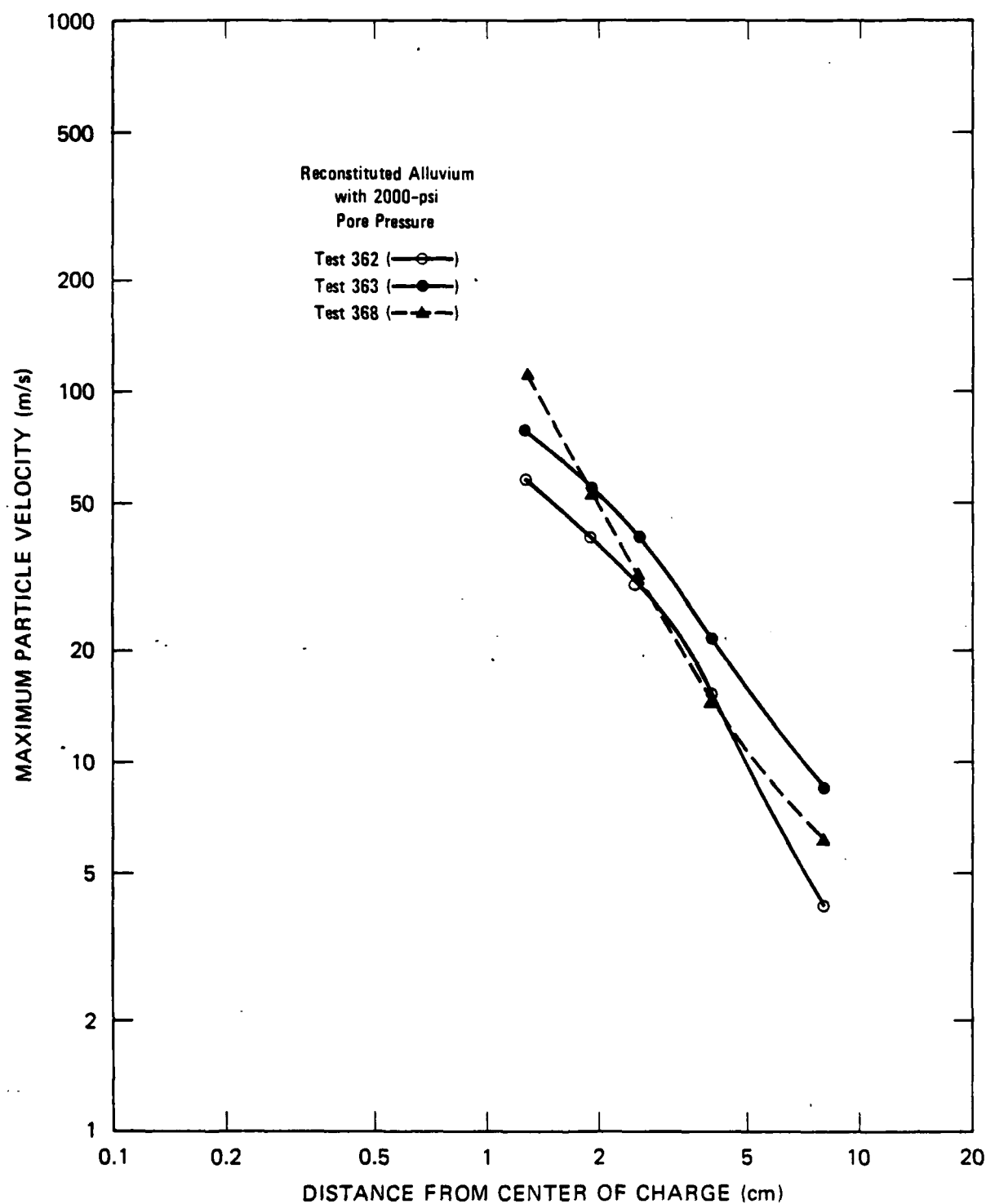
179

FIGURE 3.108   MAXIMUM PARTICLE VELOCITY VERSUS DISTANCE FROM CENTER OF CHARGE
FOR PRESSURE RECONSTITUTED ALLUVIUM WITH 2000-psi PORE PRESSURE
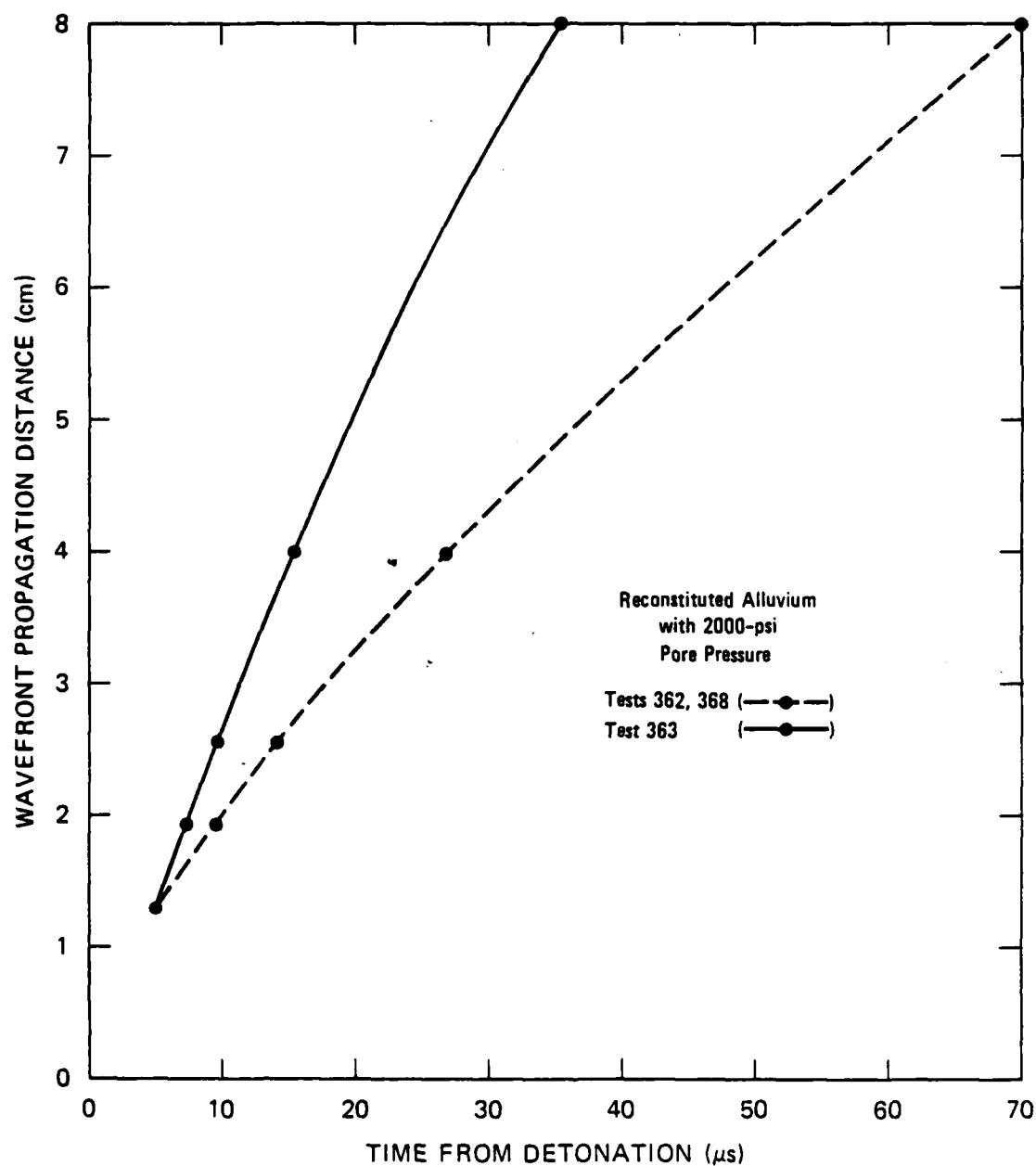
180

FIGURE 3.109 WAVEFRONT PROPAGATION DISTANCE VERSUS TIME FROM DETONATION
FOR RECONSTITUTED ALLUVIUM WITH 2000-psi PORE PRESSURE

181

RMG 2C4 Cylinder
(11 in. dia., 11 in. long)

1″

3/4″

PV5   PV6

4-9/32″ (Test 347)
4-1/8″ (Test 348)

PV3   PV4

2″

3/8-g Charge   PV1   PV2
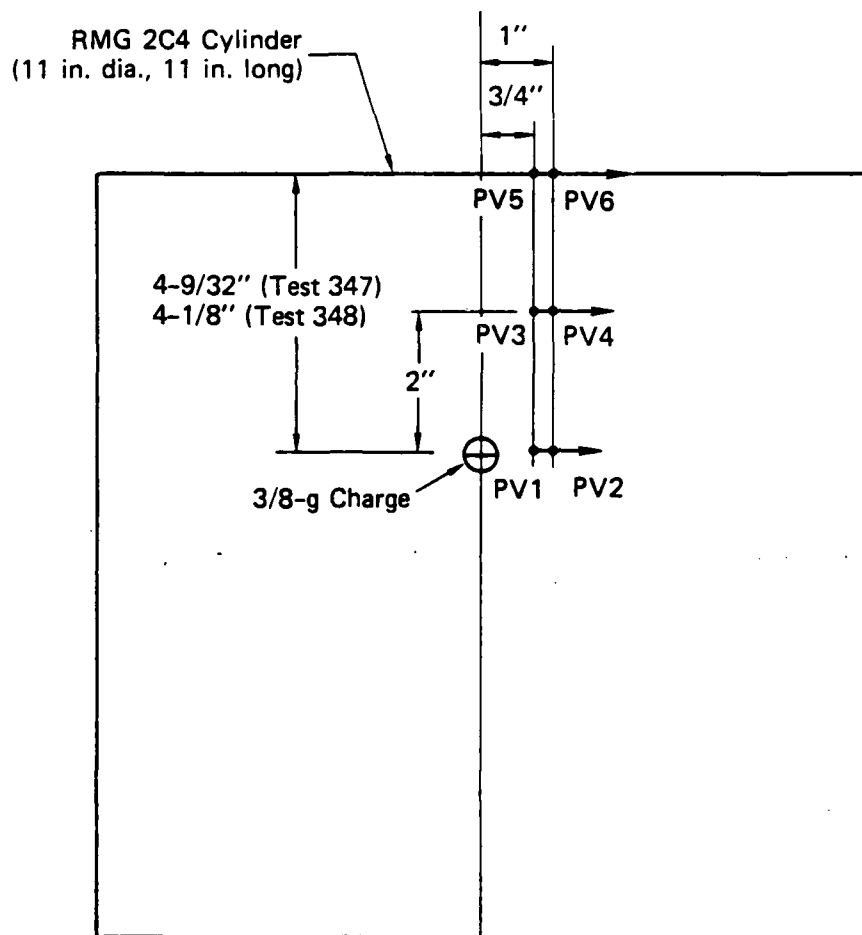
JA-5372-29

FIGURE 3.110   LOCATION OF PARTICLE VELOCITY MEASUREMENTS FOR FAILURE
THRESHOLD TESTS IN RMG 2C4

182

Particle velocity records for tests 347 and 348 are shown in Figures 3.111 through 3.113. (Note that in test 347 gages PV2 and PV4 broke before the test.) The records for the two tests are similar except for the long-term response of the surface gages (PV5 and PV6, Figure 3.113). The difference is attributed to dynamic fracture. In test 348, posttest examination of the cylinder revealed surface cracking extending along the free surface and down the sides to the plane of the charge. In test 347, no surface cracking was detected, and a subsequent hydrofracture test indicated that the vented exploded cavity was not fractured.

The particle velocity records from gages PV1 and PV2 (Figure 3.111) are representative of corresponding results from standard tests[9] on RMG 2C4 spheres subjected to 1000 psi (6.895 MPa) confining pressure. The reduction of overburden in tests 347 and 348 had negligible influence on these records because the maximum mean normal stress associated with the particle velocity pulse is much larger than the overburden, and the work done by the overburden in closing pores represents a small part of the wave energy. However, the particle velocity records from gages PV3 and PV4 (Figure 3.112) yield peak velocities less than those from the standard tests. The reduction in overburden in tests 347 and 348 influenced these records because the maximum mean normal stress at the range of PV3 and PV4 is comparable to the overburden, and a relatively large part of the wave energy is required to close pores. Standard particle velocity tests at reduced overburden should be performed to verify these results.

The depth-of-burial results from hydrofracture and particle velocity tests are summarized in Figure 3.7 (Series 3). A failure threshold curve consistent with all available results is included. As shown, the combination of a 4-inch (10.16 cm) depth-of-burial and a 500-psi (3.447 MPa) overburden pressure represents a point on the threshold of failure.

183
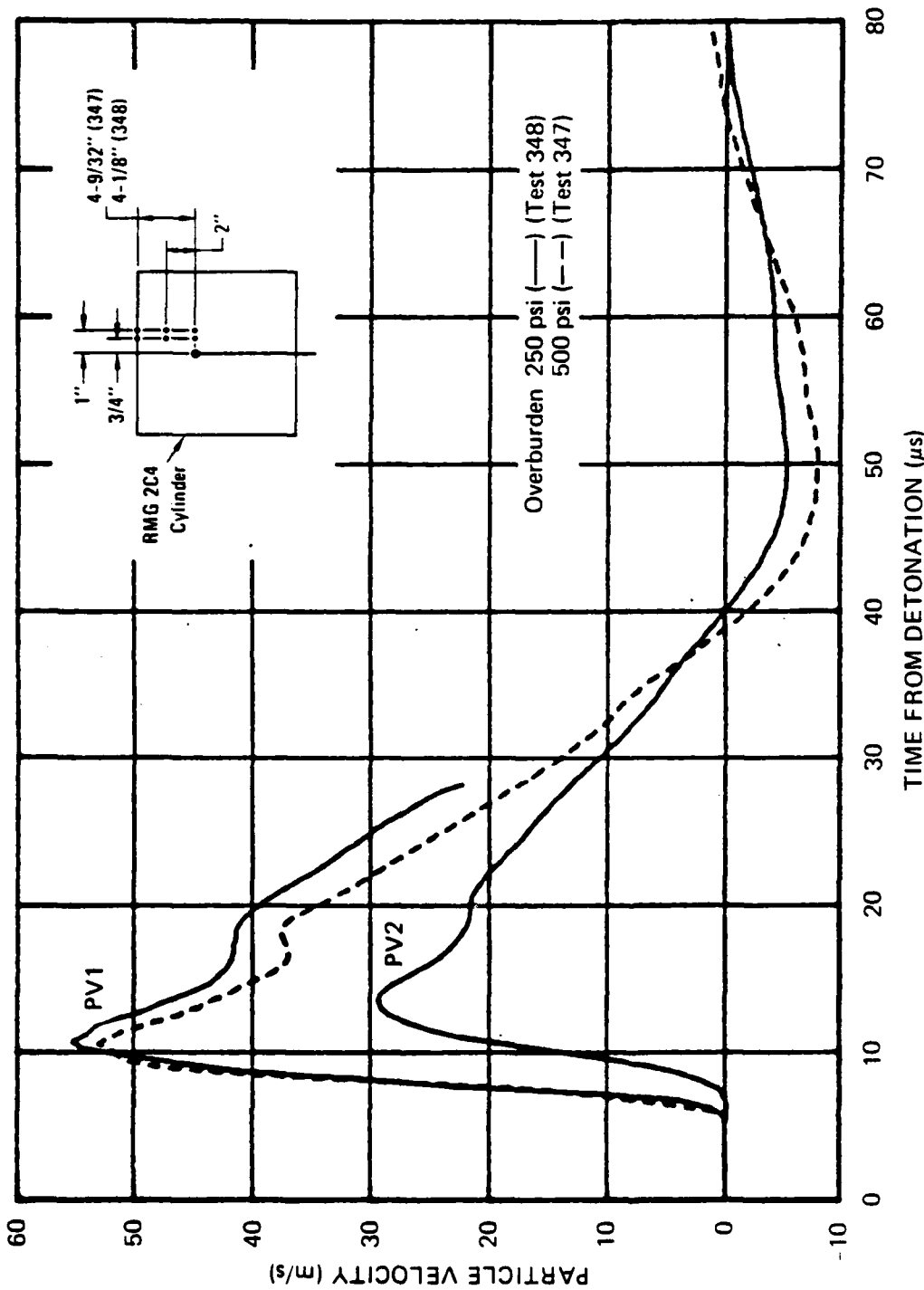
FIGURE 3.111   PARTICLE VELOCITY AT TWO LOCATIONS IN THE PLANE OF THE CHARGE
DURING FAILURE THRESHOLD TESTS IN RMG 2C4

184
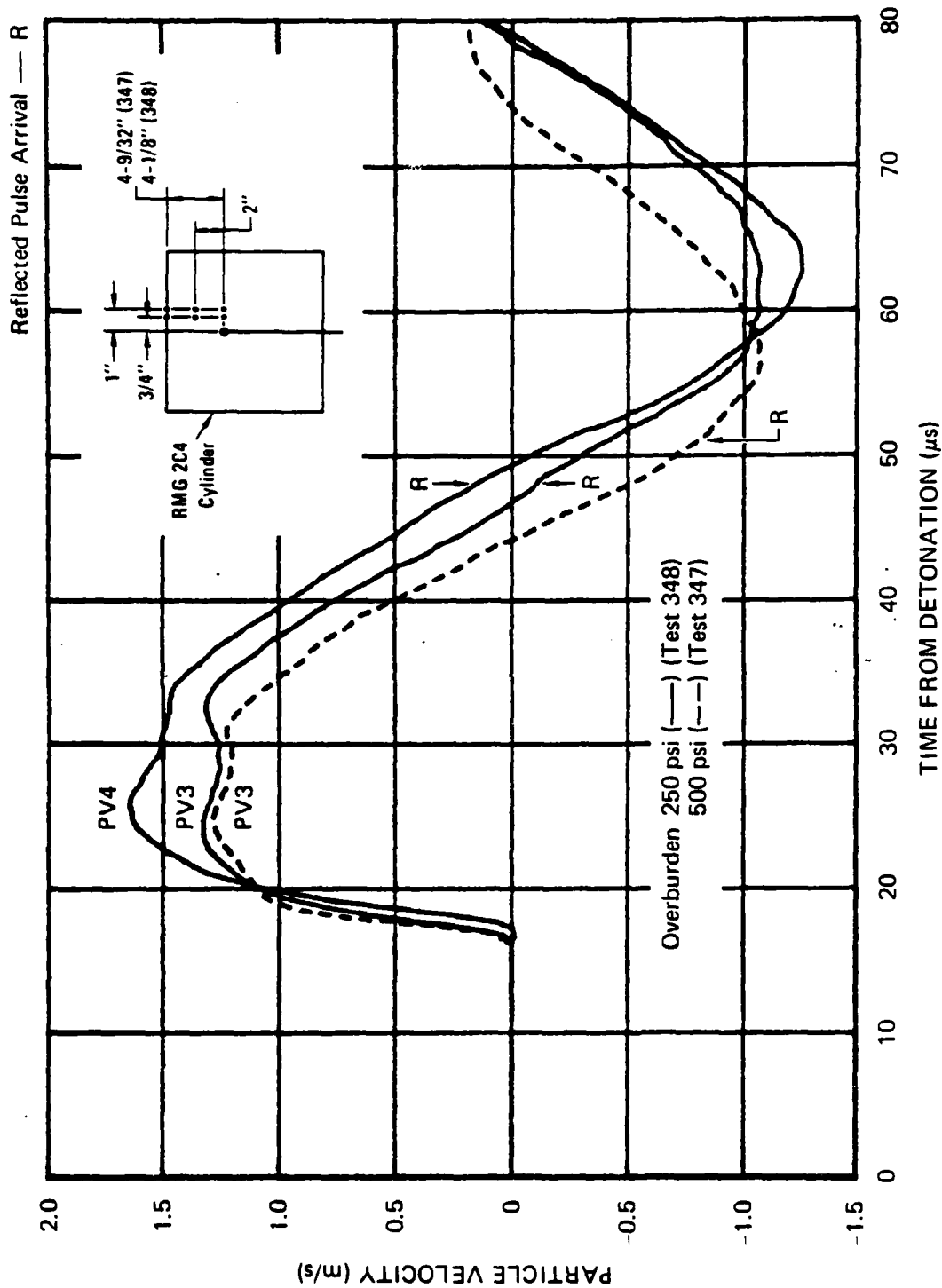
FIGURE 3.112 RADIAL PARTICLE VELOCITY AT TWO LOCATIONS ABOVE THE PLANE OF THE CHARGE DURING FAILURE THRESHOLD TESTS IN RMG 2C4

185
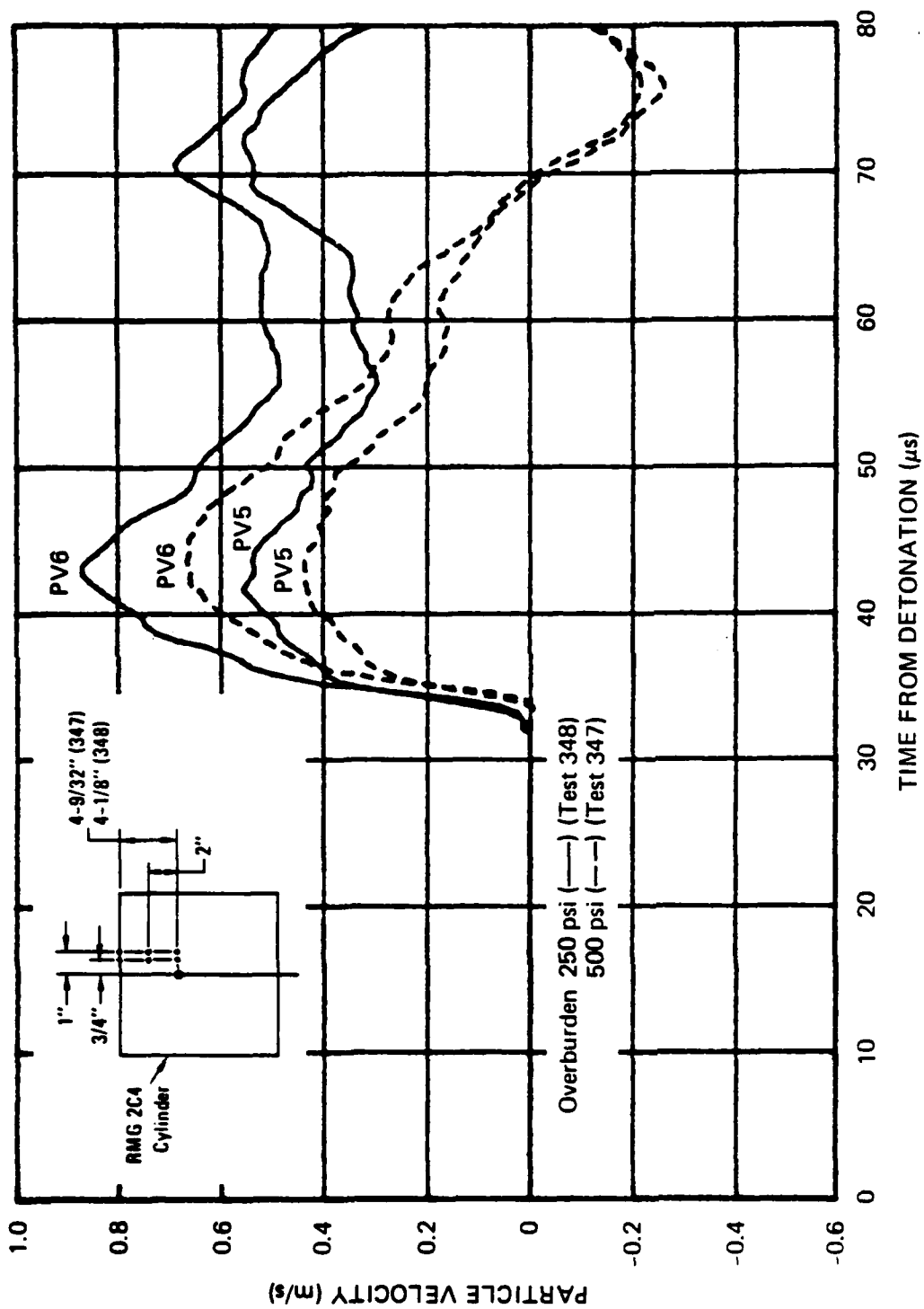
FIGURE 3.113   RADIAL PARTICLE VELOCITY AT TWO LOCATIONS ON THE FREE SURFACE
DURING FAILURE THRESHOLD TESTS IN RMG 2C4

JA-5372-36

186

3.4 STRESS AND STRAIN MEASUREMENTS

Series 14: Strain Measurements in RMG 2C4

As preliminary work for stress gage measurements, techniques were developed to measure dynamic and long-term strain in exploded cavity RMG spheres (Section 2.3).

In one configuration, loops of 4-mil-diameter (0.102-mm) constantan wire were cast concentrically about an explosive charge at four radial locations (1.27, 1.90, 2.54, and 4.00 cm). Each gage output provided a direct measure of circumferential strain (ε_θ) at a given radius (r). Figure 3.114 shows particle displacements (u) obtained from the strain measurements in test 373 through the relation $u = \varepsilon_\theta r$. For comparison, particle displacements obtained from integration of particle velocity records for tests 272, 273, and 353 are also shown. Good agreement among the results was obtained at each location. (Note that no record was obtained from the strain gage at 1.27-cm radius because of an electronic equipment problem.) Figure 3.115 shows long-term strain decay at three radii obtained from the constantan gages in test 373. Significant strain relaxation was observed for only the first 100 ms following charge detonation.

The second strain gage configuration was a standard 120-ohm constantan grid [0.32 inch (8.13 mm) by 0.32 inch (8.13 mm)] encapsulated in a 0.375-inch-diameter (9.52-mm) sphere of GE RTV 615. The RTV was considered a possible fluid-like material that would provide a hydrostatic environment for the active gage element. Two gage packages were cast in a sphere of RMG on opposite sides of a charge. The active elements were positioned 1 inch (2.54 cm) from the center of the charge. The two gages were oriented radially and circumferentially to assess the fluid-like characteristics of the RTV. Figure 3.116 shows the strain records obtained from the gages. The strain induced in the radially oriented gage was compressive, whereas the strain induced in the circumferentially oriented gage was tensile over most of the recording time. The RTV appears to have a significant dynamic shear modulus and is not a fluid-like material. However, the small strain induced in the

187

END

FILMED

DTIC
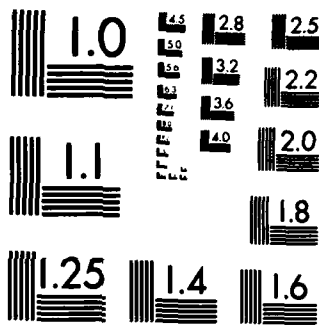
MICROCOPY RESOLUTION TEST CHART

NATIONAL BUREAU OF STANDARDS-1963-A
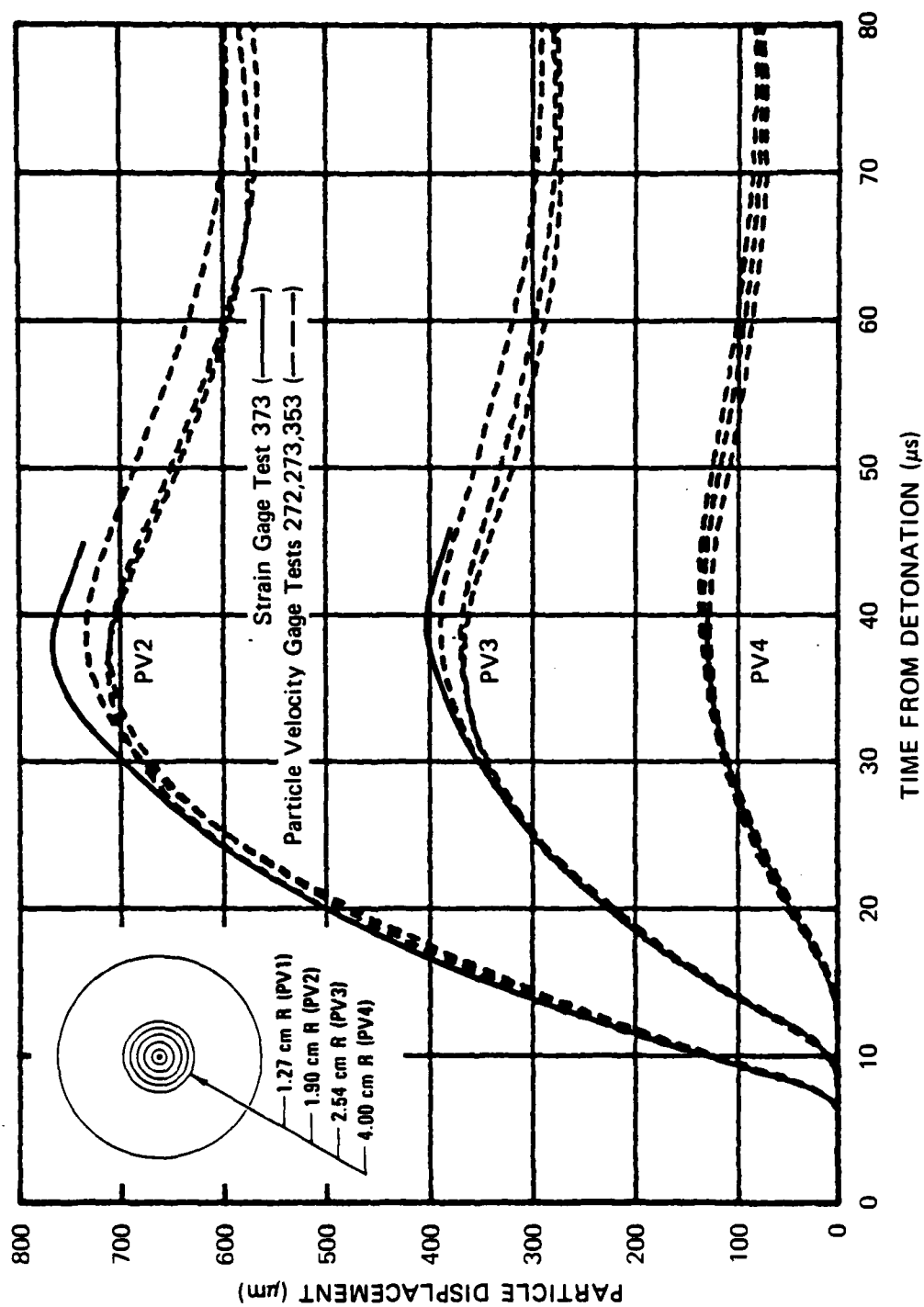
FIGURE 3.114 PARTICLE DISPLACEMENT 1.90 cm, 2.54 cm, AND 4.00 cm FROM THE CENTER OF COUPLED EXPLOSIONS IN RMG 2C4 – STRAIN GAGE VERSUS PARTICLE VELOCITY GAGE

JA-5372-89

188
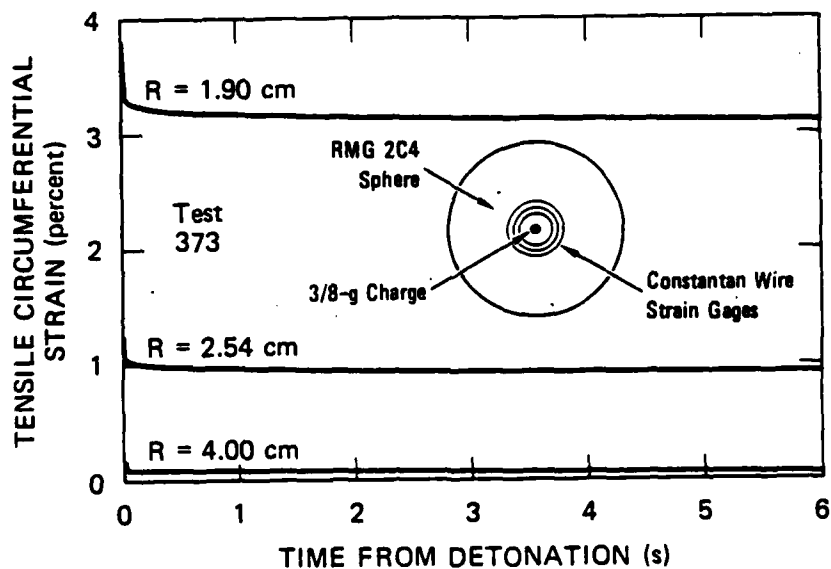
FIGURE 3.115 CIRCUMFERENTIAL STRAIN DECAY 1.90 cm, 2.54 cm, AND 4.00 cm FROM THE CENTER OF COUPLED EXPLOSION IN RMG 2C4

189
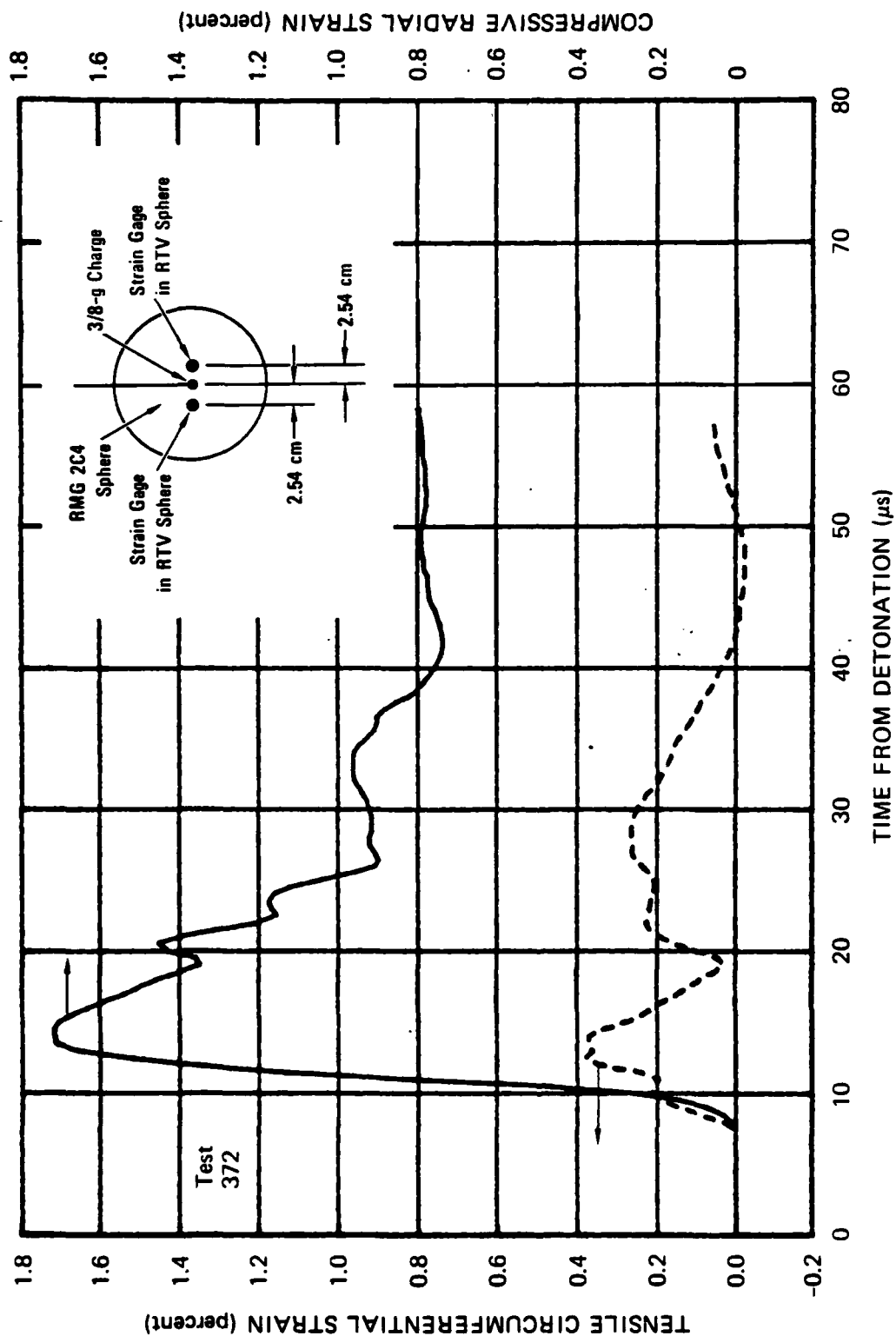
FIGURE 3.116 RADIAL AND CIRCUMFERENTIAL STRAIN 2.54 cm FROM THE CENTER OF COUPLED EXPLOSION IN RMG 2C4

JA-5372-116

190

circumferentially oriented gage indicates that the active gage element was slipping relative to the RTV. This response is beneficial in typical stress gage design where in-plane straining of the gage element should be minimized. Hence, the RTV is still considered a useful encapsulating material for stress gages.

Series 15: Stress Measurements in RMG 2C4

The development of a unique equation-of-state model for any material requires independent measurements of stress and strain. Techniques for measuring strain have been described (Series 14). Piezoresistive gages for measuring stress are being developed (Section 2.3).

A recently developed preliminary stress gage package consists of a standard 50-ohm ytterbium grid [0.25 inch (6.35 mm) by 0.25 inch (6.35 mm)] encapsulated in GE RTV 615. In one configuration, the RTV was molded into a 0.75-inch-diameter (19.05-mm) sphere. In a second configuration, the RTV was molded into a 0.75-inch-diameter (19.05-mm) and 0.125-inch-thick (3.18-mm) disk. The packages were calibrated in oil to a pressure of 1 kbar, and the ytterbium followed the hydrostatic coefficient during loading and unloading. The gages were then cast in a 12-inch-diameter (30.48-cm) sphere of RMG 2C4. The grids were positioned to measure radial stress 1 inch (2.54 cm) from the center of an explosive charge. Figure 3.117 shows the dynamic pulse measured by each gage in test 371. For comparison, a calculated pulse using an effective stress model[*] is also shown. Good agreement exists among the results near the wavefront where the in-plane straining of the ytterbium grids is small. However, the grids are eventually influenced by strain states that are different inside the sphere and disk of RTV. In addition, the inclusion effects associated with the sphere and disk influence the state of stress acting on the grids.

---

[*]Norton Kimer, S-CUBED, Del Mar, CA (private communication).
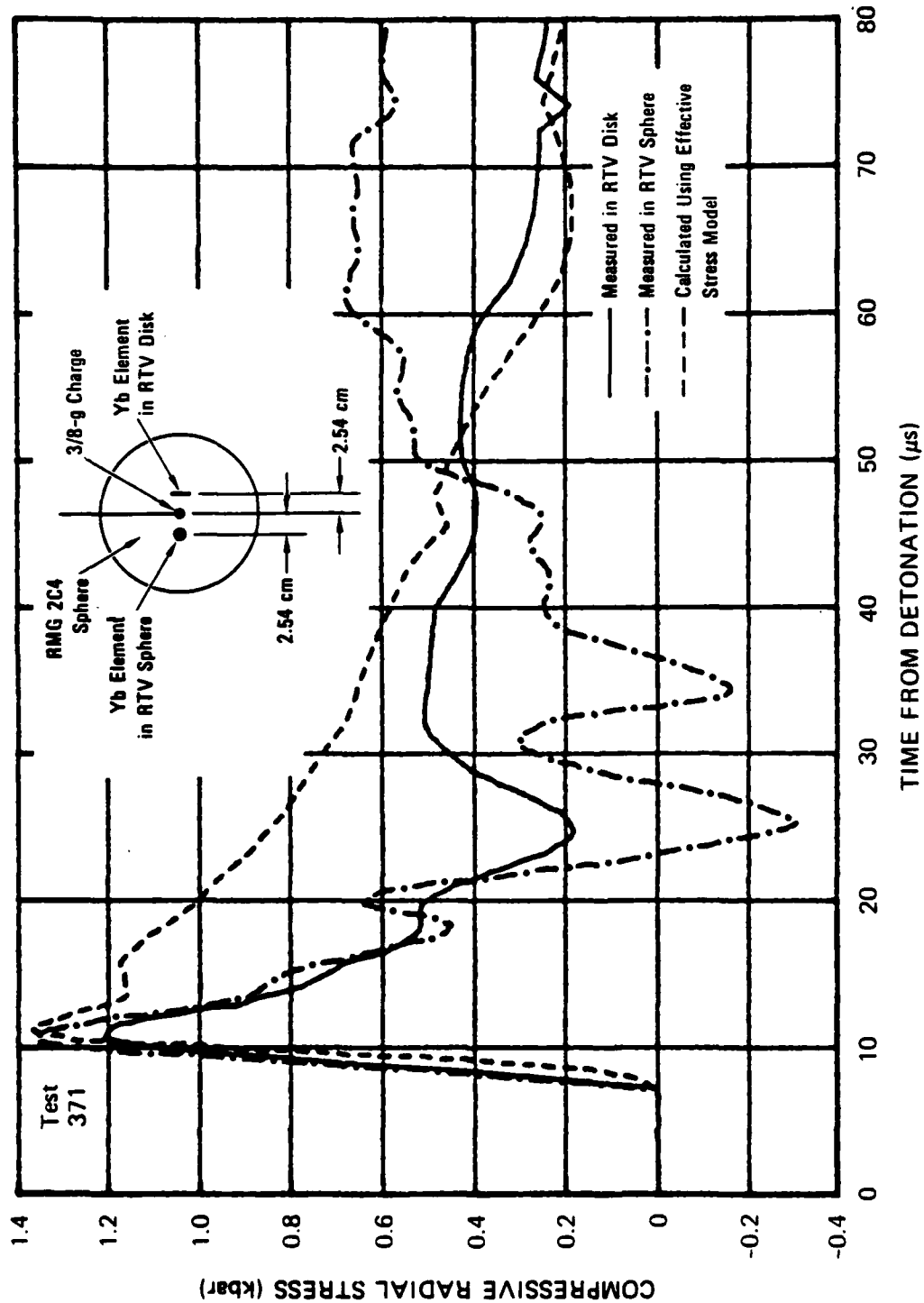
FIGURE 3.117 RADIAL STRESS 2.54 cm FROM THE CENTER OF COUPLED EXPLOSION IN RMG 2C4 — MEASURED VERSUS CALCULATED

Figure 3.118 shows the long-term radial stress decay measured by the gages in test 371. Significant stress decay appears to be limited to the first three seconds following charge detonation.
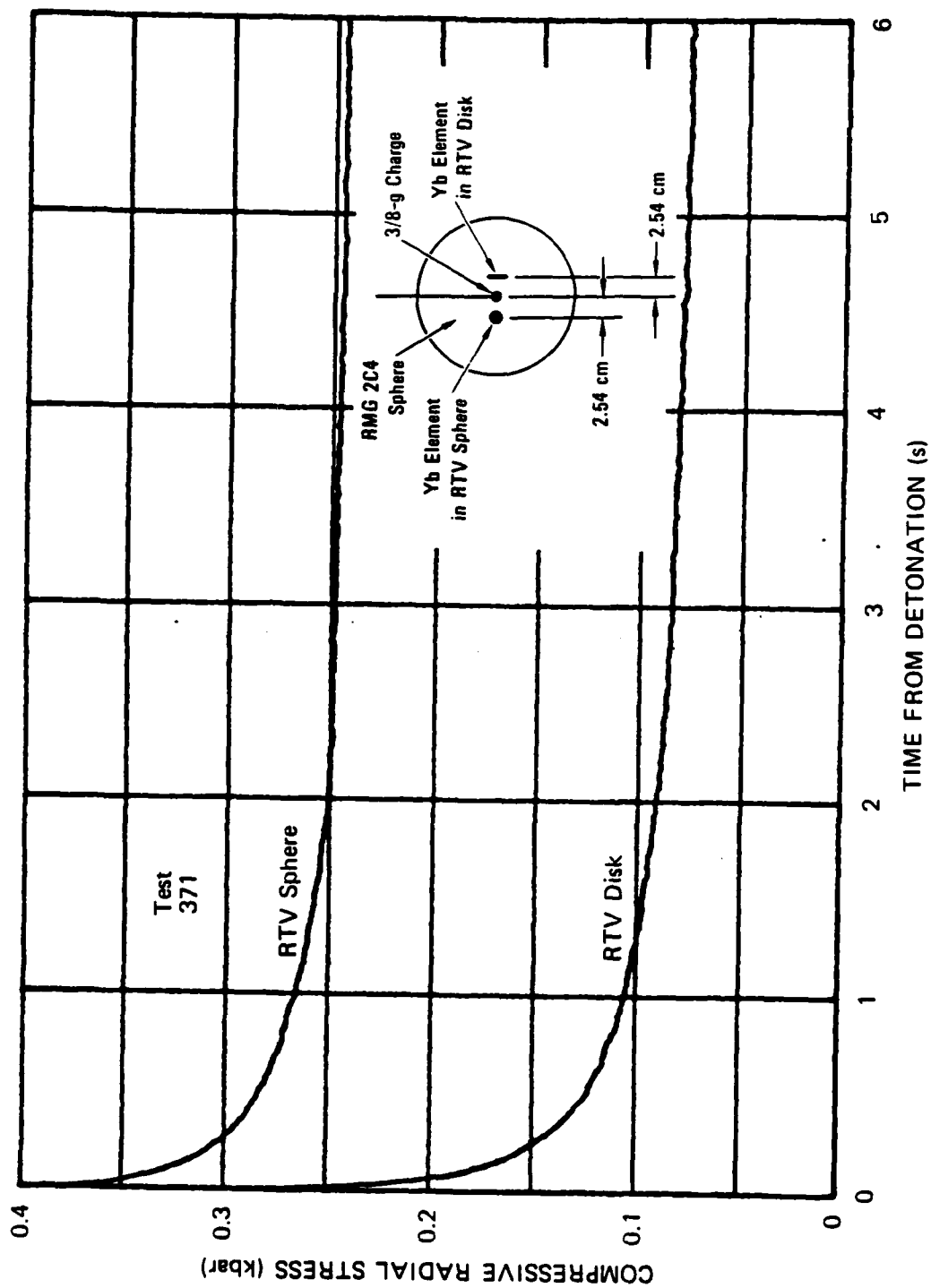
FIGURE 3.118 RADIAL STRESS DECAY 2.54 cm FROM THE CENTER OF COUPLED EXPLOSION IN RMG 2C4

JA-5372-114

REFERENCES

1. R. W. Gates and C. F. Petersen, "A Laboratory Method for Studying Stemming of Line-of-Sight Tunnels in Underground Nuclear Tests," Final Report, DNA 3058Z, Contract DNA001-72-C-0047, Stanford Research Institute (November 1972).

2. R. W. Gates, C. F. Petersen, and A. L. Florence, "Laboratory Method for Studying Stemming of Line-of-Sight Tunnels in Underground Nuclear Tests," Final Report, DNA 3592F, Contract DNA001-73-C-0122, Stanford Research Institute (December 1973).

3. A. L. Florence, "Laboratory Investigation of Stemming of Horizontal Line-of-Sight (HLOS) Underground Nuclear Tests," Final Report, DNA 3684F, Contract DNA001-74-C-0101, Stanford Research Institute (February 1975).

4. A. L. Florence, "Laboratory Investigation of Stemming and Containment in Underground Nuclear Tests," Final Report, DNA 4149F, Contract DNA001-75-C-0083, Stanford Research Institute (October 1976).

5. J. C. Cizek and A. L. Florence, "Laboratory Studies of Containment in Underground Nuclear Tests," Final Report, DNA 4846F, Contract DNA001-77-C-0025, SRI International (January 1978).

6. J. C. Cizek and A. L. Florence, "Laboratory Studies of Containment in Underground Nuclear Tests," Final Report, DNA 4847F, Contract DNA001-77-C-0025, SRI International (January 1979).

7. J. C. Cizek and A. L. Florence, "Laboratory Studies of Containment in Underground Nuclear Tests," Final Report, DNA 5601F, Contract DNA001-79-C-0094, SRI International (January 1980).

8. J. C. Cizek and A. L. Florence, Laboratory Investigation of Containment in Underground Nuclear Tests," Final Report, DNA 5731F, Contract DNA001-80-C-0040, SRI International (February 1981).

9. J. C. Cizek and A. L. Florence, "Laboratory Investigation of Containment in Underground Nuclear Tests," Final Report, DNA 6121F, Contract DNA001-80-C-0040, SRI International (December 1981).

10. J. C. Cizek and A. L. Florence, "Laboratory Investigation of Containment of Underground Explosions," Final Report, DNA TR-82-83, Contract DNA001-82-C-0053, SRI International (December 1982).

11. A. L. Florence and T. C. Kennedy, "A Simple Analysis for Containment Studies," Topical Report 76-3702-2, Contract DNA001-75-C-0083, Stanford Research Institute (August 1976).

12. L. Seaman, "SRI PUFF 3 Computer Code for Stress Wave Propagation," prepared for Air Force Weapons Laboratory, Air Force Systems Command, Kirtland AFB, New Mexico, Technical Report AFWL-TR-70-51, Stanford Research Institute (September 1970).

13. N. Rimer and K. Lie, "Numerical Simulation of the Velocity Records from the SRI Crout Spheres Experiments," Topical Report SSS-82-R-5580, Contract DNA001-82-C-0043, S-Cubed (September 1982).

14. M. B. Fogel and D. F. Patch, "Extraction of Material Property Parameters from Velocity Histories," Topical Report PT-U82-0564, Contract DNA001-82-C-0047, Pacifica Technology (August 1982).

15. J. C. Cizek, A. L. Florence, and D. D. Keough, "Experimental Study of the Effects of Faults on Spherical Wave Propagation," Final Report, DARPA Order No. 3749-A1, Contract DNA001-80-C-0287, SRI International (January 1981).

16. B. P. Bonner, A. E. Abey, H. C. Heard, and R. N. Schock, "High-Pressure Mechanical Properties of Merlin Alluvium," Lawrence Livermore Laboratory, Report UCRL-51252 (July 1972).

APPENDIX A

PARTICLE DISPLACEMENT FROM PARTICLE VELOCITY RECORDS

The particle displacement profiles in Figures A.1 through A.14 were generated by integrating the corresponding particle velocity records presented in Section 3.3.
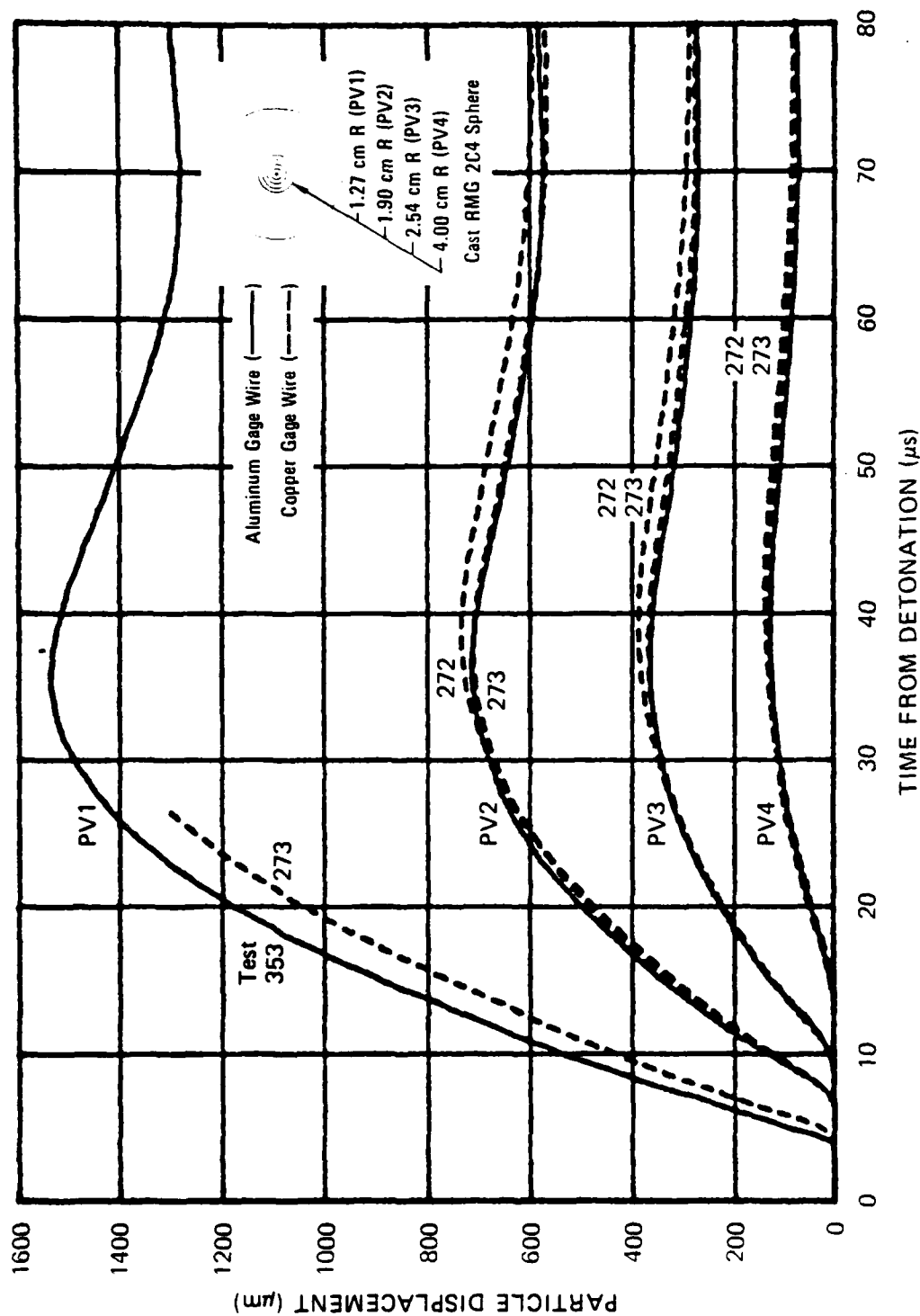
FIGURE A.1   PARTICLE DISPLACEMENT AT FOUR DISTANCES FROM THE CENTER OF COUPLED EXPLOSIONS
IN CAST RMG 2C4 — ALUMINUM VERSUS COPPER GAGE WIRE
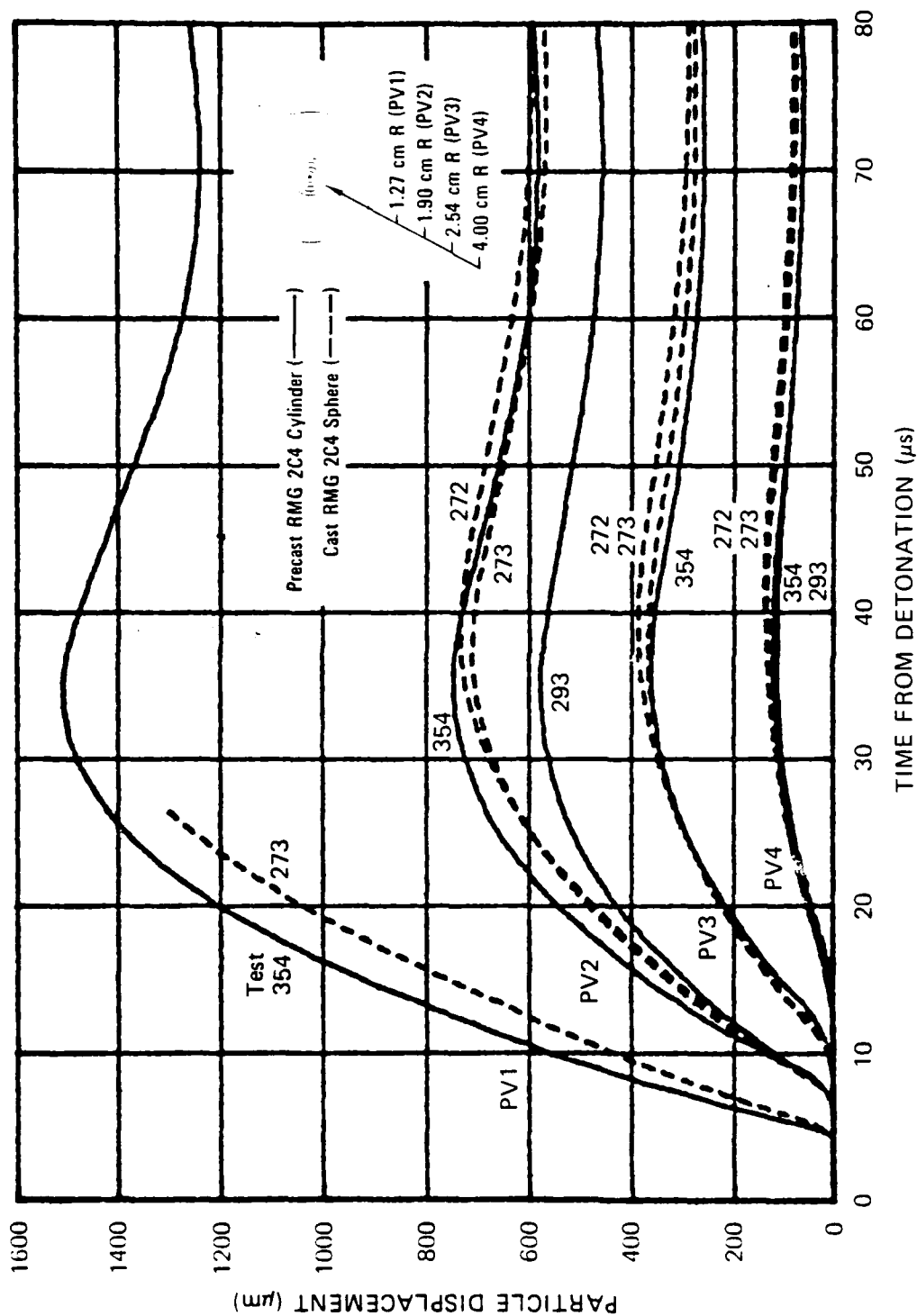
FIGURE A.2   PARTICLE DISPLACEMENT AT FOUR DISTANCES FROM THE CENTER OF COUPLED EXPLOSIONS IN RMG 2C4 – CAST VERSUS PRECAST WITH WIDE GROOVES, COPPER GAGE WIRE

JA-5372-154

A-3
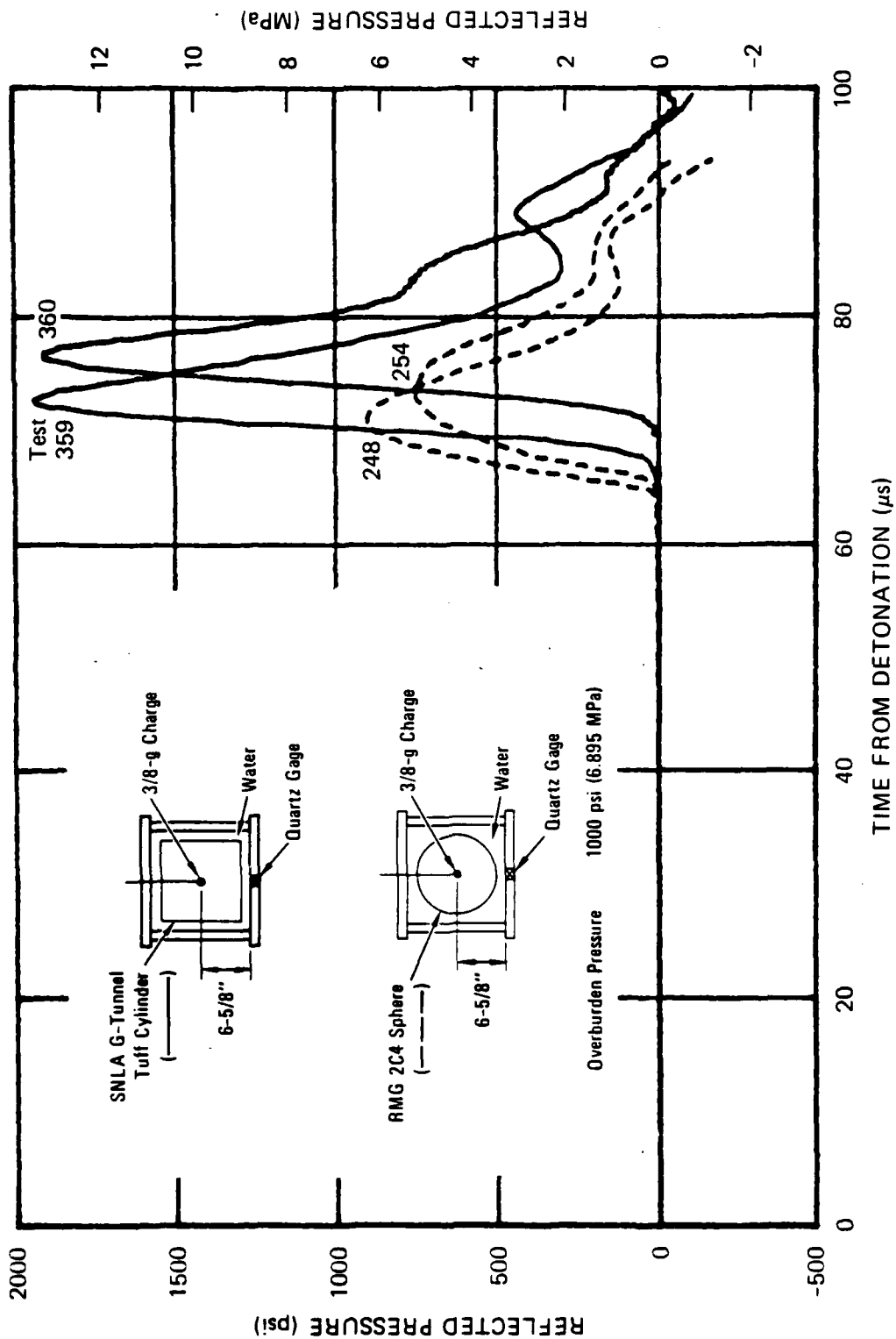
FIGURE B.1   REFLECTED PRESSURE FROM COUPLED EXPLOSIONS IN SNLA G-TUNNEL TUFF AND RMG 2C4 — HYDROFRACTURE TESTS 248, 254, 359, AND 360

JA-5372-66

APPENDIX B

PRESSURE PULSE MEASUREMENTS IN CONTAINMENT VESSEL

The pressure pulses generated during exploded cavity tests and measured by a quartz gage in the bottom of the containment vessel are presented in Figures B.1 through B.10.

A summary of results is given in Table B.1, where tests are categorized according to the relevant parameters. Maximum reflected pressure and pulse duration are listed for each test. For calculation of pulse duration, the pressure pulse was assumed to end when the pressure dropped to the initial value.
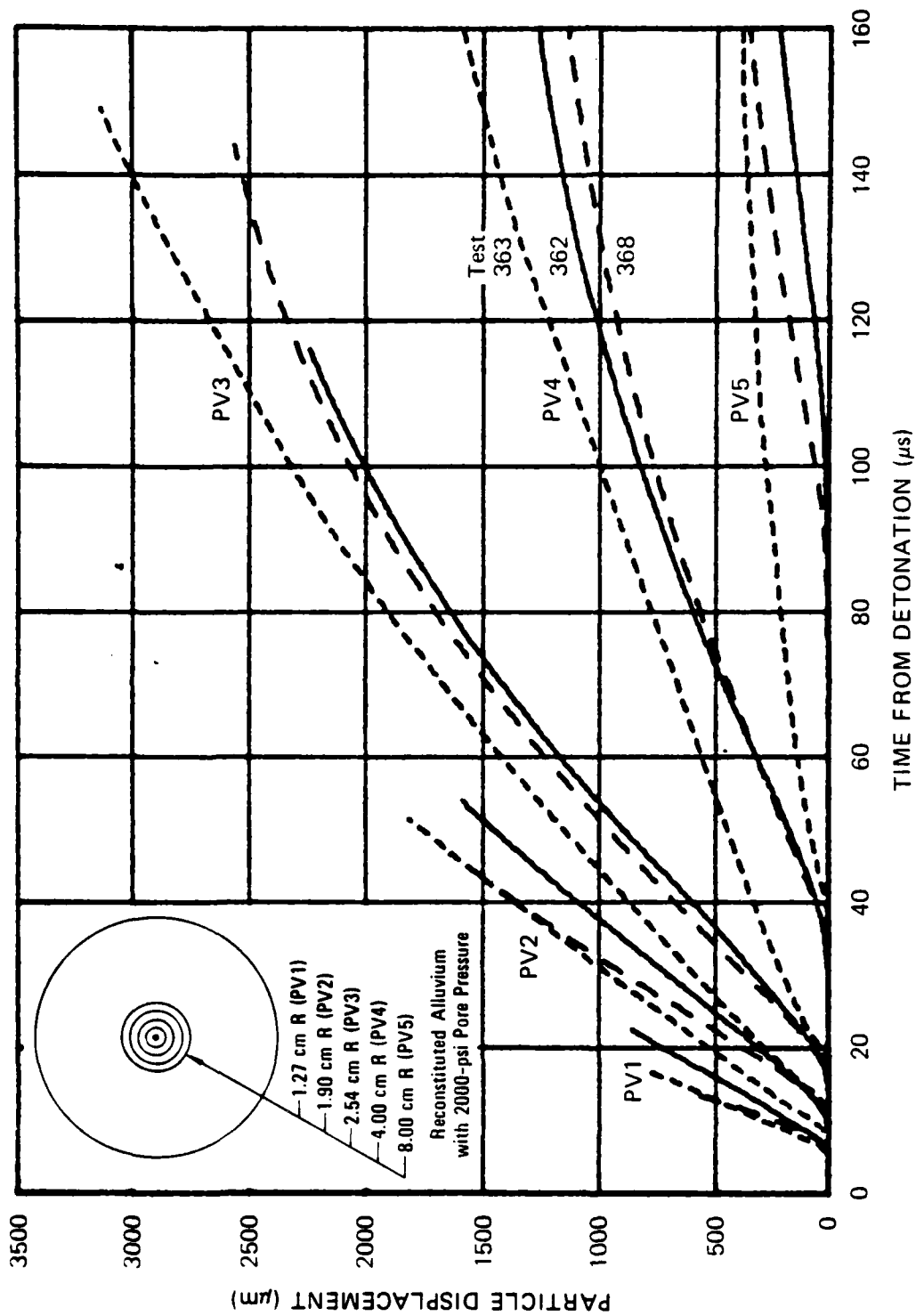
FIGURE A.14   PARTICLE DISPLACEMENT AT FIVE DISTANCES FROM THE CENTER OF COUPLED EXPLOSIONS IN RECONSTITUTED ALLUVIUM WITH 2000-psi PORE PRESSURE

JA-5372-166

A-15
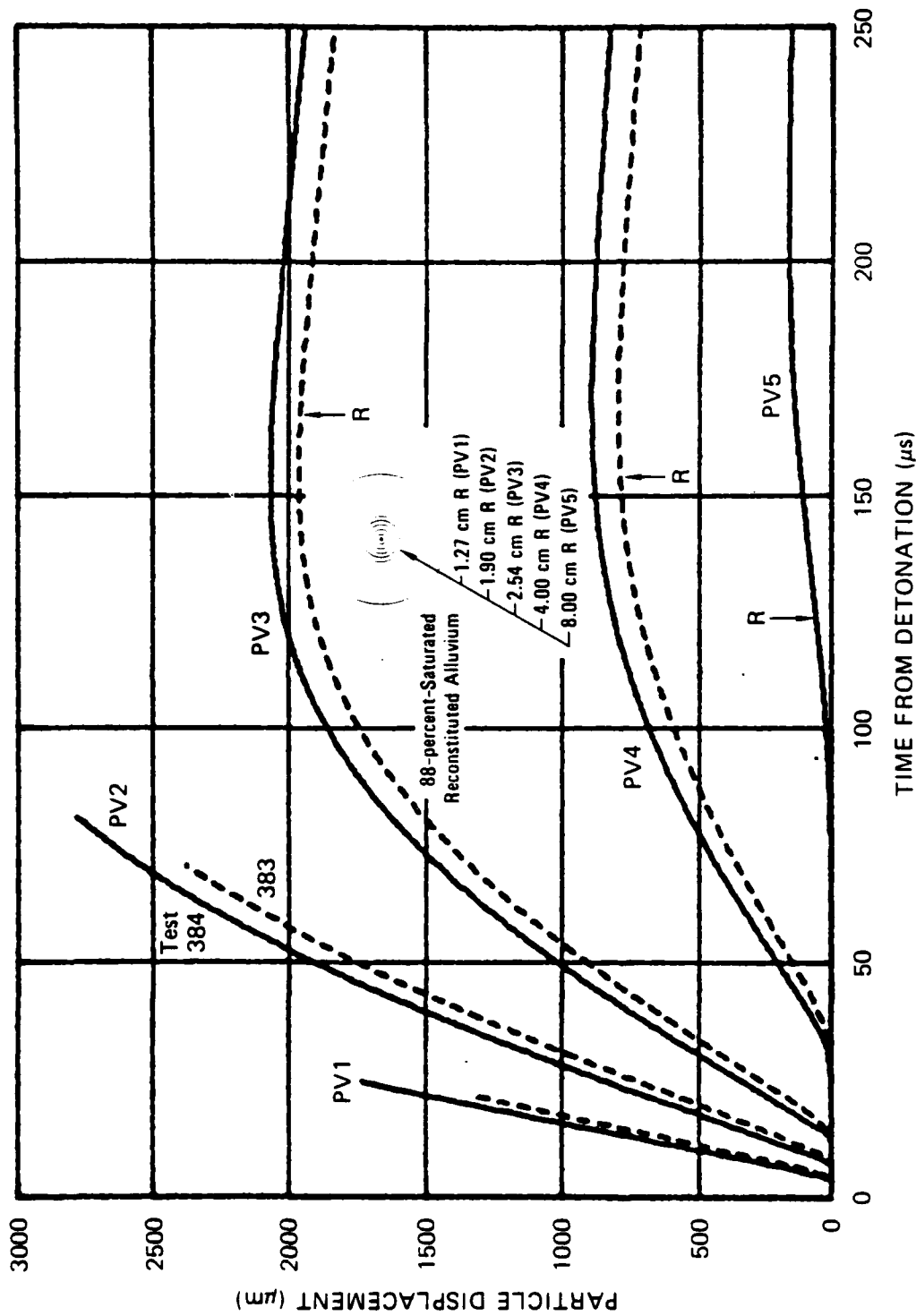
FIGURE A.13 PARTICLE DISPLACEMENT AT FIVE DISTANCES FROM THE CENTER OF COUPLED EXPLOSIONS IN 88-percent-SATURATED RECONSTITUTED ALLUVIUM

A-14
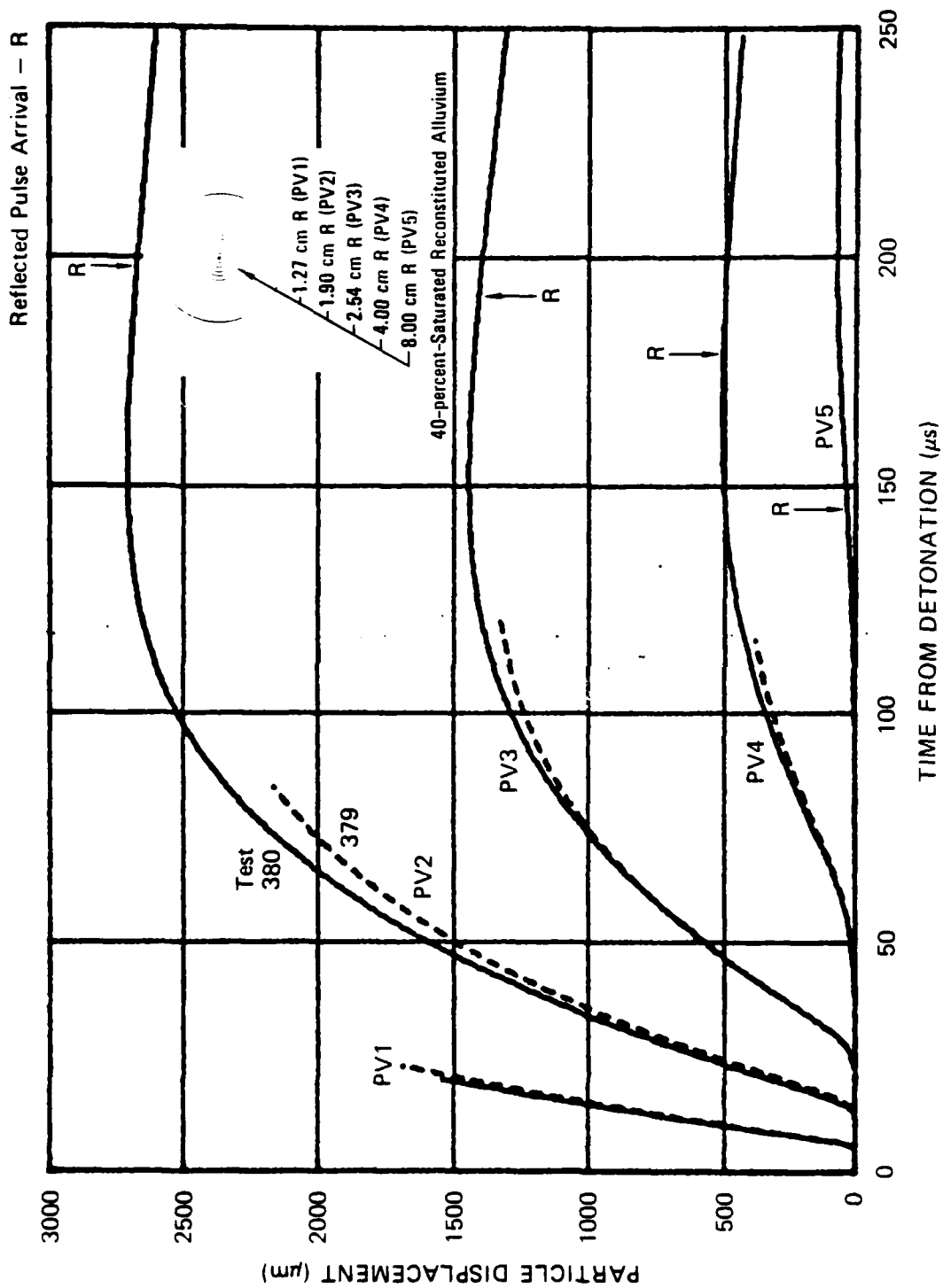
FIGURE A.12   PARTICLE DISPLACEMENT AT FIVE DISTANCES FROM THE CENTER OF COUPLED EXPLOSIONS
IN 40-percent-SATURATED RECONSTITUTED ALLUVIUM

A-13
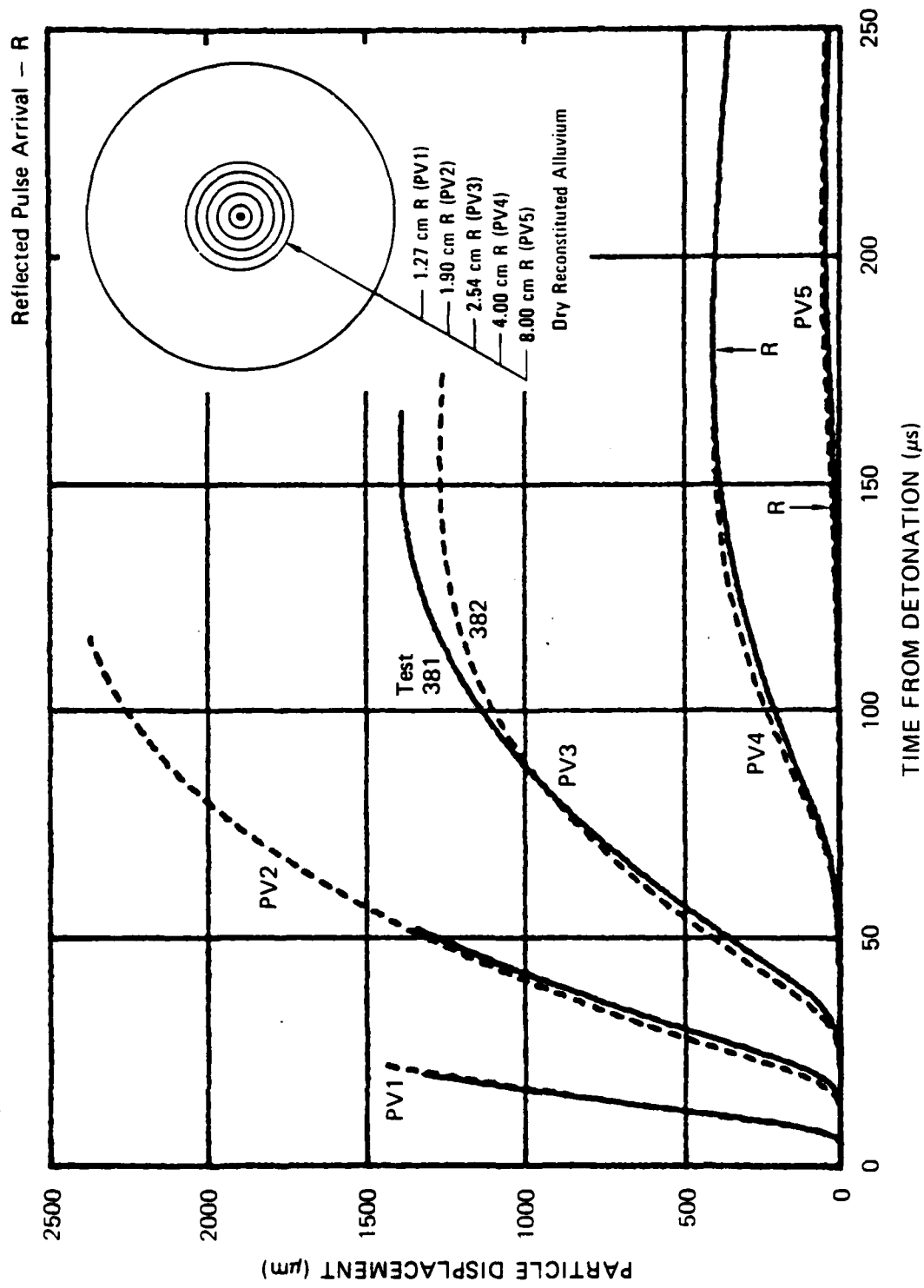
FIGURE A.11   PARTICLE DISPLACEMENT AT FIVE DISTANCES FROM THE CENTER OF COUPLED EXPLOSIONS IN DRY RECONSTITUTED ALLUVIUM

JA-5372-147

A-12
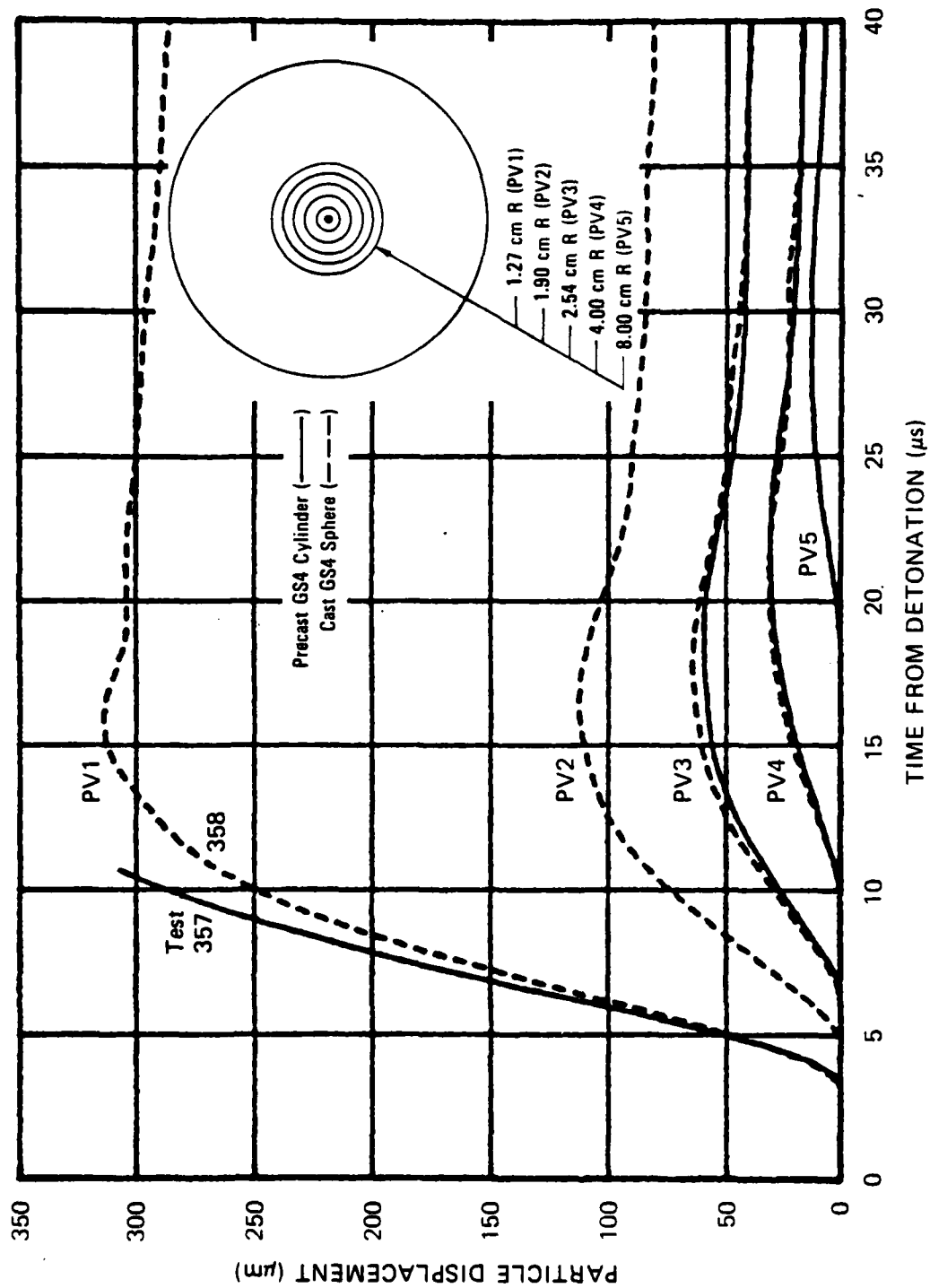
FIGURE A.10 PARTICLE DISPLACEMENT AT FIVE DISTANCES FROM THE CENTER OF COUPLED EXPLOSIONS IN GS4

JA-5372-149

A-11
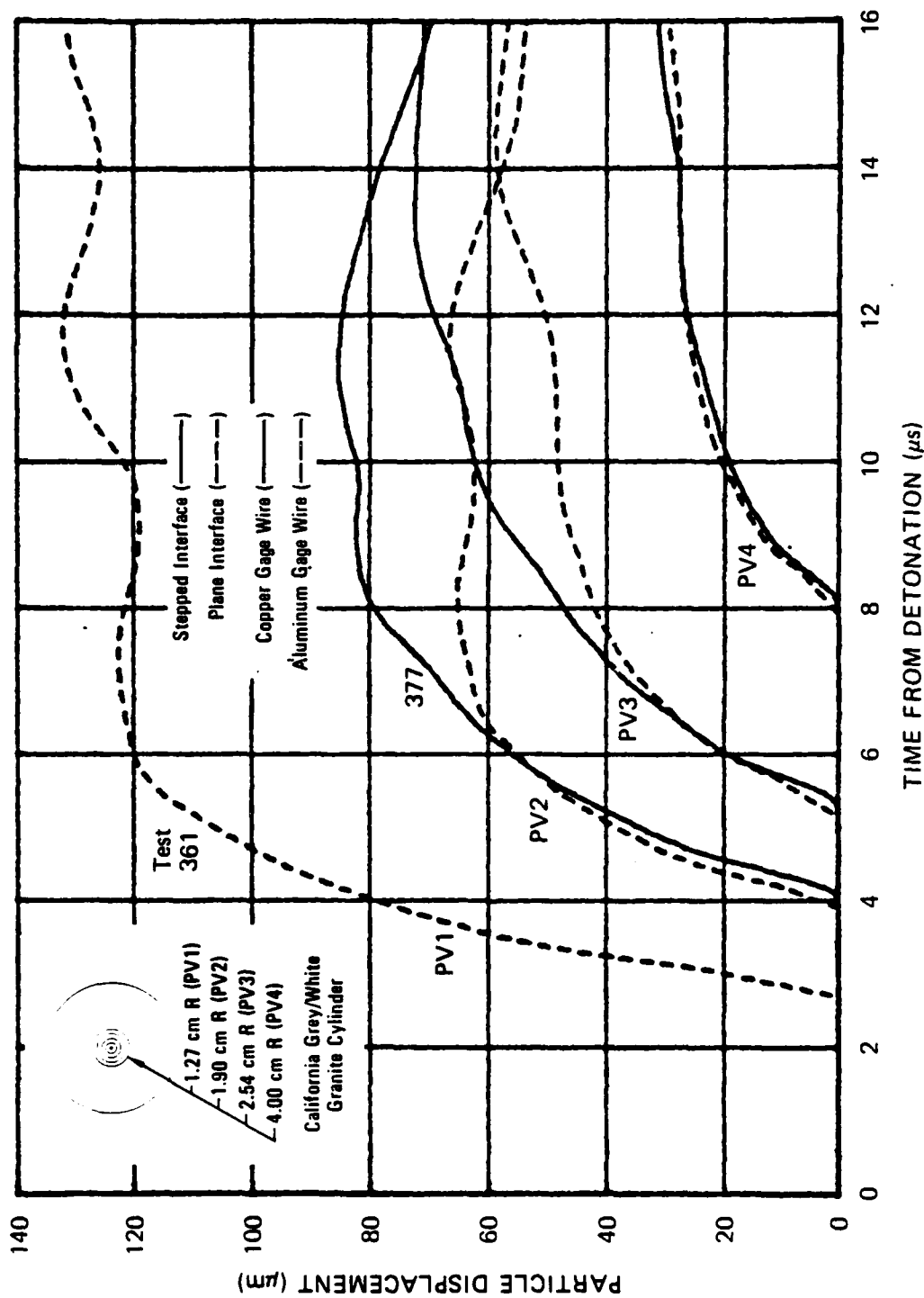
FIGURE A.9   PARTICLE DISPLACEMENT AT FOUR DISTANCES FROM THE CENTER OF COUPLED
EXPLOSIONS IN GRANITE

A-10
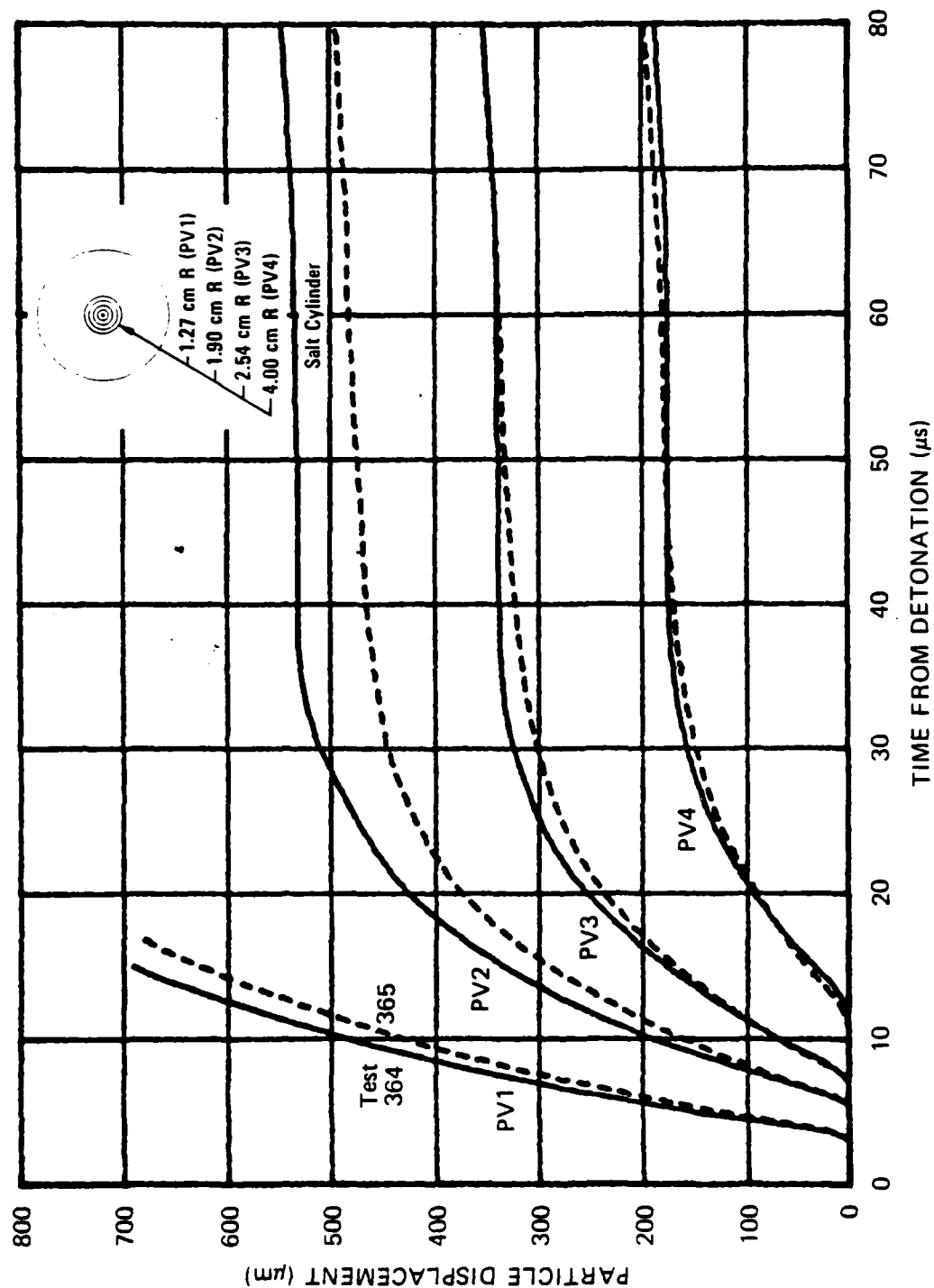
FIGURE A.8   PARTICLE DISPLACEMENT AT FOUR DISTANCES FROM THE CENTER OF COUPLED EXPLOSIONS IN SALT

A-9
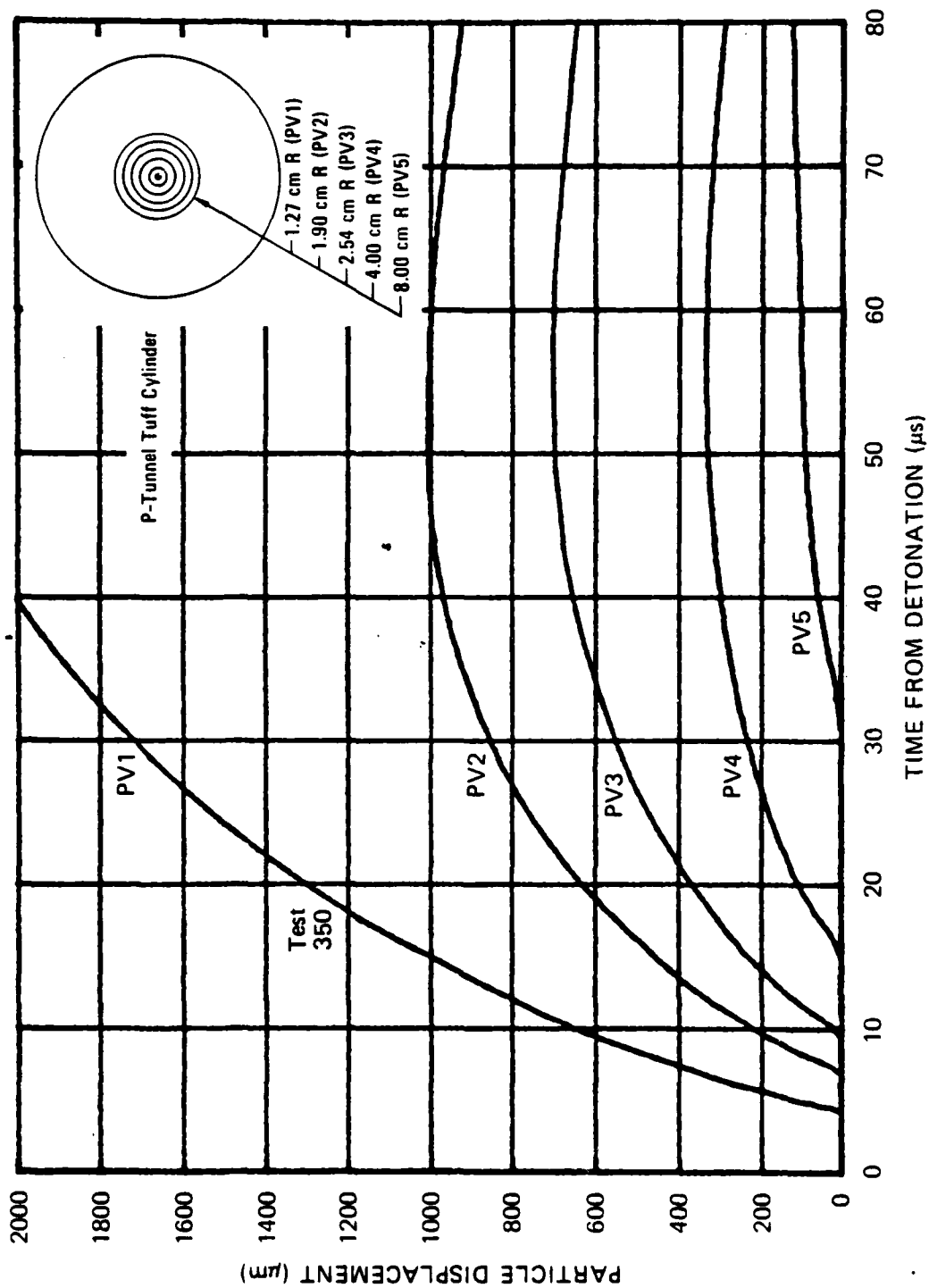
FIGURE A.7 PARTICLE DISPLACEMENT AT FIVE DISTANCES FROM THE CENTER OF A COUPLED EXPLOSION IN P-TUNNEL TUFF
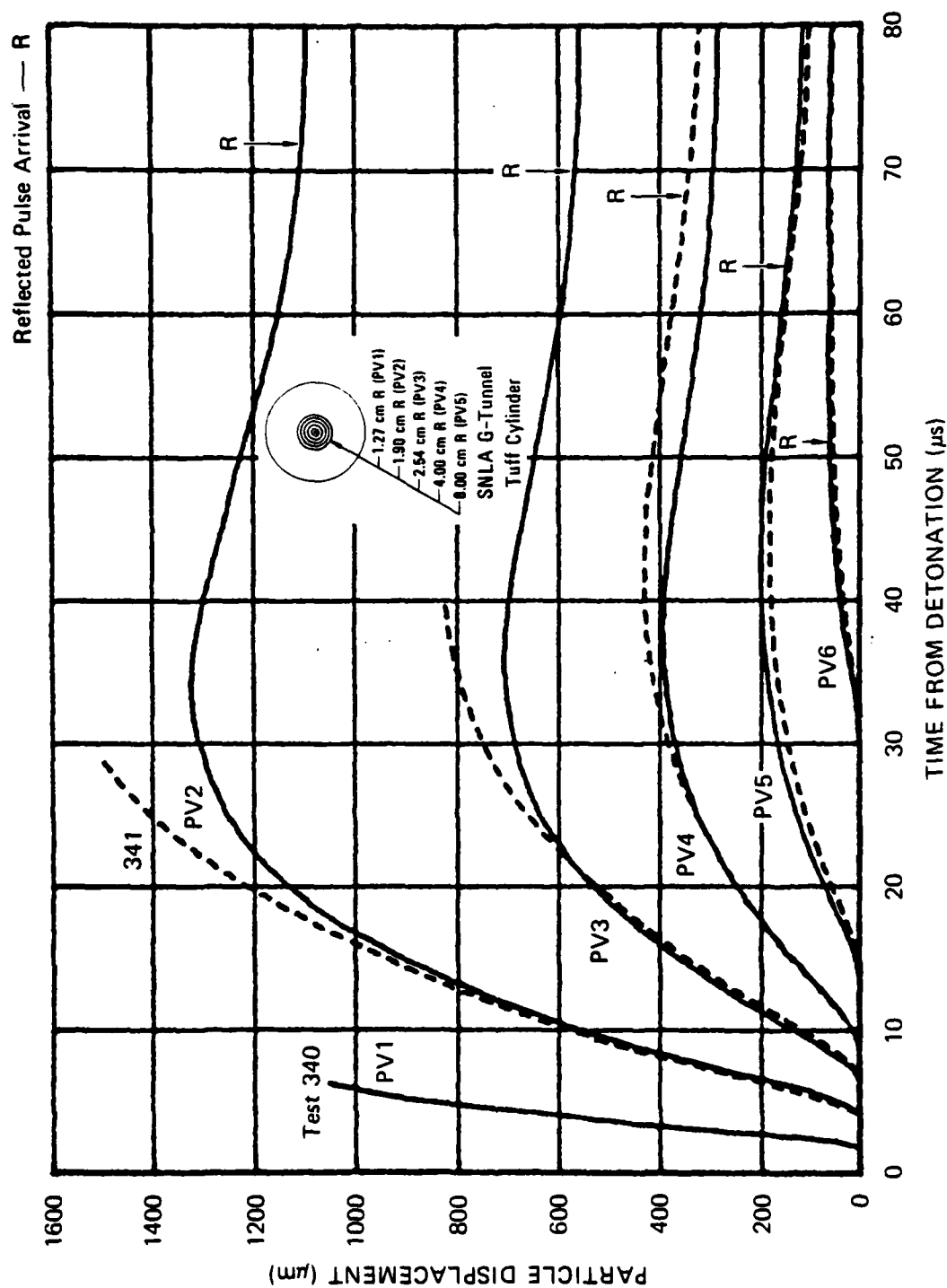
JA-5372-151

FIGURE A.6 PARTICLE DISPLACEMENT AT SIX DISTANCES FROM THE CENTER OF COUPLED EXPLOSIONS IN SNLA G-TUNNEL TUFF

A-7
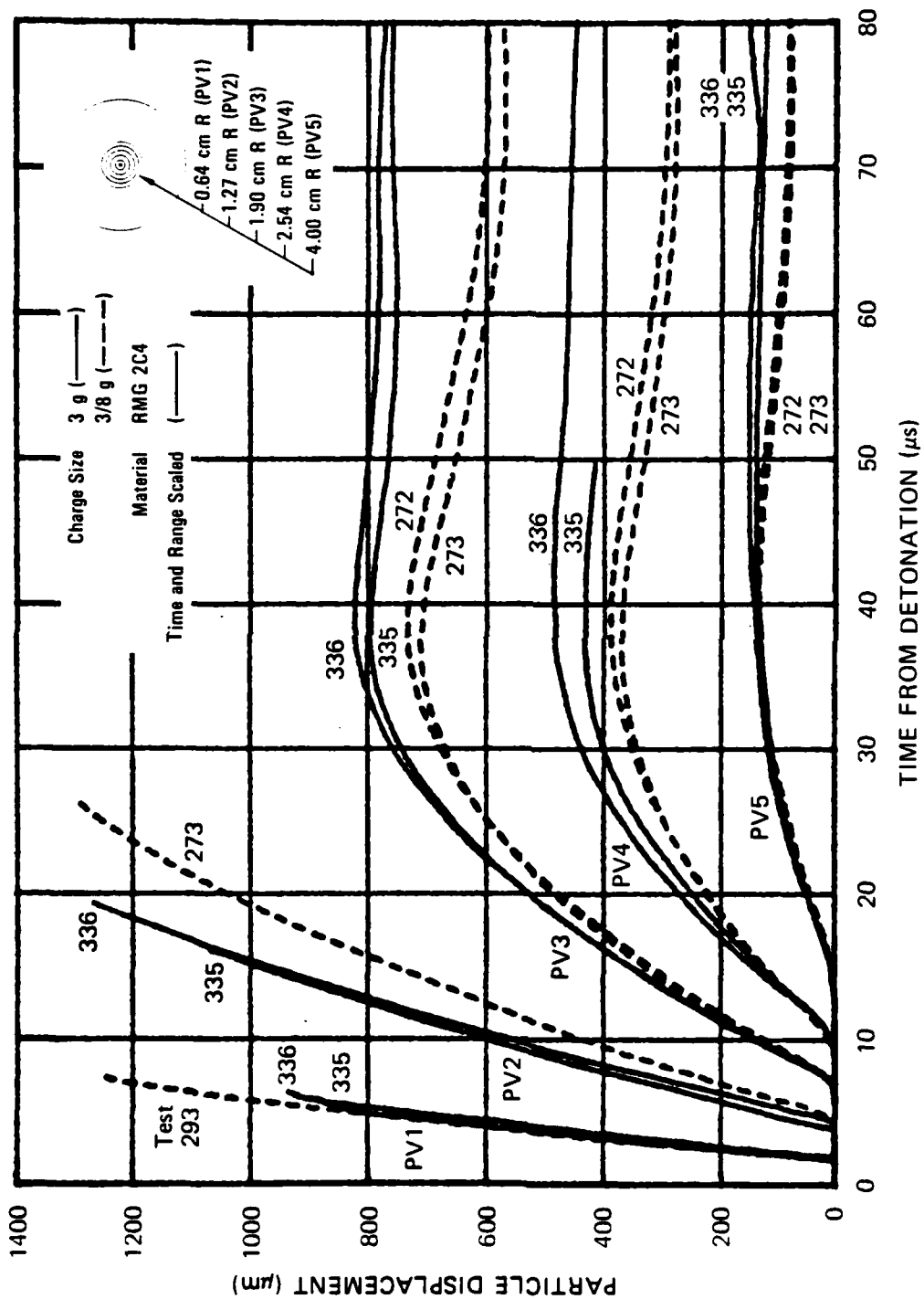
FIGURE A.5 PARTICLE DISPLACEMENT AT FIVE DISTANCES FROM THE CENTER OF COUPLED EXPLOSIONS IN RMG 2C4 — SCALING EFFECT (3 g PETN VERSUS 3/8 g PETN)

A-6
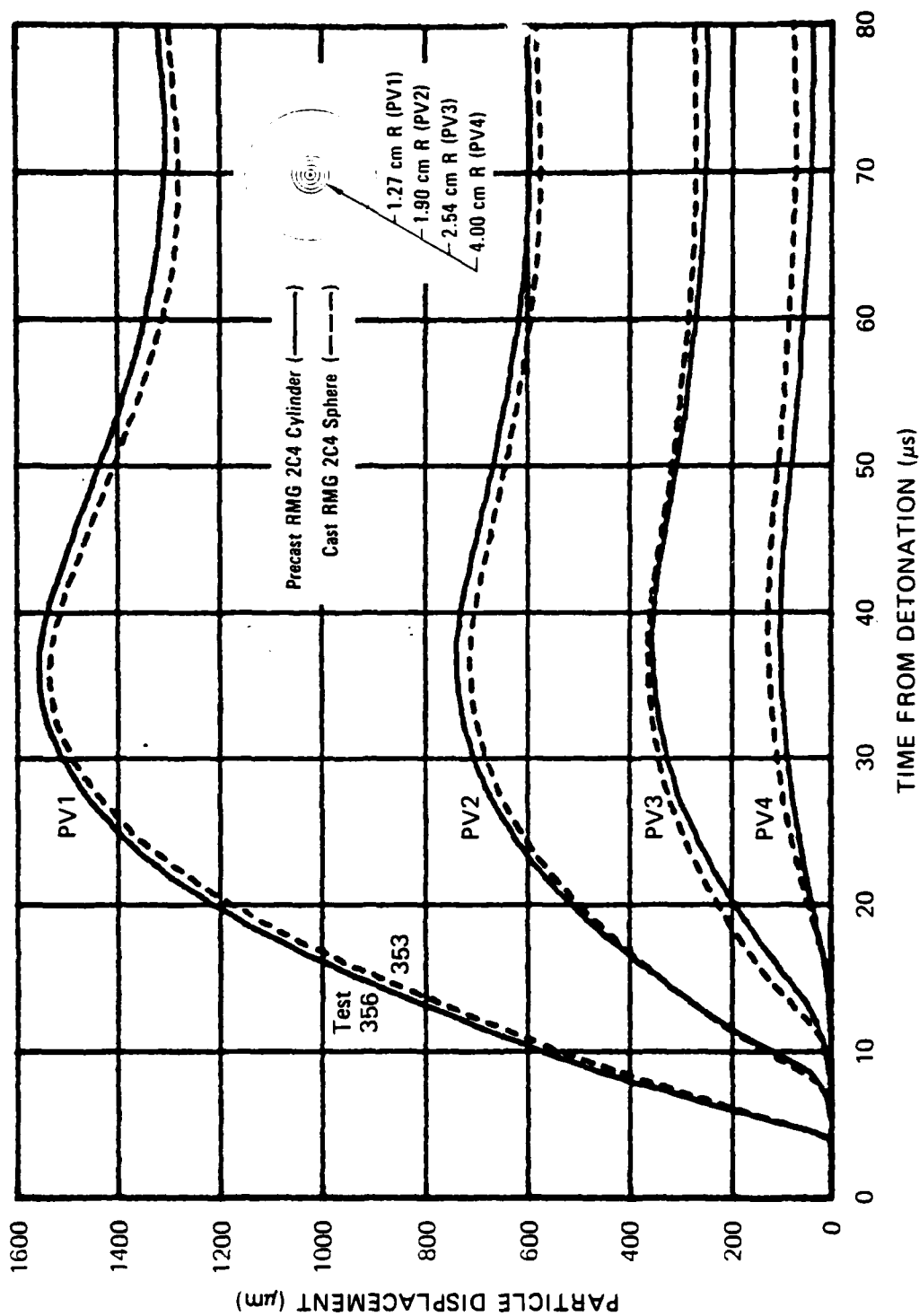
FIGURE A.4   PARTICLE DISPLACEMENT AT FOUR DISTANCES FROM THE CENTER OF COUPLED EXPLOSIONS
IN RMG 2C4 – CAST VERSUS PRECAST WITH NARROW GROOVES. ALUMINUM GAGE WIRE

JA-5372-158

A-5
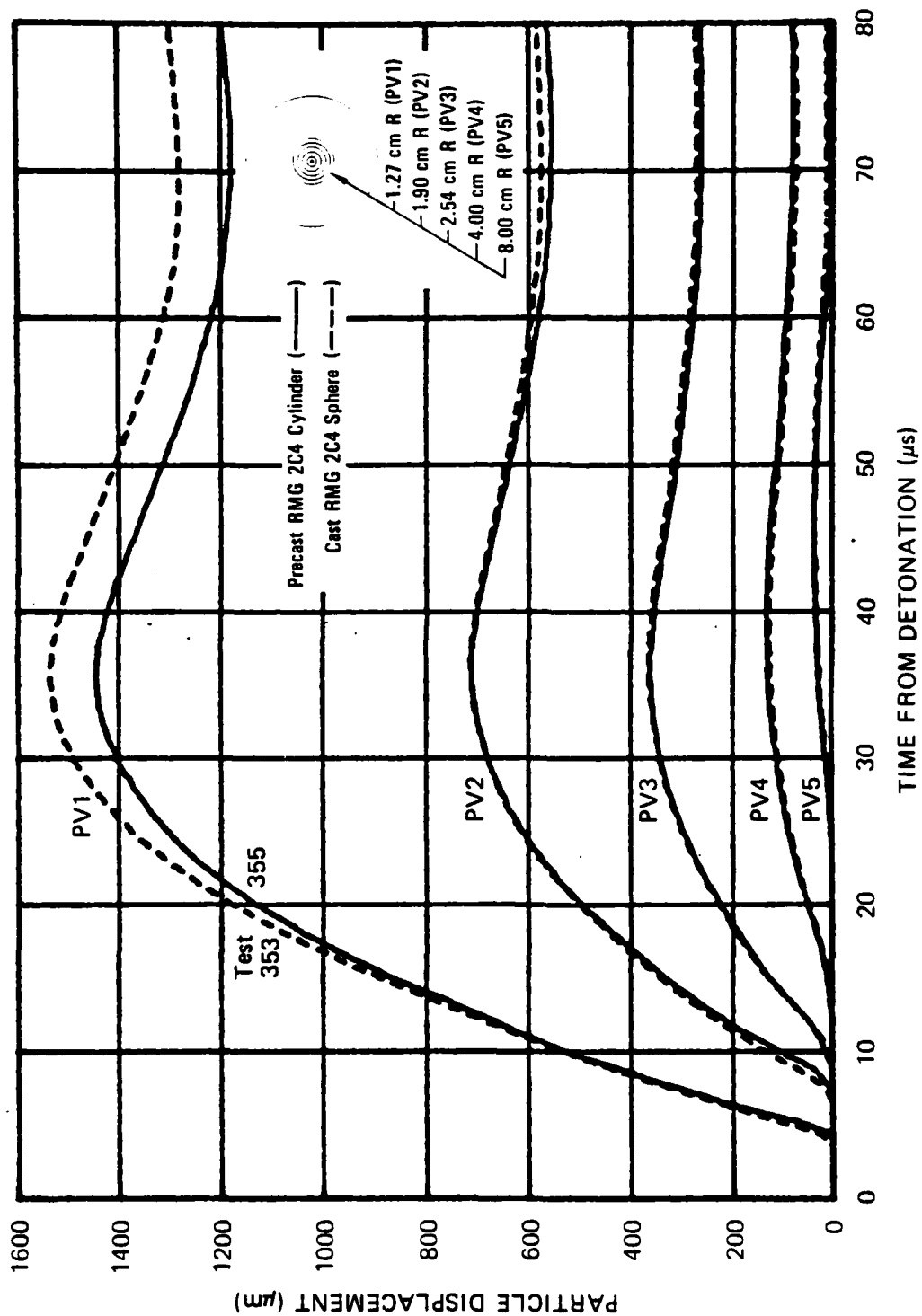
FIGURE A.3 PARTICLE DISPLACEMENT AT FIVE DISTANCES FROM THE CENTER OF COUPLED EXPLOSIONS IN RMG 2C4 — CAST VERSUS PRECAST WITH WIDE GROOVES. ALUMINUM GAGE WIRE

JA-5372-153

A-4
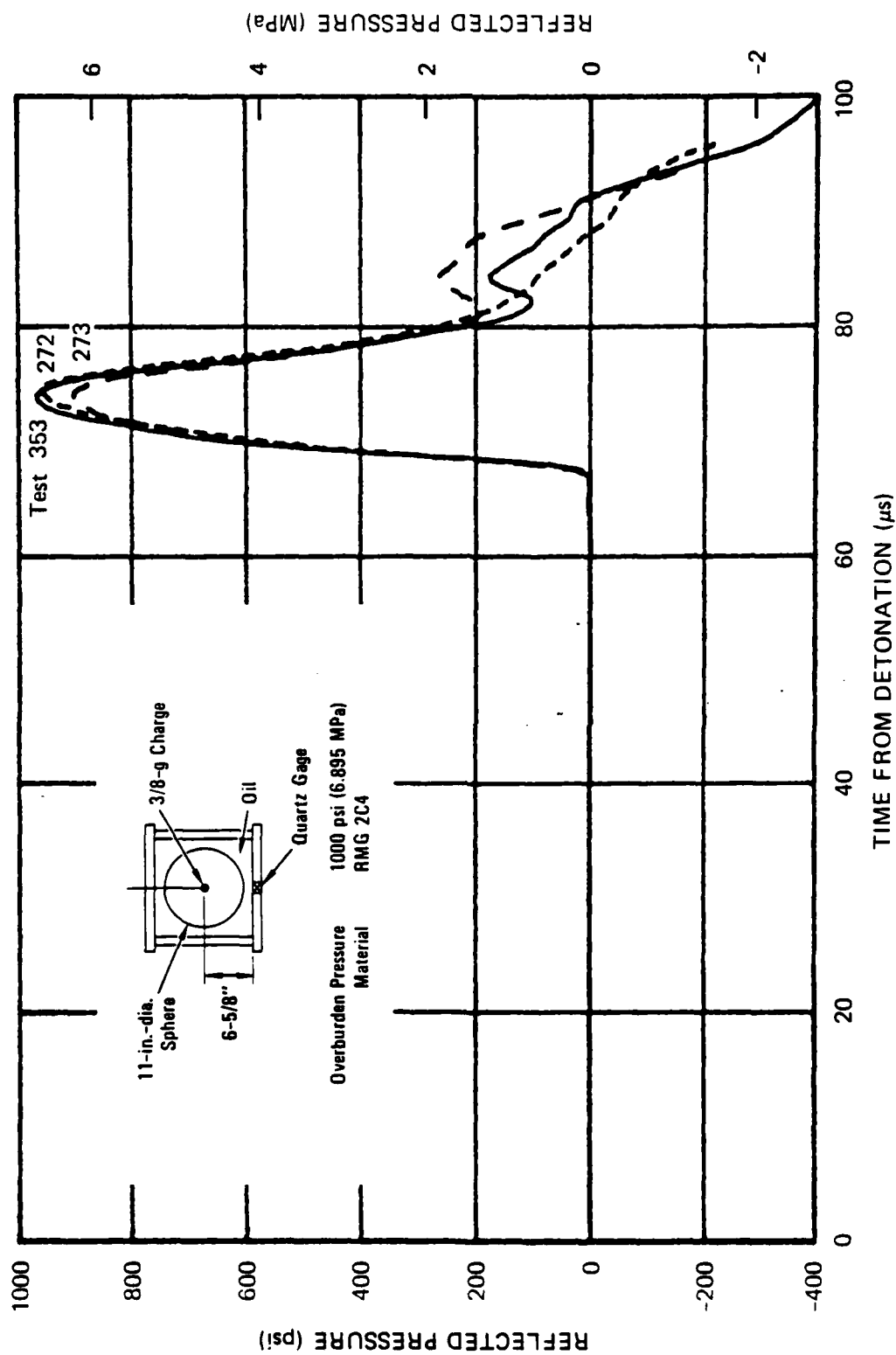
FIGURE B.2 REFLECTED PRESSURE FROM COUPLED EXPLOSIONS IN RMG 2C4 —
PARTICLE VELOCITY TESTS 272, 273, AND 353

B-3
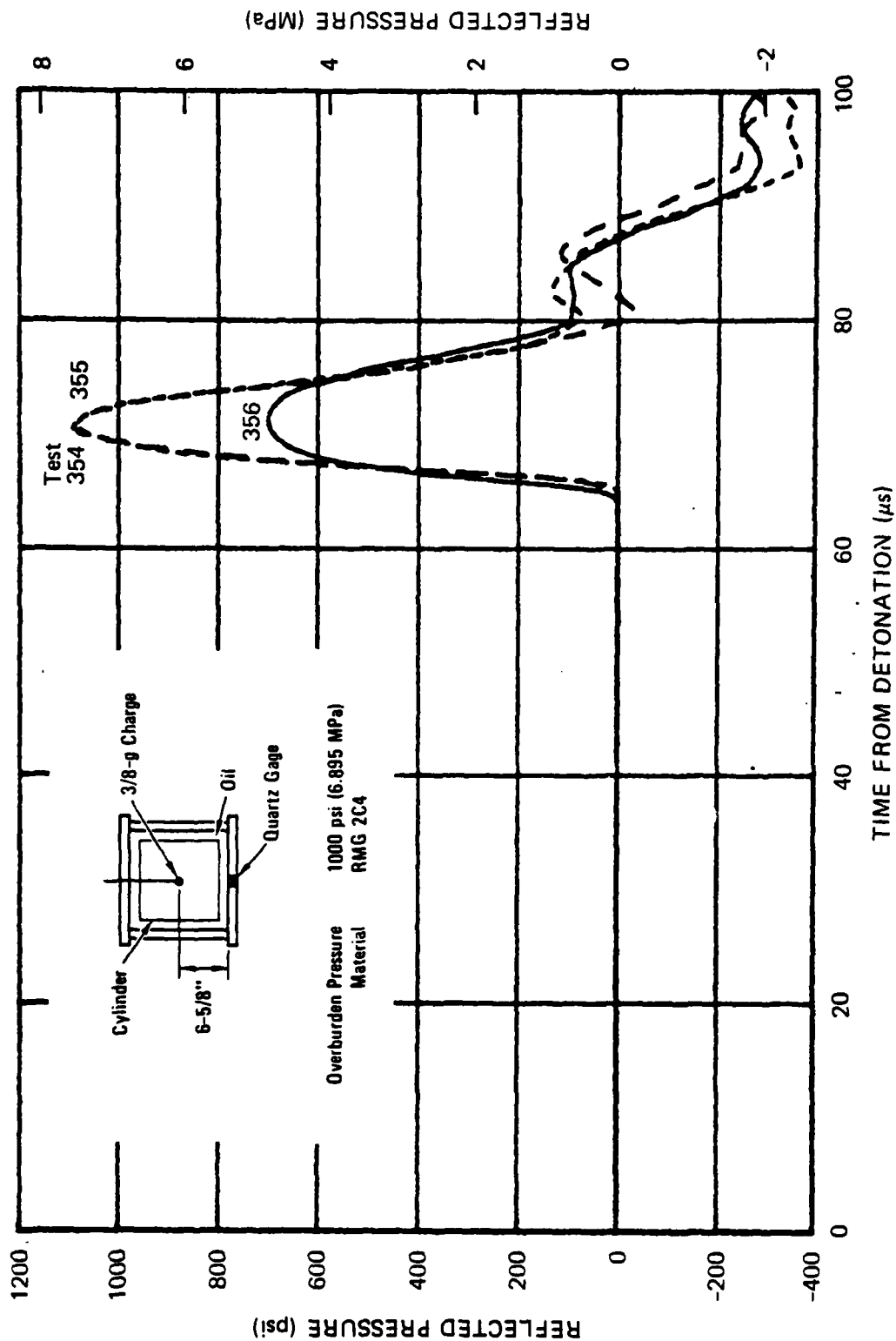
FIGURE B.3 REFLECTED PRESSURE FROM COUPLED EXPLOSIONS IN RMG 2C4 —
PARTICLE VELOCITY TESTS 354, 355, AND 356

JA-5372-110

B-4

JA-5372-18

Test
293
340
341
273
272

Cylinder
or
Sphere

3/8-g Charge

Oil

Quartz Gage

6-5/8"

Overburden Pressure   1000 psi (6.895 MPa)
Material   SNLA G-Tunnel Tuff (——)
                      RMG 2C4 (— —)

PRESSURE (psi)

1200
1000
800
600
400
200
0
-200

0   20   40   60   80   100

TIME (μs)
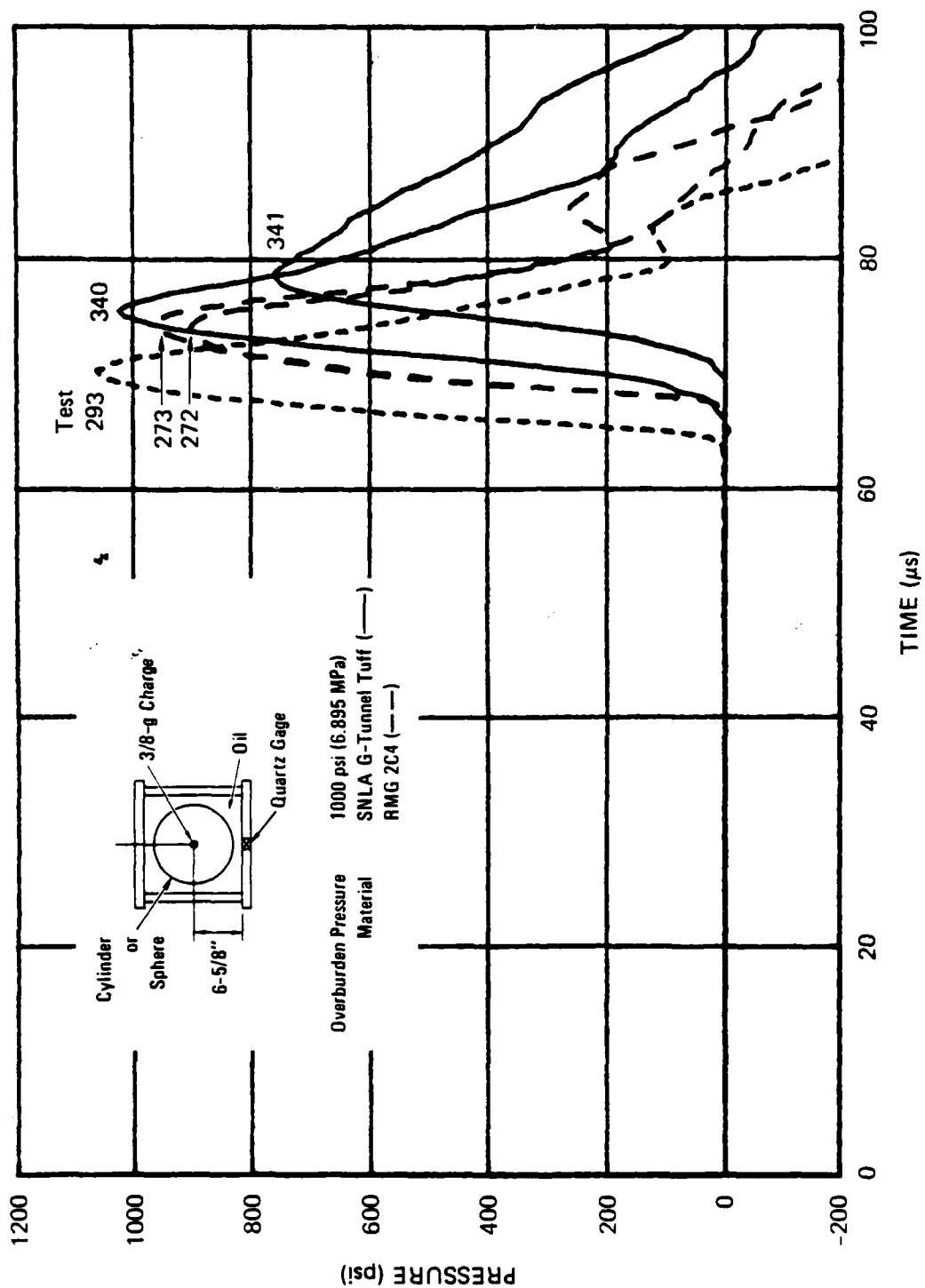
FIGURE B.4   REFLECTED PRESSURE FROM COUPLED EXPLOSIONS IN SNLA G-TUNNEL TUFF
AND RMG 2C4 — PARTICLE VELOCITY TESTS 272, 273, 293, 340, AND 341

B-5
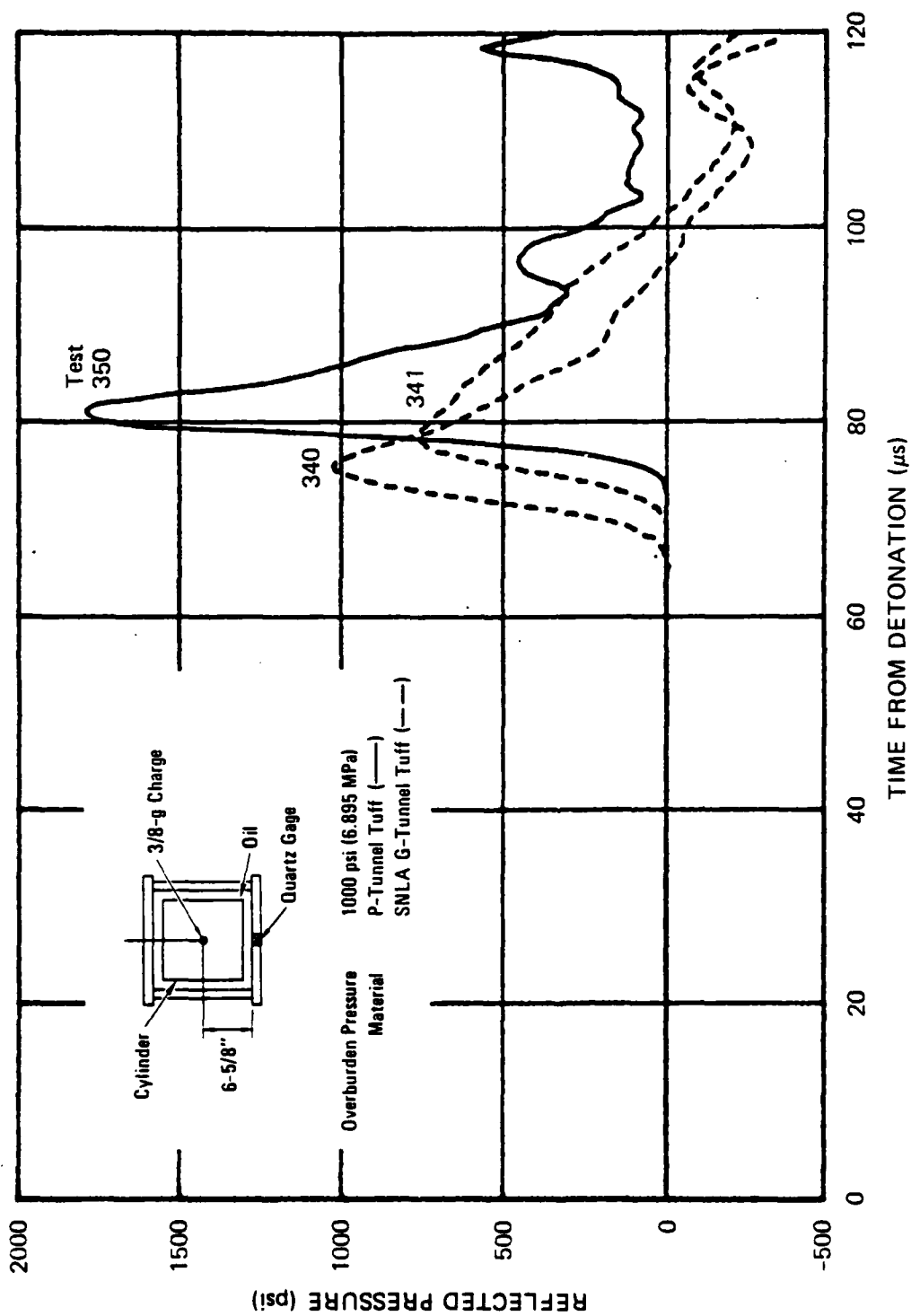
FIGURE B.5 REFLECTED PRESSURE FROM COUPLED EXPLOSIONS IN P-TUNNEL TUFF AND
SNLA G-TUNNEL TUFF – PARTICLE VELOCITY TESTS 340, 341, AND 350
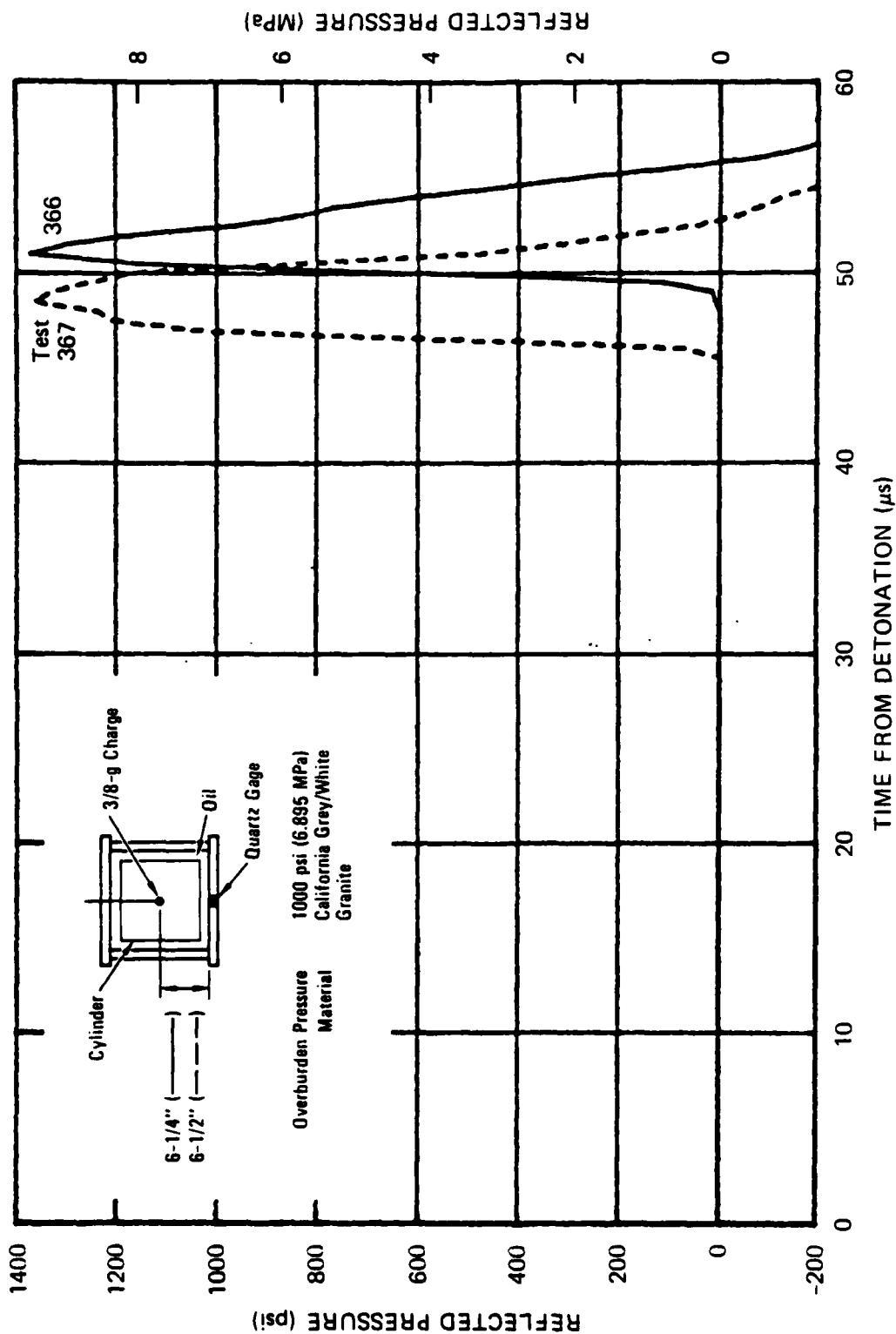
JA-5372-44

FIGURE B.6   REFLECTED PRESSURE FROM COUPLED EXPLOSIONS IN GRANITE –
FRACTURE DETECTION TESTS 366 AND 367

JA-5372-64

B-7
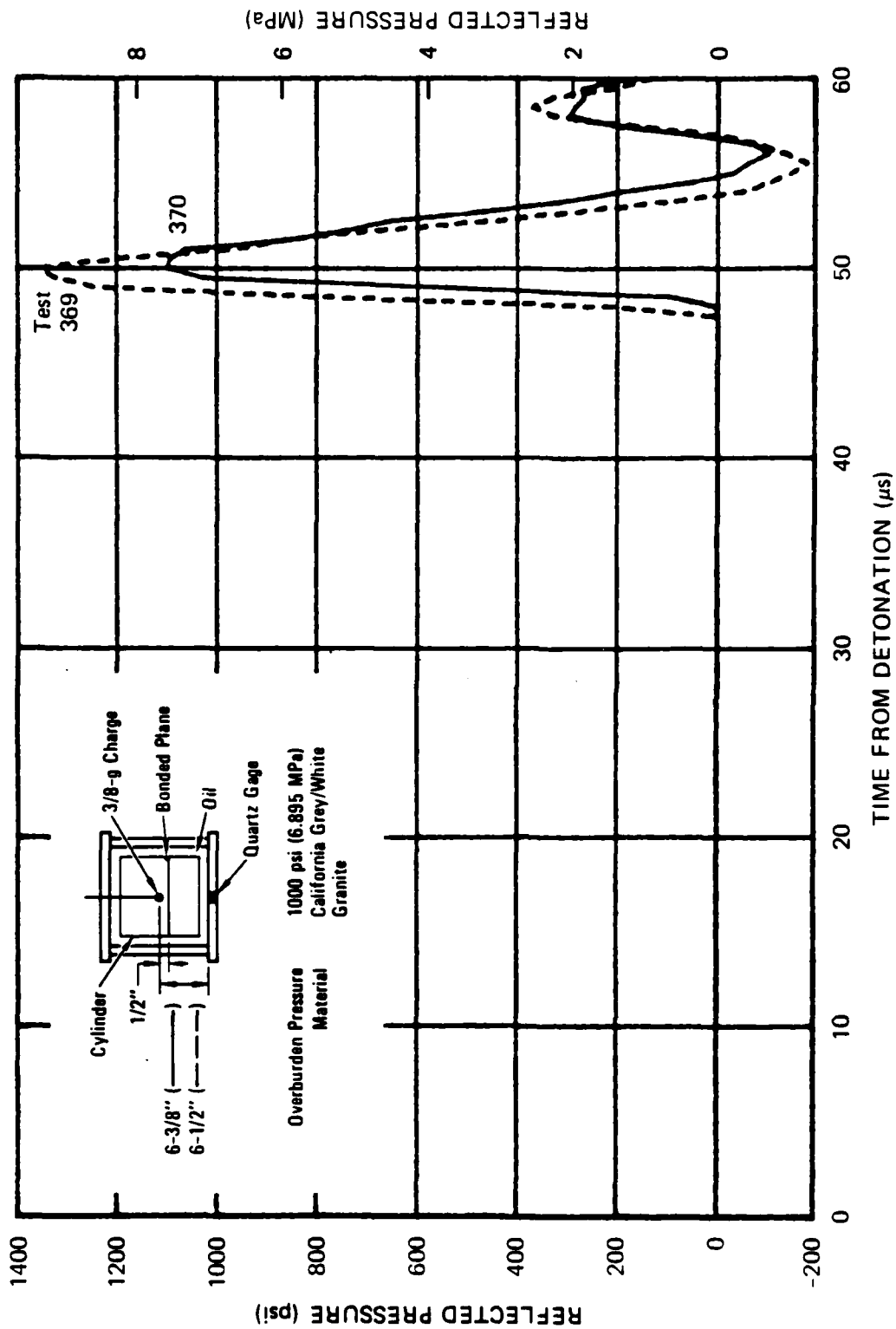
FIGURE B.7   REFLECTED PRESSURE FROM COUPLED EXPLOSIONS IN GRANITE —
PARTICLE VELOCITY TESTS 369 AND 370

B-8
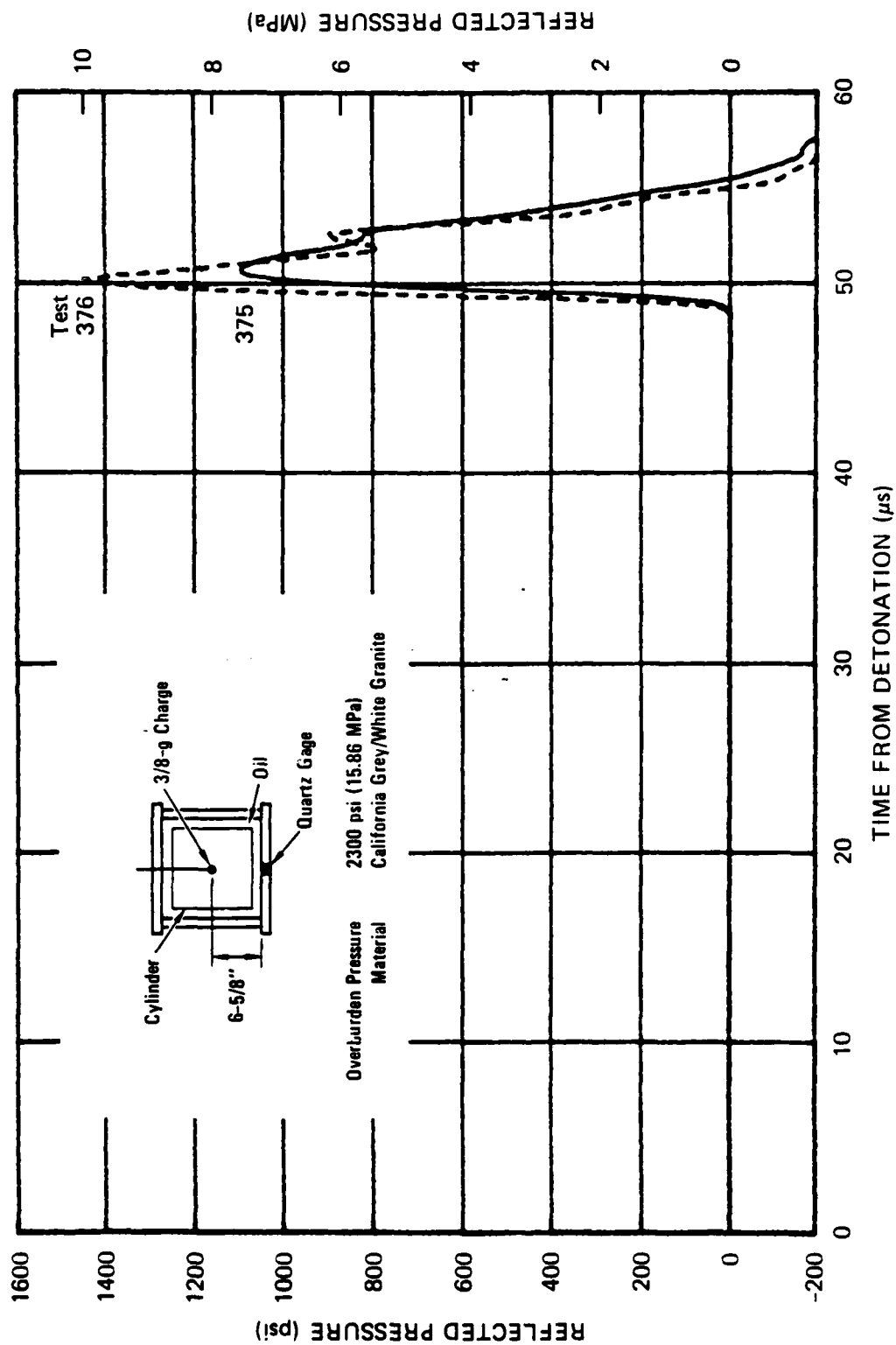
FIGURE B.8   REFLECTED PRESSURE FROM COUPLED EXPLOSIONS IN GRANITE
HYDROFRACTURE TESTS 375 AND 376

JA–5372–112

B-9
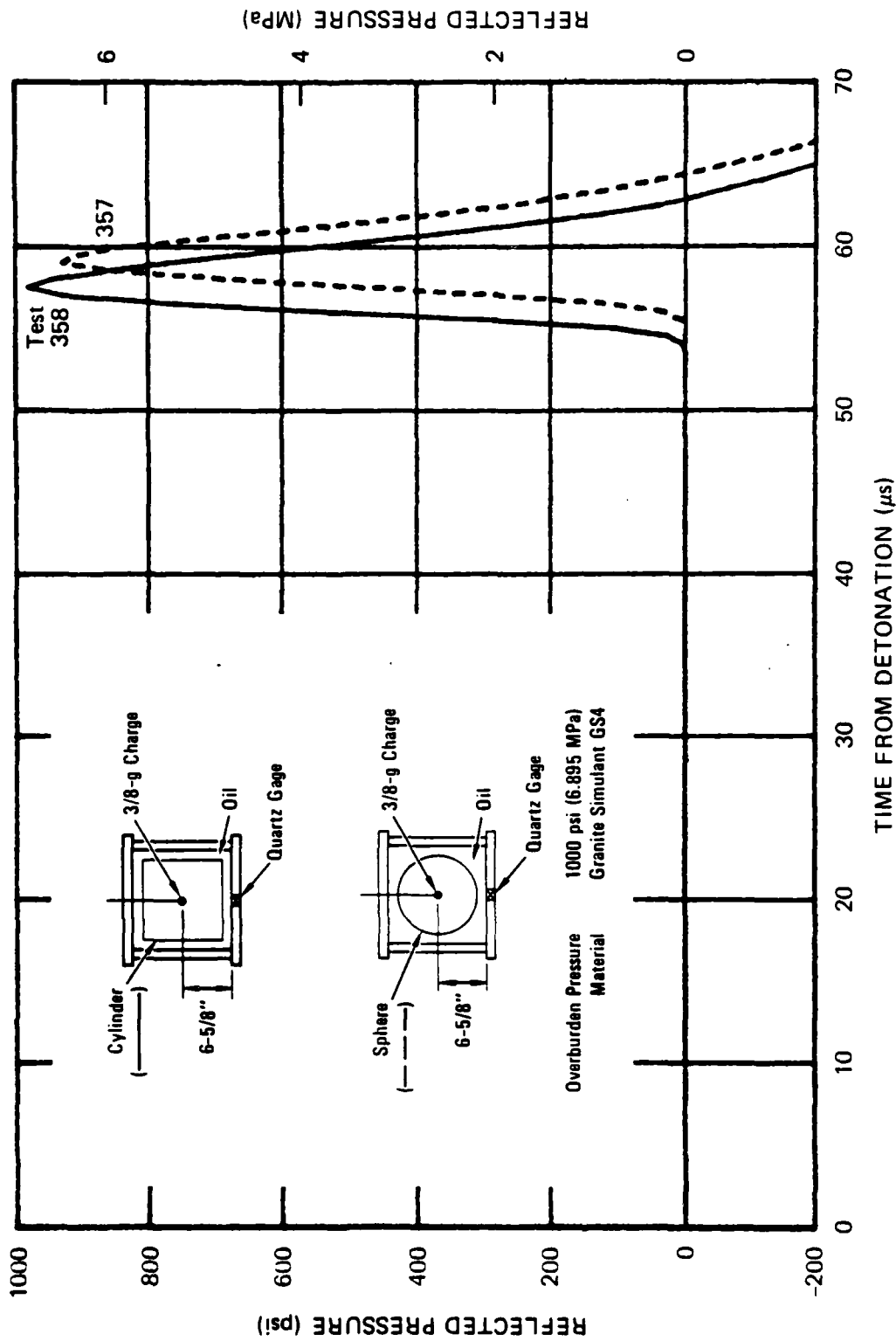
FIGURE B.9   REFLECTED PRESSURE FROM COUPLED EXPLOSIONS IN GS4
PARTICLE VELOCITY TESTS 357 AND 358

JA-5372-111

B-10
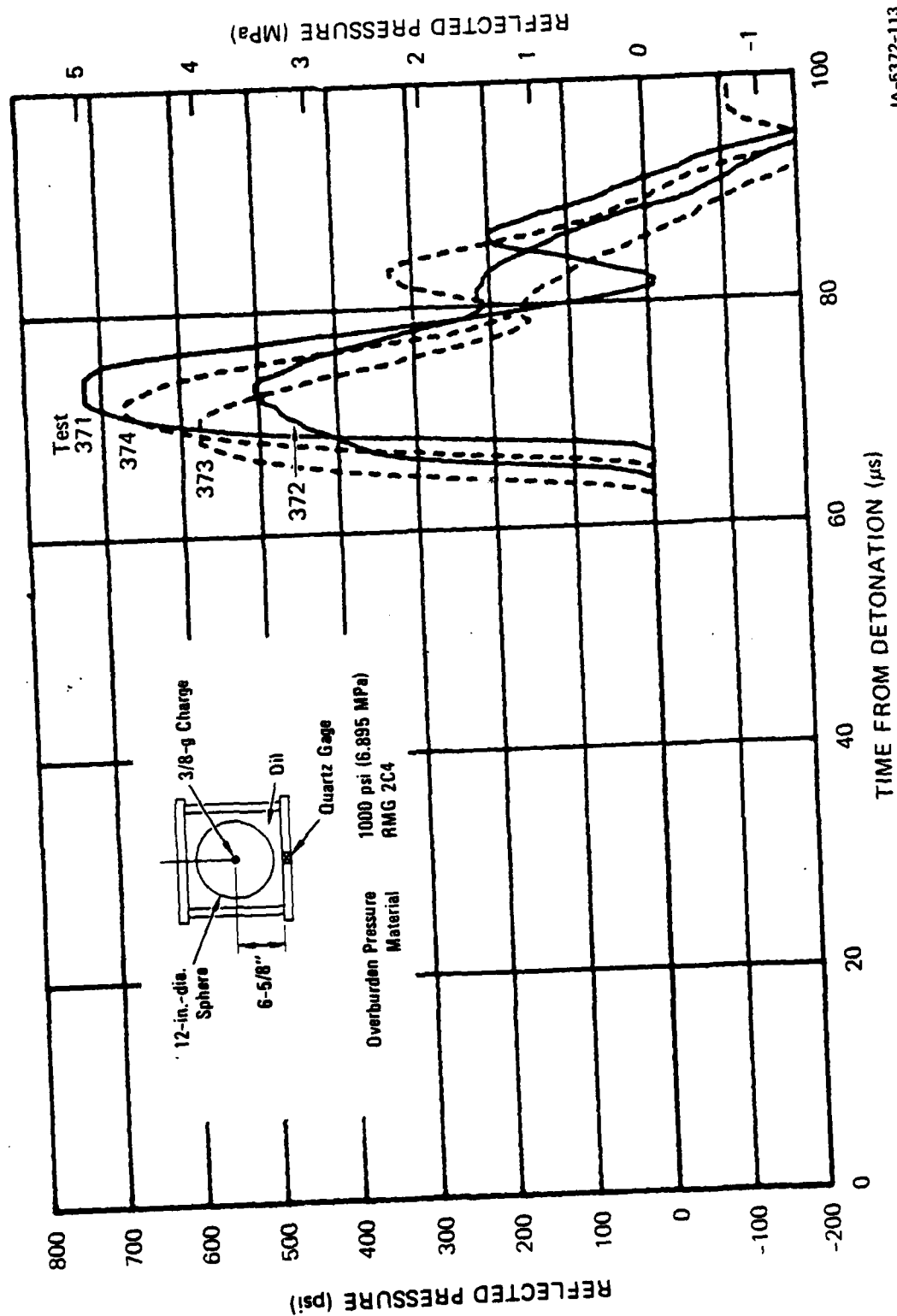
FIGURE B.10 REFLECTED PRESSURE FROM COUPLED EXPLOSIONS IN RMG 2C4 — STRESS AND STRAIN GAGE TESTS

JA-5372-113

B-11

Table B.1

SUMMARY OF PRESSURE PULSES FOR EXPLODED CAVITY TESTS

Test No.	Material	Geometry	Overburden Pressure (psi)	Overburden Fluid	Maximum Reflected Pressure (psi)	Pulse Duration (μs)
248	RMG 2C4	Sphere[a]	1000	Water	904	26.1
254	RMG 2C4	Sphere[a]	1000	Water	748	28.1
371	RMG 2C4	Sphere[a]	1000	Oil	722	24.3
372	RMG 2C4	Sphere[a]	1000	Oil	503	24.3
373	RMG 2C4	Sphere[a]	1000	Oil	575	23.1
374	RMG 2C4	Sphere[a]	1000	Oil	672	24.3
272	RMG 2C4	Sphere[b]	1000	Oil	953	21.2
273	RMG 2C4	Sphere[b]	1000	Oil	902	24.5
353	RMG 2C4	Sphere[b]	1000	Oil	966	24.2
293	RMG 2C4	Cylinder[c]	1000	Oil	1064	22.1
354	RMG 2C4	Cylinder[c]	1000	Oil	1092	22.4
355	RMG 2C4	Cylinder[c]	1000	Oil	1092	23.8
356	RMG 2C4	Cylinder[c]	1000	Oil	700	22.9
359	SNLA G-tunnel tuff	Cylinder[d]	1000	Water	1038	30.6
360	SNLA G-tunnel tuff	Cylinder[d]	1000	Water	1906	26.8
340	SNLA G-tunnel tuff	Cylinder[d]	1000	Oil	1025	29.8
341	SNLA G-tunnel tuff	Cylinder[d]	1000	Oil	754	32.3
350	P-tunnel tuff	Cylinder[e]	1000	Oil	1788	48.2
366	Granite[f]	Cylinder[e]	1000	Oil	1372	7.3
367	Granite[f]	Cylinder[e]	1000	Oil	1360	7.2
369	Granite[f]	Cylinder[e,g]	1000	Oil	1340	6.5
370	Granite[f]	Cylinder[e,g]	1000	Oil	1100	6.9
375	Granite[f]	Cylinder[e]	2300	Oil	1098	6.5
376	Granite[f]	Cylinder[e]	2300	Oil	1448	7.0
357	GS4	Sphere[b]	1000	Oil	927	8.8
358	GS4	Cylinder[c]	1000	Oil	980	9.0

a. 12 inch diameter (30.48 cm).

b. 11 inch diameter (27.94 cm).

c. 11 inch diameter (27.94 cm), 11 inches (27.94 cm) long.

d. 9-1/2 inch diameter (24.13 cm), 11 inches (27.94 cm) long.

e. 9-5/8 inch diameter (24.45 cm), 11 inches (27.94 cm) long.

f. California grey/white.

g. Bonded interface 1/2 inch (1.27 cm) below charge.

APPENDIX C

ANALYSIS OF PARTICLE VELOCITY ATTENUATION

INTRODUCTION

An existing elastodynamic analysis[1] was applied to allow us to compare experimentally determined particle velocity decay in granite with calculated elastic decay. The approach was to first assume that the particle velocity record obtained from a loop gage represents the velocity history of a spherical cavity having the same radius. Particle velocity pulses at larger radii may then be calculated and compared with experimental results.

FORMULATION

For spherically symmetric motion in a linear elastic medium, radial velocity may be expressed as[1]

$$\frac{\partial u}{\partial t} = -\frac{f''}{cr} - \frac{f'}{r^2} \tag{C.1}$$

where $u = u(r,t)$ is the radial displacement, $f = f(s)$ is the functional form for an outgoing wave, $s = t - \frac{r-a}{c}$ is the time that has elapsed after the wave has arrived (at radius r, cavity radius a, and dilatational velocity c), and $f' \equiv \frac{df}{ds}$.

The functions f' and f'' may be written[1]

$$f' = -cae^{-cs/a} \int_0^s e^{c\tau/a} v(\tau) d\tau \tag{C.2}$$

---

[1] J. C. Cizek and A. L. Florence, "Laboratory Investigation of Containment in Underground Nuclear Tests," Final Report, DNA 6121F, Contract DNA001-80-C-0040, SRI International, Menlo Park, California (December 1981).

$$f'' = -cav + c^2 e^{-cs/a} \int_0^s e^{c\tau/a} v(\tau) d\tau \qquad (C.3)$$

where $v(t) = \dfrac{\partial u(a,t)}{\partial t}$ is the cavity wall velocity. According to equation (C.1), the particle velocity is

$$\frac{\partial u}{\partial t}(r,s) = \frac{a}{r} v(s) - \left(1 - \frac{a}{r}\right) \frac{a}{r} \frac{c}{a} e^{-cs/a} \int_0^s e^{c\tau/a} v(\tau) d\tau \qquad (C.4)$$

In the next section, we examine particle velocity records from an experiment assuming a piecewise linear approximation to the cavity-wall velocity. Thus, for a velocity at $r = a$ of

$$v(t) = m_i t + b_i \qquad\qquad t_{i-1} < t < t_i$$

where

$$m_i = \frac{v_i - v_{i-1}}{s_i - s_{i-1}} \quad , \quad b = \frac{v_{i-1} s_i - v_i s_{i-1}}{s_i - s_{i-1}} \quad , \quad i = 1,2,\ldots,n \qquad (C.5)$$

and where n = number of piecewise linear segments, the particle velocity at radius r is

$$\frac{\partial u}{\partial t} = \frac{a}{r}(m_i s + b_i)$$

$$- \left(1 - \frac{a}{r}\right) \frac{a}{r} \cdot \frac{c}{a} e^{-cs/a} \sum_{j=1}^{j=i} \int_{s_{j-1}}^{s_j} e^{c\tau/a} (m_j \tau + b_j) d\tau \qquad (C.6)$$

where $s_{i-1} < s < s_i$ and

$$\int_{s_{j-1}}^{s_j} e^{c\tau/a} (m_j \tau + b_j) d\tau = \frac{m_j a^2}{c^2} \left(\frac{c}{a} s_j - 1\right) e^{(c/a)s_j} - \left(\frac{c}{a} s_{j-1} - 1\right) e^{(c/a)s_{j-1}}$$

$$+ \frac{b_j a}{c} e^{(c/a)s_j} - e^{(c/a)s_{j-1}}$$

ANALYTICAL AND EXPERIMENTAL RESULTS

The analysis was applied to California grey/white granite because the small displacements increase the possibility of elastic response within the range of the gages. Particle velocity was calculated by means of equation (C.6). A reasonably accurate piecewise linear approximation for the cavity-wall velocity was made by taking suitably small time steps.

Figure C.1 compares the theoretical and experimental decay of maximum particle velocity for the granite cylinder in test 361 (Series 9B). The particle velocity records for gages PV2 through PV4 were each used to provide cavity-wall velocity. Figure C.2 compares theoretical and experimental particle velocity pulses at PV4 (4.00 cm). The input to the calculation was the experimental particle velocity pulse at PV3 (2.54 cm). The results indicate that elastic response is being approached beyond a radius of 2.54 cm.
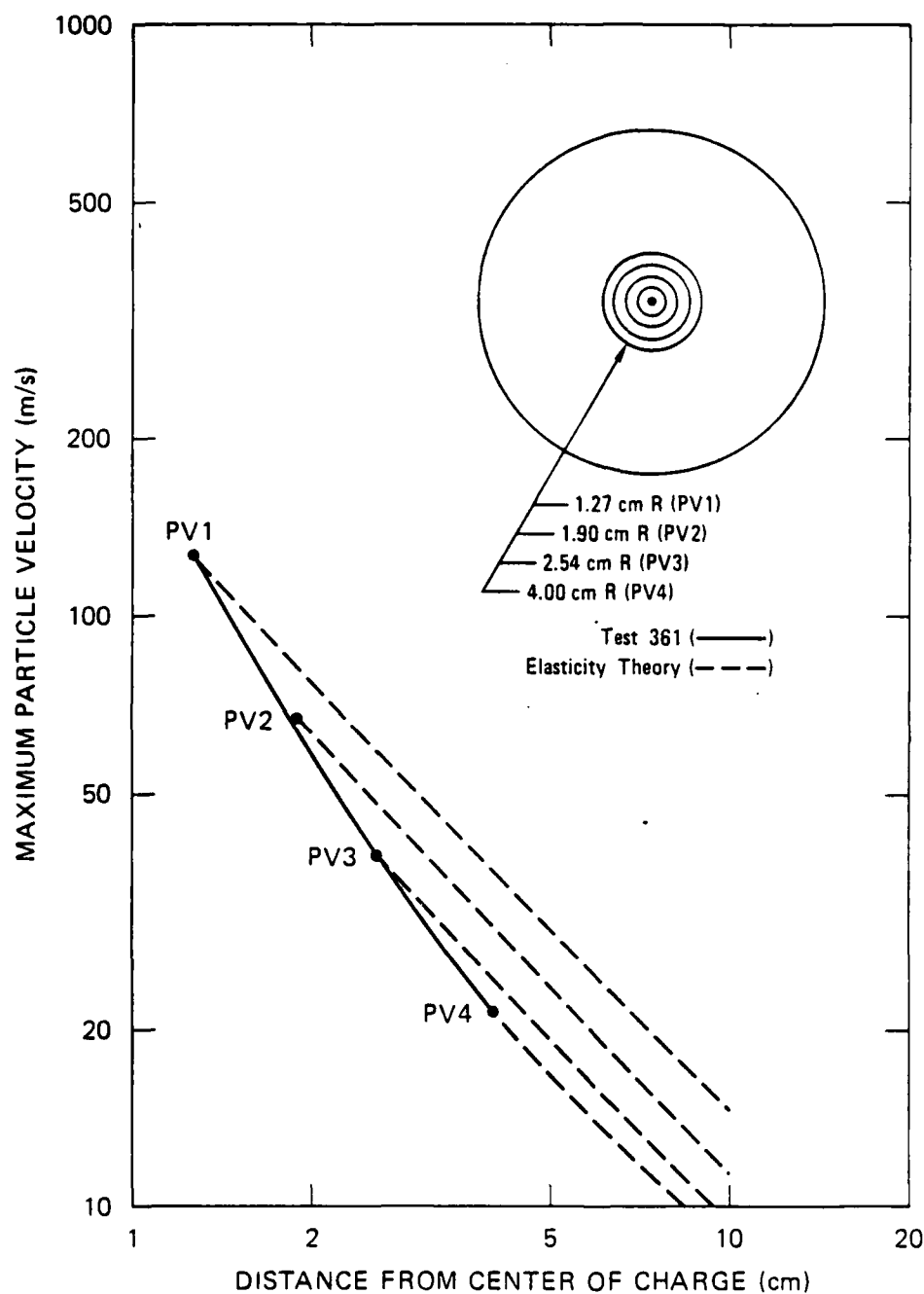
FIGURE C.1   THEORETICAL AND EXPERIMENTAL DECAY OF MAXIMUM
PARTICLE VELOCITY IN THE REGION SURROUNDING A
COUPLED EXPLOSION IN GRANITE

JA-5372-174
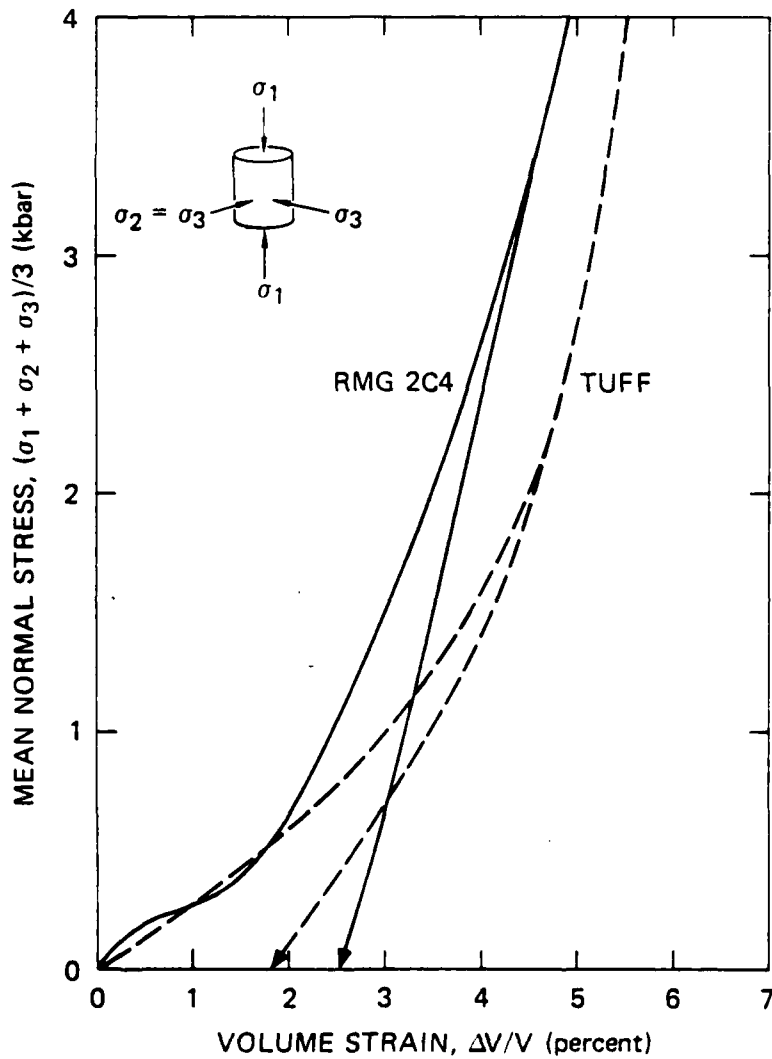
FIGURE F.2 UNIAXIAL STRAIN RESPONSE OF ROCK-MATCHING
GROUT RMG 2C4 AND NEVADA TEST SITE TUFF:
MEAN NORMAL STRESS VERSUS VOLUME STRAIN
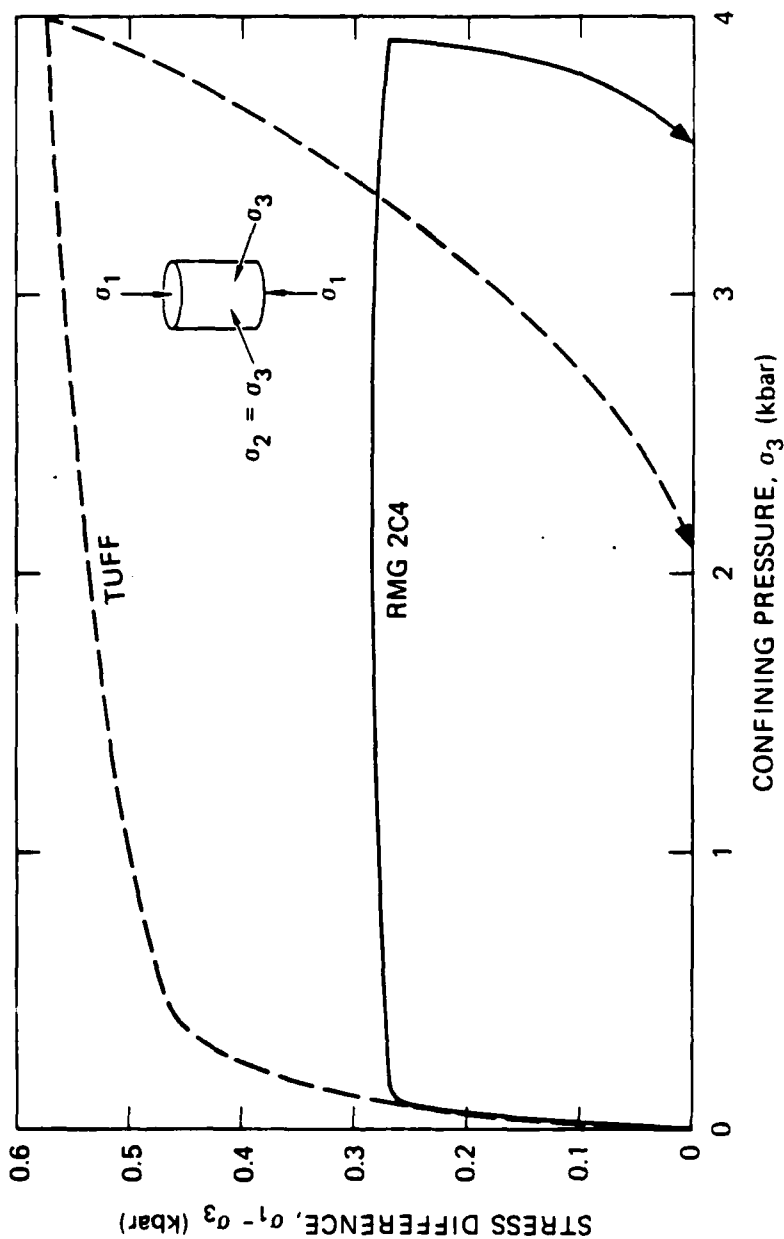
FIGURE F.1 UNIAXIAL STRAIN RESPONSE OF ROCK-MATCHING GROUT RMG 2C4 AND NEVADA TEST SITE TUFF: STRESS DIFFERENCE VERSUS CONFINING PRESSURE

JP-1289-42

Table F.3

STRENGTH PROPERTIES OF ROCK-MATCHING GROUT RMG 2C4,
WEAK (1-DAY-OLD) ROCK-MATCHING GROUT RMG 2C4,
NEVADA TEST SITE TUFFS, CALIFORNIA GREY/WHITE
GRANITE, AND GRANITE SIMULANTS GS3 AND GS4

Material	Average Strain Rate (s^{-1})	Unconfined Compressive Strength (psi)	Splitting Tensile Strength (psi)
RMG 2C4	Static	3970	530
RMG 2C4	0.15	5330	900
Weak (1-day-old) RMG 2C4	Static	600	60
Weak tuff	Static	870-1860	140-250
Strong tuff	Static	2460-5220	580-620
California grey/white granite	Static	20,660	3240
GS3	Static	8900	1110
GS3	0.15	15,900	1620
GS4	Static	9220	1370

Table F.2

PHYSICAL PROPERTIES OF ROCK-MATCHING GROUT RMG 2C4,
NEVADA TEST SITE TUFFS, GRANITE SIMULANTS GS3
AND GS4, AND RECONSTITUTED ALLUVIUM

Physical Property	RMG 2C4	Dry, 40%-, and 88%-Saturated Reconstituted Alluvium[a]	GS3 (GS4)	Typical Tuff (Weak Tuff) [Strong Tuff]
Density (g/cm^3)				
(Aged 2C4, GS3, GS4)	2.15	1.61,1.75,2.05	2.42 (2.39)	1.87 (1.96-2.13) [1.76-1.87]
Dry	1.75	1.61,1.72,1.80	2.27	1.54
Grain	2.87	2.51	2.80	2.34
Water by wet weight (%)	18.6	0,6.8,12.1	6.3	17.9
Porosity (%)	39	36,32,28	18.8	34
Saturation (%)	97-100	0,40,88	81.6	97.6
Air voids (%)	0-3	36,19,3.4	3.5	1.8
Longitudinal velocity (km/s)	3.29	1.15,1.15,1.31[b]	4.82	2.95
Shear velocity (km/s)	1.82	-	2.75	1.53
Modulus in compression (psi)	2.64 x 10^6	-	6.68 x 10^6	1.67 x 10^6
Shear modulus (psi)	1.03 x 10^6	-	2.65 x 10^6	0.63 x 10^6
Bulk modulus (psi)	2.00 x 10^6	1.2 x 10^4	4.64 x 10^6	1.55 x 10^6
Poisson's ratio	0.28	-	0.26	0.32
Permeability (μd)	3.0	-	-	-

a. At 1000 psi axial pressure under uniaxial strain.

b. 2.12 km/s in 88% saturated alluvium next to cavity.

Table F.1

MIXTURES[a] FOR ROCK-MATCHING GROUT RMG 2C4 AND GRANITE SIMULANTS GS3 AND GS4

Component	RMG 2C4 (%)
Type I-II Portland cement	32.691
Sand (20-40 Monterey)	21.896
Barite (barium sulfate)	20.848
Bentonite (gel)	2.837
CFR 2 (concrete friction reducing compound)	0.078
Water	21.650
Microballoons (Q-CEL 300)	-

Component	GS3 (%)	GS4 (%)
Type I-II Portland cement	38.573	38.573
Sand (10-30 granite)	49.295	-
Sand (16-30 granite)	-	49.295
Melment	1.035	1.035
CFR 2 (concrete friction) reducing compound)	0.252	0.252
Water	10.845	10.845

[a]Submerged in water for 28-day aging procedure with the following temperature sequence: raise to 54°C over 48-hour period, hold at 54°C for 48 hours, lower to 25°C over 36-hour period.

APPENDIX F

MATERIAL PROPERTIES

Presented here are properties of the following materials:

- Rock-matching grout RMG 2C4
- Nevada Test Site tuffs ranging from weak to strong
- California grey/white granite
- Granite simulants GS3 and GS4
- Alluvium reconstituted from NTS desert fines.

The properties include representative data selected from the results of recent Terra Tek test programs.[1-3]

Table F.1 provides the mixture and heat curing cycle for the rock-matching grout and the granite simulants. Tables F.2 and F.3 summarize available physical and mechanical properties of all the materials.

Figures F.1 and F.2 compare the uniaxial strain response of RMG 2C4 and a typical tuff. Figures F.3 and F.4 compare the uniaxial strain response of RMG 2C4 and GS3.

Figures F.5 through F.8 show the uniaxial strain response of dry, 40%-, and 88%-saturated alluvium as determined by the procedure

---

[1]D. S. Gardiner, S. W. Butters, D. O. Ennis, and A. H. Jones, "Material Properties of Nevada Test Site Tuff and Grout—With Emphasis on the DIABLO HAWK and HYBLA GOLD Events," Draft Final Report, Contract DNA001-76-C-0351, Terra Tek, Inc. (November 1977).

[2]S. W. Butters, J. M. Gronseth, and J. F. Patterson, "Material Properties of Nevada Test Site Tuff and Grout," Final Report TR 80-35, Contract DNA001-78-C-0395, Terra Tek, Inc. (May 1980).

[3]C. H. Cooley, R. H. Smith, and J. F. Schatz, "Material Properties of 2C4 Grout in Support of the Nevada Test Site Nuclear Test Program," Draft Final Report TR 81-56, Contract DNA001-81-C-0037, Terra Tek, Inc. (May 1981).

(2) Position accurately a 1/2-inch-diameter steel rod with a
     hemispherical end on the upper axis where the spherical
     explosive charge and the attached steel tube containing
     MDF will eventually be installed. This step eliminates
     any possible damage to the charge during subsequent
     loading in the Baldwin.

(3) Position accurately a prefabricated array of concentric
     circular particle velocity gages on top of the 5-inch-
     deep alluvium and concentric with the central 1/2-inch-
     diameter steel rod.

(4) Continue filling the container with alluvium in 1-inch-
     thick layers, compressing each layer in turn with 1000
     psi until the depth is 10 inches.

(5) Carefully remove the central rod and emplace the
     charge/MDF tube assembly.

(6) Fill the annular region around the charge and tube with
     layers of alluvium and tamp each layer firmly.

(7) Place the piston shown in Figure E.1 over the alluvium.

(8) Assemble the remaining apparatus.

(9) Apply a vertical stress of 1000 psi, using the hydraulic
     flatjack below the specimen.

UNIAXIAL STRAIN RESPONSE

The uniaxial strain response of dry, 40%-, and 88%-saturated
alluvium subjected to axial loads in the range 0-2 kbars was determined.
The procedure was similar to the one described above for determining the
overburden state. A thick-walled steel cylinder (6-inch height, 2-inch
internal diameter, and 6-inch external diameter) replaced the thin-
walled aluminum cylinder. Two strain gages were again mounted 90
degrees apart on the outer surface to monitor circumferential strain
during loading in the Baldwin machine. The cylinder was completely
filled with the desired mixture of desert fines and water so that the
internal pressure would be uniform along the entire length. The
internal pressure required to generate the measured hoop strain was then
calculated using a thick-walled cylinder analysis. This pressure is the
required radial (confining) stress. Volume change of the alluvium
sample was determined by measuring the displacement of a loosely fitting
steel piston. Results are presented in Appendix F, Material Properties.

Piston-plate

Alluvium
(11-7/16 in. dia. x 10 in. ht.)

Particle Velocity Loop

Solenoid

Confining Cylinder
(aluminum 1/4-in. wall)

Baseplate

Hydraulic
Flatjack
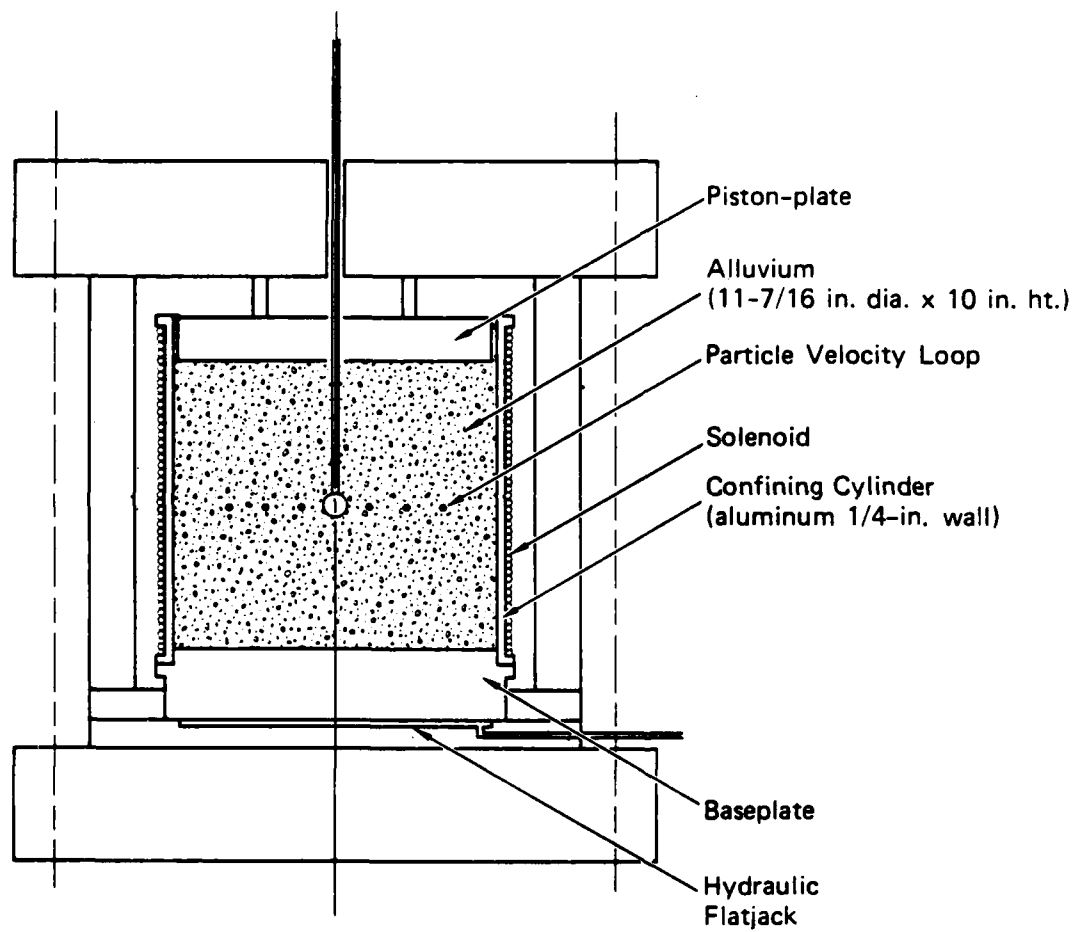
JA-5372-165

FIGURE E.1 CONFIGURATION FOR ALLUVIUM EXPERIMENTS

When the axial stress was 1000 psi, we obtained the values

$$\rho_w = 2.10 \text{ g/cm}^3 \qquad w = 0.125\rho_w = 0.263 \text{ g/cm}^3 \qquad \rho_d = 1.84 \text{ g/cm}^3$$

$$\eta = 0.267 \qquad v = 0.263 \qquad s = 0.985$$

Thus, the saturation achieved with the above improvement was 98.5%. Further improvement requires either higher accuracy or vacuum technology to remove air.

OVERBURDEN STATE

The initial uniaxial strain states for the dry, 40%, and 88% saturation alluvium samples are fixed by the initial densities at 1000 psi vertical stress of 1.61, 1.85, and 2.05 g/cm^3, respectively. It remains to determine the radial component of stress. In step (3) of the procedure for determining the saturation percentage, the alluvium sample was compressed in an aluminum cylindrical shell with a radius-to-thickness ratio (22.72) chosen to be the same as the larger aluminum cylinder containing the sample for the particle velocity experiment (Figure E.1). The container had two strain gages, which were 90 degrees apart bonded to the outer surface, to monitor the circumferential strain during loading with the Baldwin machine. We calculate the approximate hoop stress from the hoop strain and hence obtain the internal pressure on the cylinder. This pressure is the radial stress required. It turned out that the increase of radial stress with axial loading was independent of the saturation percentage. When the axial stress was 1000 psi, the radial stress was 390 psi.

PARTICLE VELOCITY SAMPLE

Figure E.1 shows schematically the experimental configuration. The procedure for preparing the alluvium samples is as follows:

(1) Fill the aluminum cylinder (11-7/16-inches internal diameter) with alluvium to a depth of 5 inches in 1-inch-deep layers. Compress each layer in turn with a vertical stress of 1000 psi by means of a Baldwin loader.

E-3

(4) Compress the wet sample by loading the piston in a Baldwin testing machine until the axial stress is 1000 psi. Weigh the water squeezed out and measure the piston displacement (to determine the final volume).

(5) Calculate the wet density at 1000 psi and the water remaining in the sample (A total of 2.05 g/cm^2 and 12.1% of wet weight, respectively, in our preparation.)

This procedure was performed in an attempt to obtain 100% saturation. However, our calculations gave 88%. These calculations are as follows:

Wet density $\qquad\qquad\qquad\qquad\qquad\qquad\qquad\qquad \rho_w = 2.05 \text{ g/cm}^3$

Weight of water $\qquad\qquad\qquad\qquad\qquad\qquad w = 0.121\rho_w = 0.248 \text{ g/cm}^3$

Dry density $\qquad\qquad\qquad\qquad\qquad\qquad\qquad \rho_d = \rho_w - w = 1.80 \text{ g/cm}^3$

Grain density (pycnometer analysis) $\qquad\qquad\qquad \rho_g = 2.51 \text{ g/cm}^3$

Porosity $\qquad\qquad\qquad\qquad \eta = (\rho_g - \rho_d)/\rho_g = 0.283 \text{ cm}^3/\text{cm}^3$

Volume of water $\qquad\qquad\qquad\qquad\qquad\qquad v = 0.248 \text{ cm}^3/\text{cm}^3$

Saturation fraction $\qquad\qquad\qquad\qquad s = v/\eta = 0.88$

In an attempt to obtain 50% saturation, we started with half of the water retained in step (2) above. In this case, the calculations gave a saturation of 40%, as follows:

$\rho_w = 1.85 \text{ g/cm}^3 \qquad w = 0.068\rho_w = 0.126 \text{ g/cm}^3 \qquad \rho_d = 1.72 \text{ g/cm}^3$

$\rho_g = 2.51 \text{ g/cm}^3 \qquad \eta = 0.315 \qquad v = 0.126 \qquad s = 0.40$

Failure to obtain 100% saturation is attributed to the inadequacy of step (2) in providing enough water retention. In other words, water can drain out of the sand while air is still in the pores. We replaced the cylindrical container with a screen base in step (2) with a cylinder that had an impermeable base and stirred in enough water to leave a thin layer of water on top. Later, this excess water is removed. This process resulted in a water retention of 19.3% of the wet weight.

APPENDIX E

## PROCEDURES FOR PREPARING ALLUVIUM SPECIMENS

In the particle velocity experiments with alluvium specimens, distortion of the circular wire loops must be prevented when the over-burden pressure is applied. The problem arises because alluvium is highly compressible. We avoided distortion of the loops by choosing an overburden state that corresponds approximately to uniaxial strain; that is, we suppressed the radial strain. We describe here the preparation of the alluvium specimens for particle velocity experiments, including determination of the saturation percentage and the overburden stress-strain state.

SATURATION PERCENTAGE

We attempted to achieve 0%, 50%, and 100% saturation percentages but obtained instead 0%, 40%, and 88%. The reason for not achieving the desired percentages is given below.

The following are steps and results of the procedure for 100% saturation:

(1) Dry and weigh a sample of NTS desert fines (W_d).

(2) Place the dry sample in a cylindrical container (12-in. height, 2-in. diameter) having a fine screen base plate. Add water slowly at the top until water begins to drain through the base plate. Determine the weight of water added (W_a) and weigh the excess water (W_e). The water retained in our preparation ($W_r = W_a - W_e$) was 15.1% of the wet weight ($W_w = W_d + W_r$; $W_r = 0.151 W_w$).

(3) Place the wet sample in a thin-walled cylindrical aluminum container (6-inch height, 4-inch internal diameter, and 0.09-inch-thick wall) with a perforated steel base plate (0.031-inch-diameter holes) and a loosely fitting piston for compressing the specimen (drained condition). The sample was 5 inches high in our preparation.

E-1
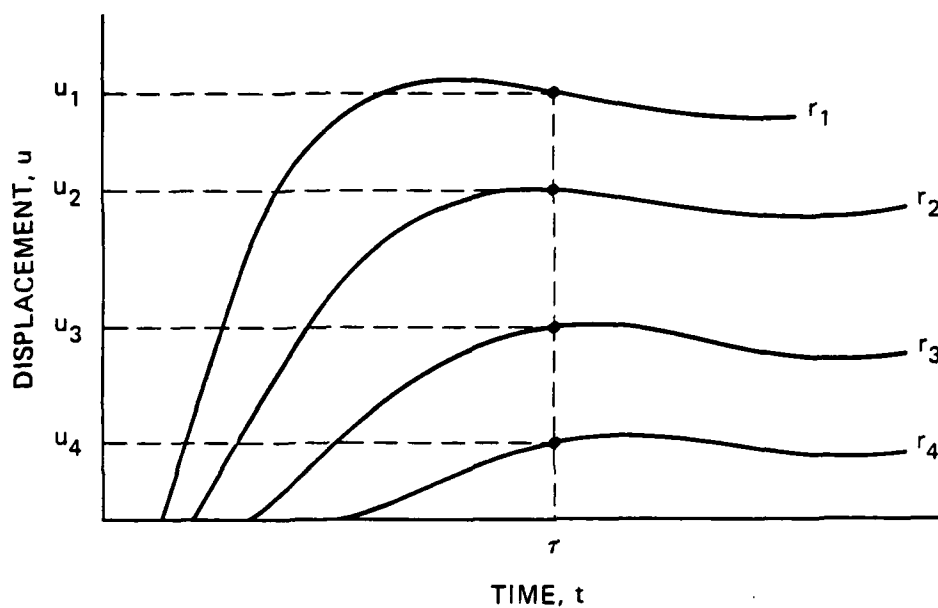
JA-5372-161

FIGURE D.1 DISPLACEMENT HISTORIES AT SEVERAL RADII OBTAINED
FROM INTEGRATION OF PARTICLE VELOCITY RECORDS
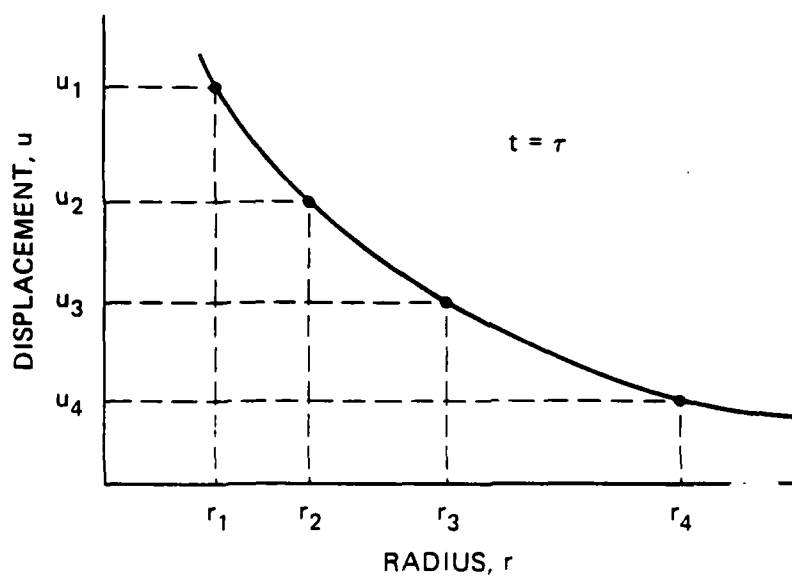
JA-5372-159

FIGURE D.2 DISPLACEMENT PROFILE AT TIME $t = \tau$

APPENDIX D

VOLUME CHANGE FROM PARTICLE VELOCITY RECORDS

The records of the particle velocities at several radii for a spherical wave provide a means of calculating the time variation of the volume change for the material between the gages. The particle velocity record at each gage location is integrated with respect to time to produce the particle displacement history there, as shown schematically in Figure D.1. At time $t = \tau$, the radial displacement at gage location r_n is u_n. Figure D.2 shows schematically the displacements u_n plotted against the radius r_n at time τ.

A spherical shell of material of outer radius r_{n+1} and inner radius r_n has changed at time τ to a spherical shell of outer radius $r_{n+1} + u_{n+1}$ and inner radius $r_n + u_n$. Hence the volume of the spherical shell at time τ is
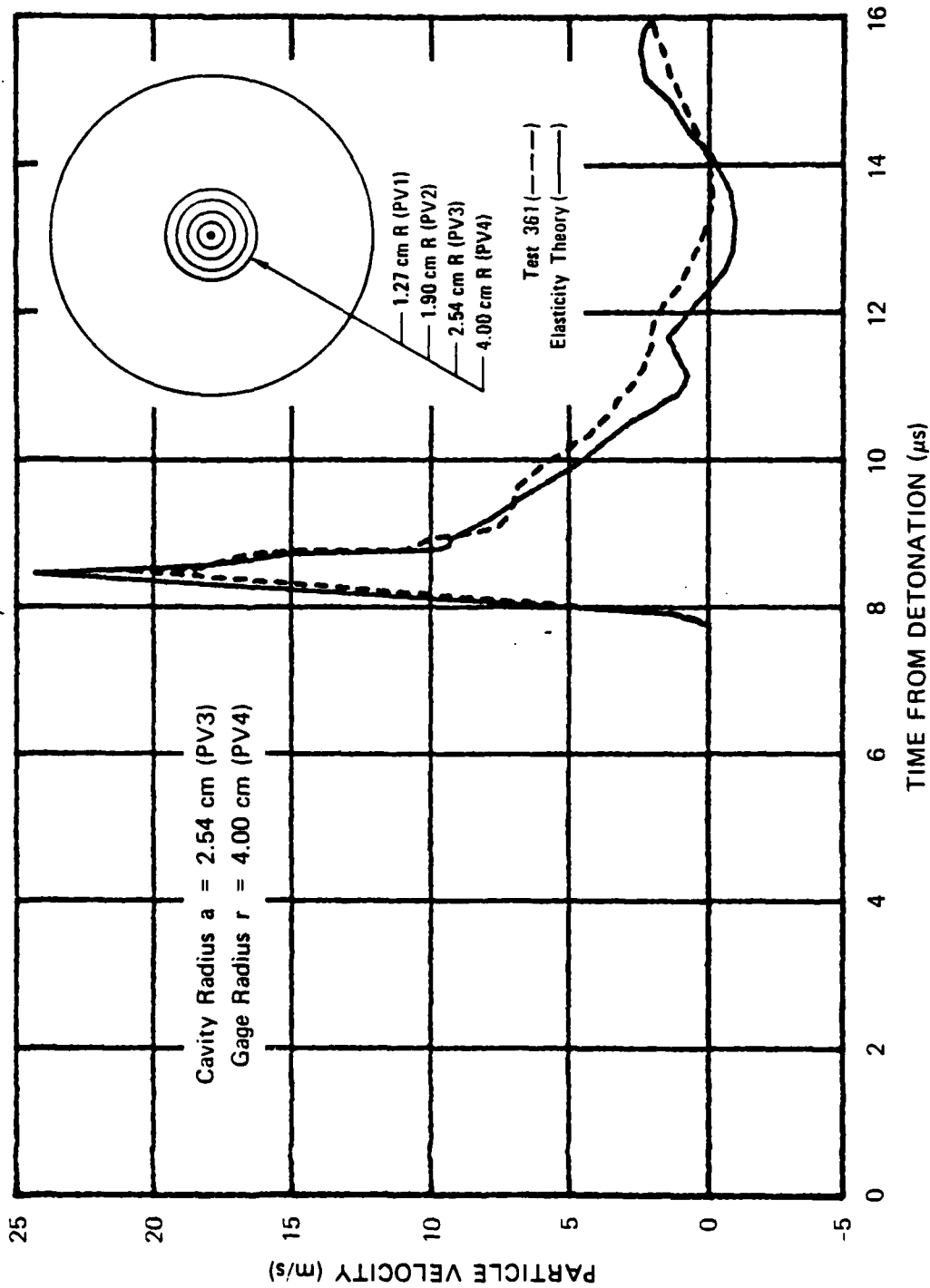
$$V_{n+1/2}(\tau) = \frac{4}{3}\pi\left[(r_{n+1} + u_{n+1})^3 - (r_n + u_n)^3\right] \qquad (D.1)$$

The volume change is therefore the value of equation (D.1) minus the original volume

$$V_{n+1/2}(0) = \frac{4}{3}\pi\left[r_{n+1}^3 - r_n^3\right] \qquad (D.2)$$

The fractional volume change at time τ is simply the difference between the volumes of equations (D.1) and (D.2) divided by the original volume of equation (D.2).

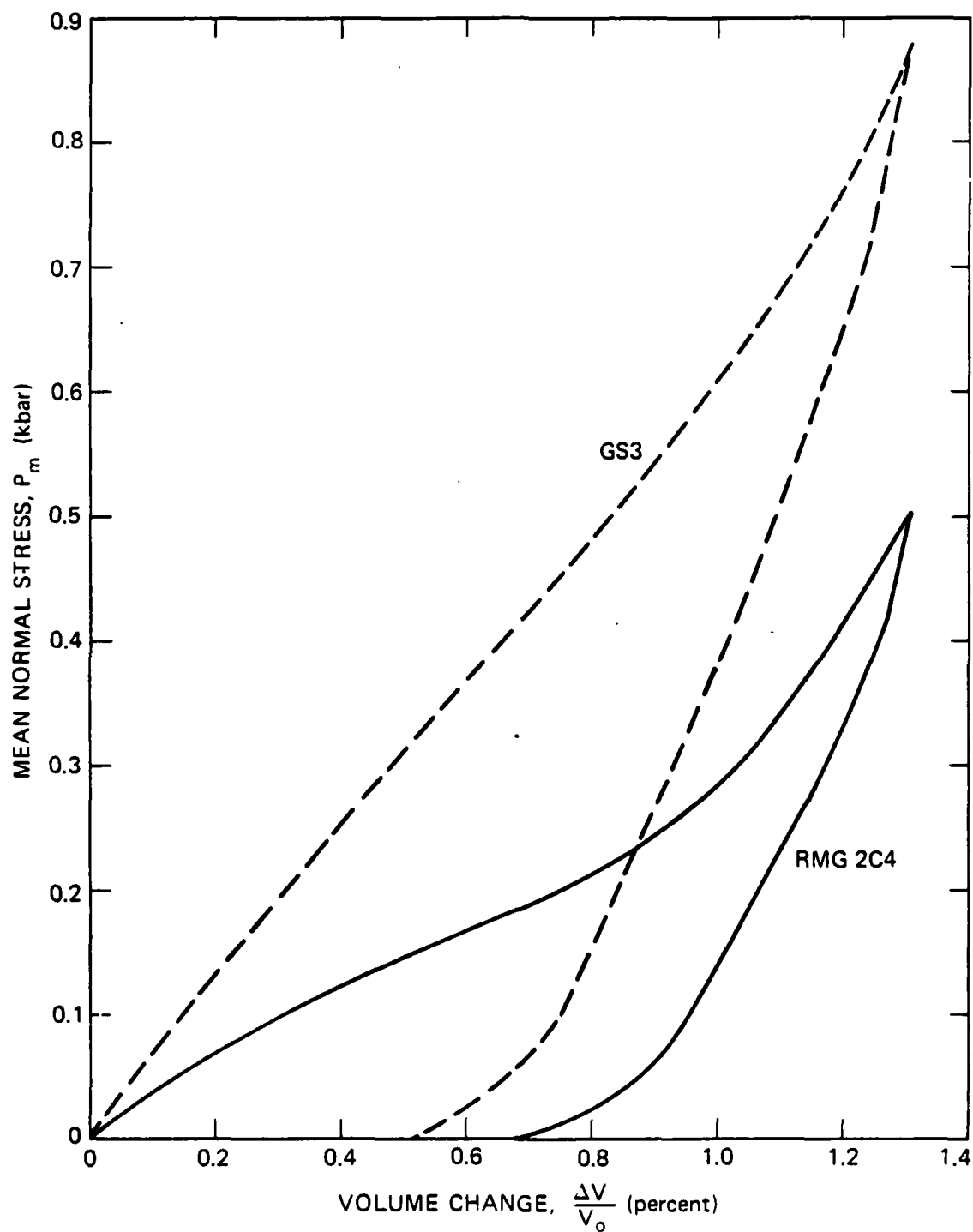The procedure was used to obtain the volume change results presented in Section 3.

FIGURE C.2   THEORETICAL AND EXPERIMENTAL PARTICLE VELOCITY 4.00 cm FROM THE CENTER
OF A COUPLED EXPLOSION IN GRANITE

JA-5372-175

C-5
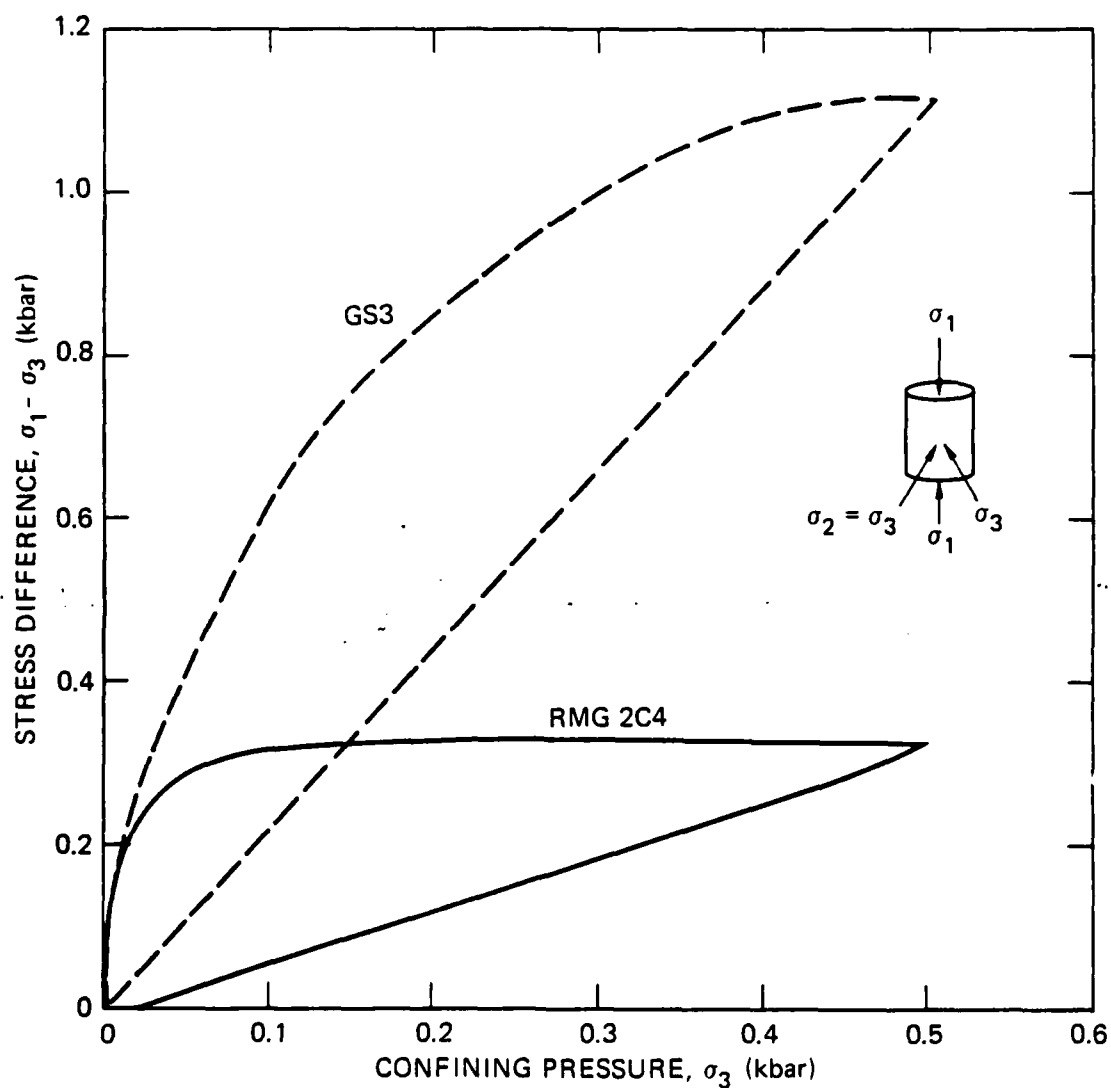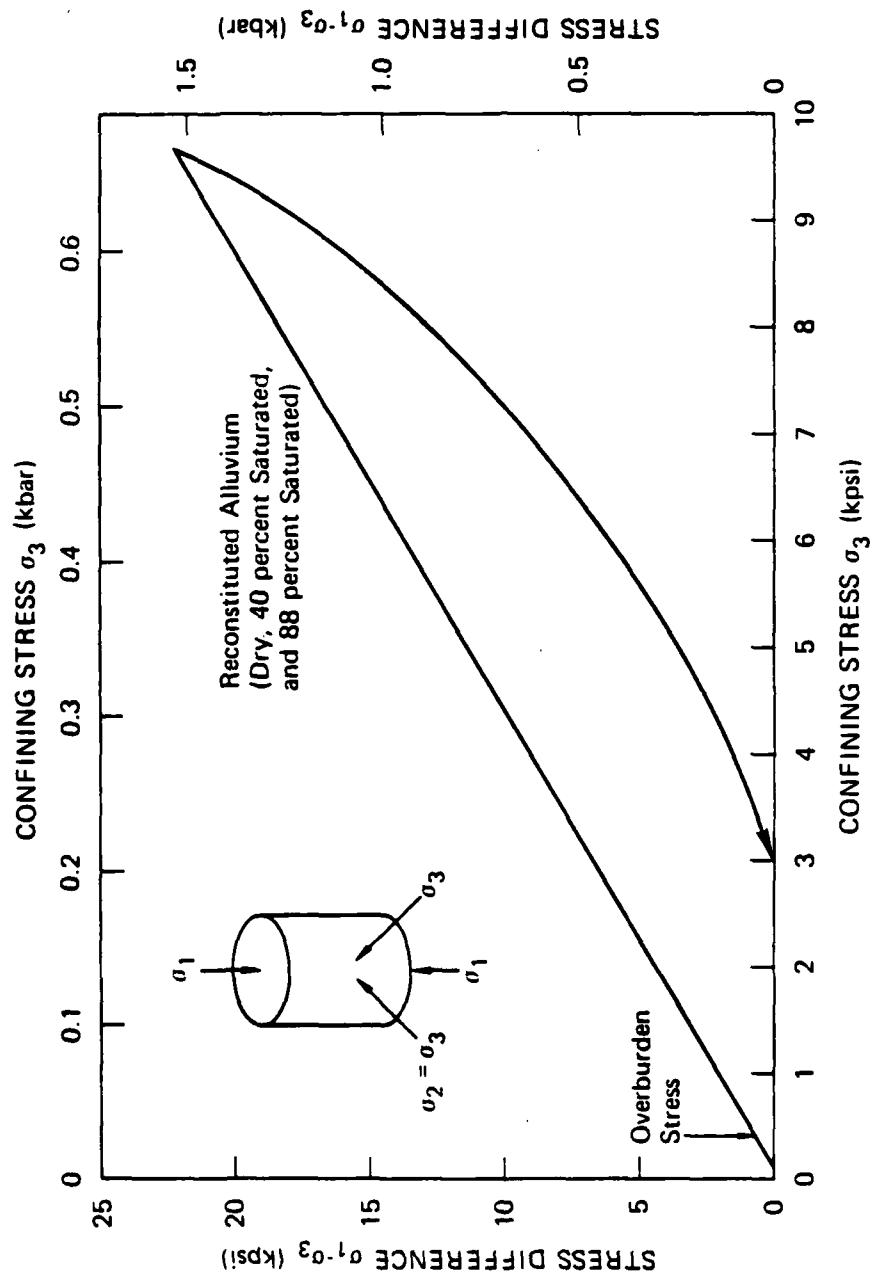
FIGURE F.3 UNIAXIAL STRAIN RESPONSE OF ROCK-MATCHING GROUT RMG 2C4 AND
GRANITE SIMULANT GS3: STRESS DIFFERENCE VERSUS CONFINING PRESSURE

MP-5958-40

F-7
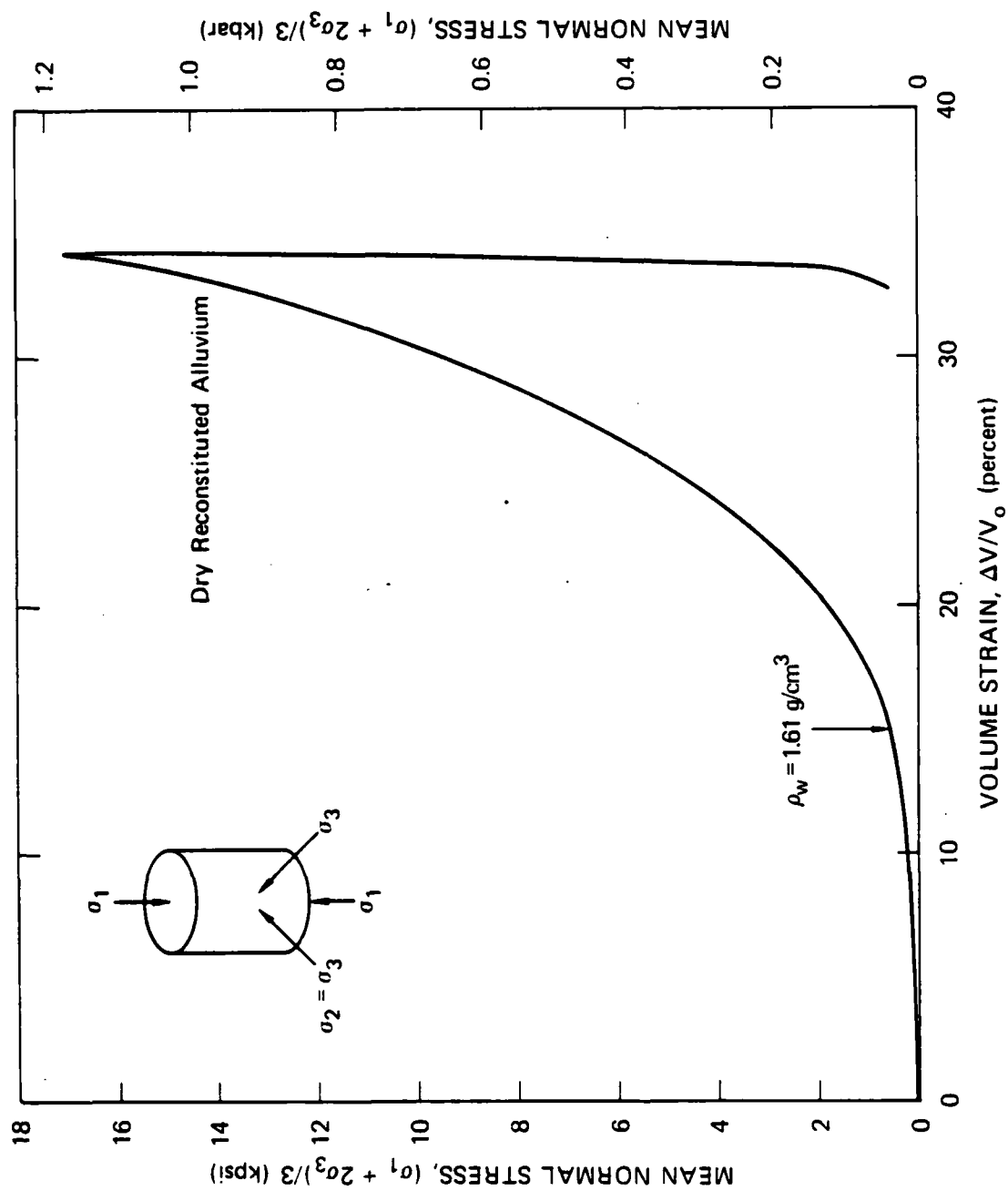
MP-5958-41

FIGURE F.4 UNIAXIAL STRAIN RESPONSE OF ROCK-MATCHING GROUT RMG 2C4 AND
GRANITE SIMULANT GS3: MEAN NORMAL STRESS VERSUS VOLUME CHANGE

F-8

FIGURE F.5 UNIAXIAL STRAIN RESPONSE OF RECONSTITUTED ALLUVIUM: STRESS DIFFERENCE
VERSUS CONFINING PRESSURE (DRAINED)

FIGURE F.6 UNIAXIAL STRAIN RESPONSE OF DRY RECONSTITUTED ALLUVIUM:
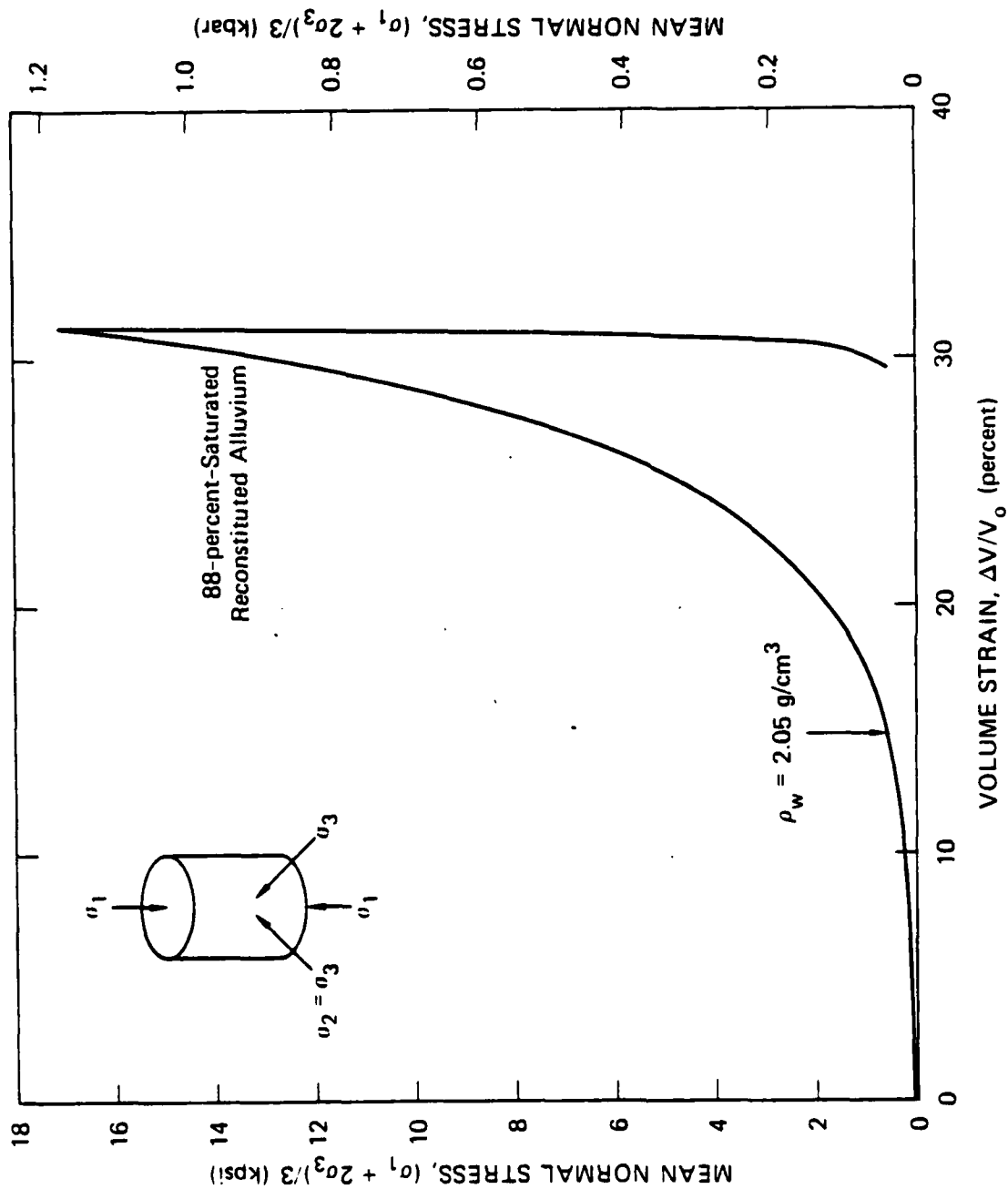MEAN NORMAL STRESS VERSUS VOLUME STRAIN

F-10
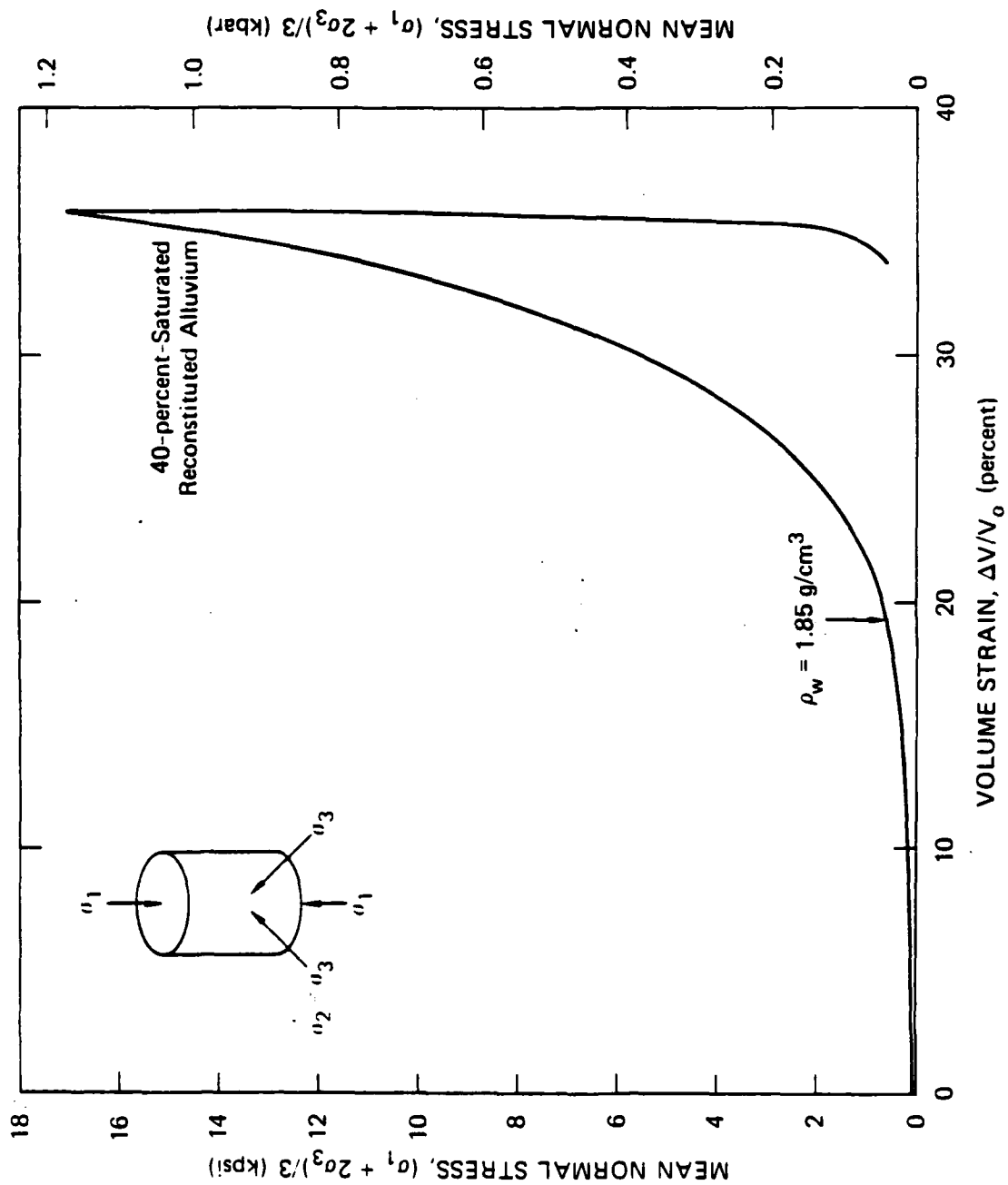
FIGURE F.7 UNIAXIAL STRAIN RESPONSE OF 40-percent-SATURATED RECONSTITUTED ALLUVIUM: MEAN NORMAL STRESS VERSUS VOLUME STRAIN (DRAINED)

JA-5372-145

F-11

FIGURE F.8   UNIAXIAL STRAIN RESPONSE OF 88-percent-SATURATED RECONSTITUTED ALLUVIUM:
MEAN NORMAL STRESS VERSUS VOLUME STRAIN (DRAINED)

F-12

described in Appendix E. Stress difference (axial minus confining) versus confining pressure during loading and unloading is shown in Figure F.5. This response was found to be independent of the initial state of saturation. The overburden stress state at which particle velocity tests were performed is designated on the loading path. Mean normal stress versus volume strain for dry, 40%-, and 88%-saturated alluvium under drained conditions is shown in Figures F.6, F.7, and F.8, respectively. The density at which particle velocity tests were performed is shown on the loading path in each figure.

DISTRIBUTION LIST

DEPARTMENT OF DEFENSE

Defense Nuclear Agency
    ATTN: SPTD, T. Kennedy
4 cy ATTN: STTI/CA

Field Command
Defense Nuclear Agency
    ATTN: FCTT, W. Summa
    ATTN: FCT, COL G. Ballantine
3 cy ATTN: FCTK, C. Keller
3 cy ATTN: FCTK, E. Rinehart

Defense Technical Information Center
12 cy ATTN: DD

DEPARTMENT OF ENERGY

Department of Energy
Nevada Operations Office
    ATTN: P. Mudra

OTHER GOVERNMENT AGENCY

US Geological Survey
    ATTN: R. Carroll
    ATTN: P. Orkild

DEPARTMENT OF ENERGY CONTRACTORS

Desert Research Institute
Attention D. Schulke Sec Off for
    ATTN: P. Fenske
    ATTN: C. Case

University of California
Lawrence Livermore National Lab
    ATTN: B. Hudson
    ATTN: F. Morrison
    ATTN: L-209, G. Higgins
    ATTN: R. Terhune
    ATTN: L. Makague
    ATTN: C. Olsen

Sandia National Laboratories
    ATTN: Org 7112, C. Mehl
    ATTN: R. Bass
    ATTN: C. Smith

DEPARTMENT OF ENERGY CONTRACTORS (Continued)

Los Alamos National Laboratory
    ATTN: F. App
    ATTN: R. Brownlee
    ATTN: C. Keller
    ATTN: T. Kunkle, ESS-5
    ATTN: B. Travis

DEPARTMENT OF DEFENSE CONTRACTORS

California Research & Technology, Inc
    ATTN: M. Rosenblatt

Kaman Tempo
    ATTN: DASIAC

Kaman Tempo
    ATTN: DASIAC

Pacific-Sierra Research Corp
    ATTN: H. Brode, Chairman SAGE

Pacifica Technology
    ATTN: D. Patch

Physics International Co
    ATTN: J. Gordon
    ATTN: H. Wampler
    ATTN: J. Shea

R&D Associates
    ATTN: P. Haas

Rand Corp
    ATTN: B. Bennett

S-CUBED
    ATTN: C. Dismukes
    ATTN: R. Duff

SRI International
2 cy ATTN: A. Florence
2 cy ATTN: J. Cizek

END

FILMED

4-85

DTIC